Aston University

Some pages of this thesis may have been removed for copyright restrictions.

If you have discovered material in AURA which is unlawful e.g. breaches copyright, (either yours or that of a third party) or any other law, including but not limited to those relating to patent, trademark, confidentiality, data protection, obscenity, defamation, libel, then please read our Takedown Policy and contact the service immediately

LIQUID-LIQUID EXTRACTION IN A PILOT SCALE ROTATING DISC CONTACTOR

by

KIFAH KAMIL MAHMOUD AL-ASWAD

A thesis submitted to
The University of Aston in Birmingham
for the degree of
Doctor of Philosophy

Department of Chemical Engineering,
The University of Aston in Birmingham. May, 1982.

PAGE NUMBERS CUT OFF IN ORIGINAL

To My Elder Brother, SABAH.

The University of Aston in Birmingham

SUMMARY

LIQUID-LIQUID EXTRACTION IN A PILOT SCALE ROTATING DISC CONTACTOR

KIFAH KAMIL MAHMOUD AL-ASWAD Ph.D. May, 1982.

A study of the hydrodynamics and mass transfer characteristics of a liquid-liquid extraction process in a 450 mm diameter, 4.30 m high Rotating Disc Contactor (R.D.C.) has been undertaken. The literature relating to this type of extractor and the relevant phenomena, such as droplet break-up and coalescence, drop mass transfer and axial mixing has been reviewed.

Experiments were performed using the system Clairsol-350-acetone-water and the effects of drop size, drop size-distribution and dispersed phase hold-up on the performance of the R.D.C. established. The results obtained for the two-phase system Clairsol-water have been compared with published correlations: since most of these correlations are based on data obtained from laboratory scale R.D.C.'s, a wide divergence was found. The hydrodynamics data from this study have therefore been correlated to predict the drop size and the dispersed phase hold-up and agreement has been obtained with the experimental data to within ∓8% for the drop size and ∓9% for the dispersed phase hold-up. The correlations obtained were modified to include terms involving column dimensions and the data have been correlated with the results obtained from this study together with published data; agreement was generally within ∓17% for drop size and within ∓14% for the dispersed phase hold-up.

The experimental drop size distributions obtained were in excellent agreement with the upper limit log-normal distributions which should therefore be used in preference to other distribution functions.

In the calculation of the overall experimental mass transfer coefficient the mean driving force was determined from the concentration profile along the column using Simpson's Rule and a novel method was developed to calculate the overall theoretical mass transfer coefficient K_{cal}, involving the drop size distribution diagram to determine the volume percentage of stagnant, circulating and oscillating drops in the sample population. Individual mass transfer coefficients were determined for the corresponding droplet state using different single drop mass transfer models. K_{cal} was then calculated as the fractional sum of these individual coefficients and their proportions in the drop sample population. Very good agreement was found between the experimental and theoretical overall mass transfer coefficients.

Drop sizes under mass transfer conditions were strongly dependant upon the direction of mass transfer. Drop sizes in the absence of mass transfer were generally larger than those with solute transfer from the continuous to the dispersed phase, but smaller than those with solute transfer in the opposite direction at corresponding phase flowrates and rotor speed. Under similar operating conditions hold-up was also affected by mass transfer; it was higher when solute transfered from the continuous to the dispersed phase and lower when direction was reversed compared with non-mass transfer operation.

Key Words: Liquid-Liquid Extraction; Rotating Disc Contactor; Dispersed Phase Hold-up; Drop Size and Drop Size Distribution; Overall Mass Transfer Coefficient

ACKNOWLEDGEMENT

The author wishes to express his gratitude to Professor G. V. Jeffreys, the Head of the Department of Chemical Engineering for providing the facilities for this research for his invaluable supervision, for his patience and encouragement, and for his continued help and constructive criticism.

The author also wishes to thank:

Dr. C. J. Mumford,

for his interest in the subject of this study and encouragement throughout this study.

The Laboratory and Technical Staff of the Department of Chemical Engineering for their assistance.

Ms S. Ellis,

for her diligence in typing this thesis.

Ms C. Johnson,

for her help in the correction of the manuscript.

And finally thanks are due to my parents for their continual encouragement during my studies.

CONTENTS

LIST OF TABLES

LIST OF TABLES (cont.)

LIST OF FIGURES

LIST OF FIGURES (Contd.)

LIST OF FIGURES (Contd..)

CHAPTER ONE

Introduction

Liquid-liquid extraction involves the separation of a liquid mixture into its components by means of a solvent in which one or more of the components is preferentially soluble. The process entails the dispersion of one liquid as droplets into a continuous phase followed by solute transfer to or from the droplets and finally separation of the dispersed phase by flocculation and coalescence.

The process has been used increasingly for separation because of the rapid world-wide development of the chemical industry and the importance of petrochemicals, wet metallurgy and synthetic fibre processes.

Liquid-liquid extraction is often applied to separate a liquid mixture when it is impracticable, or inconvenient, to obtain the desired components by distillation. Normally distillation is the most efficient method of separating a mixture into its constituents, but extraction may be preferred under the following circumstances:

i) when valuable components would be destroyed, or damaged, by the temperature required for separation by distillation.

ii) when the required component is present in the feed liquor in very small quantities,

iii) when the feed is non-volatile,

iv) when a large number of constituents in the feed have similar volatilities or form azeotropes; and/or

v) when one component only of intermediate volatility is required from a mixture composed of a large number of components.

Whilst distillation exploits differences in the volatilities of components, in extraction use is made of differences in their solubilities in a selected solvent. Following extraction it is necessary to recover the solute and solvent and this often entails fractional distillation. Any extraction process involves:

a) Bringing the solvent and solution into intimate contact;

b) separation of the two phases;

and

c) removal and recovery of solute and solvent.

A wide variety of equipment can be used to carry out steps (a) and (b) in either a continuous or stagewise manner. The equipment, their applications and advantages are discussed in Chapter 2.

The rate of solute transfer in moles per unit time N_A may be expressed as the product of an overall mass

transfer coefficient K, the interfacial area A, and the mean concentration driving force ΔC

$$N_A = KA\Delta C \qquad (1.1)$$

The overall mass transfer coefficient is dependent on the series resistance to diffusion inside the drop, outside the drop and possibly at the interface, and it is expressed mathematically by neglecting the latter terms as

$$\frac{1}{K} = \frac{1}{k_d} + \frac{m}{k_c} \qquad (1.2)$$

where m is the distribution coefficient. To maximise the rate of mass transfer in equation 1.1, an attempt is generally made to maximise A. The total interfacial area depends on the drop size and dispersed phase hold-up X, in the contactor and assuming that the drops are spherical and their diameter can be represented by a mean value d_{vs} (1).

$$A = \frac{6x}{d_{vs}}$$

where x is the dispersed phase hold-up.

A wide distribution of droplet size exists in practical contactors, dependent upon the degree of turbulence which results in break-up and recoalescence effects. The flow pattern inside and outside the individual drops, also differs. These determine, whether a droplet is 'stagnant', 'circulating' or 'oscillating'. The different coefficients for each mode of transfer are reviewed in Chapter 5.

In recent years agitated columns involving internal pulsing or rotary agitation, giving rise to increased turbulence, have found wide application. Generally they offer the advantage of flexibility, high efficiency and reasonable volumetric capacity. The most common is the Rotating Disc Contactor which was invented by Reman in 1951. The design is traditionally made from data obtained on small scale columns, with the efficiency and capacity measured in terms of heights of transfer unit and flooding flowrates respectively. However, there are several limitations in this method (2). For example, the efficiency of a column decreases with the increase in column diameter due to increased axial mixing. Wall effects may also be significant in small columns, because droplet break-up, coalescence and flow in an unrestricted continuous phase differ from those in the vicinity of the wall. Literature pertaining to the R.D.C. is reviewed in Chapter 3.

Considerable work has been done to describe R.D.C. performance in terms of droplet fundamental behaviour, i.e. drop size distribution, dispersed phase hold-up and discrete drop mass transfer coefficients, but most of this has been limited to specific cases and small scale columns. Therefore the present work comprises a study of R.D.C. hydrodynamics under mass transfer conditions and in the absence of mass transfer and to correlate mass performance using a pilot scale R.D.C.

CHAPTER TWO

Liquid-Liquid Extraction Equipment

2.1 Equipment Classification

There are two major categories of equipment for liquid extraction.

(A) Stagewise Contactors, in which liquids are mixed, extracted and separated in discrete stages. This class includes the mixer settler range of equipment.

(B) Differential Contactors, in which continuous counter-current contact is established between the immiscible phase to give the equivalent of any desired number of stages. These may be categorised as

(1) Gravity Operated Extractors

(a) Non-mechanical dispersion

(I) Baffle Plate Columns

(II) Spray Columns

(III) Packed Columns

(IV) Perforated-Plate Columns

(b) Mechanically Agitated Columns

(I) Pulsed Columns

(II) Rotary Agitated Columns

(i) The Rotating Disc Contactor

(ii) The Schiebel Column

(iii) The Oldshue-Rushton Column

(iv) The Assymetric Rotating Disc Contactor

(2) Centrifugal Extractor

A summary of the agitated column design is given in Table 2.1.

2.2 Selection of Equipment

Continuous contactors are generally preferable to mixer settlers when large throughputs are to be handled since they offer economies in agitation and power equipment cost, floor space and solvent inventory. They operate with relatively small amounts of hold-up of raffinate and extract. This is important when processing radioactive, flammable, expensive or low stability materials. In extraction processes it is necessary as a final step, or in multi-contact stagewise equipment, at intermediate steps, to separate the two phases. Rapid coalescence is desirable otherwise an excessive residence time is required or some of the continuous phase will be removed with the 'bulk' dispersed phase, resulting in reduced efficiency, capacity and loss of solvent. Hence the contactor which gives the most rapid solute transfer is not necessarily the most economic.

Table 2.1 Continuous Differential Contactors

CONTACTOR	TYPE	COMMENT
1. RDC (3)	Centrally located discs driven in compartments separated by stator rings by a central shaft.	Operation reasonably flexible; efficiency not much affected by phase flow ratio; H.E.T.S. is remarkably low, around 20 per cent of that for a simple packed tower. Hydrodynamics and mass transfer characteristics are partially known.
2. A.R.D.C. (4,5)	Similar to the R.D.C. except that the rotor is off-set from the column axis; separations of phases take place in a shielded transfer section.	Mixing and separation zones claimed to reduce backmixing; but phase entrainment does occur in settling zone reducing overall efficiency (6). No special advantages over R.D.C.
3. Oldshue Rushton (7)	Vertical column divided into compartments by horizontal stator rings with vertical baffles in each compartment . Turbine in each compartment driven by a central shaft.	Coalescence-redispersion is predominant. Stage efficiencies obtained by Oldshue and Rushton varied from 40 to 90%. H.E.T.S. was nearly half that of a simple packed tower of same diameter.
4. Ziel Extractor (8)	Vertical column terminating at top and bottom in large vessel to assist settling. The stirring mechanism consists of a shaft fitted with a number of star-shaped impellers. Vertical, reciprocal, as well as rotary motion is imposed on the impellers for effective mixing.	Theoretical efficiencies claimed to have been attained in the manufacture of phenol formaldehyde resin (8). No mass transfer data is available.

Continued . . .

Table 2.1 (continued)

CONTACTOR	TYPE	COMMENT
5. Scheibel Column (9)	Consists of alternate fully- baffled mixing sections and packed sections. Agitation is provided by centrally located impellers.	Coalescence-redispersion is predominant. Mass transfer coefficient is related by $Ka = c(\frac{\Delta\rho}{\gamma})^{1.5}$ Capacity is limited by permissible flow rate through the packing.
6. Khuni Extractor (10)	Incorporates the principles of R.D.C. Oldshue-Rushton and sieve plate columns. Divided into compartments by plates perforated only at the centre so that flow from one compartment to the next is directed towards the agitator. Each compartment has four vertical baffles. Impeller agitator is provided. End sections are large for effective settling.	Published mass transfer data are limited. Capacity and scale-up are expressed by $\frac{d}{D} = C.Re^{0.61}.We^{0.6}.Fr^{0.05}$ The design allows for only low throughputs. Modified designs have found limited application (10).
7. Pulsed Columns (1)	Phases are interdispersed by inducing a pulsating motion either by means of diaphragm pump or a valveless piston. A variety of internal packing or baffles may be used. In one design the plates are pulsed.	Commercial application is limited. Employed in the extraction of metals from radioactive solutions. Power requirements are high. No published information is available for scale-up. Mass transfer data have been reported by various authors (11,12).

Continuous columns without mechanical agitation are unsuitable for use with systems of high interfacial tension since adequate dispersions cannot be achieved throughout a continuous phase. Centrifugal extractors have relatively high capital and operating costs and the number of stages which can be accommodated in a single unit is limited. Nevertheless they are superior to all other contactors for processes requiring a low hold-up or low contact time, or if there is a low density difference between the phases (2).

Table 2.2 is a useful 'rule of thumb' method for a preliminary narrowing of the choice between the various types of extractor (13). Special process factors often govern extractor selection. Equipment installation and operating costs are of primary importance. On this basis, and dependent on the number of stages for a given application and the ease of phase dispersion/separation, an extractor selection chart can be drawn for any given feed rate range.

In general the choice of equipment for a given separation should be based on the minimum annual cost for the complete plant, i.e. extractor and ancillary equipment, as well as an operating and solvent loss costs.

Recently Logsdail (14) has described the various design considerations and process parameters to be considered in arriving at a decision on solvent extraction equipment. The various factors and choice of extractors are outlined in Table 2.3.

Table 2.2 Advantages and Disadvantages of Various Contactors (13)

Type	Capital Cost	Operating and Maintenance Costs	Efficiency	Total Capacity	Flexibility	Volumetric Efficiency	Space		Ability to Handle Systems that Emulsify
							Vertical	Floor	
Spray Tower	5	5	1	2	2	1	0	5	3
Baffle Plate Tower	4	5	2	4	2	3	1	5	3
Packed Tower	4	5	2	2	2	2	1	5	3
R.D.C.	3	4	4	3	5	4	3	5	3
Pulsed Plate Column	3	3	4	3	4	4	3	5	1
Mixer-Settler	2	2	3	4	3	3	5	1	0
Centrifugal	1	2	5	3	5	5	5	5	5

0 = Unsuitable, 1 = Poor, 2 = Fair, 3 = Adequate, 4 = Good, 5 = Outstanding(Preferred)

2.3 The Rotating Disc Contactor - Advantage and Applications

The Rotating Disc Contactor has received considerable attention as liquid-liquid extraction equipment in oil-refining, the processing of nuclear fuels and manufacture of chemical and foodstuffs (15). As in other agitated columns, e.g. the Oldshue-Rushton and Schiebel columns, mechanical energy is applied to achieve a high mass transfer efficiency. As indicated by Table 2.2 and Table 2.3 the Rotating Disc Contactor possesses several inherent advantages over other extractors, these advantages may be summarised (3, 16, 17, 18) in the following section.

2.3.1 Advantages of the R.D.C. over other Extraction Devices

(i) High efficiency, measured as low H.T.U. or H.E.T.S. values.

(ii) The ability to maintain the efficiency over a large capacity range. This is practicable because, by variation of rotor speed, the flow conditions in the contractor can be maintained at the optimum for any particular feed conditions.

(iii) It is cheap and simple to build and operate (19).

(iv) The power consumption of an R.D.C. is low and the bearing wear less in comparison with the pumps of an equivalent mixer settler, because lower speeds are required.

Table 2.3 Factor Determining the Choice of an Extractor (14)

FACTOR	CONTACTOR
1. Number of stages required:	
(i) few (2-3) stages,	All types.
(ii) (10-20) stages.	Mixer-Settler Cascade, Agitated Column.
2. Volumetric Capacity:	S.P.C.
(i) intermediate to high,	Spray or Packed Columns.
(ii) low.	R.D.C., Oldshue-Rushton Column.
3. Residence time:	
(i) short,	Centrifugal types.
(ii) long.	Mixer-Settler, Differential Contactors.
4. Phase ratio:	
(i) large,	Mixer-Settler.
(ii) moderate to low.	Other types.
5. Physical Properties:	
(i) small $\frac{\sigma}{\Delta\rho}$,	Non-agitated Contactors,
(ii) large $\frac{\sigma}{\Delta\rho}$,	Mechanically Agitated Contactors.
(iii) high viscosities.	Mechanically Agitated Contactors.
6. Direction of mass transfer:	
(i) from dispersed to continuous phase,	Mechanically Agitated Contactors.
(ii) from continuous to dispersed phase.	Little information is available.
7. Phase dispersion and hold-up:	
(i) If the phase of the highest throughput is to be dispersed,	Difficulties may be encountered in column contactors due to flooding and phase inversion.
(ii) If a low hold-up if one phase is required,	Centrifugal Contactors.
8. Presence of solid in one or both feed.	Mixer Columns, e.g. Oldshue-Rushton Contactor.

Reman (17) compared the performance of an R.D.C. with a packed column for purification of synthetic detergent and found that a single R.D.C. of 145 cm in diameter and a total height of 5.18 metre could replace two packed columns, each 122 cm diameter, and 21.34 metre in hieght for processing 75 tons/day of crude detergent solution. The erected cost of the contactor was also 45% of that for the two packed columns.

Misek (20) compared the R.D.C. against a sieve plate extractor and found that for dephenolisation of 68 cubic metre/hr of ammoniacal water with benzene, use of an R.D.C. saved 74% (81 tons) of material of construction and reduced operating cost by 72%.

2.3.2 Application of R.D.C.

There are numerous examples of the use of R.D.C. in industry. Some examples of where it has been used extensively are:

(a) Furfural Extraction of Lube Oil

This is the earliest R.D.C. extraction reported and has been very successful for the past 20 years (19, 21, 22, 23).

(b) Extraction of oxygen compounds from fruit juices with alcohol

Although this is a most difficult extraction to carry out in a mixer-settler unit, due to a tendency to

emulsify, it can be satisfactorily performed in an R.D.C. using low rotor speeds (23).

(c) Solutizer Extraction of Mercaptans

This can be performed satisfatorily with an R.D.C. (23).

(d) Propane Deasphalting

The use of an R.D.C. not only improves the yield of propane, but also gives better quality asphalt than the earlier mixer-settler processes (18, 24, 25).

(e) Phenol Recovery

An R.D.C. gives much improved efficiency over the traditional tray column (20).

(f) Extraction of Caprolactum

Use of the R.D.C. enhances efficiency, (16). It is also claimed that the R.D.C. is more economic than centrifugal extractor and superior in flexibility of operation.

CHAPTER THREE

The Rotating Disc Contactor Fundamentals

The Rotating Disc Contactor, was first introduced by Reman (3) in its simplest form, shown in Figure 3.1 and consists of a vertical cylindrical shell divided into a number of compartments formed by a series of stator rings with a rotating disc centered in each compartment and supported on a rotating shaft.

The less dense liquid introduced into the bottom, flows upwards counter-currently to the descending heavier liquid, which is introduced into the top of the column. In modern designs (25, 26), one of the phases is dispersed at either the top or bottom of the column by means of a distributor. This has been found to provide a saving in the effective column height (27). Flat rotor discs without protrusions are generally used to create uniform shearing conditions and hence obtain as small a spread in droplet size as possible. The requisite size of droplets in the effective length of the contactor is maintained by variation of the rotor speed. Interstage settling and re-dispersion is not normally practised.

3.1 Column Behaviour

The overall flow of the liquids in an R.D.C. is counter-

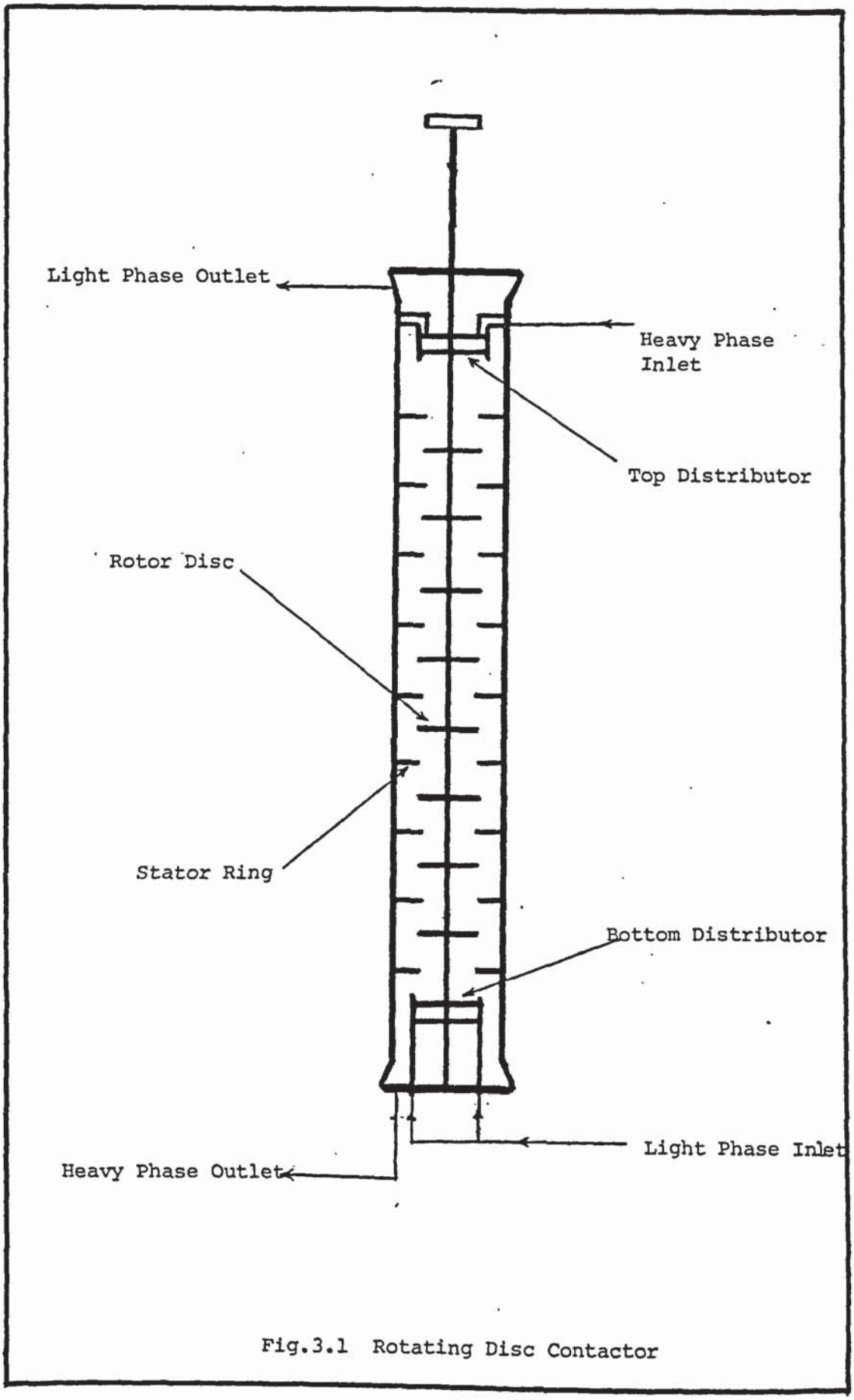

Fig.3.1 Rotating Disc Contactor

current, being established by virtue of the difference in densities of the two phases. Reman (3) suggested that the flow pattern consists of a rotation of the whole mass of liquid and that superimposed upon this rotation is a slower movement of liquid from the shaft towards the wall of the contactor in the vicinity of the discs and from the wall back towards the shaft in the vicinity of the stator rings. The resulting flow is toroidal as shown in Figure 3.2 and causes recirculation and back-mixing of both liquids within each compartment. In the absence of a distributor the dispersed phase enters the column as a continuous stream, which is rapidly broken down into droplets near the discs. If the drops are small enough they follow the vortex patterns but if they are large, they tend to move axially (28). Kung and Beckmann (29) later observed that the flow of the droplets followed two general patterns, one with very little back-mixing below a disc Reynold's number of 7.5×10^4 as illustrated in Figure 3.3, and the other with very marked back-mixing when the disc Reynold's number is higher than 7.5×10^4 and this is shown in Figure 3.4.

In a later study, Mumford (30) found that a critical minimum rotor speed existed below which a layer of dispersed phase droplets built up beneath the rotor discs. In a very recent study Laddha et al (15) suggested that the effect of column geometry may be taken into account in the estimation of the critical rotor speed which they defined as the rotor speed below which "the energy spent

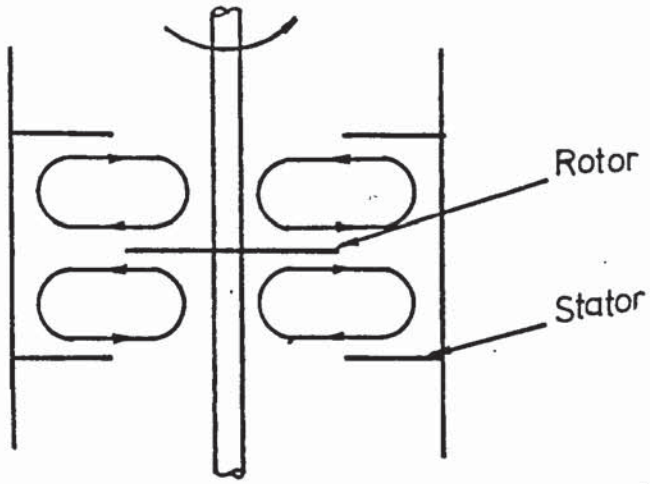

Fig. 3.2 Idealised flow pattern in a rotating disc contactor

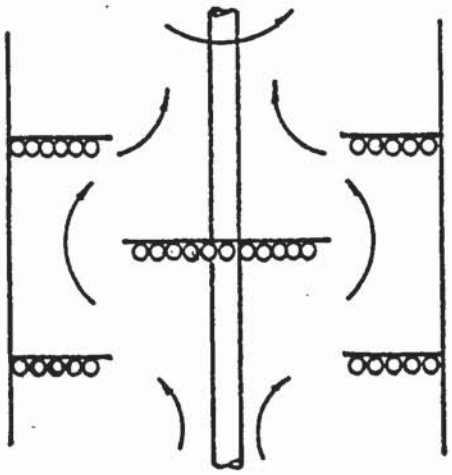

Fig. 3.3 Dispersed phase flow pattern ($Re<7.5x10^4$) in R.D.C. System: Toluene-Water

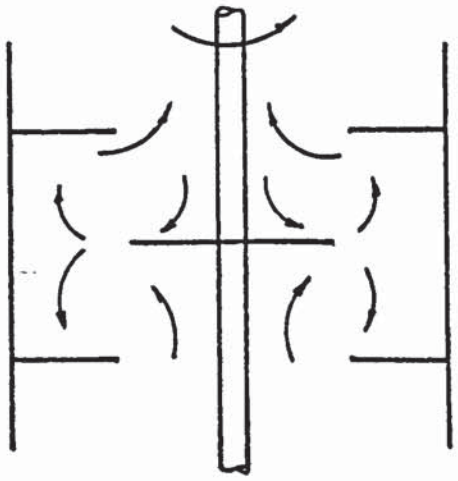

Fig. 3.4 Dispersed phase flow pattern ($Re>7.5x10^4$) in R.D.C. System: Toluene-Water

at the rotor may not be sufficient to overcome the interfacial tension forces and the break-up of dispersed phase droplets". They also produced a practical method to estimate the critical rotor speed which they found varied with the column geometries even for the same liquid system.

3.2 Power Requirements of the R.D.C.

The sizing of the driving unit in the design of R.D.C. and similar equipment in which smooth discs are used, is an important item to give maximum extraction under all conditions.

Reman et al (23) considered power requirements on the basis of mixing. They were able to correlate for any system and any R.D.C. the power number N_p with the disc Reynold s number Re , where

$$N_p = \frac{P}{\rho_m N^3 D_r^5} \quad \text{and} \quad Re = \frac{\rho_m N D_r^2}{\mu} \qquad (3.1)$$

Later Misek (31) analysed his results as well as the results of previous authors and obtained

$$N_p = B\ Re^A \qquad (3.2)$$

where A and B are constants, they were determined experimentally as

i) In the laminar region, where $Re < 6.74 \times 10^4$

$$A = -0.568 \qquad B = 6.78 \qquad (3.3)$$

ii) In the turbulent region, where Re $> 6.74 \times 10^4$

$$A = 0.155 \qquad B = 0.069 \qquad (3.4)$$

Misek (31) compared the results with those of Reman (23) the power required was only one-third of that predicted by Reman. The results obtained by Misek are shown in Figure 3.5.

3.3 Internal Geometry

The important column parameters that affect the performance of R.D.C. for a given extraction system are the column diameter Dc, the rotor disc diameter D_r, the stator ring opening D_s and the compartment height, i.e. the distance between the successive stator rings, H.

Based on the correlation plots proposed by Misek (32) the dimensions of the column internals may be roughly calculated by the following relationship in terms of column diameter D_c in cm

$$H = 0.142\ D_c^{0.68} \qquad (3.5)$$

$$D_r = 0.5\ D_c \qquad (3.6)$$

$$D_s = 0.67\ D_c \qquad (3.7)$$

Proper column geometry is of great significance since it affects both the column capacity and efficiency (17, 22, 32, 33, 34). Thus the column efficiency (17, 22) was found to increase with

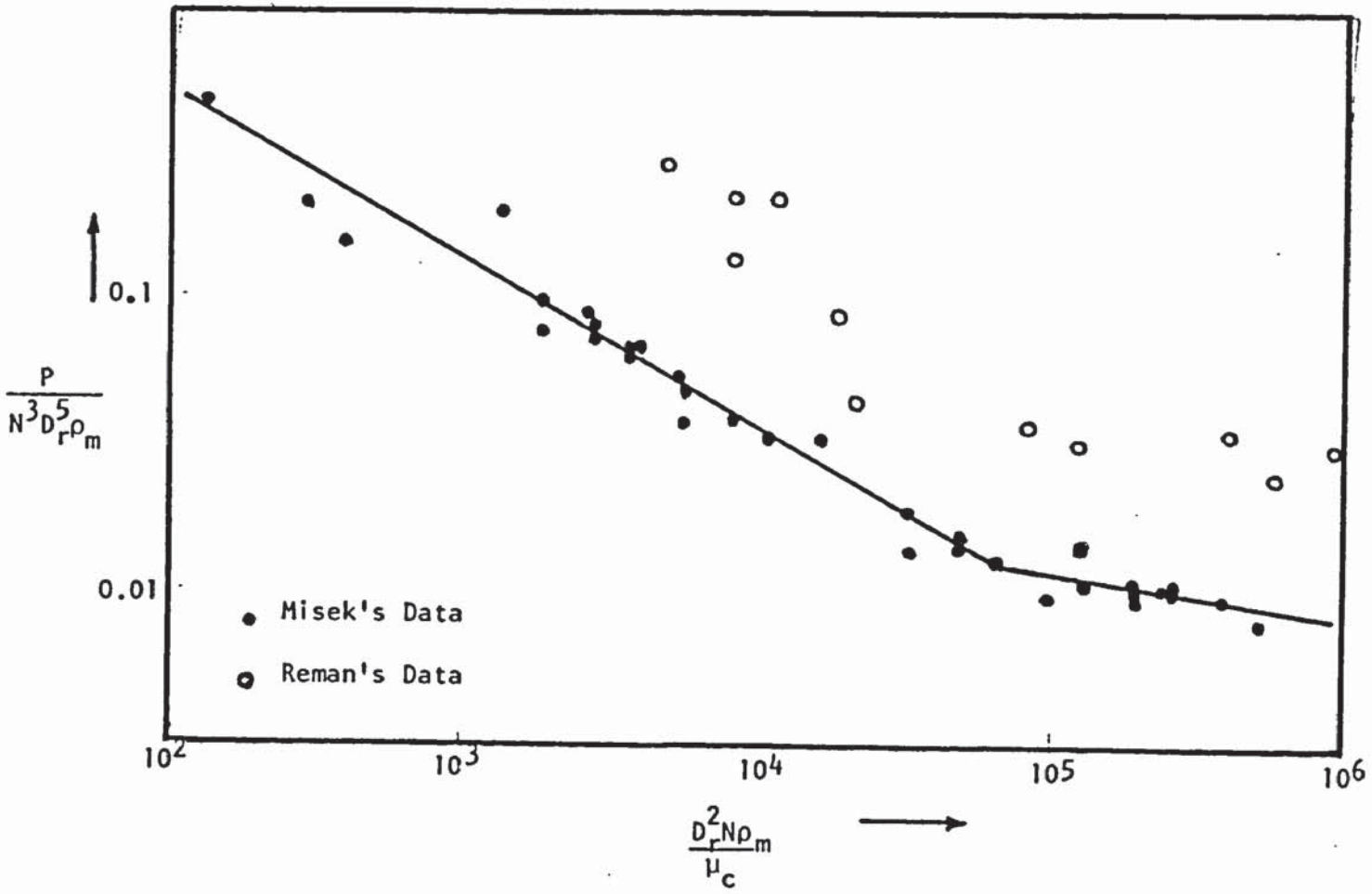

3.5 - Power Required for Agitation in an R.D.C. (31)

i) increase in diameter of rotor disc,

ii) decrease in size of the stator opening, and

iii) decrease in the height of the compartments.

Opposite effects generally apply for the capacity. Thus the need arises for optimization between efficiency and capacity. The geometry therefore selected depends upon whether,

a) the system is easily extractable, or

b) high-efficiency - low capacity, or a low efficiency but high capcity is required for a particular application and system.

In general (17, 28, 29, 32, 33, 34) for optimum design the column dimensions should have the following ratios

$$\frac{\text{Stator Opening } D_s}{\text{Column Diameter } D_c} = 0.66 \text{ to } 0.75$$

$$\frac{\text{Disc Diameter } D_r}{\text{Column Diameter } D_c} = 0.50 \text{ to } 0.66$$

$$\frac{\text{Compartment Height } H}{\text{Column Diameter } D_c} = 0.33 \text{ to } 0.50$$

3.4 Hydrodynamics

3.4.1 Hold-up

In order to determine the interfacial area of the dispersion for the mass transfer calculation using equation 1.1, either of the following should be known:

a) the drop residence time in the contactor, or

b) the fraction of the column volume occupied by the dispersed phase, i.e. the dispersed phase hold-up. In agitated contactors, the residence time distribution is rather complex and dispersed phase hold-up is therefore usually used for the estimation of interfacial area.

It has been generally reported that the hold-up increases with increasing rotor speed and dispersed phase flow rate. In 7.6 cm diameter R.D.C. Logsdail et al (28) were the first to introduce the concept of dispersed phase hold-up for the characterisation of column hydrodynamics and thus the empirical approach to the column design. These authors modified the concept of relating the slip velocity V_s of the dispersed phase to the hold-up in a two phase system (35, 36, 37), by

$$V_s = \frac{V_d}{X} + \frac{V_c}{1-X} \qquad (3.8)$$

to

$$\overline{V}_N(1-X) = \frac{V_d}{X} + \frac{V_c}{1-X} \qquad (3.9)$$

$\overline{V}_N$ is called the characteristic velocity and they defined it as the mean relative velocity of the droplets extrapolated to essentially zero flowrates at a fixed rotor speed. Many correlations have been published relating the dispersed phase hold-up to the characteristic velocity in the form of equation 3.9 with additional factors for column size (29), constriction (33) and droplets coalescence and break-up (32, 40). All these correlations are summarised in Table (3.1).

Table 3.1 Correlations of Dispersed Phase Hold-up in an R.D.C.

Author and Reference	Correlation	Column Diameter cm	Remarks
Logsdail et al (28)	$\frac{V_d}{X} + \frac{V_c}{1-X} = \overline{V}_N(1-X)$	7.62	
Kung and Backmann (29)	$\frac{V_d}{X} + k_1\frac{V_c}{1-X} = \overline{V}_N(1-X)$	15.24	k_1=2.1 for $\frac{D_s-D_r}{D_c} \leqslant \frac{1}{24}$ k_1=1.0 for $\frac{D_s-D_r}{D_c} > \frac{1}{24}$
Strand et al (33)	$\frac{V_d}{X} + \frac{V_c}{1-X} = C_R\ \overline{V}_N\ (1-X)$	15.24, 106.68	C_R=minimum constriction factor dependent on the column geometry
Misek (32, 40)	$\frac{V_d}{X} + \frac{V_c}{1-X} = \overline{V}_N(1-X)\exp\left[(\frac{Z}{\alpha} - 4.1)X\right]$	25.0, 50.0	Z=coalescence correlation factor
	$Z=1.52 \times 10^{-2}\left[\frac{D_c\rho_c}{\mu_c}(\frac{\sigma}{\rho_c d_o})^{0.5}\right]$		α=backmixing correlation factor
	$\alpha = f(d_o.\overline{V}_N.\rho_c/\mu_c)$		d_o=mean drop size

Accordingly many correlations for characteristic velocity based on dimensional analysis as a function of columns geometries as well as the physical properties of the system in use have been published. These are summarised in Table 3.2.

Most of the analyses of hold-up of the dispersed phase in an R.D.C. have been made on the basis of Pratt's (42) characteristic velocity approach (15, 28, 29). Thus the correlation of hold-up with the characteristic velocity achieved for spray columns and packed columns appears to have been applied without question to the R.D.C. in which the velocities of droplet travel are a function of external energy input.

Kasatkin et al (38) and later Murakami (39) have proposed correlation for hold-up based on dimensional analysis, but the Kasatkin (38) correlation presents difficulties in the method of treating the dimensionless groups which are based on the flooding flow rates estimated for a R.D.C. Murakami's (15) correlation is more realistic for estimating the hold-up in a R.D.C., but the exponents of the dimensionless groups were estimated by plotting the various groups and then estimating the slope of the line to obtain the exponent of the dimensionless term. Very recently, Jeffreys, Al-Aswad and Mumford (41) proposed a more practical correlation over a wide range of column diameters (5.0 cm to 45.0 cm) in which they used published data obtained in small columns for different liquid systems as well as their own data which is obtained in 45 cm

Table 3.2 Correlation of Characteristic Velocity in an R.D.C.

Author and Reference	Correlation	Column Diameter cm	Remarks
Logsdail et al (28)	$\frac{\bar{V}_N \mu_c}{\sigma} = 0.012\left[\frac{\Delta\rho}{\rho_c}\right]^{0.9}\left[\frac{g_c}{D_r N^2}\right]^{1.0}\left[\frac{D_s}{D_r}\right]^{2.3}\left[\frac{H}{D_r}\right]^{0.9}\left[\frac{D_r}{D_c}\right]^{2.7}$	7.62	
Kung and Beckmann (29)	$\frac{\bar{V}_N \mu_c}{\sigma} = k\left[\frac{\Delta\rho}{\rho_c}\right]^{0.9}\left[\frac{g_c}{D_r N^2}\right]^{1.0}\left[\frac{D_s}{D_r}\right]^{2.3}\left[\frac{H}{D_r}\right]^{0.9}\left[\frac{D_r}{D_c}\right]^{2.6}$	15.24	k=0.0225 for $\frac{D_s - D_r}{D_c} \leq \frac{1}{24}$ k=0.012 for $\frac{D_s - D_r}{D_c} > \frac{1}{24}$
Laddha et al (15)	$\bar{V}_N = 0.01\left[\frac{\sigma\Delta\rho g_c}{\rho_c}\right]^{0.25}\left[\frac{g_c}{D_r N^2}\right]^{1.0}\left[\frac{\sigma^3\rho_c}{\mu^4 g_c}\right]^{0.25}\left[\frac{\Delta\rho}{\rho_c}\right]^{0.5}\left[\frac{H}{D_r}\right]^{0.9}\left[\frac{D_s}{D_r}\right]^{2.1}\left[\frac{D_r}{D_c}\right]^{2.4}$		
Jeffreys et al (41)	$\frac{\bar{V}_N \mu_c}{\sigma} = 6.24\times10^{-3}\left[\frac{\Delta\rho}{\rho_c}\right]^{0.783}\left[\frac{g_c}{D_r N^2}\right]^{0.234}\left[\frac{D_s}{D_r}\right]^{1.778}\left[\frac{H}{D_r}\right]^{1.362}\left[\frac{D_r}{D_c}\right]^{1.922}$	45.0	For large column only

Table 3.2 (Continued)

Author and Reference	Correlation	Column Diameter cm	Remarks
Jeffreys et al (41)	$\frac{\overline{V}_N \mu_c}{\sigma} = 4.45 \times 10^{-4} \left[\frac{\Delta\rho}{\rho_c}\right]^{-0.941} \left[\frac{g_c}{D_r N^2}\right]^{-0.205} \left[\frac{D_s}{D_r}\right]^{1.601} \left[\frac{H}{D_r}\right]^{0.689} \left[\frac{D_r}{D_c}\right]^{1.786}$	7.62, 15.24, 45.0	Logsdail's and Kung's data are used in the correlation

Table 3.3 Dimensional Analysis Correlations of the Dispersed Phase Hold-up

Author and Reference	Correlation	Column Diameter cm	Remarks
Kasatkin et al (38)	$x = 1.58\left[\frac{ND_r}{V_c}\right]^{1.0}\left[\frac{V_d}{V_c}\right]^{0.96}\left[\frac{D^2_s-D^2_r}{D^2_c}\right]^{-0.7}\left[\frac{H}{H_c}\right]^{-0.426}$ $\left[\frac{\Delta\rho}{\rho_c}\right]^{-1.31}\left[\frac{\rho_c V_c D_c}{\mu_c}\right]^{-0.13}\left[\frac{\rho_c D_c V_c}{\sigma}\right]^{0.245}\left[\frac{V_c^2}{g_c D_c}\right]^{0.96}$	5.4	Hc=total column height
Murakami et al (39)	$x = 3.3\left[\frac{ND_r}{V_c}\right]^{0.55}\left[\frac{V_d}{V_c}\right]^{0.80}\left[\frac{D_s^2-D_r^2}{D_c^2}\right]^{-0.30}\left[\frac{H}{D_c}\right]^{-0.66}\left[\frac{D_r}{D_c}\right]^{0.40}$ $\left[\frac{\Delta\rho}{\rho_c}\right]^{-0.13}\left[\frac{\rho_c D_c V_c}{\sigma}\right]^{0.18}\left[\frac{V_c^2}{g_c D_c}\right]^{0.60}$	7.9, 10.5, 30.0	
Jeffreys et al (41)	$x = 1.05\times10^{14}\left[\frac{ND_r}{V_c}\right]^{0.521}\left[\frac{V_d}{V_c}\right]^{0.775}\left[\frac{D_s^2-D_r^2}{D_c}\right]^{-0.187}$ $\left[\frac{H}{D_c}\right]^{-0.873}\left[\frac{D_r}{D_c}\right]^{-0.201}\left[\frac{\Delta\rho}{\rho}\right]^{4.843}\left[\frac{\rho_c D_c V_c}{\sigma}\right]^{1.082}$ $\left[\frac{V_c^2}{gD_c}\right]^{0.892}\left[\frac{\rho_c V_c D_c}{\mu_c}\right]^{-2.367}$	7.62, 15.24, 45.0	

column. Table 3.3 shows the dimensional analysis correlations of the dispersed pahse hold-up.

3.4.2 Hold-up Profile

Dispersed phase hold-up in an R.D.C. varies in both the radial and axial direction (17, 28, 29, 33). The variation in the radial direction is generally insignificant in small columns (25). Hold-up in the axial direction was found to increase up the column, probably because a finite time is required for drop break-up. The hold-up decreases, towards the end of the column owing to the competing effects of axial diffusion of drops in the contact zone and of drop discharge into the setting zone (26).

Rozkos (44) observed similar effects in an industrial R.D.C; from the results reproduced in Figure 3.6 and 3.7, the maximum hold-up point corresponded to approximately the middle of the 'effective' column.

Rod (27) also obtained similar results in a subsequent work and derived a mathematical model on the basis that the hold-up was determined by the twin effects of droplet break-up in the mixing section and longitudinal mixing of the dispersion.

Al-Hemiri (25) studied the point hold-up along a R.D.C. 10.1 cm in diameter and he proposed the correlation.

$$\dot{x} = \left[0.0013\acute{N} + 0.38(V_d-1)-1\right](h-h^2) + 0.076(1+1/V_d) \qquad (3.10)$$

Furtural G_c = 24 m^3/hr

Oil G_d = 118m^3/hr

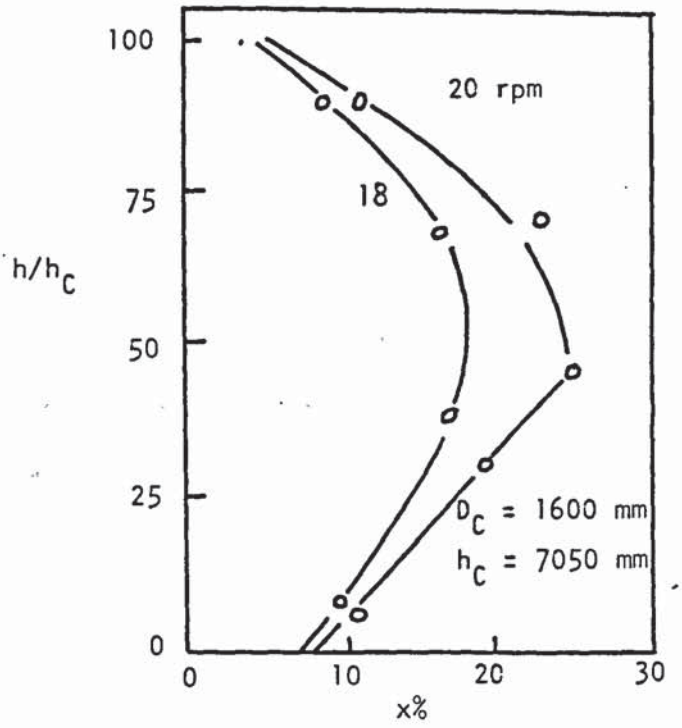

Fig. 3.6

water G_c = 45 m^3/hr

butylacetate G_d = 45 m^3/hr

D_C = 2000 mm h_C = 9500 mm

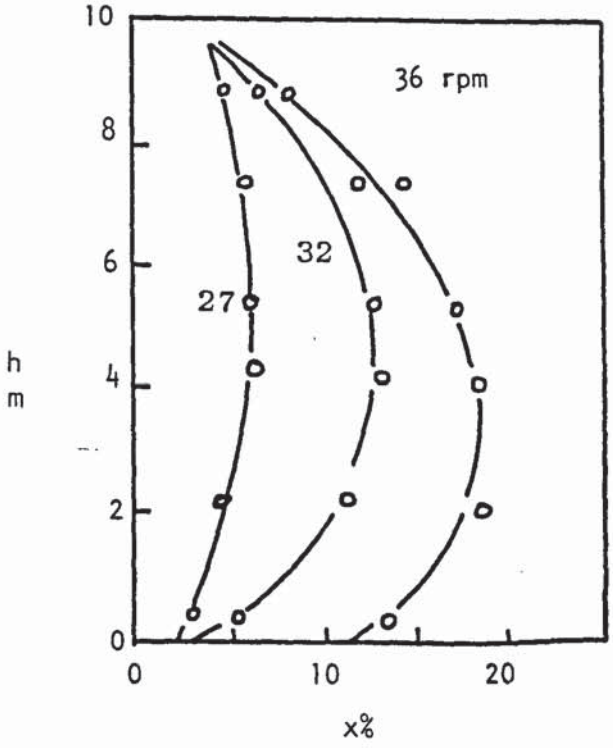

Fig. 3.7

Hold-up profile in an R.D.C. (44)

where $\dot{x}$ is the point hold-up at height h in the column. The results are illustrated in Figure 3.8. The mean of point hold-up values did not differ significantly from the above value and accordingly it was considered suitable for use in mass transfer predictions rather than a consideration of point hold-up values. An analysis of the work of Rod (27) and of Mumford (30) revealed that the above contention may only be true at low values of dispersed phase flow rate and rotor speeds.

3.4.3 Flooding

Flooding is a typical hydrodynamics phenomenon, particularly associated with differential contactors. For each flow rate of one phase, there is a corresponding maximum practical flowrate of the other phase. This maximum depends upon the system properties and the configuration of the contactor intervals. Flow in excess of the maximum causes either of the liquids to be rejected by the equipment therefore in the design of a R.D.C. it is necessary to predict the column cross-sectional area correctly for a maximum flowrate of dispersed phase for a particular flowrate of the continuous phase at each rotor speed to avoid flooding.

Reman (3, 17, 22, 45) studied the effects of system variables on the limiting capacity which was found to decrease with increasing rotor speed, disc diameter and ratio of dispersed to continuous flowrate ($\frac{V_d}{V_c}$), but to increase with increasing stator opening and compartment height.

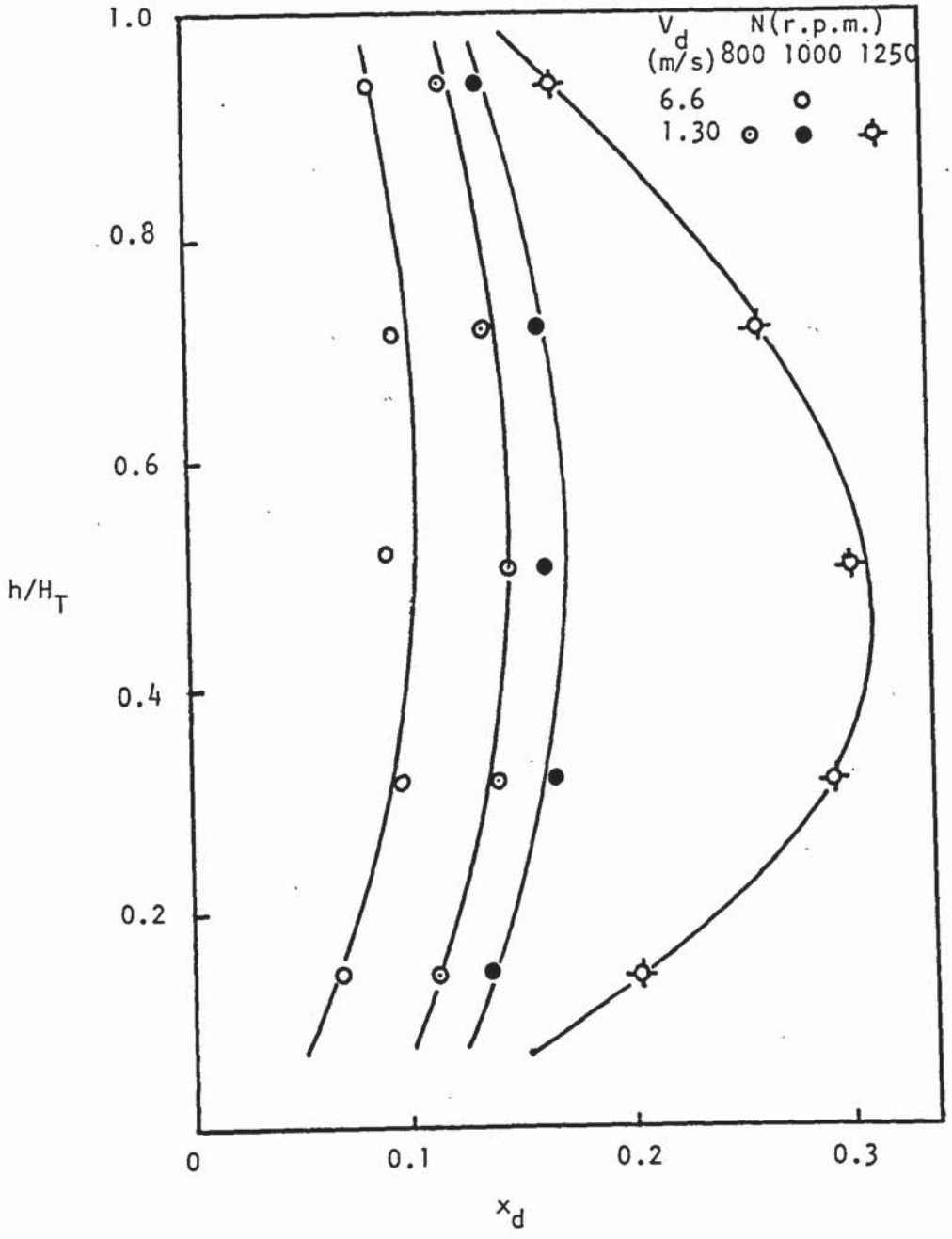

Fig. 3.8 Hold-up profile in 10.1 cm diameter R.D.C. (25)

The capacity data obtained were correlated by considering energy input per unit volume $(N^3D_r^5/HD_c^2)$ as determining the drop size of the dispersed phase. Similar work was carried out by Strand et al (33), who also included a constriction factor C_R to allow for the effect of constrictions on setlling of the drops. Thereafter C_R was defined as the minimum of the area ratio $(\frac{D_s}{D_c})^2$, $\left[1-(\frac{D_r}{D_c})^2\right]$ and $\left[(\frac{D_s+D_r}{D_c})\sqrt{(\frac{D_s-D_r}{D_c})^2+(\frac{H}{D_c})^2}\right]$ in their analysis, and they found that the procedure was valid for columns up to 106.7 cm in diameter. This correlation is inconclusive because the physical properties of the liquid system are not included e.g. interfacial tension which is an important factor in determining drop size and hence settling rates, and the volumetric capacity of the contactor. However, a rough guide to the power input group operating range has been given, which is shown in Figure 3.9 (45).

Logsdail et al (28) derived a relation between the dispersed phase flow rate, the continuous flowrate and flooding hold-ups by asserting that, at the flooding points, the flowrates reach a maximum. Introduction of this condition into equation 3.9 followed by differentation and setting $(\frac{dVd}{dx_f})$ and $(\frac{dVc}{dx_f})$ equal to zero, results in

$$V_{d.f} = 2\,\overline{V}_N\,X^2{}_f(1-X_f) \qquad (3.11)$$

$$V_{c.f} = \overline{V}_N(1-X_f)^2(1-2X_f) \qquad (3.12)$$

Elimination of $\overline{V}_N$ from equations 3.11 and 3.12 gives an expression relating the hold-up at flooding X_f and flow-rate $L = \frac{V_{d.f}}{V_{c.f}}$, thus

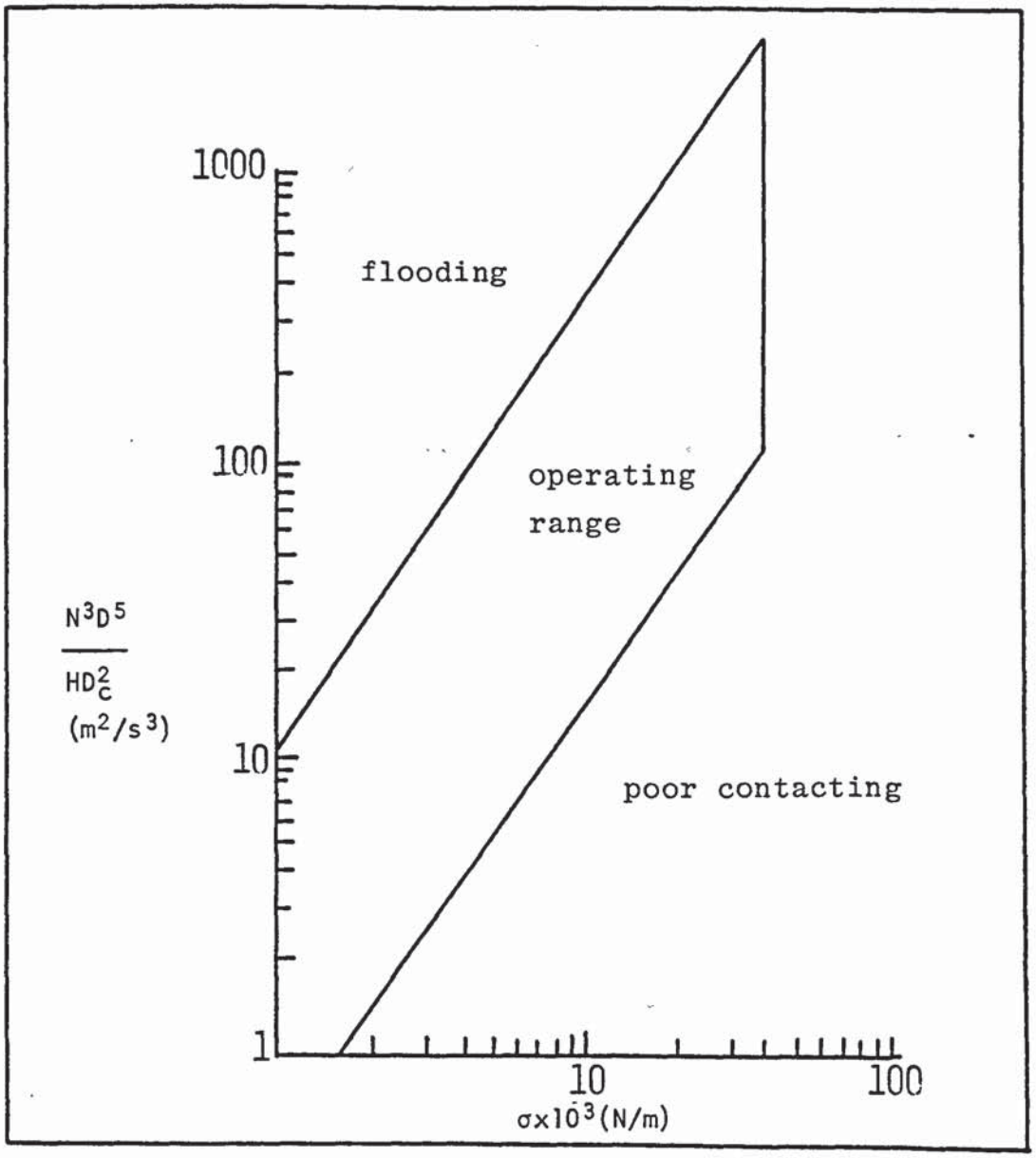

Fig. 3.9 R.D.C. Power input group operating range (45).

$$X_f = \frac{(L^2+8L)^{0.5} - 3L}{4(1-L)} \qquad (3.13)$$

However, this method is not strictly applicable when the mean drop size and hence $\overline{V}_N$, are not constant over the entire hold-up region involved, e.g. in the presence of mass transfer, drop size may increase owing to enhanced coalescence. In non- mass transfer studies, however, Logsdail et al (28) obtained good agreement between their experimental data and equation 3.13.

Misek (46) applied a similar procedure to that of Logsdail et al (28) for his proposed hold-up equation (Table 3.1). After elimination of $\overline{V}_N$ the final expression obtained -as:

$$\frac{V_{d.f}}{V_{c.f}} = \frac{2X_f^2\left[1-X_f+(Z-4.1)(X_f-\frac{X_f^2}{2} - \frac{1}{2})\right]}{(1-X_f)^2\left[1-2X_f+(Z-4.1)(X_f-X_f^2)\right]} \qquad (3.14)$$

where Z is coalescence correlation factor (Table 3.1).

3.4.4 Phase Inversion

The limiting capacity of an agitated contactor has recently been defined to be either by flooding or phase inversion (7, 9, 47), depending on the system characteristics, column geometry, materials of construction and operating parameters.

Phase inversion in liquid-liquid systems refers to a particular flow condition when the continuous phase becomes dispersed and vice versa. This occurs when the

dynamic equilibrium between droplet break-up and coalescence is shifted towards coalescence. Phase inversion studies in continuous counter-current devices have been limited. Al-Hemiri (25) first observed phase inversion in a 10.1 cm diameter R.C.D. using a toluene-water system. At a specific operating condition with toluene dispersed the onset of phase inversion occurred in the bottom compartment giving rise to a very large 'slug'; this possessed a high terminal velocity and travelled up the column and eventually dispersed in the upper compartments. With further increase in dispersed phase flow the effect was repeated at an increased frequency until all other compartments reached their phase inversion hold-ups, i.e. complete inversion obtained in the mixing section, with the column still operating counter-currently. Typical results are illustrated in Fig. 3.10. From the theoretical analysis of the phenomenon, Al-Hemeri (25) proposed the following model to predict the hold-up of inversion.

$$\frac{V_c}{V_d} = \frac{1}{K}\left[1-1.5\left(\frac{1}{X_i}\right) + 0.5\left(\frac{1}{X_i 2}\right)\right] \qquad (3.15)$$

where K is a geometric constant

$$K = 1.0 \text{ at } \frac{D_s - D_r}{D_c} > \frac{1}{24}$$

$$K = 2.1 \text{ at } \frac{D_s - D_r}{D_c} \leq \frac{1}{24}$$

To account for the effects correlated by Misek (40), Table 3.1 was used in subsequent calculations to form a modified

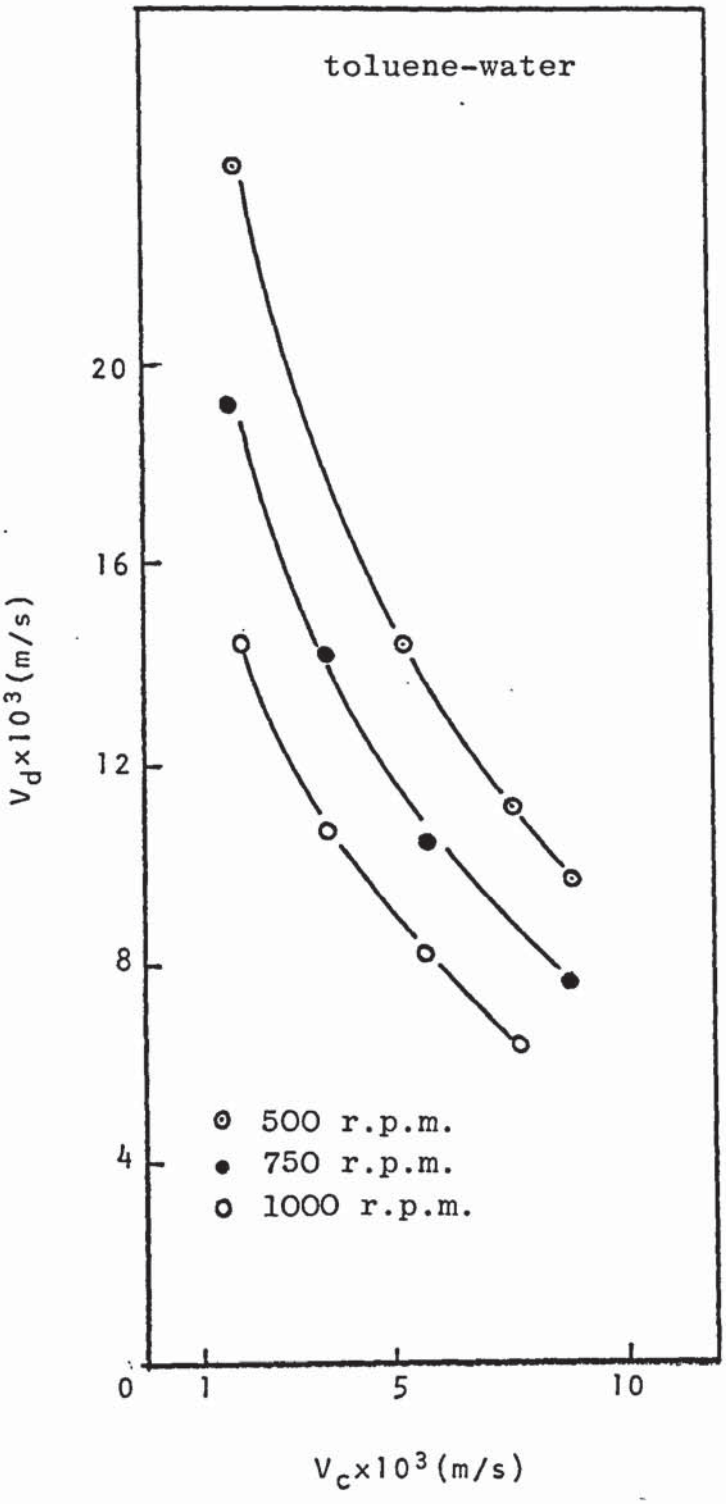

Fig. 3.10 Phase inversion curves for a non-wetted disc column

equation (25).

$$\frac{V_c}{V_d} = 1 - \frac{1}{X_i} - \frac{1}{aX_i^2} + \frac{2}{a^2X_i^3} + \frac{2b}{a^3X_i^4} \qquad (3.16)$$

where a = 4.1 and b = 2.1.

Arnold (47) subsequently studied phase inversion with the system water-toluene in 15.2 cm diameter Oldshue-Rushton column. Contrary to Al-Hemeri's observations, inversion occurred on a cyclical basis. When one particular compartment had inverted the inversion passed on to the next compartment and proceeded up the column. After a finite time the phases in the original compartment re-inverted again and the whole sequence was repeated. The hold-up values at inversion ranged from 0.55 to 0.80 and were very dependent on the energy input.

Sarkar (26) using the systems of butyl acetate-water and toluene-water, was able to generate phase inversion in a 10.1 cm diameter R.D.C. and a 10.1 cm diameter Oldshue-Rushton column. As in Arnold's (47) studies, contrary to Al-Hemeri's findings, the phase inversion was again found to be cyclical in both contactors. Reinversion occured in each compartment after a finite time as the whole process was being repeated indefinitely. A model for predicting hold-up values at phase inversion in an R.D.C. was proposed.

$$R_r = 1 - \frac{a}{x_i} + \sum_{K=2}^{K} \sum_{J=1}^{J} \frac{b^k}{X_i^J} \qquad (3.17)$$

where R_r = phase flow ratio (continuous to dispersed).

$a = 1.5 \qquad b = 0.5$

x_i = hold up at inversion

The model was tested for Rr<1.0 and was found to be in good agreement with the experimental results.

Sarkar (26) correlated the time for re-appearance of the inversion slug in a compartment as

$$t = 0.048\ (Z)^{0.66}\ (X)^{0.33}\ (D_{tr})^{-1.0} \qquad (3.18)$$

where Z = volume of the compartment

X = hold-up

D_{tr} = drop diffusion coefficient, which may be predicted from the expression

$$D_{tr} = \alpha(\varepsilon)^{0.33}\ (\lambda)^{1.33} \qquad (3.19)$$

where α = constant dependent on the continuous phase density.

ε = energy input per unit mass

λ = characteristic eddy length

The deviation of experimentally determined times from those predicted by this correlation was within 25%; at higher energy input rates the deviation was negligible.

3.5 Axial Mixing

Circulation and back mixing in extraction columns reduce the number of theoretical stages (efficiency). If the backmixing is very severe, the column may extract less than corresponding to one theoretical stage (48).

Many investigations have been performed to determine the axial mixing effect which is usually presented in the form of axial mixing coefficient, E_c for the continuous phase and E_d for the dispersed phase. These are equivalent to the respective eddy diffusivities. Most of these investigations have used tracer techniques to measure the backmixing in the phase in which the tracer should be only soluble. Several attempts have been made to correlate the axial mixing coefficients E_c and E_d, in a R.D.C. with the column geometry as well as operating parameters (V_c, V_d, N). Most of these correlations are listed in Table 3.4. Two mathematical models were the bases of these correlations.

a) Diffusion model

b) Back-flow model

Both of these models, as well as some others, have been discussed in Section 3.7.1. Westerterp and Landsman (49) in their analysis of experimental data showed that the axial mixing coefficient of the continuous phase E_c, at constant stirring speed showed a linear relationship with liquid superficial linear velocity.

$$\frac{E_c}{V_c H} = \left[0.5 + 6.5 \times 10^{-3}\left(\frac{D_r N}{V_c}\right)\right] \frac{1}{N_c} \qquad (3.20)$$

where N_c = number of compartments in the R.D.C.

Strand et al (33) considered the overall axial mixing process in the continuous phase to be made up of two main compartments, an eddy diffusion type or backmixing contribution and a Taylor type diffusion which is present especially in

Table 3.4 Correlations for Backmixing in R.D.C.

Author and Reference	Correlation	Column Diameter cm	Remarks
	(A) Backmixing in the continuous phase		
Westerterp et al (49)	$\frac{E_c}{V_c H} = \left[0.5 + 6.5 \times 10^{-3}\left(\frac{D_r N}{V_c}\right)\right]\frac{1}{N_c}$	4.1-5.0	Diffusion Model
Strand et al (33)	$\frac{(1-X)E_c}{V_c H} = 0.5 + 0.09(1-x)\frac{D_r N}{V_c}\left(\frac{D_r}{D_c}\right)^2\left[\left(\frac{D_s}{D_c}\right)^2 - \left(\frac{D_r}{D_c}\right)^2\right]$	10.0 - 105.0	Diffusion Model
Stemerding et al (51)	$\frac{E_c}{V_c H} = 0.5 + 0.012\ \frac{D_r N}{V_c}\left(\frac{D_s}{D_c}\right)^2$	7.6 - 213.4	Back-flow Model
Murakami et al (60)	$\frac{E_c}{V_c H} = 0.5 + 0.18\ \left(\frac{D_r N}{V_c}\right)^{0.8}\left(\frac{V_d}{V_c}\right)^{0.4}\left(\frac{D_s^2 - D_r^2}{D_c^2}\right)^{0.6}\left(\frac{H}{D_c}\right)^{-0.4}\left(\frac{D_r}{D_c}\right)^{2.5}$	7.9 - 30.0	Back-flow Model
Blazej et al (57)	$\frac{E_c}{V_c H} = 3.23 \times 10^6\left[\frac{D_r N(1-X)}{V_c}\right]^{-1.73}\left[\frac{V_d(1-X)}{V_c X}\right]^{0.443}\left[\frac{\rho H_c V_c}{\mu_c(1-X)}\right]^{-1.34}$	6.5	Diffusion Model

Table 3.4 (Cont..).

Author and Reference	Correlation	Column Diameter cm	Remarks
Venkataramana et al (56)	$\frac{E_c}{V_c H} = 0.5 + 0.028 \left(\frac{D_r N}{V_c}\right)\left[\frac{D_s - 0.5D_c}{D_c}\right]$	7.6-10.0	Diffusion Model Back-flow Model
	(B) Backmixing in the dispersed phase.		
Strand et al (33)	$\frac{XE_d}{V_d H} = 0.5 + 0.09X\left(\frac{D_r N}{V_d}\right)\left(\frac{D_r}{D_c}\right)^2\left[\left(\frac{D_s}{D_c}\right)^2 - \left(\frac{D_r}{D_c}\right)^2\right]$	10.0-105.0	Diffusion Model
Miyauchi et al (59)	$\frac{E_d}{V_d H} = 0.5 + 0.017X\left(\frac{D_r N}{V_d}\right) N_p^{0.33} \left(\frac{D_c}{H}\right)^{0.5}$	15.0	Back-flow Model
Misek (61)	$\frac{E_d}{V_d H} = 0.5 + 15.77X\left(\frac{D_r N}{V_d}\right)\left(\frac{N_p D_r^5 D_s^6}{D_c^8 H}\right)^{0.33}$ where $N_p = 0.069\left(\frac{\rho_c D_r^2 N}{\mu_c}\right)^{-0.155}$	25.0 - 50.0	Diffusion Model
Rod (62)	$\frac{E_d}{V_d H} = 0.7 + 0.02\, C_R X\left(\frac{D_r N}{V_d}\right)$	7.6-10.0	Diffusion and Back-flow Model
Blazej et al (58)	$\frac{E_d}{V_d H} = 5.46 \times 10^{-34}\left[\frac{D_r N X}{V_d}\right]^{3.66}\left[\frac{V_d(1-X)}{V_c X}\right]\left[\frac{\rho_c H_c V_d}{\mu_c X}\right]$	6.5	Diffusion Model

the forward direction Stainthorp and Sudall (50) conducted experiments to estimate axial mixing under no solute transfer, as well as under solute transfer conditions their results were in fair agreement with those of Strand et al (33). Stemerding et al (51) observed that the axial mixing coefficient of the continuous phase may be correlated as follows:

$$E_c = K_1 V_c + K_2 N \qquad (3.21)$$

where K_1 = 0.5 H for finite rotor speed.

Equation 3.21 may be compared with the relationship between E_c and F_B, the the back-flow factor from the back-flow model as derived by Misek (52)

$$\frac{E_c}{V_c H} = 0.5 + \frac{F_B}{V_c} \qquad (3.22)$$

Stemerding et al (51) indicated that F_B, the mean actual rate of interstage mixing per unit area of column cross-section, may be taken to be proportional to D_s^2, the area of stator opening and $D_r N$ the pumping effect of rotor. The following correlating correlation has been proposed by Misek (53) for estimation of F_B in equation 3.22

$$F_B = K_3 N D_r \qquad (3.23)$$

$$K_3 = -0.00212 + 0.00434 \left(\frac{D_s}{D_c}\right)^2 + 0.0264 \left(\frac{D_r}{D_c}\right)^2 \qquad (3.24)$$

Miyauchi et al (59) using a semi-theoretical analysis postulated that the back-flow factor F_B could be related to the Power Number (N_p), by the following equation

$$\frac{F_B}{D_r N} = 0.017(N_p)^{1/3} \left(\frac{D_c}{H}\right)^{1/2} \left(\frac{D_s}{D_c}\right)^2 \qquad (3.25)$$

where $N_p = \frac{P}{\rho_m N^3 D_r^5}$ and P is the power spent per compartment. Equation 3.25 was shown to correlate the data of Miyauchi et al (59) for R.D.C. as well as Oldshue-Rushton columns and data of Westerterp et al (49) and Stermerding et al (51).

Bruin (54) studied the geometry effects on axial mixing of the continuous phase in the R.D.C. More frequently Elenkov et al (55) have studied the axial mixing in a 5.1 cm diameter R.D.C. using both single phase and two phase flow. Their data when compared with the Strand et al relationship (33) showed considerable deviation. They observed that Ec values obtained in single phase experiments were two-fold higher than the data obtained in two phase flow experiments. This is contrary to the observations of other reported investigations (50, 51).

Blazej et al (57,58) proposed a correlation to estimate the axial mixing in the dispersed phase E_d and another correlation to estimate the continuous phase E_c, in a laboratory scale R.D.C. of 6.5 cm in diameter. They compared their data with other worker correlations. They found that the Strand relation (33) was the most convenient for the E_d in spite of the fact that it was originally derived for continuous phase.

Finally Venkataramana et al (56) studied the axial mixing in the continuous phase in two R.D.C. of 7.6 cm and 10.0 cm in diameter and they proposed a correlation for the

axial mixing coefficient E_c and they compared the predicted value from their correlation as well as from other investigators correlations (33, 49, 51, 53, 59). The predicted values from their correlation show good agreement with the experimental values more than the predicted values from the other correlations.

3.6 Wetting Effects.

The effect of the wetting characteristics of the column walls and internals upon column performance is of particular importance in column design by scale up procedures. The performance of a large column may be significantly different from a laboratory column, due to differences in the material of construction and the frequency, and thoroughness, of cleaning.

The terms wetting and non-wetting are generally used to describe whether or not a liquid spreads on a particular solid surface. In many instances when a liquid is placed upon a surface it will not completely 'wet', but remain as a drop with a certain angle of contact exhibited between the liquid and the solid. The spreading coefficient is defined in terms of the contact angle and the surface tension of the liquid (63,64).

Since the efficiency of mass transfer in an extraction column depends upon interfacial area and turbulence in either or both phases, the degree of wetting exhibited by the internals, i.e. walls, stators, rotors, or packing, may have a significant effect. Conflicting results have been reported in the literature (65, 66, 67, 68, 69), but it is generally accepted that a higher efficiency is obtained

when continuous phase wets the internals. For example, Davies et al (70) found that the transfer rate of phenol from a dispersed aqueous phase in a dispersed phase wetted R.D.C. to a kerosene phase was less than that achieved using a conventional R.D.C. It has frequently been observed that preferential wetting of the column internals by the continuous phase deteriorated in time. This results in a change in the mode of operation, possibly at the expense of extraction efficiency. The effects were noted in a laboratory scale pulsed plate column by Coggan (12), who observed different types of dispersion at different times. These were reproduced in Figure 3.11.

In a later study, using an aqueous continuous phase and organic dispersion in a R.D.C., Scheibel column and Oldshue-Rushton column sections. Mumford (30) was able to detect a variation in the wetting properties (in the form of increased coalescence of the dispersed phase) on the glass and stainless steel column internals. This was attributed to the deposition of dirt ot impurities on the column internals.

To produce a dispersion with a narrow drop size range from the distributor, the distributor plate should be preferentially wetted by the continuous phase. In a study of the formation of droplets from a circular orifice at varying contact angles Hayes et al (71) found that, as the contact angle was increased, i.e. as the dispersed phase wetted the plate, relatively large droplets were formed before breaking away under the action of gravity.

Al-Hemeri (25) studied the performance of a range of sytems of various rotor designs, such as stainless steel or

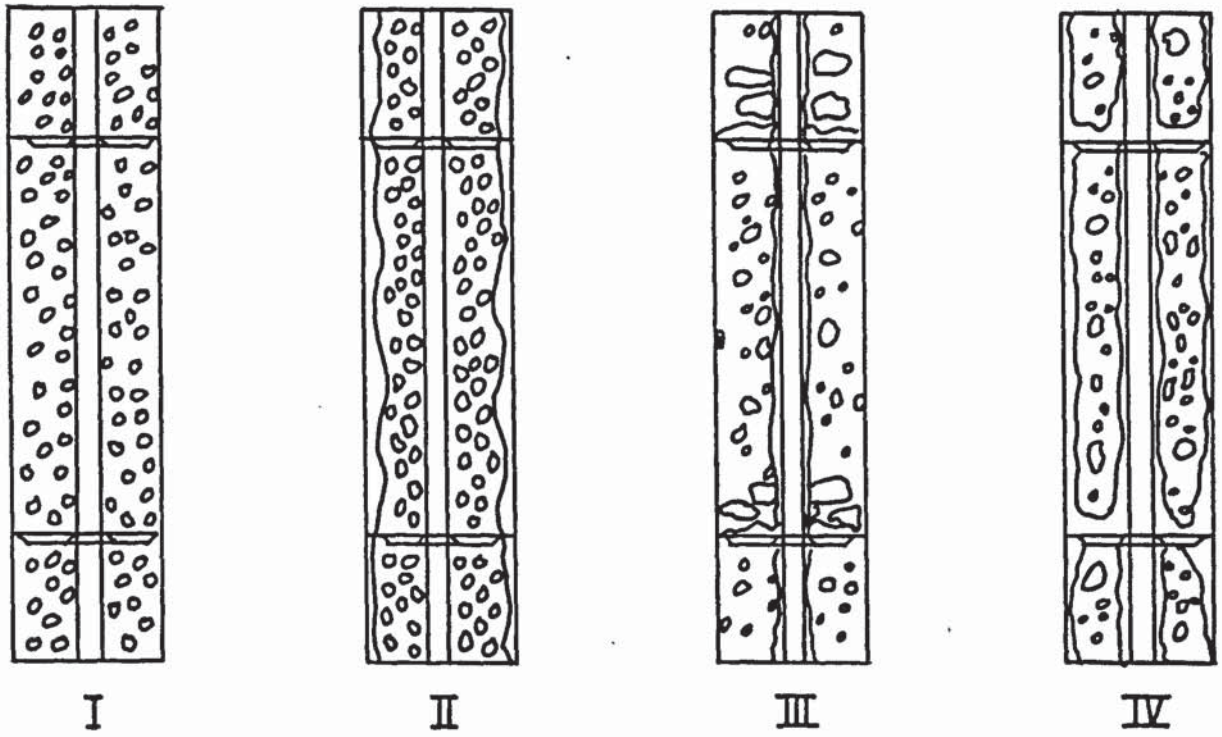

(columns shown in half section)

Type I Non-coalescer dispersion. The discontinuous phase wets none of the surfaces in the column and does not coalesce.

Type II Wall-coalescing dispersion. The discontinuous phase wets the column wall and forms a continuous moving layer.

Type III Plate-coalescing dispersion. The discontinuous phase wets the plate cartridge but not the wall. Droplets are large.

Type IV Plate and wall coalescing. The discontinuous phase wets all the surfaces within the column and coalesces rapidly on contact. It runs down (or up) the column wall and the cartridge tie rod.

Fig.3.11 Effect of Wetting on the Type of Dispersions (12)

p.t.f.e. discs or polypropylene cones, in a 10.1 cm diameter R.D.C. with a stainless steel stator. Comparison of results for wetted and non-wetted rotors can be summarised as

1) Average hold-up decreased with the wetted rotors.

2) Phase inversion, instead of flooding, defined the limiting capacity of the column with wetted rotor.

3) Under non-mass transfer conditions a different drop break-up mechanism involving sheet and ligament disruption, existed with rotors.

4) With the system studied, i.e. Toluene-Acetone-Water, rotor wettability had no significant effect on mass transfer efficiency.

Although it appears from Al-Hemeri's (25) work that rotor wettability has no appreciable effect on mass transfer efficiency, the possibility remains of higher mass transfer rates due to coalescence and redispersion phenomena in wetted disc columns.

3.7 Mass Transfer Efficiency.

Mass transfer studies in a R.D.C. have been carried out by various workers and the effect of different parameters on the overall efficiency assessed. Reman and Olney (17) observed that the efficiency increased with increasing specific load, peripheral speed and ratio of dispersed to continuous phase flow rate, but decreased with increasing stator opening and compartment height. They also found that

enhanced backmixing reduced the efficiency at high rotor speeds and specific loading. Data was interpreted by plotting efficiency against power input as illustrated in Figure 3.12.

In a subsequent work, Logsdail et al (28) employed the system toluene-acetone-water and butylacetate-acetone-water and produced a correlation to calculate the overall mass transfer unit of the form.

$$\left(\frac{(H.T.U.)_{oc}}{V_c}\right)\left(\frac{g^2\rho_c}{\mu_c}\right)^{1/3} X = \left(\frac{X}{K_{oc}a}\right)\left(\frac{g^2\rho_c}{\mu_c}\right)^{1/3} =$$

$$K\left(\frac{\mu_c g}{\bar{V}_N{}^3(1-X)^3\rho_c}\right)^{2m/3}\left(\frac{\Delta\rho}{\rho_c}\right)^{2(m-1)/3} \qquad (3.26)$$

The constant K, exponent m and the characteristic velocity $\bar{V}_N$ were determined by experiment. An accuracy to within 20% was obtained.

In a later study, Al-Hemeri (25) interpreted mass transfer data by comparing observed mass transfer coefficients with values calculated from models of the stagnant drop, circulating drop, oscillating drop and fresh surface models (118). Generally best agreement was obtained with the last two models and it was suggested that the total mass transfer comprised the net effect of a large number of oscillations and complete cycles of formation and coalescence. On this basis, he developed the expression

$$\sum_{n=1}^{n}\left[\sum_{i=1}^{i}\int\left[\frac{dC}{(C-C^*)}\right]_i\right]_n = \sum_{n=1}^{n}\left[\sum_{i=1}^{i} A_i/V_i \int K_i dt\right]_n$$

(3.27)

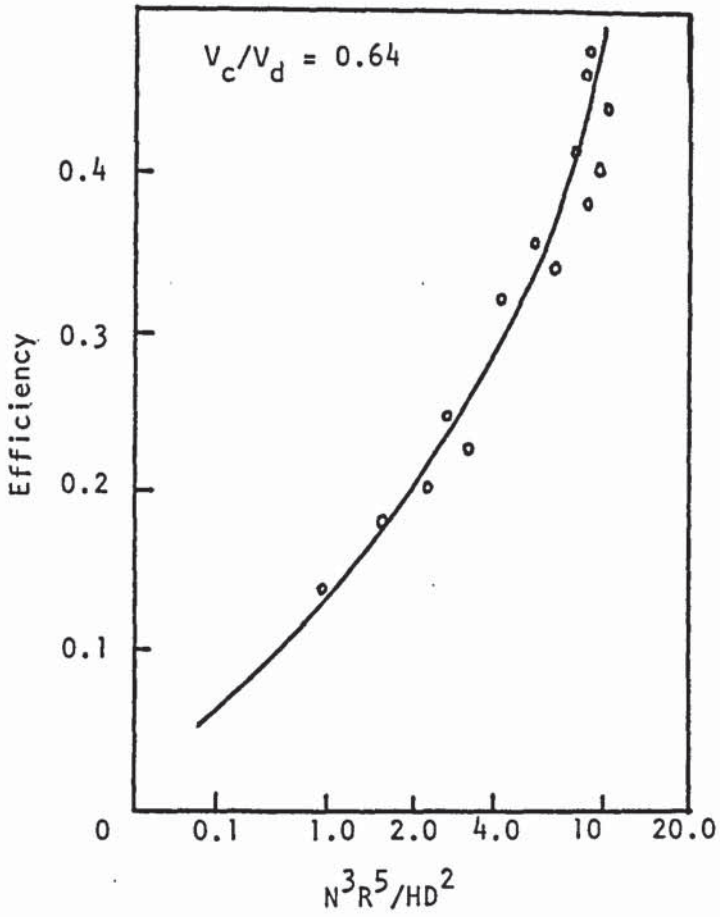

Fig. 3.12 R.D.C. Efficiency for system Water-Kerosene-Butylamine (17)

where n is the total number of compartments and i refers to the particular period, viz. formation, free rise, drop oscillation etc. The above mass transfer model relies on the single drop correlations for transfer coefficients and therefore its application to an agitated interfacing multidrop system is of doubtful validity.

In a recent study, Laddha et al (15) have distinguished two operating regions, below and above the critical rotor speed, and they proposed a correlation for each region

Region I below the critical rotor speed

$$K_{od}a = CX(1-x)\left(\frac{g^3\Delta\rho^3}{\sigma\rho_c^2}\right)^{0.25} (\psi_1)^{-1} \qquad (3.28)$$

where c = 0.068

and

$$\psi_1 = \left[(S_c)_d^{0.5} + m (S_c)_c^{0.5} \right] \qquad (3.29)$$

Region II above the critical rotor speed

$$K_{od}a = 0.95x(1-x)\left(\frac{g^3\Delta\rho^3}{\sigma\rho_c^2}\right)^{0.25} \left(\frac{g}{D_r N^2}\right)^{0.5} (\psi_1)^{-1} (\psi_2)^{-\frac{1}{2}} \qquad (3.30)$$

where $$\psi_2 = \left(\frac{\sigma^3\rho_c}{\mu_c^4 g}\right)^{0.25} \left(\frac{\Delta\rho}{\rho_c}\right)^{0.6} \qquad (3.31)$$

The maximum deviation for the experimental data was found to be ∓ 23.8% and the deviation due to the axial mixing which was not taken into account, was found to be

equal to ∓ 22.5% when it was compared to the method suggested by Strand et al (33) using the relationship given by Sleicher (48). This indicates that axial mixing does affect mass transfer rate to some extent even in a laboratory scale R.D.C. The above correlations are valid only when the dispersed phase flows as discrete droplets without preferentially wetting the column internals.

3.7.1 Mass Transfer Models in Agitated Columns

The simplest mass transfer model is that which neglects axial mixing and assumes piston flow of the phases through the column. This situation is shown diagrammatically in Figure 3.13.

If X_R and Q_R are the solute concentration and the flowrate of the raffinate phase

$$(N.T.U.)_{O.R} = \int_{X_{R2}}^{X_{R1}} \frac{dX_R}{(1-X_R)\ln\frac{(1-X_R^*)}{(1-X_R)}} = \frac{H_c}{(H.T.U.)_{O.R}} \qquad (3.32)$$

$$(H.T.U.)_{O.R} = \frac{Q_R}{K_R a (1-X_R)_{o.m} C_{R.av}} \qquad (3.33)$$

where

$$(1-X_R)_{o.m} = \frac{(1-X_R^*)-(1-X_R)}{\ln\frac{1-X_R^*}{1-X_R}} \qquad (3.34)$$

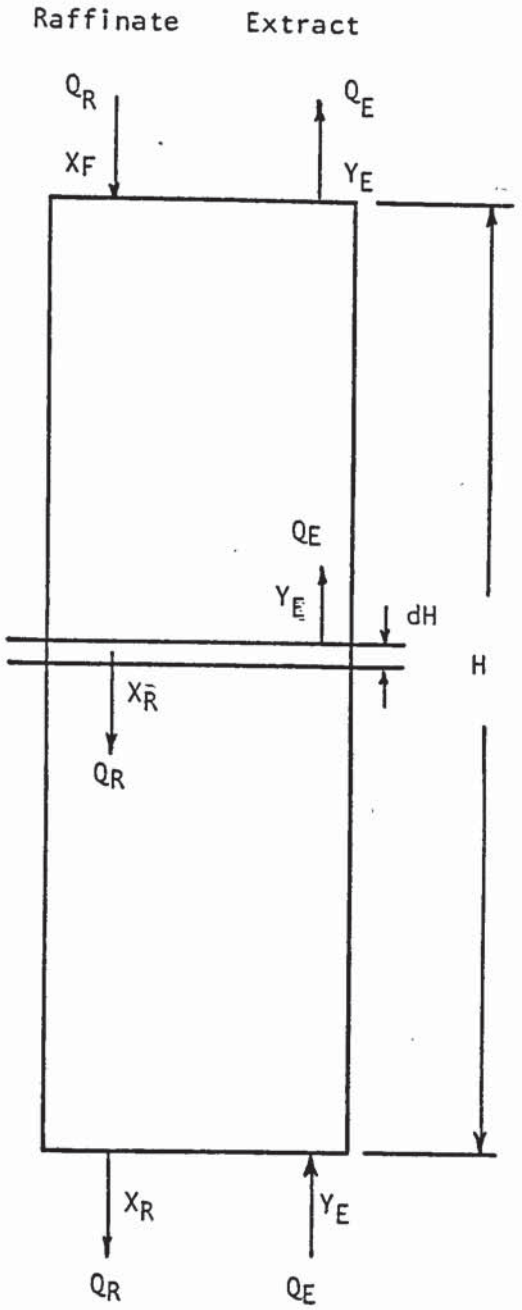

Fig. 3.13 Piston Flow Model

and

$$C_{R.av} = \frac{C_{RM1} + C_{RM2}}{2}$$

where C refers to total concentration of all substances present in the raffinate phase.

Better prediction of mass transfer efficiency has been shown to be possible by including the effect of the axial mixing inthe process of the mass transfer modelling. Four such models are discussed below.

(i) Stage Model

This is the simplest model to describe mass transfer with longitudinal mixing in counter-current extraction columns (73). A diagramatic representation of the model is shown in Figure 3.14.

In this model each stage is assumed to be perfectly mixed so that the solute concentrations in streams leaving any stage are identical with those in the same phase throughout the stage. Axial mixing is characterized only by the number of stages required. The use of this model is only recommended for cases where the extent of the axial mixing in both phases is similar and where its influence on the mass transfer is not high. Miyauchi et al (74) considered that the model could only be used when,

a) Interdroplet coalescence is frequent, or

b) The drop size distribution would narrow and the distribution coefficient m, hold-up x and mass transfer coefficient K constant.

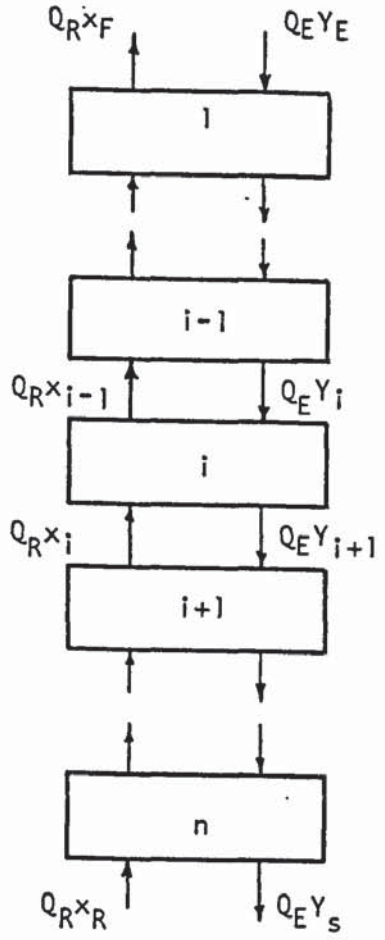

Fig. 3.14 Stage Flow Model

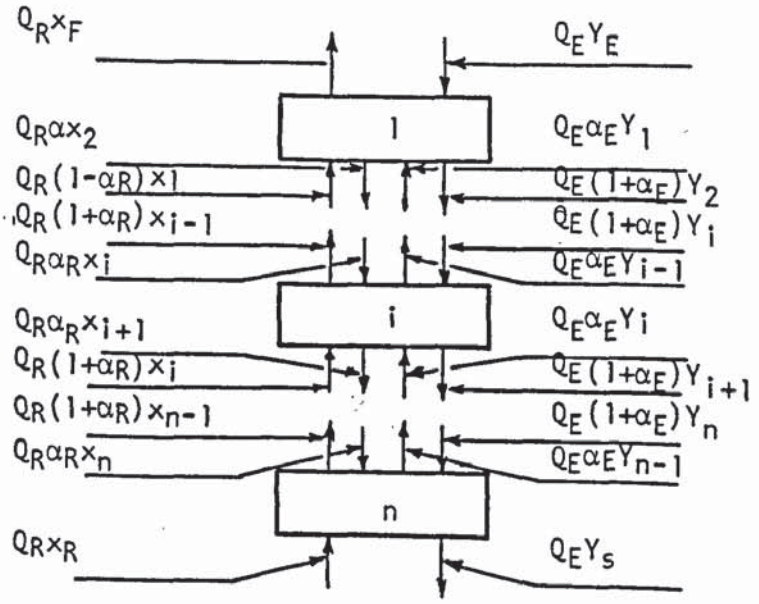

Fig. 3.15 Back Flow Model

A material balance on ith stage is described by (1, 52)

$$Q_R(X_i - X_{i-1}) = Q_E(Y_{i+1} - Y_i) \qquad (3.35)$$

and the mass transfer in the ith stage by

$$X_i - X_{i-1} = \frac{K_x aH}{Q_R}(X_i - X_i^*) \qquad (3.36)$$

The boundary conditions are

$$X_o = X_F \qquad Y = Y_E$$

$$X_n = X_R \qquad Y_{n+1} = Y_s$$

Analytical solution is required for Equations 3.35 and 3.36 for the linear case, and graphical solution is required for the non-linear case (48).

(ii) Back Flow Model

This model describes flow conditions in a counter-current extractor when one phase is entrained in the main flow of the other in a stagewise system. From Figure 3.15 a material balance on the ith stage is represented by

$$Q_R\left[(1-\alpha_R)X_{i-1} - (1+2\alpha_R)X_i + \alpha_R X_{i+1}\right] =$$

$$-Q_E\left[-\alpha_E Y_{i-1} + (1-2\alpha_E)Y_i - (1+\alpha_E)Y_{i+1}\right]$$

$$= NH.a \qquad (3.37)$$

and the mass transfer described by the relation

$$N = K_R(X_i - X_i^*) \qquad (3.38)$$

The governing finite difference equation is obtained by combination of Equations 3.37 and 3.38. The boundary conditions result from the balances around the end stages:

for i=1:

$$Q_R(X_F-X_1) + Q_R\alpha_R(X_2-X_1) = K_Ra(X_1-X_1^*)H \qquad (3.39)$$

for i=n:

$$Q_R(X_{n-1}-X_n) + Q_R\alpha_R(X_{n-1}-X_n) = K_Ra(X_n-X_n^*)H \qquad (3.40)$$

$$X_n = X_R$$

An analytical solution for the linear case has been provided by Hartland et al (75). For the general case a graphico-numerical procedure is required (76).

(iii) Diffusion Model

This model describes solute transfer within the phase from loci of higher concentration to those of lower concentration as a diffusional process, i.e. the mass flux is proportional to concentration gradient. From Figure 3.16 a material balance over a height element dH is:

$$-Q_R\frac{dX}{dH} + e_R\frac{d^2X}{dH^2} = -Q_E\frac{dy}{dH} - e_E\frac{d^2y}{dH^2} = N.a \qquad (3.41)$$

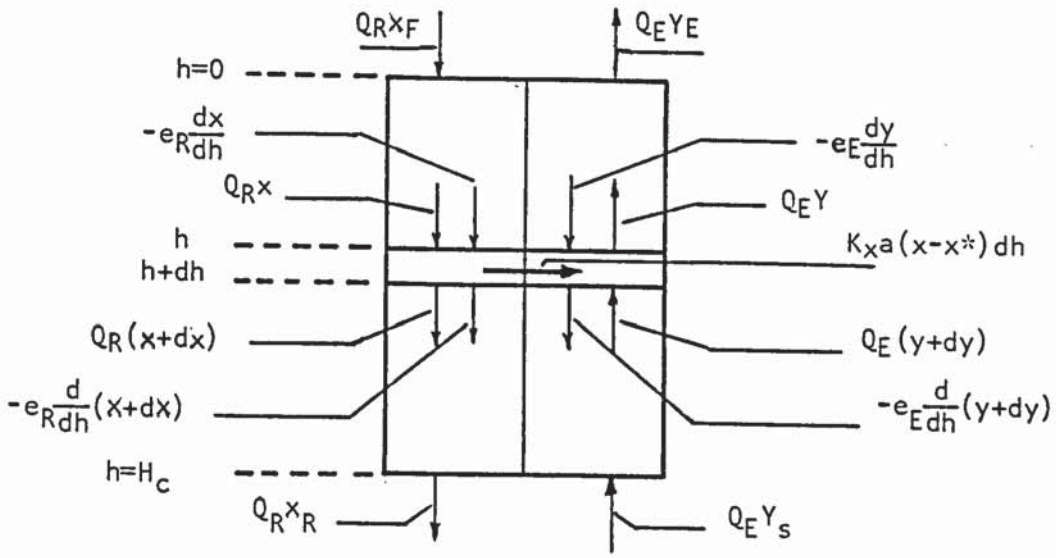

Fig. 3.16 Diffusion Model

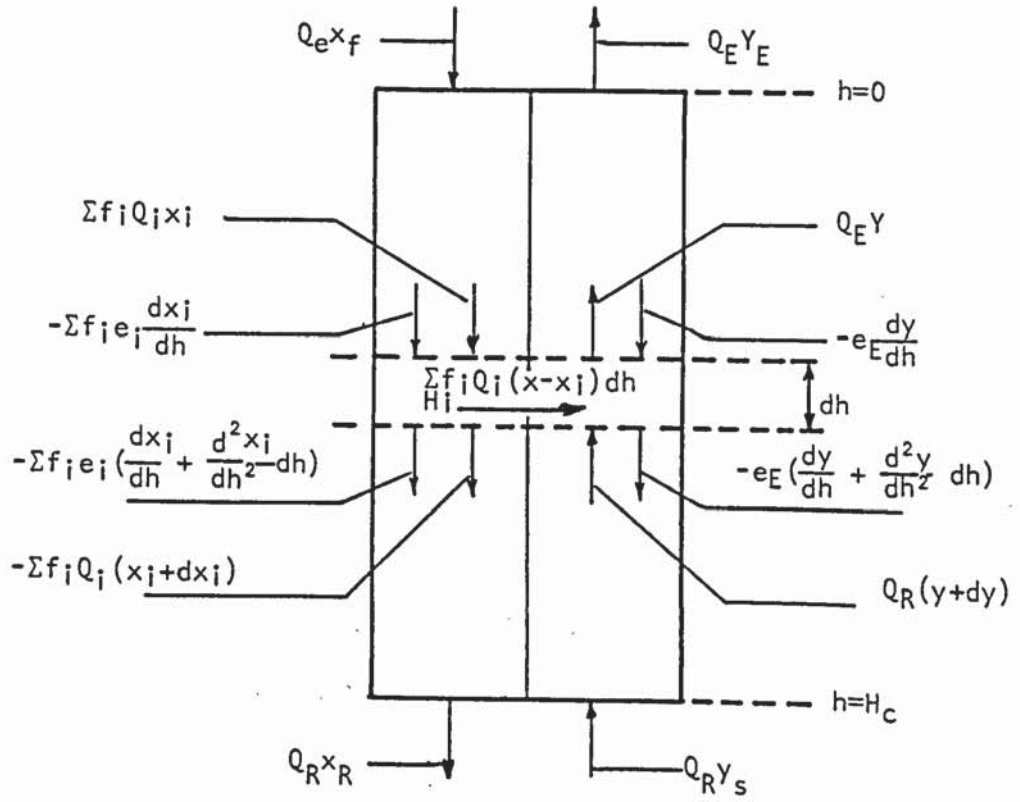

Fig. 3.17 Combined Mode with Forward mixing

The mass transfer between the phases is given by

$$N = K_R (X-X^*) \qquad (3.42)$$

The boundary conditions are obtained by performing material balances for both ends of the column thus (77)

$$Q_R X_F = Q_R X - e_R \frac{dx}{dH}: \quad \frac{dy}{dH} = 0 \quad \text{at} \quad H=0$$

$$Q_E y_S = Q_E y + e_E \frac{dy}{dH}: \quad \frac{dX}{dH} = 0 \quad \text{at} \quad H=H_c$$

The dispersion coefficients e_R and e_E outside the mass transfer sections are considered to be zero.

Again a graphico-numerical procedure is required for the general case (52). For the linear case several solutions have been obtained (48, 75).

(iv) Combined Model with Forward Mixing

Later studies on longitudinal mixing in the dispersed phase (78, 79) have shown that neither the diffusion or the back-flow models describe the mixing of the dispersion phase with sufficient accuracy for these cases where the dispersed phase has a significant polydisperse character and coalescence - redispersion takes place. This is especially true for agitated columns operating with high hold-ups. Another mechanism of axial mixing then arises due to different rise velocities of drops of differing sizes. This phenomenon influences the residence time distribution of the dispersed phase. This has been called 'forward mixing' to distinguish

it from back-mixing (79). Thus the combined model takes account of both mechanisms of longitudinal mixing, the diffusion and back-flow.

Olney (78) considered the effect of polydispersity and derived a mathematical model for R.D.C. Analytical solutions were not provided for the complex differential equations but Misek and Rod (52) used the same method as for the diffusion model and provided a numerical solution. A diagramatic representation shown in Figure 3.17.

CHAPTER FOUR

Droplet Phenomena

The phenomena of 'coalescence-redispersion' is highly pronounced in the R.D.C. It significantly controls the hydrodynamics and mass transfer characteristics of the column. Thus a fundamental understanding of drop interaction, i.e. drop break-up and coalescence phenomena is important in the context of the present work.

In a continuous counter-current extractor the dispersed phase may be introduced into the continuous phase via a distributor in an attempt to obtain a uniform initial drop size distribution. However, despite careful design of the distributor, with equi-sized sharp-edged perforations, a wide range of drop sizes are observed in all agitated counter-current contactors. This drop size distribution in the agitated column results from the coalescence-redispersion mechanism arising from the application of the external energy.

In studies with a variety of organic liquid dispersed in water in a pilot scale R.D.C. section, it was found that, in the absence of mass transfer, interdrop coalescence was negligible until flow rates approach the flooding point (80). Hence in the absence of any special interfacial effects associated with mass transfer the column appears to function as a discrete drop contacting device. However, both the break-up and formation mechanisms, and interdroplet phenomena merit consideration since they

are fundemental to the understanding of how columns operate.

4.1 Drop Formation

The rate of mass transfer in any liquid-liquid system is affected by the rate of the formation of the droplets, their rate of passage through the continuous phase and finally their rate of coalescence. The regime of drop formation in the agitated columns is independent on agitator speed and hold-up, but only on the linear velocity of the dispersed phase through the distributor mass transfer during drop formation has already been discussed in Section 5.1.

The volume, V_f, of drop released from a nozzle may be presented as a function of the time of formation t_f, in the form shown in Figure 4.1 (82). In region (I), the drop volume, V_{min}, is independent of the time of formation, and can be estimated with fair accuracy by a method by Harkins and Brown (83). Region (II) has been the subject of extensive studies and many correlations have been proposed, e.g. those of Treybal and Howarth (84) and Null and Johnson (85). However, both correlations have been found to be unsatisfactory over a wide range of liquids properties and nozzle geometries (86). Probably the most satisfactory correlation for predicting drop size is that proposed by Scheels and Meister (87). This has the form,

$$V_F = F\left[\left(\frac{\pi\sigma D_N}{\Delta\rho g}\right)+\left(\frac{20\mu_c Q D_N}{d_F^2 \Delta\rho g}\right)-\left(\frac{4\rho_d Q U_N}{3g\Delta\rho}\right)+4.5\left[\frac{Q^2 D_N^2 \rho_d \sigma}{(g\Delta\rho)^2}\right]^{1/3}\right] \quad (4.1)$$

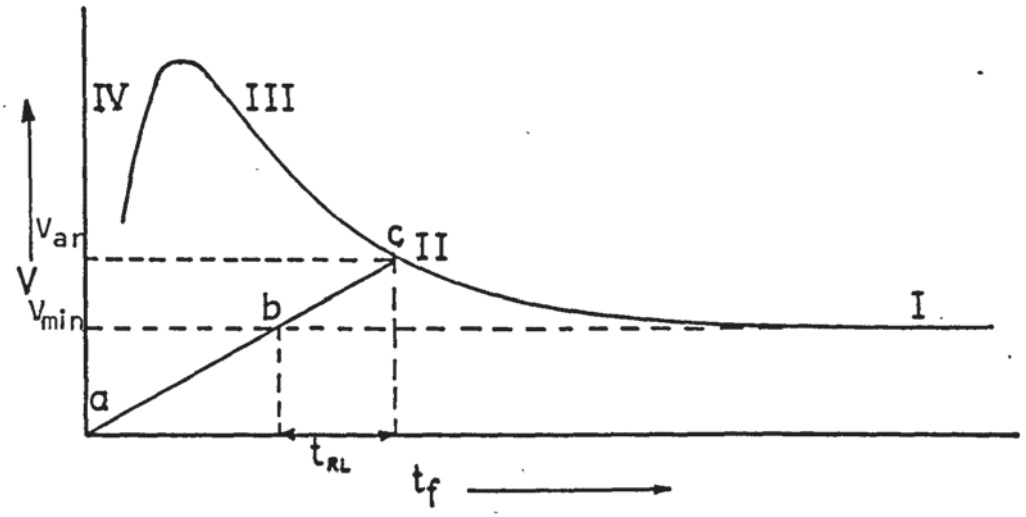

Fig. 4.1 The relation between drop volume and time of formation (82).

where F is the Harkins-Brown (87) correction factor, which can be estimated from a plot of F Vs $D_N(F/V_F)^{1/3}$ (87). Little work has been published regarding region (III), in which jetting from the nozzle, becomes apparent (87), in region (IV) jetting is fully developed and drop formation takes place at the end of a Rayleigh jet (82).

4.2 Droplet Break-up

In turbulent systems deformation of drops is caused by various interacting forces e.g. energy transmitted by the impeller or impact against the container walls and internals, or impact between drops.

In an agitated liquid-liquid system, droplets break-up occurs when:

(a) the magnitude of the dynamic pressure acting upon a drop, surpasses the magnitude of the cohesive surface forces, and

(b) the droplet stays in the high shear zone for sufficient period of time.

Kolmogoroff (88) first studied turbulent flow in a stirred tank and developed a theory of local isotropy. This postulated that in turbulent flow instabilities in the main flow amplifies existing disturbances and produces primary eddies which have a wavelength, or scale, similar to that of the main flow. The large primary eddies are also unstable and disintegrate into smaller and smaller eddies until all their energy is dissipated by viscous

flow. Hinze (89) considered the fundamentals of the break-up process and characterised them by two dimensionless groups.

(1) Weber number $N_{we} = \frac{p}{\sigma/d}$

(2) Viscosity group: $N_{vi} = \frac{\mu_d/d}{(\rho_d \sigma/d)^{\frac{1}{2}}}$

Deformation increases with increasing N_{we} until, at a critical N_{we}, break-up occurs. For break-up to result from viscous stresses the drop must be small compared to the region of viscous flow (89). Break-up due to dynamic pressure fluctuation have been considered by Hinze (89). In this regime, changes in velocity over a distance equal to the drop diameter cause a dynamic pressure to develop: this pressure determines the magnitude of the largest drop pressure. Hinze (89) extended Kolmogroff's (88) energy distribution to predict the size of the maximum stable drop in a turbulent field as,

$$d_{max} = C\left(\frac{g_c \sigma}{\rho_c}\right)^{3/5} \cdot \bar{\varepsilon}^{-2/5} \qquad (4.2)$$

where C is a constant. The value of C was calculated as 0.725 based on an analysis of the rotating cylinder data of Clay (90). Strand et al (33) suggested that the coefficient C can be adjusted to match specific conditions accompanying mass transfer and the tendency of drops to coalesce and break-up. An illustration of the application of the Hinze (89) equation for drop break-up an R.D.C. has been provided by experimental work (33) in a 15.2 cm diameter R.D.C. where for an organic phase

dispersed, the range of C varied between 0.4 to 0.6. Again from the work of Kolmagoroff (88) and later Levich (91), Jeffreys and Mumford (92) suggested that the stable drop radius can be represented by

$$r_{s.d} = \sqrt{2}\ \left(\frac{\sigma}{K_f \rho_c}\right)^{3/5} \left(\frac{L^{2/5}}{V^{6/5}}\right) \qquad (4.3)$$

where K_f is the Kolmogoroff constant ≈ 0.5 and V is the velocity component in the vicinity of rotor disc. It has been proposed that Equation (4.3) can be applied to an R.D.C. provided that the discs were non-wetted by the dispersed phase. However, the drop size calculated is the maximum in the turbulent system so that an empirical relationship has to be introduced to obtain a representative size. Table 4.1 summarises the important correlations for drop size in the absence of solute transfer in an R.D.C.

Misek (32, 40) studied the break-up of drops in an R.D.C. and identified three regions of operation depending on the Reynold number (Re). The correlations proposed for each region are given in Table 4.1. Mumford and Al-Hemiri (93) proposed a correlation for estimating the drop size in any compartment as a result of their studies for a 10.1 cm diameter R.D.C. and in very recent work, which is part of the present study, Jeffreys, Al-Aswad and Mumford (41) proposed two correlations to predict the drop size in a large R.D.C., as well as a laboratory scale R.D.C. These are based on a dimensional analysis that includes the column geometry. Also in a recent study Blazej et al (94) have proposed

Table 4.1 Correlations for Drop Size in the Absence of Solute Transfer in R.D.C.

Author and Ref.	Correlation	Column Diameter cm	Remarks
Strand et al (33)	$d_{max} = C\left(\frac{\sigma g_c}{\rho_c}\right)^{3/5} \varepsilon^{-2/5}$ where $\varepsilon = 4P/(\pi H_c D_c^2 \rho_c)$	15.2	C = Constant dependent on solvent dispersed value range 0.4 to 0.6
Jeffreys and Mumford (92)	$r_{s.d} = \sqrt{2}\left(\frac{\sigma}{K_f \rho_c}\right)^{3/5}\left(\frac{L^{2/5}}{V^{6/5}}\right)$	10.2	For discs non-wetted by dispersed phase
Misek (32, 40)	(i) $\frac{d_o N^2 D_r^2 \rho_c}{\sigma \exp(0.0887\Delta D)} = 16.3\left(\frac{H}{D_c}\right)^{0.46}$ where $\Delta D = \frac{D_c - D_r}{2}$	25.0	For $Re > 6.0\times10^4$ $Re = \frac{D_r^2 N \rho_c}{\mu_c}$
	(ii) $\frac{d_o N^2 D_r^2 \rho_c}{\sigma \exp(0.0887\Delta D)} = 1.345\times10^{-6}\,(Re)$		d_o = mean drop size when $Re < 6.0\times10^4$
	(iii) $d_o = 0.38\left(\frac{\sigma}{\Delta\rho g_c}\right)^{0.5}$		when Re is very low

Continued . . .

Table 4.1 (Continued)

Author and Ref.	Correlation	Column Diameter cm	Remarks
Mumford and Al-Hemiri (93)	$\frac{d_{32}}{D_r}=4.7\times10^{17}X^{0.225}\left[\frac{\bar{N}'D_r\mu_c}{\sigma}\right]^{2}\left[\frac{\bar{N}'D_r^{2}\rho_c}{\mu_c}\right]^{-3.33}\left[\frac{\mu_d}{\mu_c}\right]^{0.23}\left[\exp(0.4(\frac{n}{N_c}))\right]$	10.1	N'=Rotor speed r.p.m. n=the compartment number
Jeffreys, Al-Aswad and Mumford	(i) $\frac{d_{32}}{D_r}=5.52\times10^{-8}\left[\frac{\bar{V}_dH\rho_c}{\mu_cX}\right]^{1.14}\left[\frac{\bar{N}^2D_r^{3}\rho_c}{\sigma}\right]^{-0.14}\left[\frac{V_d^{2}}{g_cD_cX^{2}}\right]^{-0.38}\left[\frac{n}{N_c}\right]^{0.06}$	45.0	
	(ii) $\frac{d_{32}}{D_r}=1.48\left[\frac{\bar{V}_dH\rho_c}{\mu_cX}\right]^{=0.23}\left[\frac{\bar{N}^2D_r^{3}\rho_c}{\sigma}\right]^{-0.004}\left[\frac{V_d^{2}}{g_cD_cX^{2}}\right]^{-0.44}\left[\frac{\Delta\rho}{\rho c}\right]^{-0.57}\left[\frac{H}{D_c-D_s}\right]^{=0.24}\left[\frac{n}{N_c}\right]^{-0.07}$	10.0-45.0	

correlations to estimate a drop size distribution and the drop size in 6.5 cm diemeter R.D.C. under mass transfer conditions for water-acetone-toluene system. The drop size correlation is

$$\frac{d_{32}}{D_r} = 1.43 \left[\frac{Vd(1-X)}{VcX}\right]^{0.45} \left[\frac{DrN(1-X)}{Vc}\right]^{-0.565} \left[\frac{\rho_c H_c V_c}{\mu_c(1-X)}\right]^{-0.117} \qquad (4.4)$$

Most of the models published to-date predict mean drop size in the agitated column, but there is always a distribution of mean drop sizes along the column length (25, 41, 47, 78). Thus the assumption of a single mean drop size may lead to serious error in the interpretation of mass transfer data in a column. In the presence of mass transfer, the mean drop size is dependent upon the direction of transfer. Thus, it appears that the design of a rotary contactor, such as R.D.C. or Oldshue-Rushton column, based on a mean drop size throughout the length of the column and in which the drop size correlations are based on data for specific conditions is not reliable. Without exception direct experimental investigation is necessary for precise design.

4.3 Droplet Coalescence

Coalescence phenomena is important to the hydrodynamics of any extraction column, since interdrop coalescence in the agitated zone is one factor determining the equilibrium drop size generated in the column and coalescence is required at the interface near the dispersed

phase outlet to achieve phase separation. Within the agitated zone the drop size is determined by a balance between break-up and coalescence. This size determines the interfacial area and drop rise velocity. The height of the dispersed phase separation zone depends on the ease with which phase coalescence occurs at the interface. This is also a function of the drop size generated.

The coalescence rate depends on the system properties, drop size and coalescence mechanism. There are three separate mechanisms of coalescence in any column.

(i) Drop interface coalescence.

(ii) Drop-drop coalescence.

(iii) Drop-solid surface coalescence.

Mechanism (i) always occurs in the settling section where phase separation takes place. Mechanism (ii) usually occurs in the mixing section, as well as in the settling section when a layer of uncoalesced drops accumulates. Mechanism (iii) is a special case of drop coalescence on the column internals and/or the column wall, if it is wettable by the dispersed phase.

4.3.1 Coalescence Fundamentals

In general, coalescence is a simple fusion of two or more macroscopic quantities of the same substance. Coalescence took place because the free energy associated with the large interfacial area between the phases can be

decreased by aggregation or coalescence of the dispersed phase droplets. From energy balance considerations coalescence of a liquid dispersion would be expected until ultimately two layers are formed. Coalescence generally occurs in three steps.

(i) Flocculation of drops.

(ii) Collision and drainage of the continuous phase film until it reaches a critical thickness.

(iii) Rupture of the film.

The coalescence time depends on the drainage and rupture of the continuous phase film, factors affecting these steps control the coalescence process. These factors have been well documented by Lawson (95), some of these factors are summarised in table 4.2.

4.3.2 Drop-Interface Mechanism

Coalescence of single drops at a plane interface consists of five distinct steps: (95, 96).

1. Approach of the drop to the interface and the subsequent deformation of the drop and interface profiles;

2. The damping of oscillations caused by the impact of the drop at the interface;

3. Formation and drainage of a continuous phase film between the drop and its bulk interface;

Table 4.2 Factors Affecting Coalescence Time *(95)*

Variable (increasing)	Effect on coalescence time	Explanation in terms of effect on continuous film drainage rate
1. Drop size	Increase	More of the continuous phase film
2. Distance of fall	Increase	Drop 'bounces' and film is replaced
3. Interfacial tension	Decrease	More rigid drop, less continuous phase in films
4. Phase $\Delta\rho$	Increase	More drop deformation, more continuous phase in film
5. Phase viscosity ratio $\frac{\mu c}{\mu d}$	Decrease	Either less continuous phase in film or higher drainage rate
6. Temperature	Decrease	Increase phase viscosity ratio
7. Temperature gradients	Decrease	Film distorts
8. Curvature of interface towards drop:		
a) concave	Increase	More continuous phase in film
b) convex	Decrease	Less continuous phase in film
9. Presence of a third component		
a) suffactants	Increase	Forms 'skin' around drop, film drainage inhibited
b) mass transfer into drop	Increase	Sets-up interfacial tension gradients which oppose film flow
c) mass transfer out of drop	Decrease	Sets-up interfacial tension gradients which assist flow of film

4. Rupture of the film; and

5. Drop contents desposition into the interface

The sum of steps 1 and 2 is refered to as the pre-drainage time. This is generally of the order of 0.1 seconds and step 5 as post-drainage step which takes about 0.05 seconds. Thus coalescence time may be considered as the sum of the times taken by steps 3 and 4 and can be of order of several seconds.

A distribution in the coalescence time for identical drop sizes has been reported in many investigations (97, 98, 99). This distribution has been found to be approximately Gaussian.

Although a number of correlations for coalescence time have been proposed by various workers in terms of the ratio of number of drops not coalescing in time t to the total number of drops examined, controversy has arisen over their validity and reproducibility (92). This is probably because studies have been carried out under varying conditions (98, 100). Presence of electrolytes or surfactants is expected to affect the interfacial tension which in turn may reduce or increase the film drainage process.

4.3.3 Drop-drop Coalescence Mechanism

Inter droplet coalescence occurs frequently in mixing section of the agitated contactors like the R.D.C. and Oldshue Rushton column though the effect is more

pronounced in the latter.

The analysis of drop-drop coalescence which represents a more dynamic situation in agitated systems is rather difficult on two counts. Firstly, it is difficult to reproduce a controlled collision between two drops which have not been restrained in some way. Secondly, there is an inherent randomness in the manner in which the drops rebound or coalesce. Thus drop-drop coalescence studies necessitate consideration of both collision theory and the coalescence process. It follows that the prediction of coalescence frequency requires a knowledge of both collision frequency and coalescence probability.

From the above consideration and using a purely theoretical approach, Howarth (103) developed an equation to relate the frequency of coalescence with dispersed phase hold-up in a homogeneous isotropic turbulent flow.

$$\psi = \left[\frac{24X_S\overline{V}^2}{d^3}\right] \exp\left[-\frac{3V^{*2}}{4\overline{V}^2}\right] \qquad (4.5)$$

where ψ is coalescence frequency, $\overline{V}^2$ is the mean square Langragian turbulent velocity fluctuation, V* is the critical approach velocity. Although this equation showed good agreement with Madden and Damerell's (104) observation for water drops dispersed in toluene in an agitated tank, doubt has been expressed as to the applicability of Howarth's model to real situations (30)

due to the restrictive assumptions made in the derivation.

There is little data on coalescence in agitated columns. In a pilot scale R.D.C. with kerosene-water system, Davies et al (70) found that drop-drop coalescence was not significant up to a hold-up of 10%. Misek (32), however, asserted that interdrop coalescence in a R.D.C. may be significant at hold-up values of about 18% or more. From fundamentals it would be expected that the prerequisites for a significant frequency are high drop collision frequency and a high hold-up of the dispersed phase. Thus in a subsequent study by Mumford (30) of the R.D.C., interdroplet coalescence was only significant at conditions approaching flooding.

In a later study, Misek (105) characterised the dispersion by hydraulic mean drop diameter and assumed that these drops exactly followed the turbulent fluctuations in the continuous phase. Every collision of droplets was assumed to result in coalescence. Since drop-drop coalescence can take place, either in the bulk of liquid or at the wall of the column, Misek (105) proposed a different correlation for each case. For coalescence in the bulk of the fluid

$$\ln \frac{d}{do} = K_1(n_o d^3)V_o^{0.5}\left(\frac{D_c\rho}{\mu}\right)^{0.5} = K_2 X\left(\frac{\sigma}{d_o\rho}\right)^{0.5}\left(\frac{D_c\rho}{\mu}\right)^{0.5}$$

$$= Z_1 X \qquad (4.6)$$

and for coalescence at the column wall.

$$\ln \frac{d}{d_o}=K_3(n_o d^3)V_o(\frac{D_c\rho}{\mu})=K_4X(\frac{\sigma}{d_o\rho})^{0.5}(\frac{D_c\rho}{\mu})=Z_2X \qquad (4.7)$$

The values of Z_1 and Z_2 were determined indirectly based on phase flow-rate measurements using Misek's equation (Table 3.1). Only a fair agreement was obtained with the above equations when they tested experimentally for a number of binary systems in various agitated columns like the R.D.C., Oldshue-Rushton column and Scheibel column. A value of 1.59×10^{-2} for the constant K_2 in Equation 4.6 was claimed to be independent of the type of mixer. However, it is doubtful whether coalescence characteristics in columns as different in Operation as the R.D.C. and Oldshue-Rushton can properly be represented by a single operation (30). Furthermore, the equations make no allowance for the known variation in the case of coalescence with drop size.

Drop coalescence with solid surfaces is strictly a case of "wetting properties" which have been considered in Section (3.6).

It appears from the above review that although drop-interface coalescence is well understood, knowledge on drop-drop coalescence is very limited. This is due to the inherent complexity of the process and it has not been possible as yet to observe in detail the behaviour of a swarm of drops in a turbulent field.

4.4 Drop Size Distribution

In all practical liquid-liquid contacting devices, the dispersed phase exists predominantly as discrete drops. In order to analyse extraction data the assumption commonly made is that these drops are spherical and of uniform size. This permits the use of a discrete drop size in the mass transfer calculations. Olney (78) and Stainthorp et al (50) reported that such assumption may lead to serious errors due to the fact that there is a distribution of mean drop size along the column length. If there is a large range of drop sizes in a column the drop size distribution f(d) must be included in the analysis.

In most agitated contactors drop size distribution is a result of the competing effects, viz., the generation of new drops by break-up due to shear or local turbulence in the bulk flow, and of droplet coalescence due to the interaction effects (104, 106). This size distribution is bounded by an upper limit or maximum stable drop size (89, 107, 108) which in the absence of coalescence will be determined by the size of the nozzles, and a lower limit or minimum size, dependent upon the prevailing break-up processes. This minimum size, may be dictated by the size that is just entrained by the continuous phase (78).

There is a considerable disagreement over the shape of the drop size distribution curve in an agitated system.

Some investigations report a normal distribution (109, 110, 111, 112), while others found the distribution to be log-normal (41, 78, 113, 114, 115). This is of practical significance in the analysis of the performance of an extraction column. Thus for a fixed volumetric throughput, a comparison of the two types of dispersion is given in Table 4.3 (47). Table 4.3 shows that a normal distribution, where the mode is equal to the mean, results in more drops being nearer to the mean size would be preferable to a log-normal distribution for predicting the characteristics of an extraction column. However, Chartes and Korchinsky (114) confirmed Olney's (78) conclusion that the drop size distribution in an R.D.C. obeys the upper limit distribution proposed by Mugele and Evans (108).

$$\frac{dv}{dr} = \frac{\delta}{\sqrt{\pi}} \exp(-\delta^2 r^2) \qquad (4.8)$$

where $r = \ln\left(\frac{a'd}{d_m - d}\right)$ (4.9)

The upper limit distribution is modified log-normal distribution which may be compared with the standard form of the log-normal distribution

$$\frac{dv}{dr} = \frac{\delta}{\sqrt{\pi}} \exp(-\delta^2 r^2) \qquad (4.10)$$

where $r = \ln \frac{d}{d_{vg}}$ (4.11)

where d_{vg} is the geometric mean drop diameter.

Chartres and Korchinsky (114) have shown that Olney's (78) data are accurately represented by the

Table 4.3 Comparison between Normal and Log-Normal Distribution Dispersion.

Property of Dispersions	Normal Distribution	Log-normal Distribution
Proportion of smaller droplets	Lower	Higher
Mean mass transfer coefficient	Higher because more drops are circulating	Lower- more stagnant drops
Interfacial area	Lower	Higher
Settling Rate	Higher	Lower
Tendency to flood column	Lower	Higher

upper limit distribution rather than the log-normal distribution. In addition Korchinsky and Azimzadeh-Khateylo (115) found that the upper limit distribution accurately represented the drop size data in an Oldshue-Rushton column. They emphasised the importance of applying drop size distribution in the mass transfer calculation instead of using the Sauter mean diameter (d_{32}). Olney (78) has also shown that d_{32} may not be the proper mean drop size to represent the transfer rate for the total drop population and concluded that the upper limit distribution will represent the drop size distribution in an R.D.C. The significance of the distribution parameters a' and δ was emphasised. In another recent study Chartres and Korchinsky (116) stated that the size of sample drops used to represent a dispersion is also extremely important. They also point out the marked effect of inlet

drop size on column drop size and measured extraction efficiency. Finally in a very recent study, Jeffreys, Al-Aswad and Mumford also confirmed the accurate representation of the upper limit density distributions of Mugele and Evans (108) for the drop samples in large R.D.C. They compared the Sauter mean diameter d_{32} calculated by the volume-surface diameter equation.

$$d_{32} = \frac{\Sigma n_i d_i^3}{\Sigma n_i d_i^2} \qquad (4.12)$$

and d_{32} calculated from equation proposed by Mugele and Evans (108)

$$d'_{32} = \frac{d_m}{1 + a' e^{0.25\delta^{-2}}} \qquad (4.13)$$

Both d_{32} and d'_{32} were in a very good agreement.

CHAPTER FIVE

Mass Transfer Fundamentals

The rate of mass transfer in all extraction equipment depends on the overall mass transfer coefficient, the interfacial area, and the driving force, as given by Equation 1.1. The overall mass transfer coefficient depends on the rate of diffusion inside, across the interface and outside the droplet. Therefore the mechanism of solute transfer from or to a single drop is fundamental to the overall transfer process in practical equipment.

In considering mass transfer, the life span of a droplet inside a contactor may be divided into three stages

(i) formation time at the distributor,

(ii) travel time through the continuous phase,

(iii) coalescence time at the bulk interface in the separation zone.

mass transfer occuring, to some degree, at each stage. In agitated columns the magnitude of contributions from (i), (ii) and (iii) will be dependent on the rate and frequency of droplet coalescence and re-dispersion.

5.1 Mass Transfer During Drop Formation

Various workers have measured the extent of mass transfer during drop formation. Sherwood (117) observed that 40% of the overall transfer occured during the formation period, but recent investigations (81, 118, 119, 120) have shown the amount to be around 10%. However, Sawistowski (120) has shown that the prediction of precise extraction rates during drop formation is difficult because of the rapid changes in interfacial tension, and the interfacial area of the droplet, which occur during this period. Nevertheless, many mathematical expressions have been proposed to predict dispersed phase mass transfer coefficient during drop formation. These are summarised in Table 5.1. All these expressions, in which mass transfer is assumed to be entirely controlled by diffusion, are based on one of the following theoretical models

1) the model of an ageing, rigid boundary layer which increases in the surface area,

2) in the ageing boundary layer, the concentration gradient increases because of increase in surface area due to stretching, this is known as the 'balloon model',

3) the 'fresh surface' model. Here the boundary layer ages as with a rigid layer. Surface is increased by addition of fresh surface element,

4) for the boundary layer a flow pattern has been developed in which a varying rate of stretching occurs.

Further the following conditions have been assumed to hold in the derivation of the expression in all cases.

(i) the interfacial concentration is that at saturation,

(ii) mass is transported by diffusion perpendicular to the interface,

(iii) the process of diffusion is slow compared with the process of drop growth,

(iv) variations in the diffusion coefficient in the direction of flow may be neglected.

Skelland and Minhas (121) concluded that the above models are unrealistic because they fail to allow for the effects of internal circulation, interfacial turbulence and disturbances caused by detachment. A modified expression was proposed for the mass transfer coefficient,

$$K_{df} = 0.0432 \left(\frac{d}{t_f}\right)\left(\frac{V_n^2}{dg}\right)^{0.089} \left(\frac{d^2}{t_f D_N}\right)^{-0.334} \left(\frac{\mu_d}{\sqrt{\rho_d d\sigma}}\right)^{-0.601} \qquad (5.9)$$

This correlation represents the overall mass transfer occuring during formation, which includes mass transfer during drop growth, during the detachment of the drop and the influence of the rest drop. Around 25% deviation was obtained from the experimental values. This model did not however consider the rate of formation as one of the variables

Table 5.1 Correlation for Mass Transfer During Drop Formation

Author and Reference	Correlation	Equation Number
Licht and Pensing (130)	$K_{df}=\frac{6}{7}\left(\frac{D_N}{\pi t_f}\right)^{0.5}$	5.1
Heertjes et al. (119)	$K_{df}=\frac{24}{7}\left(\frac{D_N}{\pi t_f}\right)^{0.5}$	5.2
Groothuis et al (72)	$K_{df}=\frac{4}{3}\left(\frac{D_N}{\pi t_f}\right)^{0.5}$	5.3
Coulson and Skinner (123)	$K_{df}=2\sqrt{\frac{3}{5}}\left(\frac{D_N}{\pi t_f}\right)^{0.5}$	5.4
Heertjes and de Nie (122)	$K_{df}=2\left[\frac{ro}{a_d}+\frac{2}{3}\right]\left(\frac{D_N}{\pi t_f}\right)^{0.5}$	5.5
Heertjes and de Nie (82)	$K_{df}=\frac{14}{3}\left[\frac{ro}{a_d}+\frac{1}{3}\right]\left(\frac{D_N}{\pi t_f}\right)^{0.5}$	5.6
Ilkovic (131)	$K_{df}=1.31\left(\frac{D_N}{\pi t_f}\right)^{0.5}$	5.7
Angelo et al (118)	$K_{df}=\frac{2}{\tau}\sqrt{\tau}\left(\frac{D_N}{\pi t_f}\right)^{0.5}$	5.8

affecting mass transfer, whereas Heertjes et al (122) and Coulson and Skinner (123) observed mass transfer at higher frequencies of drop formation.

Mass transfer studies in connection with different rates of formation have, to date, been limited. The only significant work is due to Popovich et al (124). Based on the fresh surface model and associated difusion mechanism of transport, he derived the following expression for the prediction of mass transfer rate.

$$E_F.V_d = \frac{4n}{2n+1} \int_o^1 \left[(1-y^2)dy.(C^*-C_o)\left(\frac{D_n}{\pi}\right)^{0.5} B_p t^{(2n+1)/2} \right] \qquad (5.10)$$

where n and B_p are defined by the surface area $A=B_p t^n$ and $y=(1-t/t_1)^{\frac{1}{2}}$, t is the time at which a fresh surface element is formed and t_1 that when mass transfer is considered. The above model is applicable to drops with a moderate rate of formation given by

$$1.28\text{x}10^4 \leq \left(\frac{d^2}{t_f D_N}\right) \leq 12.31\text{x}10^4$$

In case of formation at high speed, i.e. Re > 40, large contributions to mass transfer are caused by strong circulation in the drop. However, no theory or experimental data has been presented of high speed drop formation. Mass transfer at low rates of formation has not been studied in detail either; the only information available

suggests that mass transfer in these circumstances is comparable to that with drops formed at moderate speed on which is superimposed the contribution of free convection (82).

5.2 Mass Transfer During Drop Travel through the Continuous Phase

Mass transfer during drop travel through the continuous phase is significantly influenced by the hydrodynamic state of the drop, i.e. whether it is stagnant, circulating or oscillating. The mechanism of transfer differs in each case. Circulation or oscillation induces intense mixing inside the drop resulting in a high mass transfer rate to, or from, the drop. Conversely, a rigid or stagnant drop, in which internal mixing is completely inhibited, has a lower mass transfer rate. Oscillations commence in regimes of flow for which droplet Reynolds number Re>200. Below this circulation predominates (125). Good agreement, however, has often been found between the rates of mass transfer for oscillating drops and those with rapid internal circulation, although in several instances (118, 126), the rates were considered to be much higher for oscillating drops. Although mass transfer is dependent on the hydrodynamic state of the drops, the presence of a wake behind the moving drop may considerably affect the overall transfer rate (127, 128, 129). Few attempts have been made to quantify this effect which may be pronounced in quiescent flow. The only significant work is due to Kinard et al (129) who developed an equation to modify the driving force due to entrainment of a wake behind the drop. Later, Forsyth et al (127) proposed a

theoretical analysis of the effect in spray columns. Wake phenomena have little significance in turbulent flow systems however because the continuous phase is continually renewed and the wake is not allowed to develop. Furthermore in agitated systems the wake contents are readily mixed with the continuous phase.

5.3 Mass Transfer in the Dispersed Phase

In agitated columns the proportion of mass transfer which occurs during droplet travel would be expected to be very much greater than during release or detachment from the inlet distributor. The coefficient of mass transfer inside the droplet depends on the degree of internal circulation. Circulation rate is known to increase with the droplet diameter and with the ratio of the viscosity of the continuous phase to that of the dispersed phase. Thus Hadamard (132) showed that the liquid inside the droplet would circulate at droplet's Reynold number ($d\rho_c V/\mu_c$) greater than 1.0, and Levich (133) postulated that circulation would occur between Reynolds number of 1.0 and 1500. Levich (133), as well as Garner and Skelland (134), considered that the surface tension of the dispersed phase would affect the circulation rate. Recently Al-Hassan (135) showed that Reynolds number is insufficient to explain the hydrodynamics state of the drop. The complex interaction as well as other properties characteristics had to be considered in addition to Reynolds number. Droplet Reynold number, however, may be used as a rough guide to determine the hydrodynamics state of the drops as following:

(i) stagnant droplets or rigid droplets when $Re<1.0$,

(ii) circulating droplets when $1.0 \leq Re<200.0$

(iii) oscillating droplets when $Re \geq 200$.

Clean liquid systems with different properties produce drops with widely different mass transfer characteristics. The range of behaviour from stagnant drops to oscillating drops are therefore considered below.

5.3.1 Stagnant Droplets

These are generally very small droplets, usually less than 1.0 mm in diameter, with no internal circulation and molecular diffusion is considered to be the dominant mechanism. For the case if no resistance to mass transfer in the continuous phase. This situation is adequately represented by the Newman's (136) relation.

$$E_m = \frac{C_o - C_f}{C_o - C^*} = 1 - \frac{6}{\pi^2} \sum_{n=1}^{\infty} \frac{1}{n^2} \exp\left(\frac{-n^2 \pi^2 Ddt}{r^2}\right) \qquad (5.11)$$

Vermulen (137) found that Newman's model could be closely approximated by the empirical expression

$$E_m = \left[1-\exp\left(\frac{-\pi^2 Ddt}{r^2}\right)\right]^{-0.5} \qquad (5.12)$$

which for values of E_m less than 0.5, reduces by a series expansion neglecting higher order terms to:

$$E_m = \pi\left(\frac{Ddt}{r^2}\right)^{\frac{1}{2}} \qquad (5.13)$$

Correlation for the mass transfer coefficient based on a linear concentration-difference driving force is proposed by Treybal (1) as

$$k_d = \frac{4\pi^2 D d}{3r} \qquad (5.14)$$

5.3.2 Circulating Droplets

The circulating droplets are those in which the fluid inside the drop is in a state of rapid circulation. This circulation is laminar at droplet Reynnolds numbers less than 1.0 and turbulent at Reynolds number greater than 1.0. As a result of these phenomena, the fluid inside the drop is completely mixed and this results in a higher mass transfer coefficient.

A theoretical analysis of mass transfer inside a circulating droplet with laminar circulation has been made by Kronig and Brink (138). They assumed that circulation rate was sufficiently rapid to maintain the streamlines at constant, but different concentrations. Hence mass transfer occurs by molecular diffusion in a direction perpendicular to the streamlines. The rate of mass transfer inside circulating drops was shown to be far greater than in stagnant drops. They proposed a correlation for a droplet in this situation neglecting the resistance to mass transfer in the continuous phase.

$$E_m = 1 - \frac{3}{8} \sum_{n=1}^{\infty} A_n^2 \exp\{-\lambda_n \frac{16Ddt}{r^2}\} \qquad (5.15)$$

where A_n and λ_n are eigenvalues. Heertjes et al (119) presented values for A_n and λ_n for values of n from one to seven. Calderbank et al (139) proposed an empirical approximate to equation 5.15 as

$$E_m \simeq 1 - \exp\{\frac{2.25Ddt}{r^2}\} \qquad (5.16)$$

An approxiamte expression for the mass transfer coefficient was also prepared by Kronig and Brink (138) for circulating droplets under laminar circulation as

$$k_d \simeq \frac{17.9\,Dd}{d} \qquad (5.17)$$

Alternatively, Handlos and Baron (140) considered the case of a fully turbulent drop, with circulation pattern simplified to concentric circles. It was assumed that the liquid between two streamlines became really mixed after one circuit. They proposed a correlation for mass transfer coefficient for droplets under turbulent circulation as

$$k_d = \frac{0.00375\ V_t}{\left[1 + \mu_d/\mu_c\right]} \qquad (5.18)$$

Equation 5.18 has been verified experimentally, by Skelland and Wellek (141) and Johnson and Hamilec (142). However Olander (143) observed some deviation when applying the Handlos and Baron model to cases involving short time of contract. This is due to the fact that, in the derivation of equation 5.18, only the first term of the series which appeared in the mathematical evaluation has been used (143).

This is permissible only when the contact times are large. Thus Olander (143) proposed a correlation for the actual mass transfer coefficient kd.

$$k_d = 0.972 k_{HB} + 0.075 \frac{d}{t} \qquad (5.19)$$

where k_{HB} is the mass transfer coefficient calculated by means of Handlos and Baron's model. Equation 5.19 is for cases where there is no resistance in the continuous phase.

5.3.3 Oscillating Droplets

When a droplet reaches a certain size it begins to oscillate about an ellipsoidal shape. This usually happens when the drop Reynolds number exceeds 200 in a continuous phase of low viscosity. The cause of the onset of this oscillation is not yet fully understood. However, Gunn (144) suggested that oscillations would ensue when the periodic force produced by the detachment of wake eddies had the right frequency to self exite vibrations. Droplet oscillations are not necessarily restricted to oblate-prolate, or spherical-oblate oscillations. As droplet size increases beyond the point where oscillations begin, the droplet oscillation tends towards a more random fluctuation in shape (125).

Garner and Tayeban (126) found that for a given droplet size oscillation was greater for systems with a low continuous phase viscosity, a low interfacial tension and a low dispersed phase viscosity. Garner and Haycock (145)

found that the period of oscillation was dependent on the physical peoperties of the liquid-liquid system, particularly the densities. Johnson and Hamielec (142) reported that once oscillations were set up in drops the effective diffusivities as high as 52 times the molecular value. Garner and Skelland (134) reported that the rate of mass transfer of an oscillating nitrobenzene drop in water was 100% greater than that for an equivalent stagnant drop. Rose and Kinter (125) proposed a model for mass transfer from vigorously oscillating, single liquid drops moving in a liquid field based upon the concept of interfacial stretch and internal droplet mixing. Their model takes into account both an amplitude factor and the frequency of drop oscillations. They stated that oscillations break-up internal circulation streamlines and turbulent internal mixing is achieved. The proposed model gives

$$E_m = 1-\exp\left[\frac{-2\pi D E}{V}\int_{t_o}^{t_f}\frac{1}{f_1(t)}\left\{\left(\frac{3V}{4\pi W}\right)^2+\frac{1}{2\alpha}\ln\frac{1+\alpha}{1-\alpha}+W\right\}dt\right] \tag{5.20}$$

where $$\alpha = \frac{W-(3V/4\pi W)^2}{W} \tag{5.21}$$

$$W = (a_o + a_p/\sin 0.5\ \omega t1)^2 \tag{5.22}$$

$$f_1(t)\ \frac{(a_o{}^2 b-(a-X_o)^2(b_o-X_o))-2a_bX_o+bX_o{}^2}{a^2-2aX_o+X_o{}^2} = X \tag{5.23}$$

$$a = a_o + a_p|\sin 0.5\ \omega t| \tag{5.24}$$

and

$$b = \frac{3V}{4\pi a^2} \tag{5.25}$$

A correlation to estimate the frequency of oscillation was proposed by Schroeder and Kintner (146) gives

$$\omega^2 = \frac{\sigma b_1}{r^3} \frac{n(n+1)(n-1)(n+2)}{\left[(n+1)\rho_d + n\rho_c\right]} \tag{5.26}$$

where $b_1 = \frac{d_e^{0.225}}{1.242}$ (5.27)

and n is the mode of oscillation, when n=0,1 correspond to rigid body motion. The fundamental mode correspond to n=2.

Rose and Kintner (125) also proposed a correlation to calculate the dispersed phase mass transfer coefficient of an oscillating droplet as

$$k_d = 0.45\ (D_d\omega)^{0.5} \tag{5.28}$$

Angelo et al (118) also based their model on surface stretch and internal mixing of the drop. They expressed the periodic change of the surface area for an oscillating droplet as

$$A = A_o(1+\varepsilon \sin^2 \omega t) \tag{5.29}$$

where

$$\varepsilon = \frac{A_{max}}{A_o} - 1 \tag{5.30}$$

Equation 5.29 allows an analytical integration of the resulting mass transfer relations and yields the following relation for the mass transfer coefficient

$$k_d = \left[\frac{4Dd\omega(1+\varepsilon_o)}{\pi}\right]^{\frac{1}{2}} \qquad (5.31)$$

where $\varepsilon_o = \varepsilon + \frac{3}{8}\varepsilon^2$ (5.32)

Another model for oscillating droplets was proposed by Ellis (147) which is based on the assumption that oscillating droplets could be divided into different regions of mass transfer. This division of the droplet is not in agreement with the physical phenomena of drop oscillation and also the shape of the drop is not a sphere during oscillation (135).

5.4 Mass Transfer in the Continuous Phase

The overall mass transfer process between dispersed and continuous phase, includes the contribution of mass transfer in the continuous phase. This is very difficult to estimate due to the wake of the drop. Thus the process usually described as an overall process for the whole drop, using the continuous mass transfer coefficient. This coefficient may be evaluated in terms of the resistance in the film surrounding the drop through which the transfer takes place by molecular diffusion and mass transfer coefficient becomes

$$k_c = \frac{Dc}{X_c} \qquad (5.33)$$

where X_c is a continuous phase fictitious film thickness. A great number of investigations have been done to derive a theoretical or empirical correlation for the continuous phase mass transfer coefficient. Summaries of these investigations can be found in the work of Linton et al (148), Sideman et al (149) and Griffith (150). All of the theoretical expressions have been derived for stakes flow.

The internal droplet circulation has an importance effects on the outside mass transfer coefficient k_c. The different mechanisms of mass transfer in the continuous phase from or to a droplet, dependent on the hydrodynamics state of the droplets are therefore considered below.

5.4.1 From and To Stagnant Droplets

For the case of a rigid drop theoretical analysis by Garner and Suckling (151) and Garner and Jenson (152) based on the boundary layer theory, have shown that the rate of mass transfer from or to a solid sphere can be correlated by a general equation of the form

$$Sh = A + C\ Re^m\ Sc^n \qquad (5.34)$$

where A, C, m and n are constants.

Examples from the literature are reproduced in Table 5.2. Equation 5.35 in Table 5.2 has been proposed by Linton et al (148) and recommended by Griffiths (150). However, in a study by Rowe et al (43), Equation 5.36 was proposed which included a term accounting for the diffusion process. Both Equation 5.35 and 5.36 make no

allowance for the effect of the wake, and therefore, Kinard et al (129) proposed Equation 5.37 which includes the wake effect.

5.4.2 From and To Circulating Droplets

Many studies (126, 138, 142) have indicated that the continuous phase mass transfer coefficient is increased when circulation occurs inside a droplet and this is explained by the reduction in the boundary layer thickness. The correlations proposed to describe the mass transfer coefficient of the continuous phase surrounding a circulating droplet are similar to those given for stagnant drops, i.e. k_c found via a Sherwood number relation. These correlations are given in Table 5.2. The proportionality constant in Equation 5.38 may be lower than 1.13 due to the existence of a wake under practical conditions. Thus Garner and Tayeban (126) proposed Equation 5.39 with a constant of 0.6. In another study Garner et al (154) using a partially miscible binary liquid-liquid system of low interfacial tensions, observed that the exponent of Schmidt groups for fully circulating potential flow, is one-half, and for stagnant drop is one-third. Hence they proposed Equation 5.40 with a Schmidt number exponent of 0.42.

In a recent study by Mekasut et al (155) on the transfer of iodine from aqueous continuous phase to carbon tetrachloride drops the resistance to mass transfer was assumed to be solely in the continuous phase. The Sherwood number was

Table 5.2 Correlation for Continuous Phase Mass Transfer Coefficient

Author and Reference	Correlation	Equation No.	State of Drops	Comment
Linton and Sutherland (148)	$Sh_c = 0.0582(Re)^{0.5}(Sc)^{0.33}$	5.35	Stagnant	Ignore diffusion and wake effect
Rowe et al (43)	$Sh_c = 2+0.76(Re)^{0.5}(Sc)^{0.33}$	5.36	Stagnant	Account for diffusion process
Kinard et al (129)	$Sh_c = 2+(Sh_c)+0.45(Re)^{0.5}(Sc)^{0.33}$	5.37	Stagnant	Include diffusion process and wake effect
Boussinesq (153)	$Sh_c = 1.13(Re)^{0.5}(Sc)^{0.5}$	5.38	Circulating	Claimed to be valid for many systems
Garner and Tayeban (126)	$Sh_c = 0.6(Re)^{0.5}(Sc)^{0.5}$	5.39	Circulating	Inapplicable to Re>450
Garner et al (154)	$Sh_c = -126+1.8(Re)^{0.5}(Sc)^{0.42}$	5.40	Circulating	For partially miscible binary system of low interfacial tensions
Mekasut et al (155)	$Sh_c = 1.04(Ga)^{0.49}$	5.41	Circulating	Ga is Galileo number $Ga=d^3\rho_c^2 g/\mu_c^2$
Garner and Tayeban (126)	$Sh_c = 50+0.0085(Re)(Sc)^{0.7}$	5.42	Oscillating	Successfully used by Thorsen et al (156)
Yamaguchi et al (157)	$Sh_c = 1.4(Ré)^{0.5}(Sc)^{0.5}$	5.43	Oscillating	$Ré=\rho_c \omega d_e^2/\mu_c$
Mekasut et al (155)	$Sh_c = 6.74(Ga)^{0.34}$	5.44	Oscillating	Ignore the effect of infrequency of oscillation

correlated with the Galileo number ($Ga = d^3\rho_c^2 g/\mu_c^2$) in Equation 5.41 for drops less than 0.26 cm in diameter.

5.4.3 From and To Oscillating Droplets

Many workers (141, 142, 158) have used correlations to estimate mass transfer rates for oscillating drops with turbulent internal circulation, but the effect of oscillation cause higher rates of mass transfer than circulation (125, 126). Garner and Tayeban (126) proposed the most acceptable correlation to predict the mass transfer coefficient of continuous phase surrounding an oscillating droplet. They reported a Schmidt number exponent more than 0.5 because, for oscillating drops, there is less dependence on diffusivity (135). Yamaguchi et al (157) proposed Equation 5.43 with a modified Reynolds number ($Ré = \rho_c \omega d_e^2/\mu_c$) for oscillating drops, which neglects the drop velocity. They reported that the maximum deviation of the data from that predicted is approximately ± 20%. Finally a new approach was used by Mekasut et al (155) who correlated the Sherwood number with the Galileo number in Equation 5.44 to predict the mass transfer coefficient of the continuous phase for oscillating drops. They ignored the effect of the frequency of the oscillation drop.

The influence of the wake, in the case of oscillating drops, is even more difficult to assimilate. Hendrix et al (159) observed that oscillation of drops resulted in irregular oscillation of the wake, and that the wake diminished rapidly with the distance travelled by the drop and did not

follow the drop closely.

5.5 Mass Transfer During Coalescence

Mass transfer in a coalescing environment is a rather complex process. As outlined in Chapter 4, numerous studies have been made of coalescence mechanisms, but there is little information as to the effects of mass transfer on coalescence and vice versa. Many investigators have found that coalescence rates are greatly affected by the presence of mass transfer. The rates were also dependent on the direction of transfer. Groothuis and Zwiderweg (160) observed enhanced coalescence when the transfer was from the dispersed to the continuous phase. Sawistowski (161), from studies in agitated columns by Al-Hemeri (25) and Arnold (47) observed that this was only applicable if the solute decreases the interfacial tension. McFerrin and Davidson (162), using the system water-di-isopropylamine-salt, in which the solute salt increased the interfacial tension, found that the transfer into the drop aided coalescence and out of the drop hindered it. Heertjes and de Nie (82) concluded that the effect of mass transfer on the rate of coalescence of drops in binary systems could not be entirely explained by interfacial phenomena alone as suggested by previous workers.

Little information is available on the effect of coalescence on mass tranfer. Johnson and Hamielec (142) proposed a highly simplified expression for k_{dc} for a drop coalescing immediately upon reaching the phase boundary. Mass transfer was regarded as occurring according to the penetration theory

and the time of exposure of the layer was taken to be the same as the time of drop formation

Thus

$$k_{dc} = \left(\frac{D_d}{\pi t_f}\right)^{0.5} \qquad (5.45)$$

Similar results were reported by Licht and Conway (163) and Coulson and Skinner (123) but, Skelland and Minhas (121) subsequently criticised the above models and concluded logically that the amount of mass transfer during coalescence is insignificant compared to that during drop-formation. Therefore for all practical purposes transfer during coalescence might be ignored, though they correlated their experimental results for mass transfer coefficient during drop coalescence as

$$\frac{k_{dc}t_f}{d} = 0.1727\left(\frac{\mu_d}{\rho_d D_d}\right)^{-1.115}\left(\frac{\Delta\rho g d^2}{\sigma}\right)^{1.302}\left(\frac{V_t 2 t_f}{D_d}\right)^{0.146} \qquad (5.46)$$

The average absolute deviation from the data was around 25%. The insignificant mass transfer during drop coalescence has been confirmed by Heertjes and de Nie (82, 164) who argued that drainage of drop-contents in a homophase does not allow entrainment of continuous phase in the homophase. Further since coalescence on impact with an interface is almost instantaneous (of the order of 3×10^{-2} sec), very little mass transfer is expected. This is particularly true in the case of agitated columns where efficient mass transfer occurs in the column proper. Reference here is only made to the coalescence of drops at an interface and substantial work

has been performed with regard to mass transfer during interdroplet coalescence. However, generally the coalescence of drops in swarms causes an increase in drop size, and thus oscillation, and a decrease in surface area. These factors counteract each other with respect to mass transfer rate.

5.6 Overall Mass Transfer Coefficient

The overall mass transfer coefficient is the sum of the individual phases mass transfer coefficient as given by Equation 1.2. The resistance to mass transfer in one of the phases is often predominant, and design can then be based on that phase. The determination of which phase is controlling the mass transfer requires the knowledge of the time for a droplet to attain 60% or 90% solute concentration. The phase requiring the larger time is controlling the mass transfer. The time t, may be estimated from the following equations (30). For the dispersed phase

$$\frac{Qt}{Qo} = 1 - \exp\left[-2.25\left(\frac{4D_d\pi^2 t}{d^2}\right)\right] \qquad (5.47)$$

and for the continuous phase

$$\frac{Qt}{Qo} = 1 - \mathrm{erf}\left[\frac{X}{\sqrt{4D_c t}}\right] \qquad (5.48)$$

5.7 Application of Single Drop Mass Transfer Models to Agitated Extraction Columns

Although studies of mass transfer in agitated contractors are an extension of single drop behaviour to swarms, the direct application of single drop data is of limited value, because of the complex interaction between drops of different sizes in a swarm. The basic differences may be summarised as

1. In the case of single drop mass transfer, the driving force may be evaluated to a reasonable degree of accuracy. Difficulties arise in the estimation for an agitated column owing to axial mixing.

2. Mass transfer coefficient predicted from a single drop model are usually considerably lower than values obtained in agitated systems. This is due to the phenomena of coalescence-redispersion and associated surface renewal effects which predominate in an agitated contactors.

3. Drop break-up may lead to a higher surface area but a lower mean mass transfer coefficient due to the change in mode of mass transfer.

4. A wide range of drop sizes exists in the column giving rise to different modes of mass transfer and also a residence time distribution.

Application of single drop mass transfer models become doubtful to design an industrial agitated contactor, due to the presence of dirt, impurities and surface active agents.

Most of mass transfer correlation presented in sections 5.3 and 5.4 apply to pure systems with the minimum of impurities under ideal conditions, and these seldom exist in practice.

5.8 Mass Transfer and Interfacial Instability

Various types of ancilliary flows generated at the interface and in the layers immediately adjacent to it are usually classified as interfacial turbulence. Such turbulence induces a substantial increase in the rate of mass transfer between the two phases. Thus transfer rates may be much higher than predicted from a proper combination of single-phase rate coefficients on the assumption of a quiescent interface.

Sterling and Scriven (165) in their analysis of this phenomena, suggested that interfacial turbulence is usually promoted by

1. Solute transfer out of the phase of higher velocity;

2. Solute transfer out of the phase in which its diffusivity is lower;

3. Large differences in kinematic viscosity and solute diffusivities between the two phase;

4. Steep concentration gradients near the interfaces;

5. Interfacial tension that is highly sensitive to solute concentration;

6. Absence of surface active agents.

Sterling and Scriven (165) showed that some systems may be stable with solute transfer in one direction yet unstable with transfer in the opposite direction. Orell and Westwater (166) have confirmed some of the above conditions. Maroudas and Sawistowski (167) in their study on the simultaneous transfer of two solutes across liquid-liquid interface found that both solutes produced spontaneous interfacial disturbances, termed 'eruptions', during mass transfer in either direction. This is contrary to the stability criteria of Sternling and Scriven (165). Mass transfer in the eruptive regime, however, cannot be explained by penetration and surface renewal theories (26).

Sehrt and Linde (168) observed that the presence of spontaneous interfacial convection in rising and falling drops will affect the drag coefficient in addition to the rate of mass transfer. This is due to reduction the extent of internal circulation in the drop and thus increases the form drag.

Haydon's (169) developed a theory implying that spontaneous interfacial turbulence should occur with transfer of solute in either direction. Maroudas and Sawistowski (167) found their experimental results agreed with Haydon's theory, They also concluded that Sterling and Scriven theory is too simple to give a reliable criterion of interfacial instability. Finally, Davies (170) reported an interesting quantitative result for the extraction of acetic acid from benzene drops rising through water, that the rate of mass

transfer of acetic acid is higher by a factor of 5.9, if 5% butanol is initially present in the benzene. Butanol causes spontaneous interfacial turbulence which accelerates the transfer of acetic acid. With 10% of butanol in benzene, the acetic acid transfer is 8.8 times higher than without the butanol (171).

5.9 Effect of Surface Active Agent

A trace amount of surface-active substances, unknown in structure and concentration, are frequently present in commercial equipment. This leads to difficulties in interpreting the performance of plant in terms of experimental and theoretical studies of mass transfer. These surface-active materials can be surfactant, impurities or metallic colloids from pipe fittings. The presence of a surface layer of a surface-active material, has a significant effect on the rate of mass transfer and interfacial tension. This is due to the introduction of a surface resistance to diffusion across the interface. The reduction in mass transfer rate can be large and this will introduce an additional resistance into the "resistance-additivity" equation. Thus reduction in interfacial tension will become less dependent on solute concentration and the interface compressibility will also decrease, thus adversely affecting surface renewal (161). In addition surface viscosity will increase and tends to slow down any movements in the surface. It has been demonstrated that surface active materials make droplets more rigid and cause the mass transfer rates to approach that of stagnant droplet (155, 172, 173, 174). This is because

the droplet internal circulation is reduced due to the presence of the surface active materials which will sweep back towards the rear of the moving drop (175). Garner and Hale (172) showed that the addition of small quantities of teepol (0.015% by volume) to water reduce the rate of extraction of diethylamine from toluene drops to 45% of its original value. An even greater reduction (68%) has been reported by Lindland and Terjesen (174) and about 70% by Holm and Terjesen (173) using a stirred liquid-liquid extractor. Huang and Kintner (176) in their study of mass transfer characterisitcs, showed that the surface film reduces both the extent of internal circulation and also the area of the interface being renewed. The mass transfer rate to or from oscillating drops is also affected by traces of surface-active materials. This may be due to surface tension gradients and the rigidity of the surface inhibiting the surface movement of the drop as it oscillates (170), 177).

CHAPTER SIX

Experimental Investigation

The objectives of the experimental investigation were to study the hydrodynamics of an R.D.C. under mass transfer conditions and in the absence of mass transfer using a 450 cm diameter and 4.30 m height pilot scale R.D.C. The hydrodynamic investigations included

a) Study the effect of phase (flow rate) ratios on the contactor hold-up and drop size distribution.

b) Study of the effect upon the overall mass transfer coefficient of the operating conditions via rotor speed and phase ratios.

6.1 Description of Equipment

A flow diagram of the equipment is shown in Figure 6.1 and a general arrangement in Figure 6.2. The process lines and the feed and effluent tanks were arranged so that column was accessible from all sides to facilitate sampling and photography, and all valves were within easy reach. Drain points were incorporated at the lowest points in the system. The basic equipment was identical with that described by Khandelwal (2). However, the whole process lines were

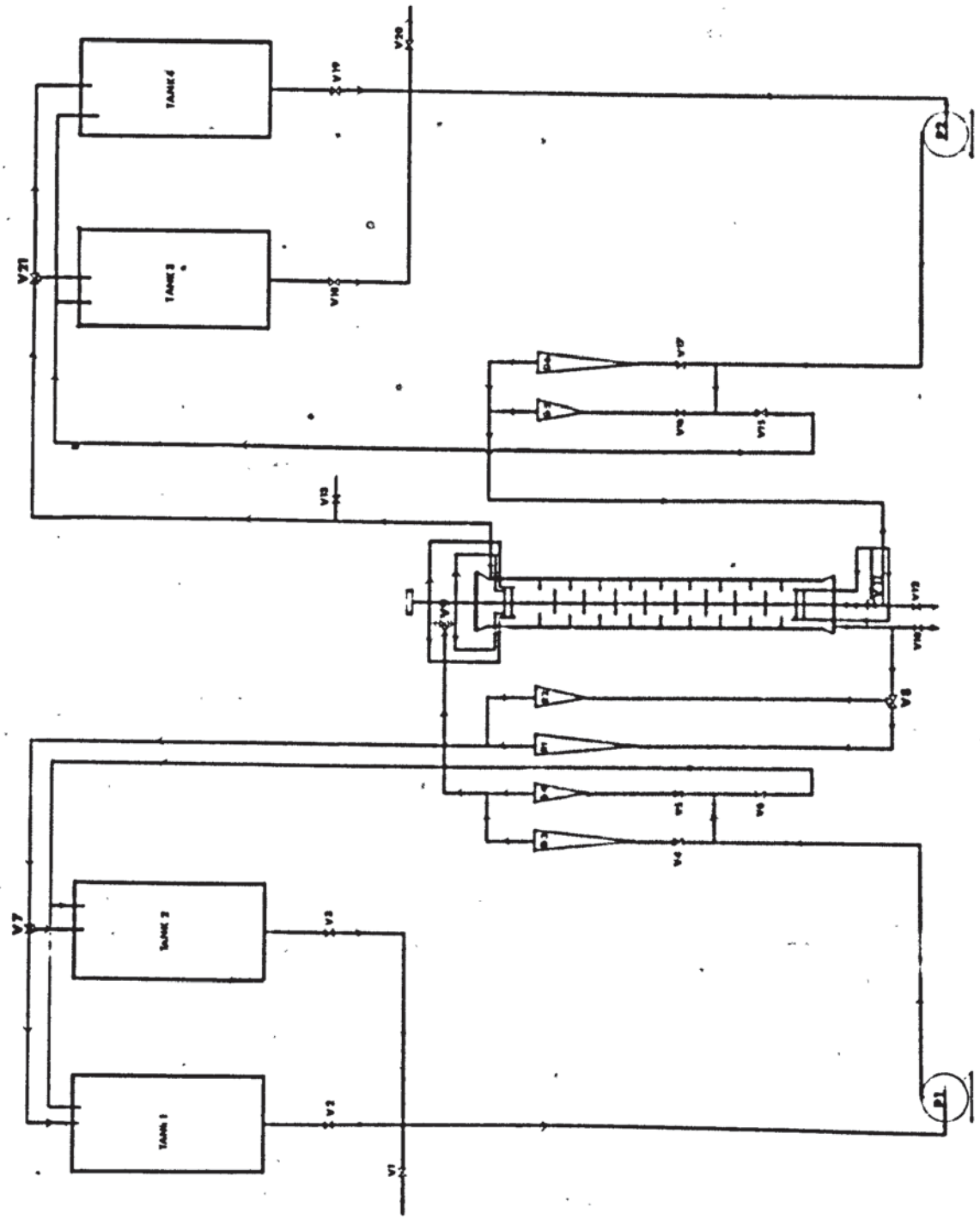

Figure 6.1 Schematic flow diagram

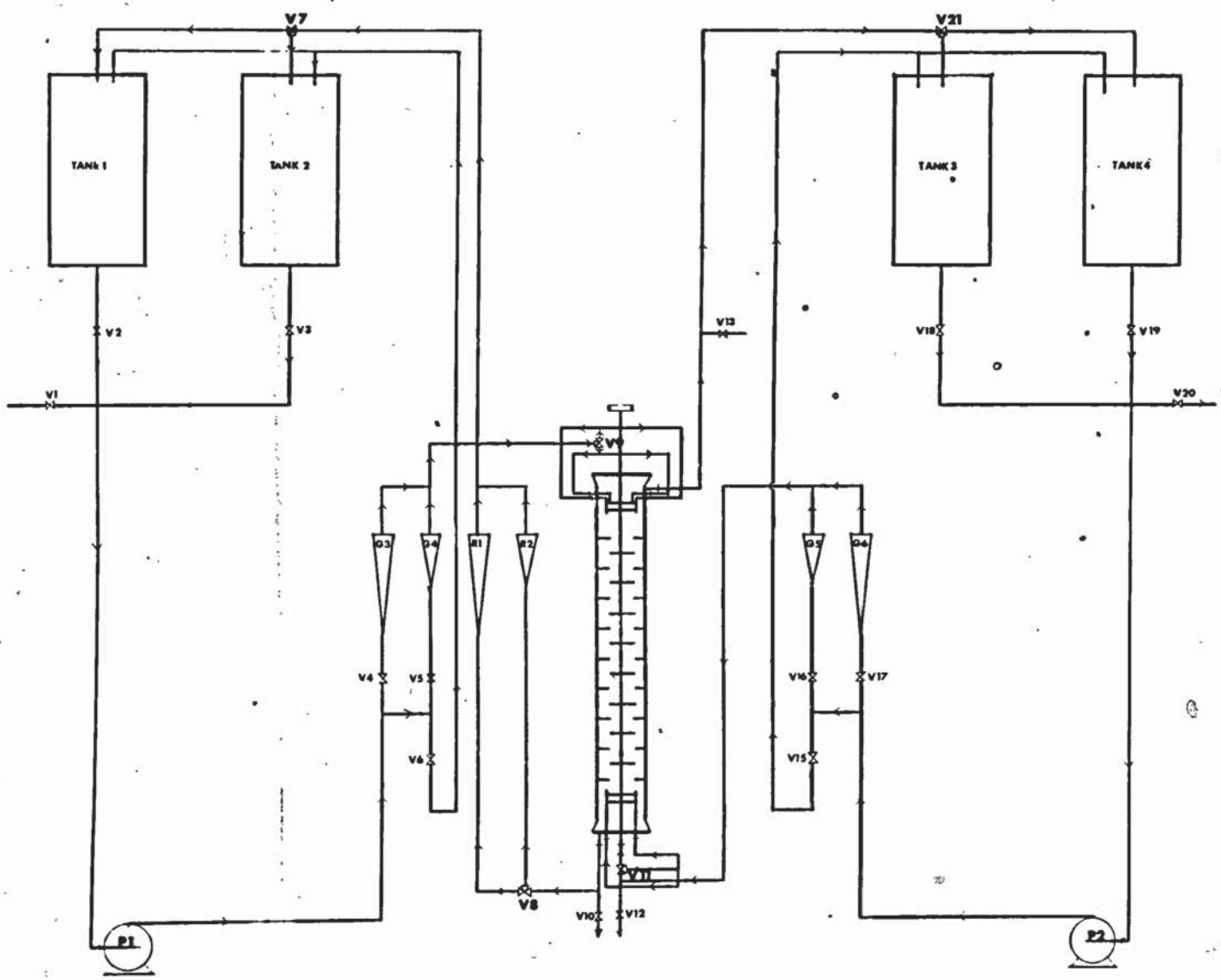
V7
V21
TANK 1
TANK 2
TANK 3
TANK 4
V2
V3
V18
V19
V1
V13
V20
V9
G3
G4
R1
R2
G5
G6
V4
V5
V16
V17
V6
V15
V11
V8
V10
V12
P1
P2

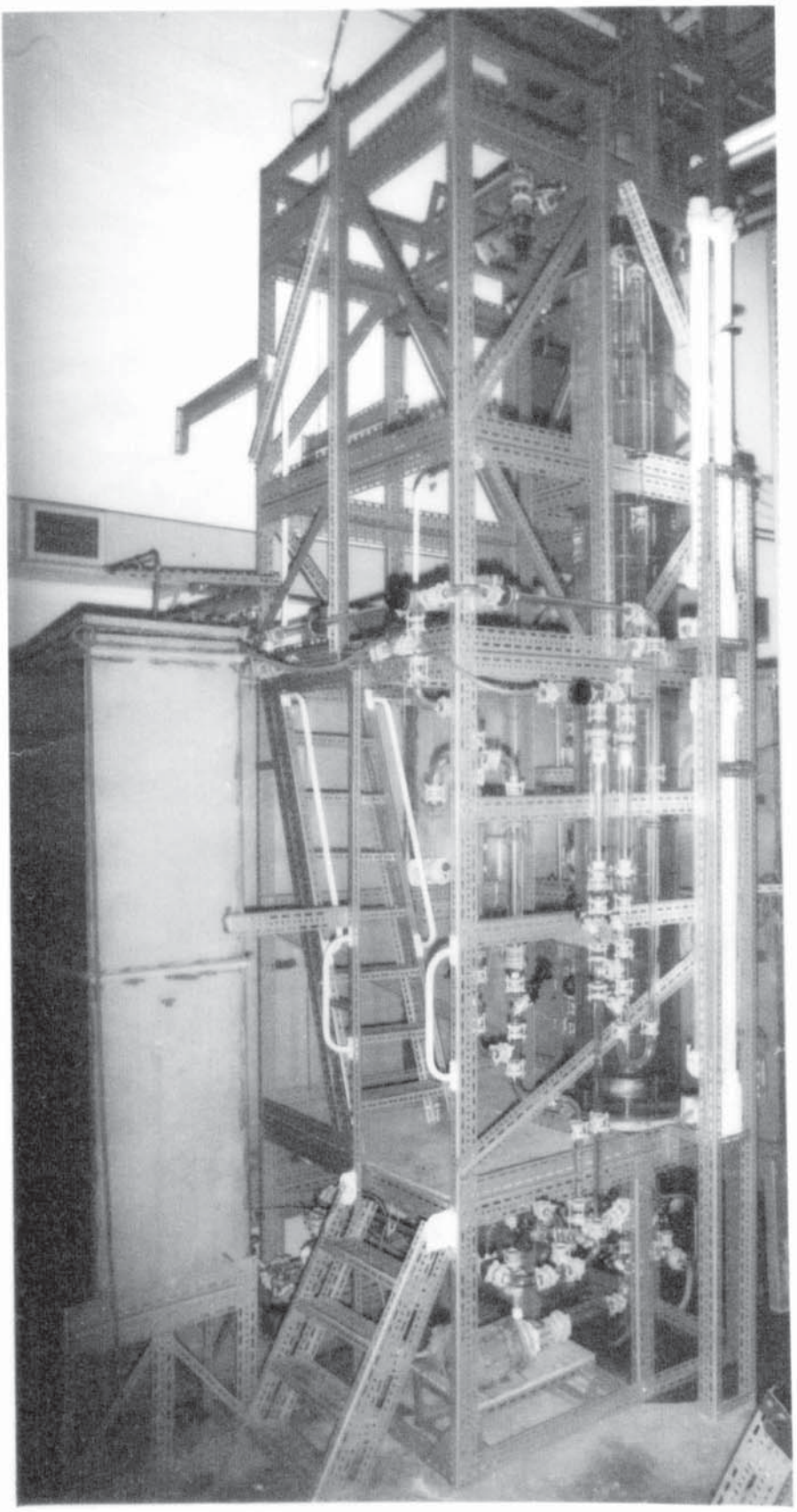

Figure 6.2 General Equipment Arrangement

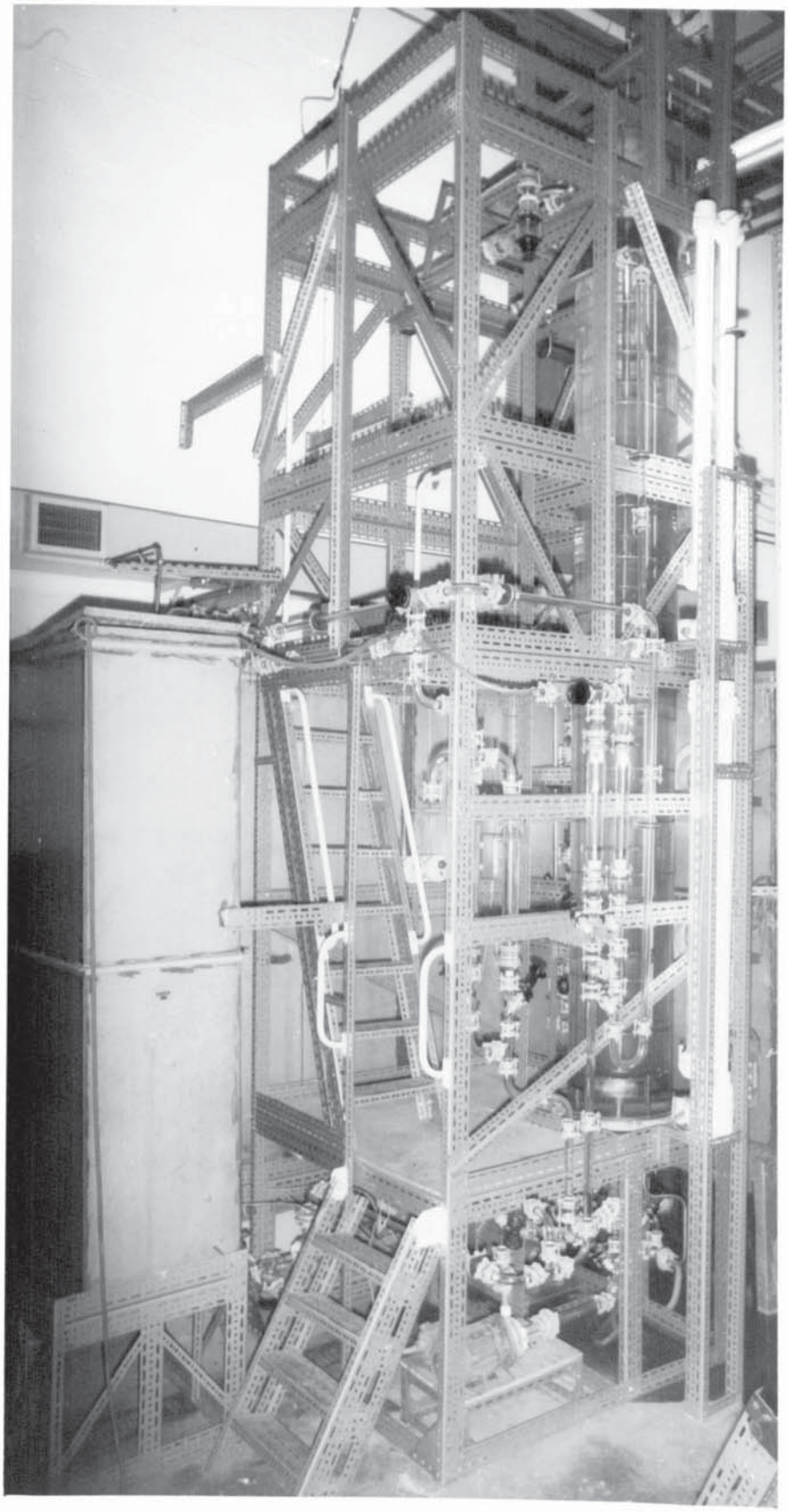

repiped to eliminate some of bottle neck points and to increase flexibility in operation. As illustrated in Figure 6.2 a two-storied steel angle structure, with wooden working platforms was constructed for the equipment. All the central valves and instruments were located on the first floor of this structure so that the contactor could be operated by one person.

The column consisted of a 45.0 cm diameter, 430 cm height, Q.V.F. glass section divided into 14 compartments each 22.5 cm high. The diameter of the discs was 22.5 cm and that of the stator openings 33.75 cm, these dimensions were in accordance with published design specifications (17, 21, 28, 29, 32, 33, 34). Nine sample points were provided over the column height including one at the outlet and another at the inlet. Each point comprised a 1.0 cm diameter hole fitted 0.6 cm in diameter tube with a quick-acting toggle valve.

The column internals were fabricated entirely from 18/8 stainless steel, and were machined to obtain a close fit at the column walls. The stators were supported by means of four equispaced 0.6/cm diameter stainless steel rods. The thickness of the discs and the stators was 0.2 cm. The discs were supported by means of a grub screw through the collar of the disc. This was countersunk into the collar to eliminate any effect on the pattern of agitation. In any event, the neighbourhood of the collar is effectively a dead zone and any disturbances caused by protruding screws would be very small (30). The discs had straight edges since discs with sharp or tapered peripheries would have

increased the axial mixing effects (32). The rotor shaft was fabricated from 2.5 cm O.D. stainless steel rod in two sections threaded at the centre, and it was supported at three points, via at the top and bottom distributors and in the centre, by means of P.T.F.E. bearings.

The heavy phase was introduced into the top of the column either via a side entry, or through the distributor plate. This was to facilitate operation with the heavy phase constituting either the continuous or dispersed phase. Similar provisions were made for the entrance of the light phase. However, the bottom distributor was 'water wetted' which is recommended for introduction of organic phase into an aqueous continuous phase, and the top distributor was 'organic wetted' for introduction of aqueous phase into organic continuous phase (25).

Figure 6.3 shows the construction of the bottom distributor with the P.T.F.E. bearings for the central shaft and the type of slot (4 in all) for feed to the distributor plate was designed on the conventional basis, using the correlation by Treybal (1, 84). The distributor plate, 30.5 cm in diameter, contained 700 holes each of 0.16 cm diameter, arranged on a 1.0 cm triangular pitch. The distributor was located 20.0 cm below the first compartment so that initial droplet formation was unaffected by agitation.

The top distributor shown in Figure 6.4 was constructed of 10 guage stainless steel but the perforated plate was of

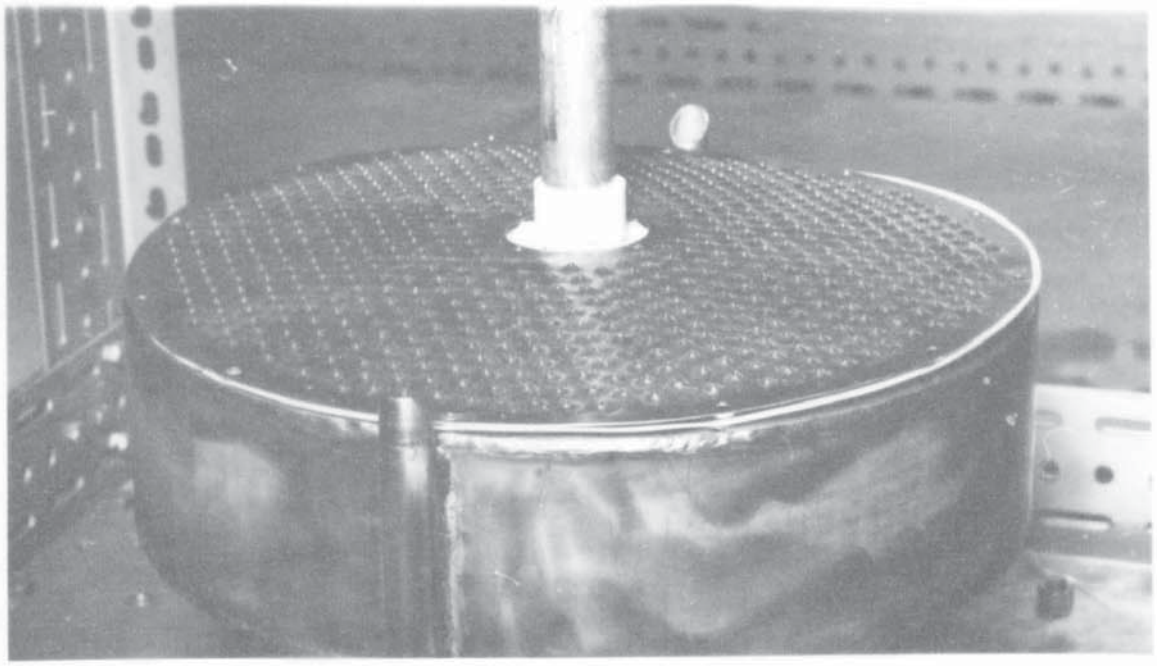

(a) With distributor plate on

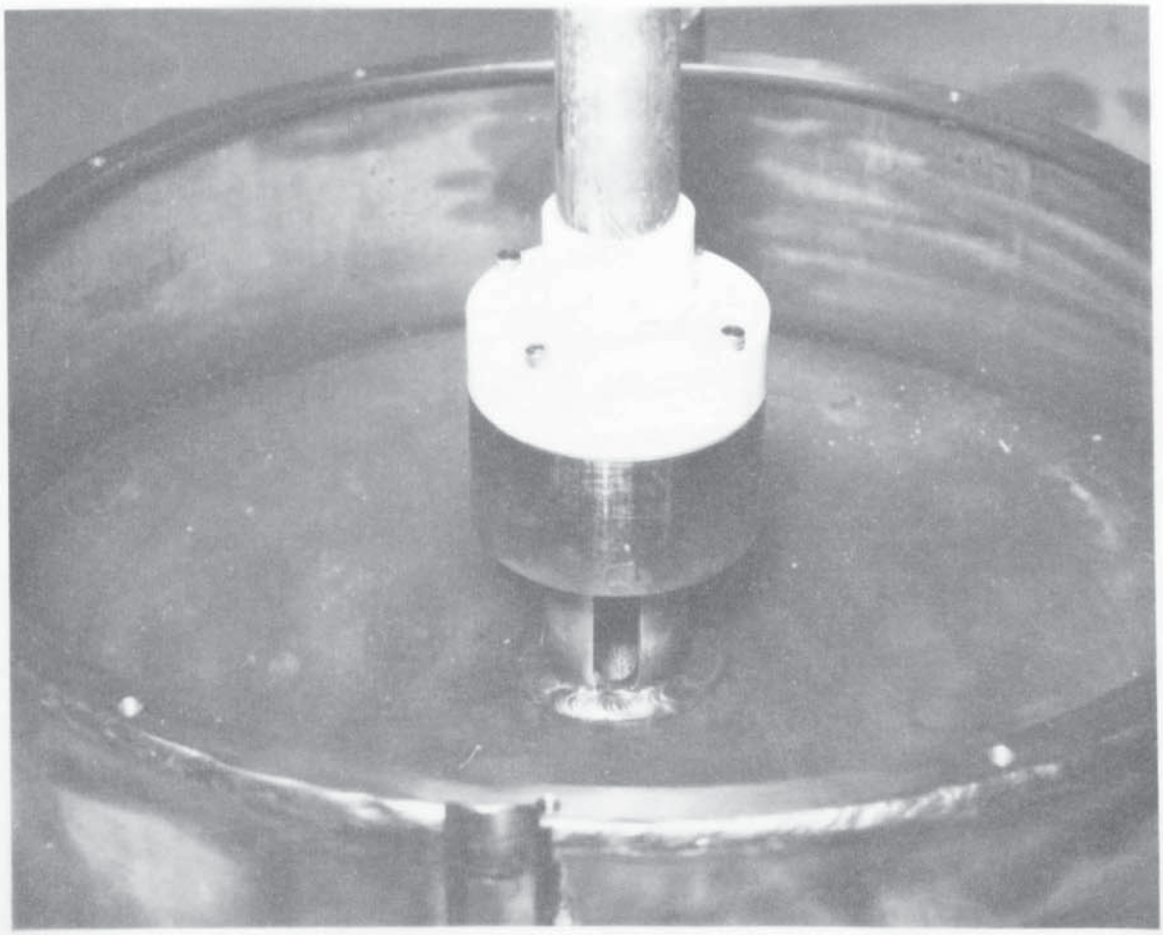

(b) With distributor plate removed to show the P.T.F.E. bearing for the central shaft and type of slot (4 in all) for feed to the distributor

Figure 6.3 The bottom distributor construction

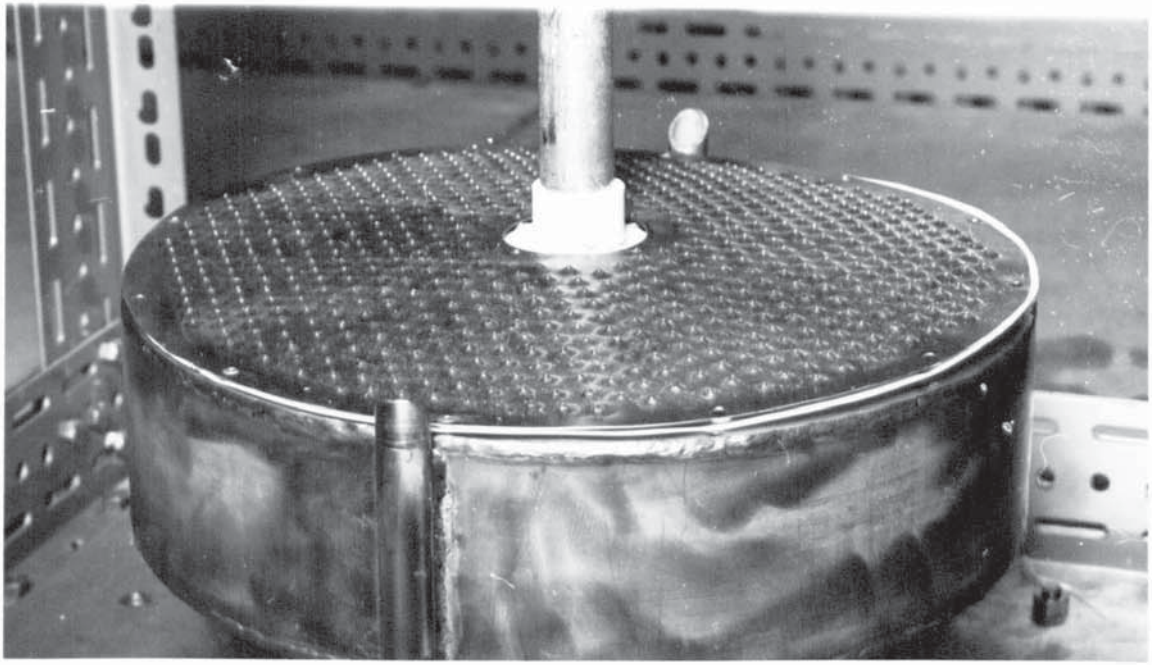

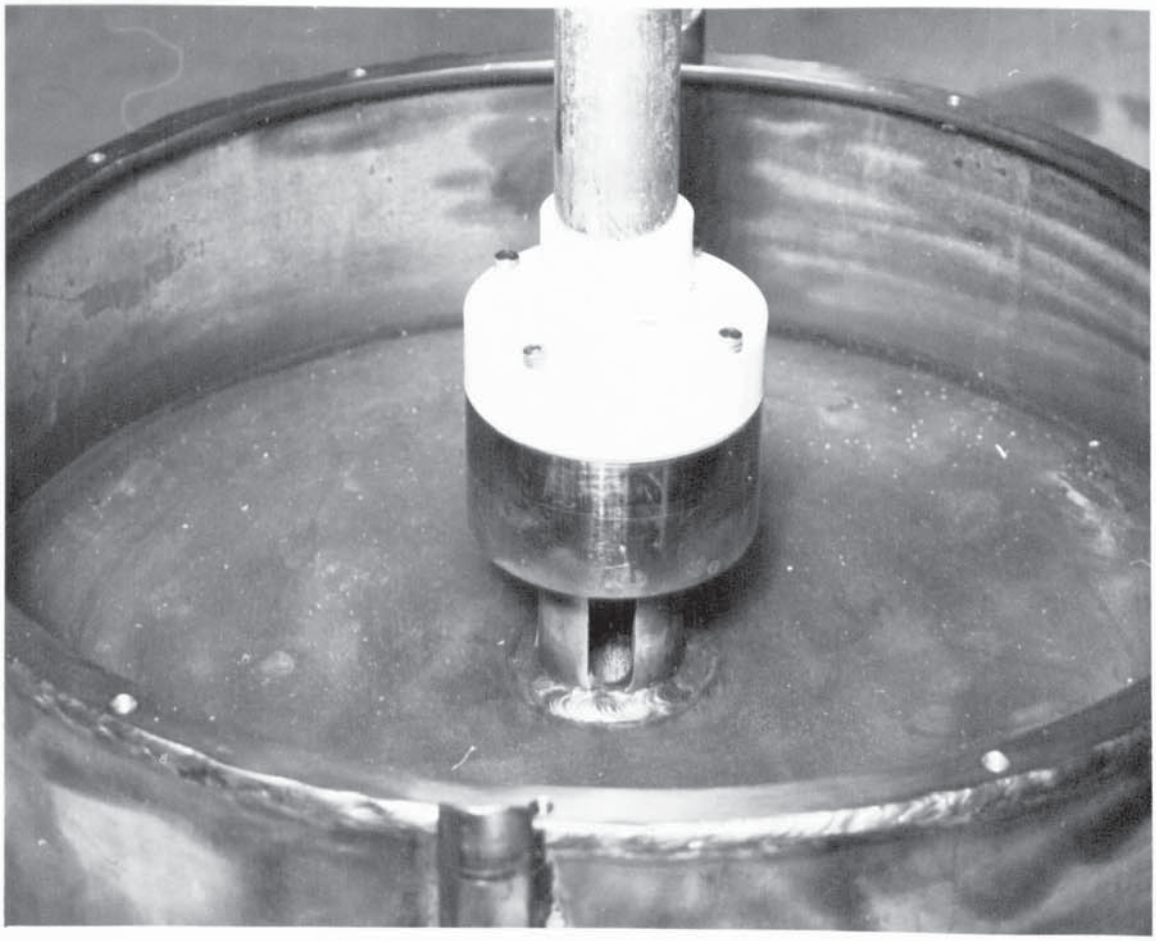

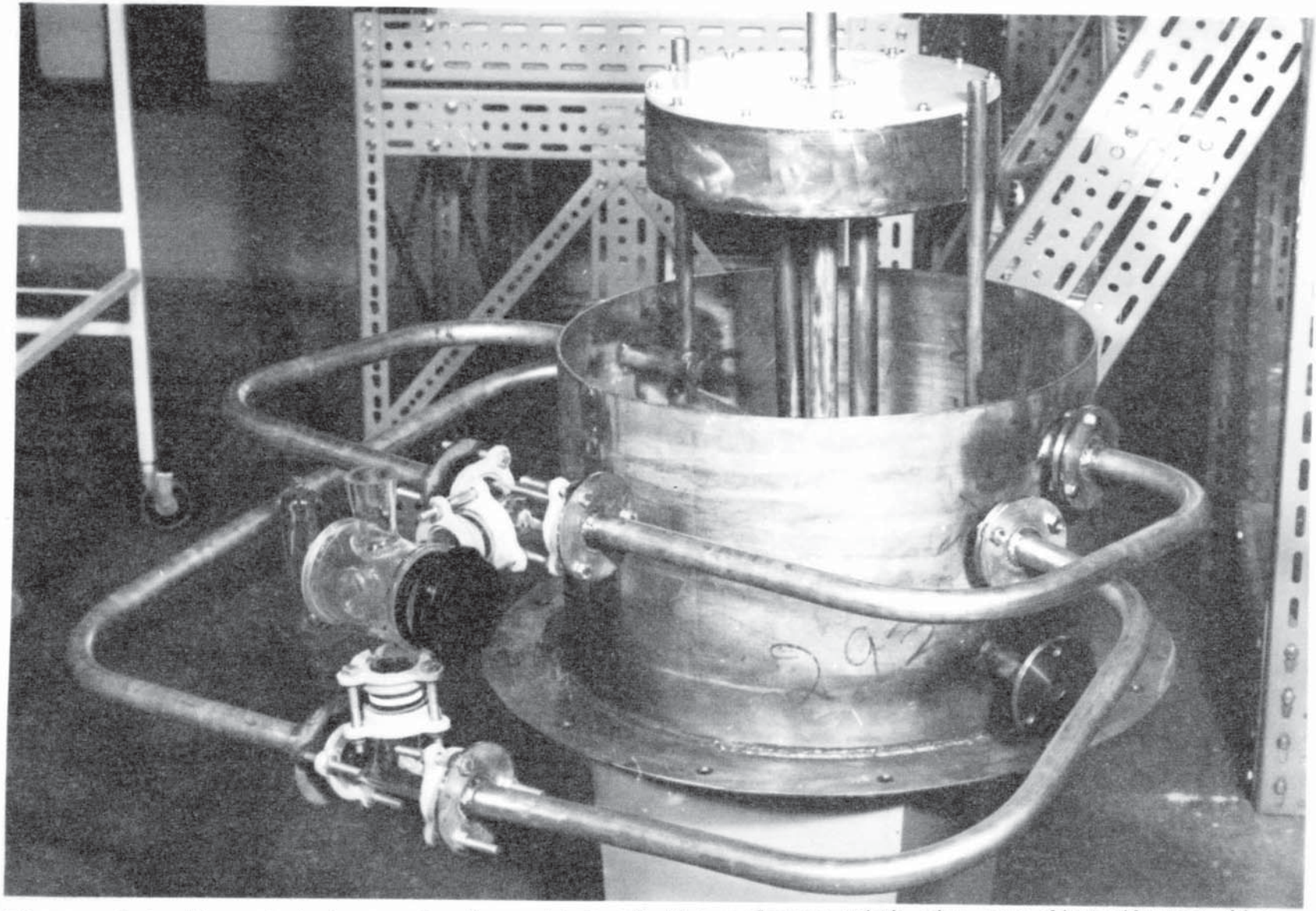

Figure 6.4 Top stainless steel section of the columns with the top distributor (in inverted position outside the column).

0.6 cm thick polypropylene, with 0.16 cm size holes drilled at 1.0 cm triangular pitch. As shown in Figure 6.4 a 30.0 cm long and 45.0 cm diameter stainless steel section fabricated from 10 guage sheet, provided the light phase coalescence section and incorporated outlet as well as heavy phase inlets.

The plates at the bottom and in the centre of the column were fabricated from 0.6 cm thick stainless steel. The bottom plate was drilled and incorporated pipes for the bottom distributor inlets and outlets.

6.1.1 Associated Equipment

The agitator shaft was driven by a 0.25 H.P., 240 volt. single phase, A.C. variable speed flame proof electric motor. The speed of the rotor was controlled by a gear box. The speed varied from 75 to 500 r.p.m. The speed of rotation was measured by a Comark electronic tachometer with 0-3000 r.p.m. range used in association with a photo-electric probe located in level with a mark on the shaft at the top of the column.

Four stainless steel rectangular tanks, each with dimensions of 3.44 m x 1.22 m x 0.61 m and a capacity of 1815 litres, were used as feed tanks and receivers. A recycle line was provided for each phase for use during feed preparation and for mutual saturation of the phases by recirculation in a closed loop.

Two p.v.c. flame proof pumps, each capable of supplying 50 - 100 lit/min against a head of 6 m - 3 m, were used for

the heavy phase. The first pump was used to feed the column, while the second pump was used to transfer the continuous phase from the bottom of the column into the receiver tank. The second pump was used to circulate the continuous phase to the top of the column in the study of the hydrodynamics in the absence of mass transfer as well. A third powerful stainless steel pump of capacity 120 litres against the head was used for the light phase.

Light phase flow was measured by two rotameters with stainless steel floats and a maximum capacity of 160 litres/min and 60 litres/min respectively. The heavy phase flowrate at both the inlet and outlet were also measured using two rotameters with stainless steel floats and a capacity of 100 litres/min and 50 litres/min respectively. All rotameters were installed in parallel to each other to obtain fine control.

No provision was made for temperature control of the equipment environment but temperature was always within 18.5 - 20.0^{o}C. The equipment was in fact located in an isolated pilot plant room provided with flameproof switchgear and lighting and an efficient low level air extraction system.

6.2 Selection of Liquid-Liquid System

The storage and use of a relatively large quantity of solvent, i.e. about 1500 litres, required a low cost solvent to a fixed specification. Therefore the liquid-liquid system selected for this study was

clairsol-350-acetone-water (physical properties of the liquid-liquid system were given in Appendix 1). This was based mainly on the following considerations.

1. Low volatility of clairsol-350 and relatively low toxicity, flash point > 71°C and hence a reduced fire hazard compared with other commercially available solvents (e.g. kerosene, toluol, dobane). The low volatility resulted in both low vapour concentrations in the pilot plant during open handling operations and low solvent losses.

2. The kinematic viscosity in the range 2 - 3 cs, interfacial tension with water in the range 20 - 40 dyne/cm and density 0.785 of clairsol-350 result in a system of the type ideal for operation with an agitated column (2).

3. Physical properties of clairsol-350 is very close to that of kerosene. So availability of results from other studies for comparison is possible.

A disadvantage with the use of clairsol-350, was that with ordinary filtered tap water an interfacial scum accumulated over a period.

6.3 Experimental Techniques

6.3.1 Cleaning Procedure

A 1% to 2% solution of Decon-90 decontaminant was used to clean the column, tanks and the process lines. The column was filled with this solution and left overnight; next morning it was pumped through all parts of the equipment for

1 - 2 hours with the agitator running and then drained. The equipment was then flushed with tap water 4 - 5 times and finally rinsed with water. Owing to the nature of contacting, and the liquid system used, there was a tendency for dirt and other impurities to be deposited on the column internals in preference to the rest of the equipment, so that great attention was paid to cleaning, which was repeated during each series of experiments. Great care was taken to effectively drain all low points and pipe sections to avoid any retention of surfactant.

6.3.2 System Purity Checks

The system purity was checked at regular intervals during the experimentation, by measuring the relevant system properties, i.e. density, viscosity, interfacial tension and the individual surface tension of the component liquids. Whenever a significant discrepancy (more than 5%) was observed in the values of these properties, the liquids were discarded. Due to the scale of equipment and its operations some changes in the system properties were unavoidable. This was observed during initial non-mass transfer runs when filtrated tap water aggravated the formation of an interfacial scum. This scum was removed by complete rejection of the water phase and rejection of the bottom settled layer in the clairsol-350 phase, followed by equipment washing using the method already described in Section 6.3.1.

6.3.3 Measurement and Calibration

Acetone concentrations were determined by measurement of relative absorbance of ultra-violet ray. Calibration charts for relative absorbance against concentration were prepared by measuring the relative absorbance of solutions of known acetone concentration. The data are given in Appendix 2. Only small quantities of samples of the liquid under test, i.e. about 10 mls, were required for this method.

A Pye unichem ultra-violet spectraphotometer (SP 1800) was used for the measurement of relative absorbance of the sample placed in 2 mm size cell. The apparatus was first zeroed by inserting a liquid blank in both cells. The best calibration condition for the working range of acetone concentrations in both places (0 - 10%) was found to be at band-width equal to 3.0 nm and wave-length of 310 nm for the clairsol phase solutions and 300 nm for the for the water phase solutions. The cells as well as the samples were maintained at a constant temperature of 20.5 ∓ 0.2 ^{o}C in a thermostat water bath for about one hour before the measurement made.

The above method was chosen from three methods of analysis previously used to measure acetone concentration in water and organic solutions (25, 26, 135). The other two methods were refractive index and Messinger iodoform method (178). The measurement of refractive index did not give reproducible results and it was observed that the same sample gave a large difference in refractive index. However,

it was difficult to make an accurate calibration curve for a three component system.

Messinger iodoform method (178) did not give any satisfactory results. This is probably due to the sensitivity of the chemicals involved to light, temperature and time. Since it depends upon the reaction of an alkaline solution of acetone (NaoH + acetone) with an excess of iodine to form iodoform according to the equation:

$$CH_3COCH_3 + 3I_2 + 4NaOH \longrightarrow CH_3I + 3NaI + CH_3COONa + 3H_2O \qquad (6.1)$$

The above reaction is a very slow reaction and it should be allowed to stand for at least one hour in a "black bag" and in an ice water bath. However, the method of relative absorbance is very convenient and gave very accurate reproducible results and was chosen for the analysis in this study. The physical properties of Clairsol-350 via viscosity, density, surface and interfacial tension in the presence of the solute was also determined. It was found necessary to determine the acetone at different concentrations to estimate the variation in these properties due to the presence of solute and to use the exact value of any property at any solute concentration in the mass transfer calculation. The filtrated tap water density and the densities of clairsol-acetone solutions were measured using a specific gravity bottle at 20.5 $\mp$ 0.1 ^{o}C.

The viscosities were determined by timing the passage of the fluid through a capillary immersed in a bath of constant temperature of 20.5 $\mp$ 0.1°C, i.e. by Cannon Fenske Viscometer (type BS/IP/CF).

Interfacial and surface tensions were measured with ring tensionmeter (torsion balance) at 20.5 $\mp$ 0.1°C. The measurement of the interfacial tension was done with water saturated with the clairsol. The results of all the above measurements of the mentioned physical properties are shown in Appendix 2.

6.3.4 Determination of Equilibrium Distribution Diagrams

Equilibrium concentrations were determined by making up mixtures on a weight basis to represent points below the mutual solubility curve (179). Each mixture was contained in a stoppered flask and brought to equilibrium by repeated shaking and standing for several hours in a thermostat bath at 20.0°C. The layers were then separated using a separating funnel and the sample analysed using the relative absorbance method. The equilibrium diagrams for the ternary systems used, viz. Clairsol 350-Acetone-Water, are given in Appendix 2.

6.3.5 Photography and Associated Techniques

Two still cameras, a Nikkormat 35 mm and a Pentax 35 mm were employed for this photography. The flameproof tube lights placed in the rig, although essential for visual observation, provided insufficient illumination for

photography; therefore the lighting was provided by a 1000 watt quartz-iodine lamp. The method of lighting was to place a 1000 watt photo flood lamp behind the column and take the photographs with back lighting. Ilford 400 ASA films were employed in most cases. Aperture opening, shutter speed and focal length were adjusted according to densometer reading. In most cases a shutter speed of 1/1000 second was found to give best results specially at high rotor speed. Three photographs were taken for each event. A photograph of the whole compartment was preferred to one of a very small section of the compartment. This was because large number of drops i.e. nearly 300 drops, were required per photograph for Sauter mean drop size estimation. Distortion due to curvature was found to be negligible in large column diameter (25, 26, 47). The depth of field was typically less than 6 cm.

CHAPTER SEVEN

Experimental Procedures and Results

7.1 Non-Mass Transfer Studies

The non-mass transfer investigation were performed in support of the main study to provide a good understanding of large scale R.D.C. hydrodynamics via dispersed phase hold-up, drop size and drop size distribution; this in addition of knowing the limiting capacity of the equipment via flood phenomena. Some repetition of earlier studies in the same equipment by Khandelwal (2) was necessary. This is due to the use of different liquid-liquid systems and due to minor modifications in the equipment.

7.1.1 Flooding Phenomena

As discussed in Chapter 3, flooding rates represent the maximum volumetric capacity of a contactor under a given set of conditions. In this work flooding was characterised by the complete rejection of the dispersed phase, a dense layer of droplets at the heavy phase outlet at the bottom of the column. This was the conventional flooding phenomena described in the literature (25, 26, 33). The operating procedure used for determining flooding flowrates was:

The column was filled with the continuous phase up to the plane to be occupied by the interface, generally a

distance of 50 cm from the top of the column. With the agitator stationary and no continuous phase flow, the dispersed phase was admitted to the column. When the build-up of bulk dispersed above the interface was completed and the coalesced layer of the dispersed phase started to flow from the dispersed phase outlet, to be recycled to the reservoir, the agitator was then started and its speed adjusted to the required value. The dispersed phase hold-up steadily increased and the continuous phase which was displaced was allowed to flow out of the column via the outlet valve. The continuous phase was then admitted to the top of the column at the desired rate. Careful control of the outlet flowrate of the continuous phase was necessary to maintain the interface at constant level at the top of the column by adjusting the outlet valves of the continuous phase. Steady state was indicated by the interface level remaining steady. The dispersed phase flow rate was then increased incrementally until flooding occurred. Sufficient time was allowed for steady state conditions to be reestablished following each increase which was found to be about five minutes. On occasion temporary increases in the continuous phase outlet flow were necessary to maintain a constant interface position during the re-establishment process. Both the dispersed phase and continuous flowrates were recorded at the flooding point. As a check the dispersed phase flowrate was then decreased by about 10%, to allow the column to revert to normal operation, and then increased until flooding re-occured. Intense mixing was observed immediately prior to flooding, this was also reported by previous workers (2, 25, 26, 47).

Flooding was more easily recognisable at high rotor speed, viz 300 r.p.m. This is due to the generation of very small drops becasue of intensive break-up processes The terminal velocities of these droplets was very much less than the downward velocity of the continuous phase, and they were therefore carried out of the column with that phase.

The flooding flowrate results are reproduced in Fig. 7.1.

7.1.2 Drop Size and Drop Size Distribution

Preliminary observations confirmed that, as reported by other workers (2, 25, 26, 30, 40, 180), drop size and drop size distribution were not greatly affected by continuous phase flowrate. Therefore observation and photography of droplet phenomena were carried out with a constant continuous phase flowrate.

Drop sizes were measured in compartments 2, 4, 6, 10, 14 and at the distributor compartment 0, which did not contain a rotating disc and this was considered as the inlet drop size. For each condition two or three photographs were taken after hydrodynamic equilibrium was attained. The criterion for equilibrium was taken as a steady interface level and its attainment normally required about 7 to 10 minutes. The photographic techniques have been described in paragraph 6.3.5.

Drop size measurements were taken from A4 size prints with approximately 1 to 2 times magnification, a typical print for drop size measurement in the absence of mass transfer is shown in Figure 7.2. Magnification of 5 to 6 times was reported earlier to give better accuracy (30), but in this

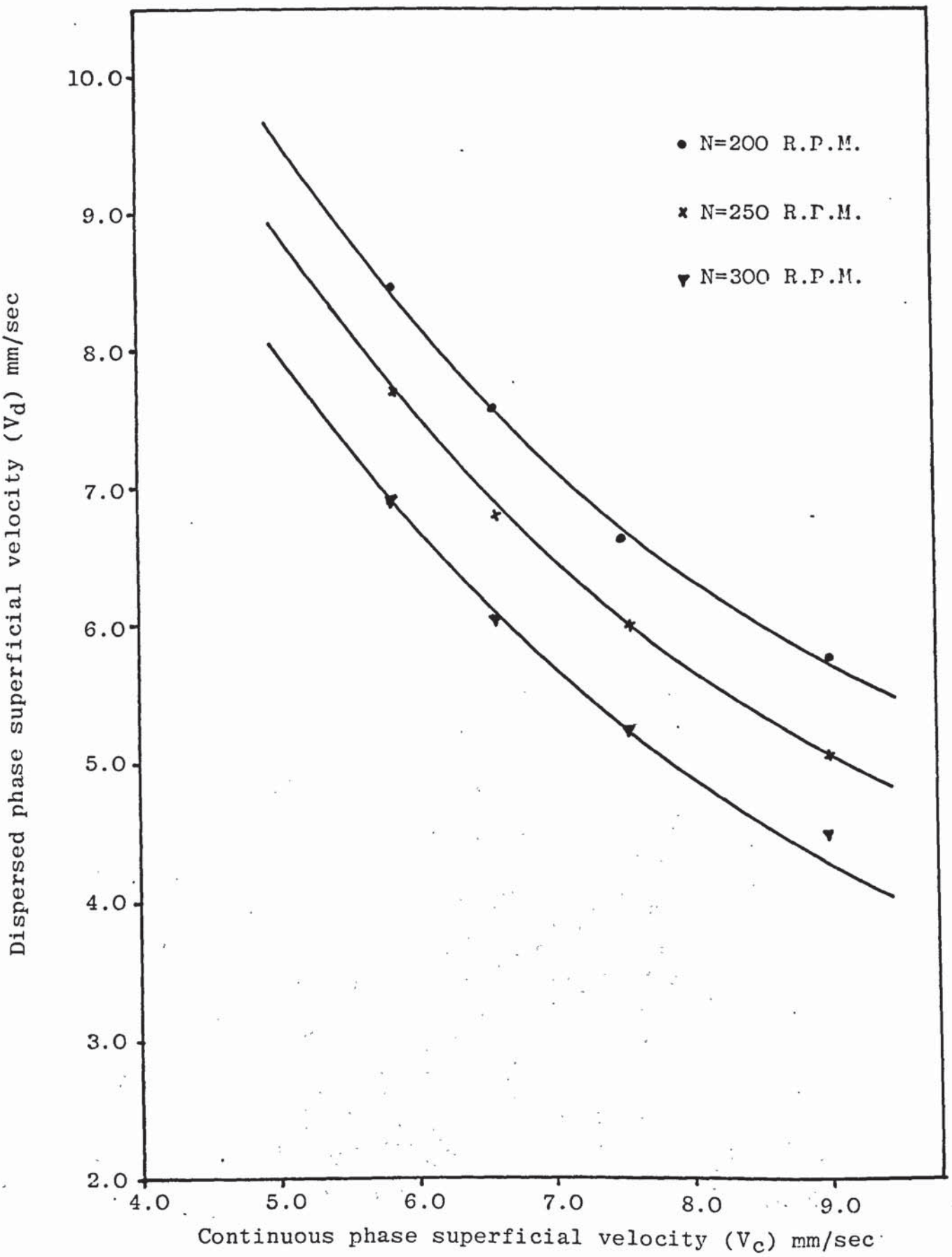

Fig. 7.1 Flooding curves at different rotor speeds

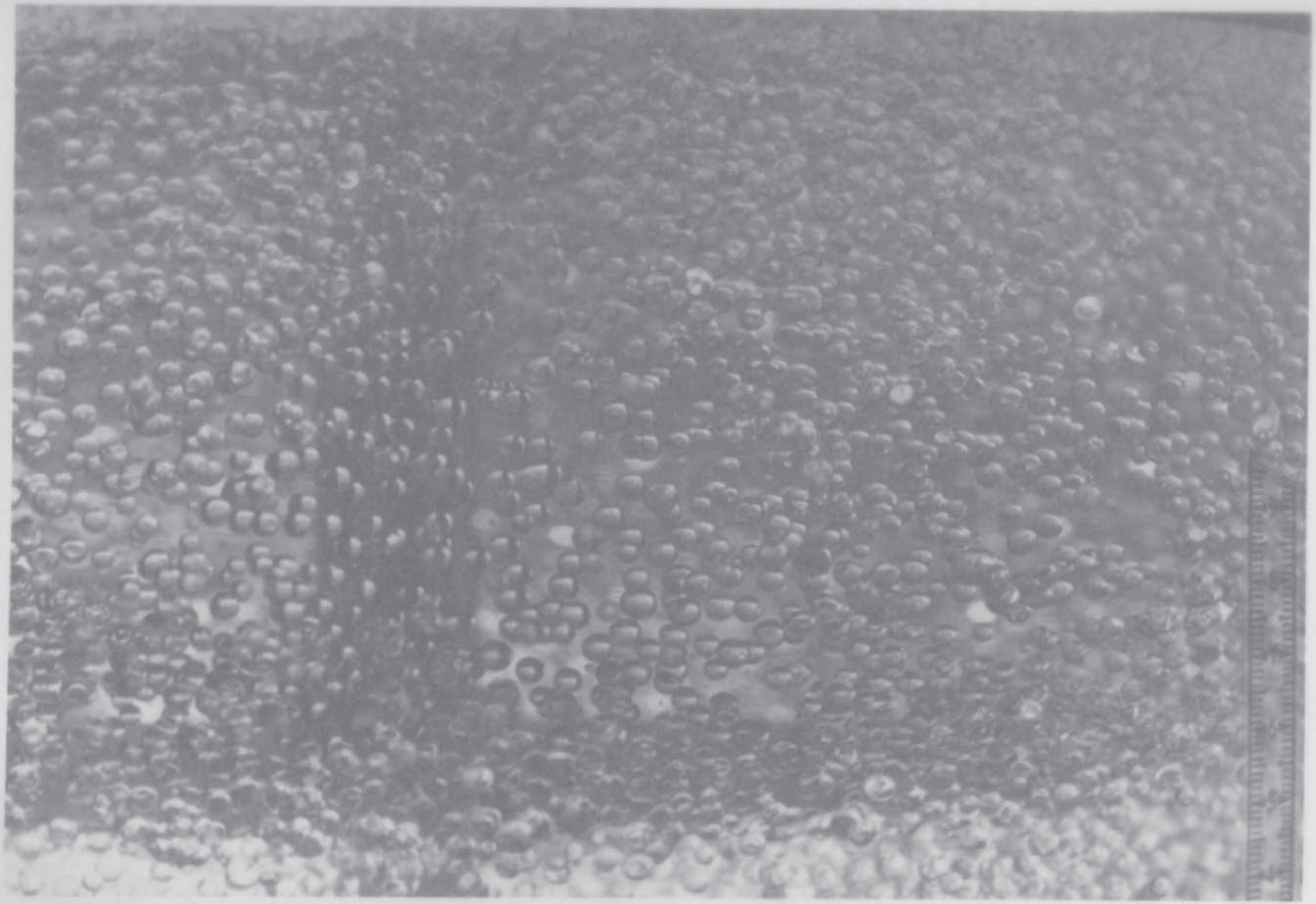

Compartment No.6 Magnification = 1.25 Rotor speed = 200 r.p.m.

Figure 7.2 Typical print for drop size measurement

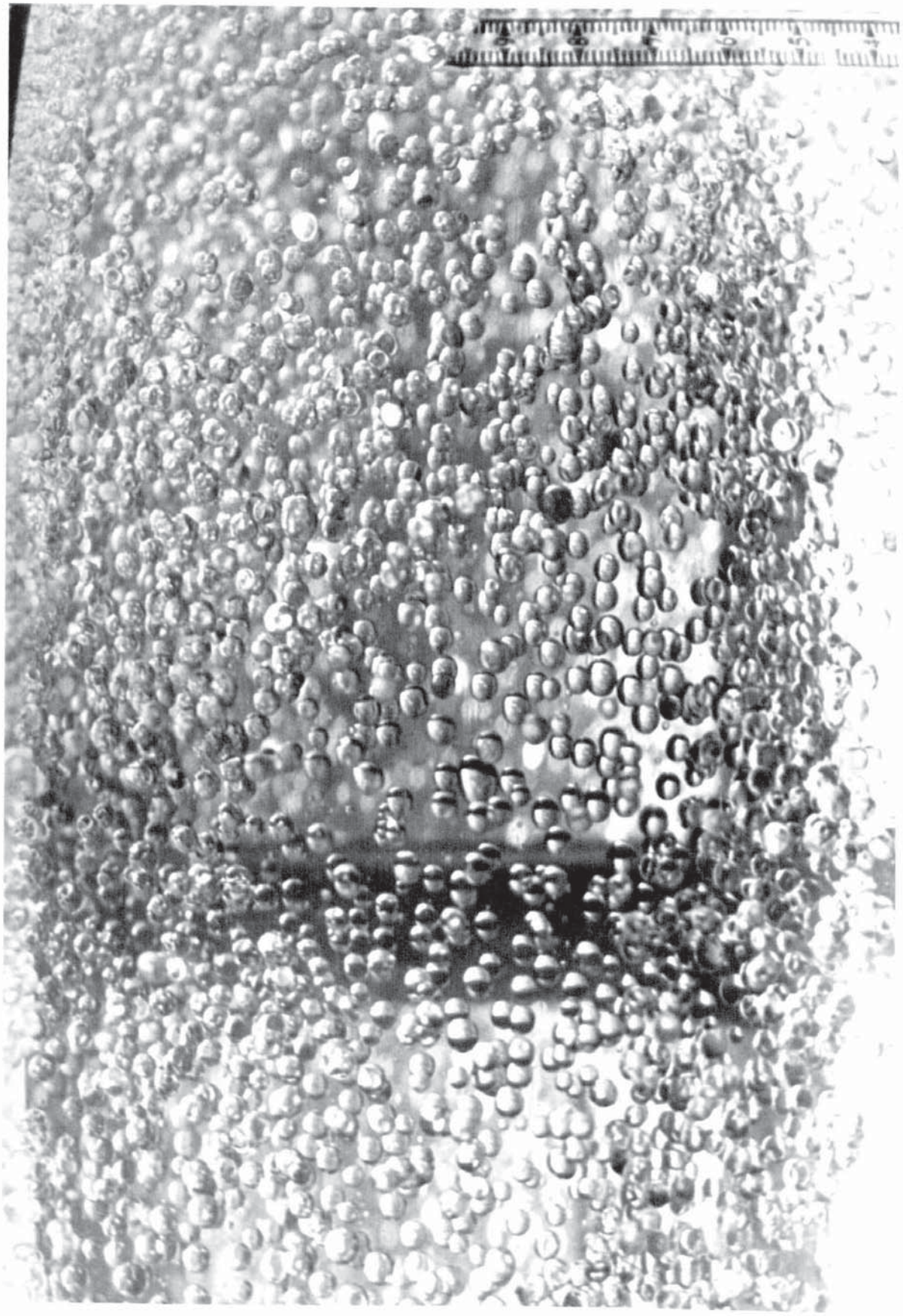

work this was impractical due to the large number of prints to be analysed (about 500 prints). Moreover a whole compartment had to be photographed to give adequate representation of drop size distribution and the actual size of the compartment was 45.0 cm x 22.5 cm. Conversely, smaller magnification factor would tend to give slightly larger Sauter mean drop diameter because of very small drop size either remained indistinct or did not fall into the counting range.

A Carl-Zeiss particle size analyser was used to analyse the photographs T4.Z.3. Ellipsoids were recorded as spheres of equivalent diameter.

Sauter mean drop diameter was evaluated from

$$d_{32} = \frac{\Sigma nd^3}{\Sigma nd2} \qquad (7.1)$$

A total of more than 200 drops were counted in a random manner from each photograph. The variation of drop size along the column height in the absence of mass transfer is plotted in Figure 7.3. A typical drop size distribution as drop size cumulative volume against drop diameter for compartment No.14 for two rotor speeds, viz 200 r.p.m. and 300 r.p.m. is shown in Figure 7.4. These were chosen arbitrarily from all of the data for all the compartments and many different rotor speeds to check the drop size distributions.

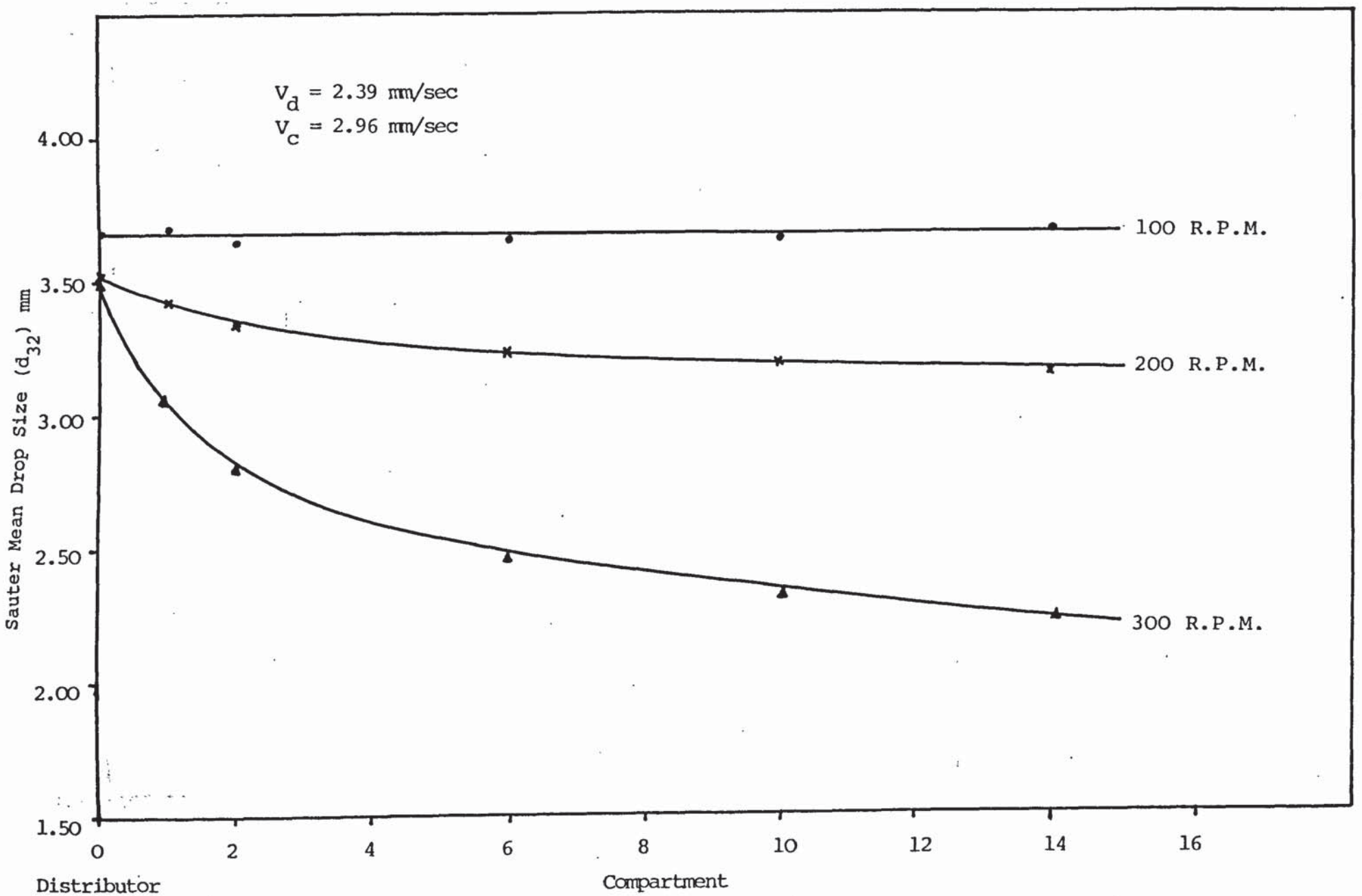

Figure 7.3 - Drop Size Profile Along Column

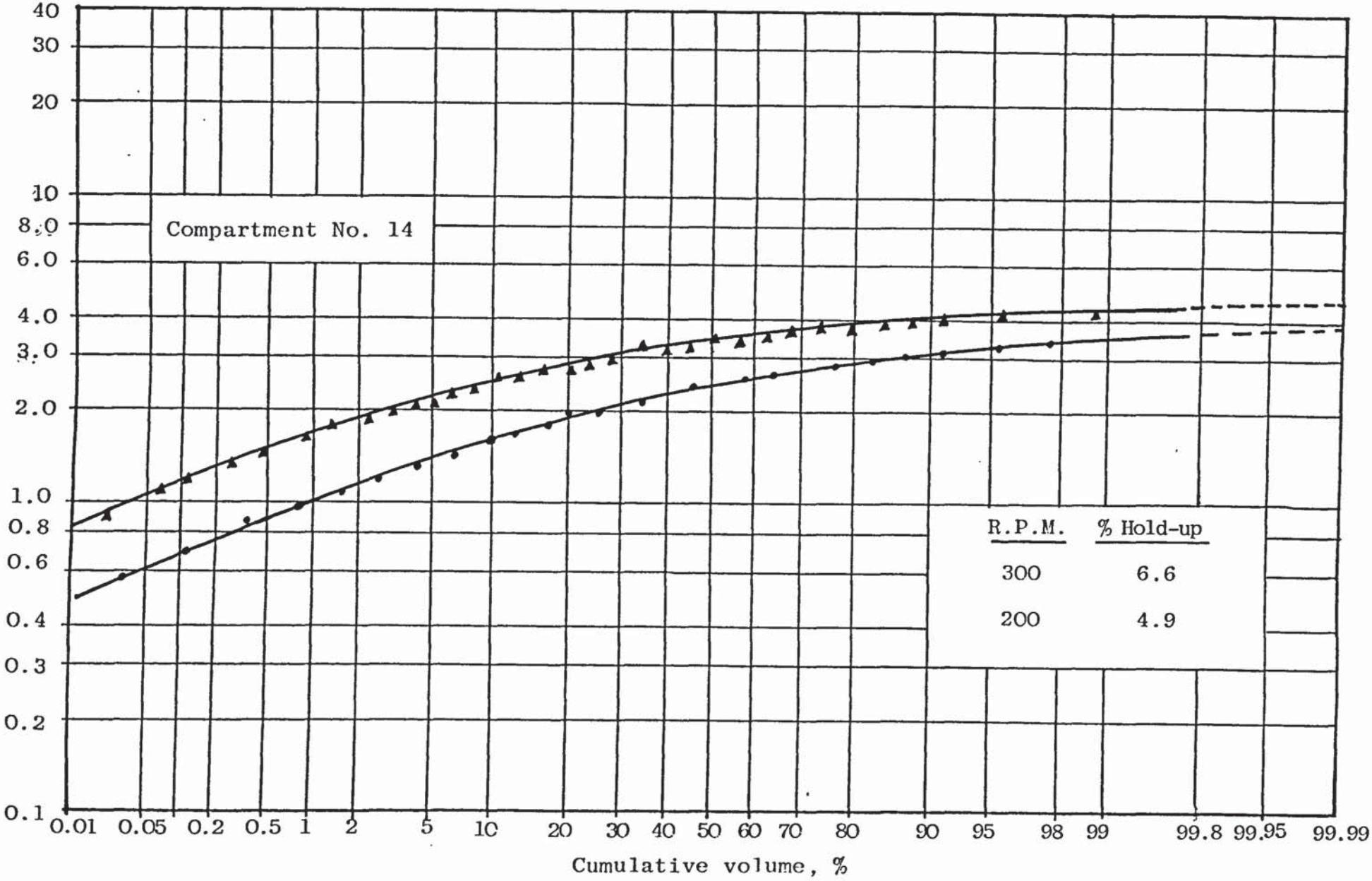

Fig. 7.4 Drop size distribution for compartment No. 14 at different rotor speed

7.1.3 Dispersed Phase Hold-up

Only the average values of the dispersed phase hold-up have been determined in this work. The simultaneous shut-off method (28, 34, 38, 39) was applied by operating the column under the desired conditions, and when the steady state had been attained and measured by steady interface level, all the inlet and outlet valves were closed rapidly and the rotor stopped to allow the dispersion to settle under gravity and displace the interface. The average hold-up was then determined by dividing the shift in the position of the interface by the effective height of the column, i.e. the height from the bottom distributor to the previous position of interface. This method was found to be satisfactory, and was in agreement with some other workers (2, 25, 26), although in an earlier work (30) it was reported to give poor accuracy and reproducibility.

Typical results of the variation of average hold-up against dispersed phase superficial velocity V_d at various rotor speeds are reproduced in Figure 7.5. Figure 7.6 shows the variation of average hold-up against rotor speed at various dispersed phase superficial velocity V_d. Finally the effect of the continuous phase flow rate upon the average hold-up is shown in Figure 7.7 where the average hold-up is plotted against the dispersed phase superficial velocity V_d at various continuous phase superficial velocity V_c at constant rotor speed.

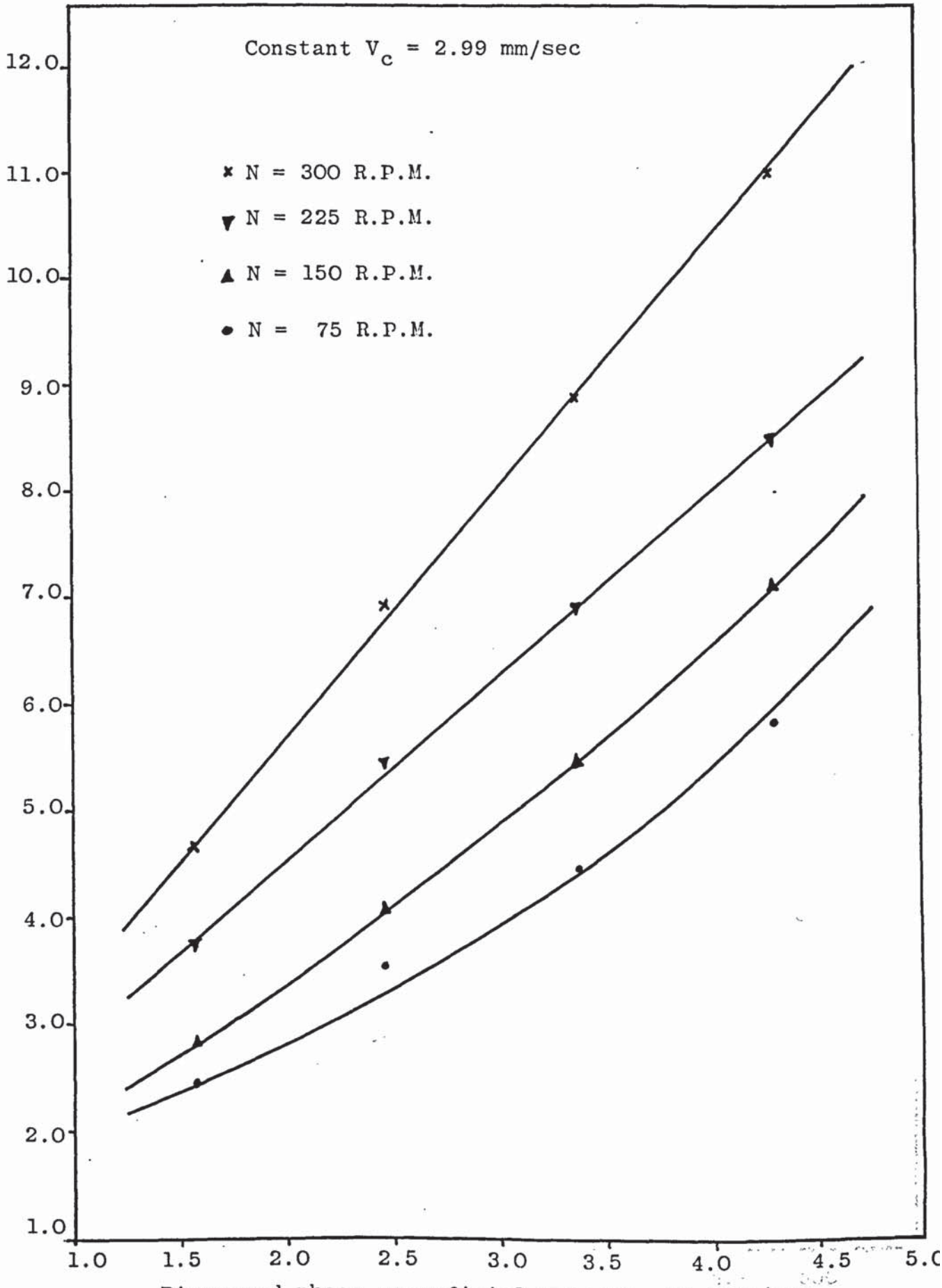

Fig. 7.5 Hold-up vs dispersed phase superficial velocity

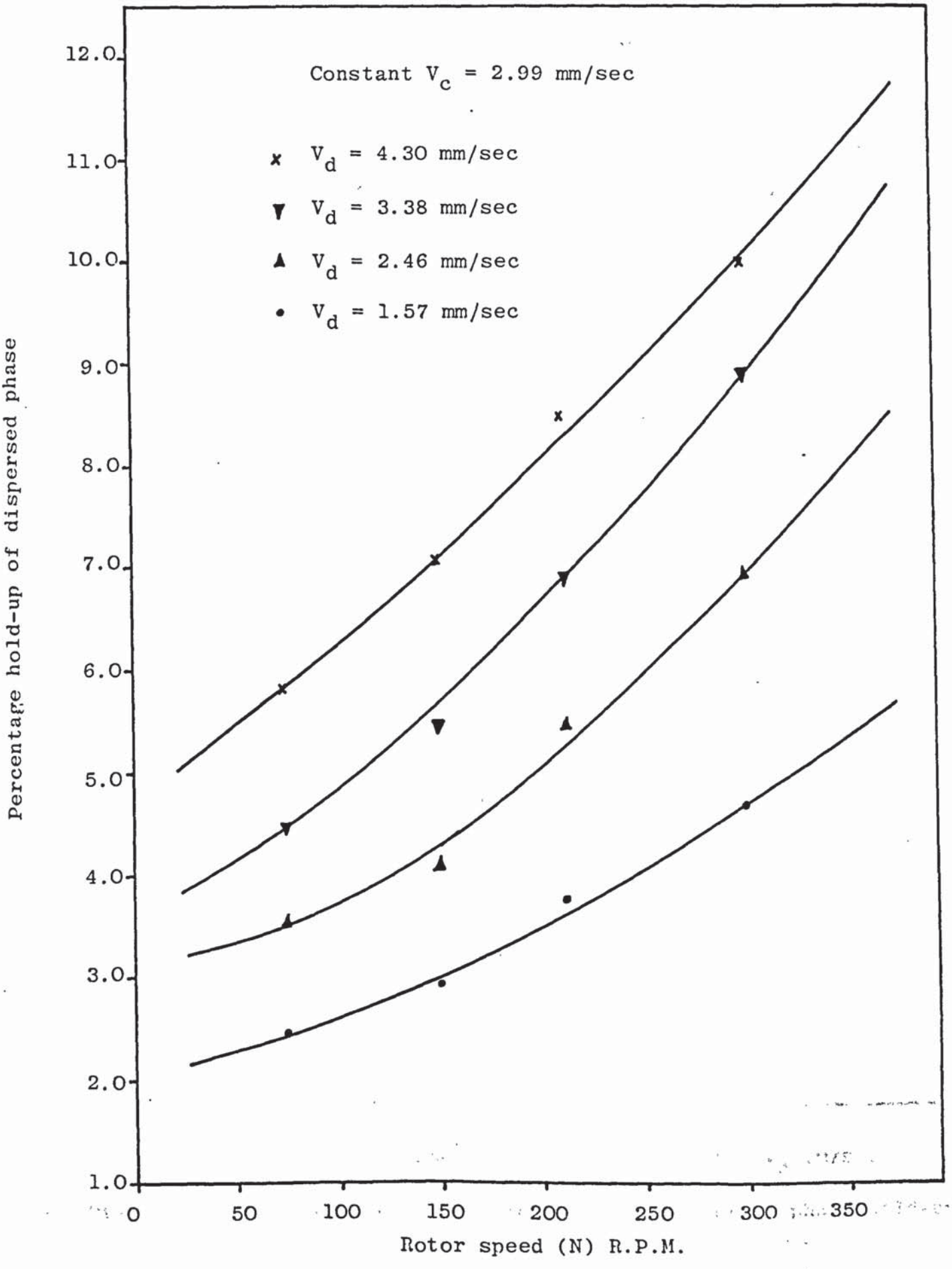

Fig. 7.6 Hold-up vs rotor speed

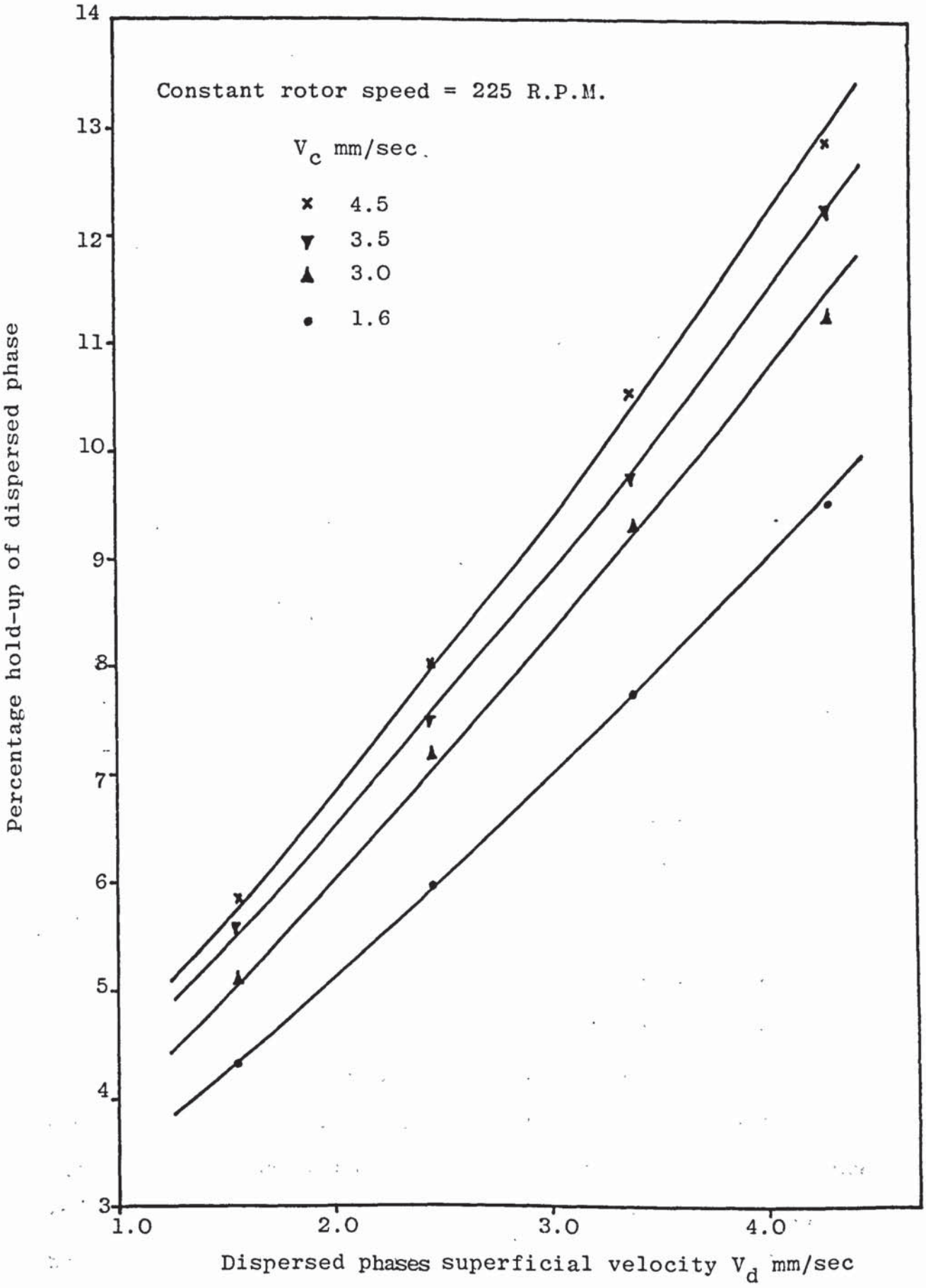

Fig. 7.7 The effect of phase velocities on dispersed phase hold-up

7.2 Mass Transfer Studies

The column extraction efficiency, as well as its hydrodynamics under mass transfer conditions, were carried out at different acetone concentration in the feed stream and mass transfer in both directions were studied i.e. from dispersed to continuous or from continuous to dispersed. Hydrodynamics did not include the flooding test since it is impractical to carry out separate experiments to measure flooding rates in such a large column because this would have to consume large quantities of solvents and solute. There were no continuous distillation facilities available to recover the solute quantities either. However, all the mass runs were carried out below 70% of the flooding flowrates obtained during the non-mass transfer experiments as recommended by Treybal (1).

7.2.1 Dispersed Phase Hold-up

The average hold-up measurements were made during the individual mass transfer runs, as described in Section 7.1.3.

No attempt has been made to plot the hold-up against operating parameters because of change of more than one parameter during the mass transfer experiments. However, the dispersed phase hold-up was found to increase with an increase in either phase flow rates or rotor speed which are the same situations as in non-mass transfer experiments, but the percentage hold-up under mass-transfer is different from that under non-mass transfer for the same operating parameters. This depends upon acetone concentration and

direction of mass transfer. The results are presented in Table 8.3 in the next chapter.

7.2.2 Drop Size and Interfacial Area Estimation

Drop sizes were measured within the same compartments mentioned in Section 7.1.2 during each mass transfer run when solute transfer from either phase to the other. Two or three photographs were taken for each compartment throughout the column length for the purpose of drop size measurements, a total of 350 photographs were taken. During the preliminary experiments an attempt was made to determine a 'representative' compartment in order to reduce the number of photographs requiring analysis and to simplify the estimation of the interfacial area with/^{out} affecting the accuracy of mass transfer calculations.

Compartment No. 6 has been chosen as a 'representative' compartment for the average drop size in the column for the following reasons:

a) The arithmetical average of Sauter mean drop diameter $\bar{d}_{32}$ over the whole column is closest to that of compartment No. 6. This is approximately shown by Figure 7.8 for drop size profile throughout the column at constant acetone concentration .

b) According to literature (2, 25, 33) the maximum peak of the hold-up is in the middle of the column. So d_{32} in this section will give more realistic average diameter for a wide drop size distribution.

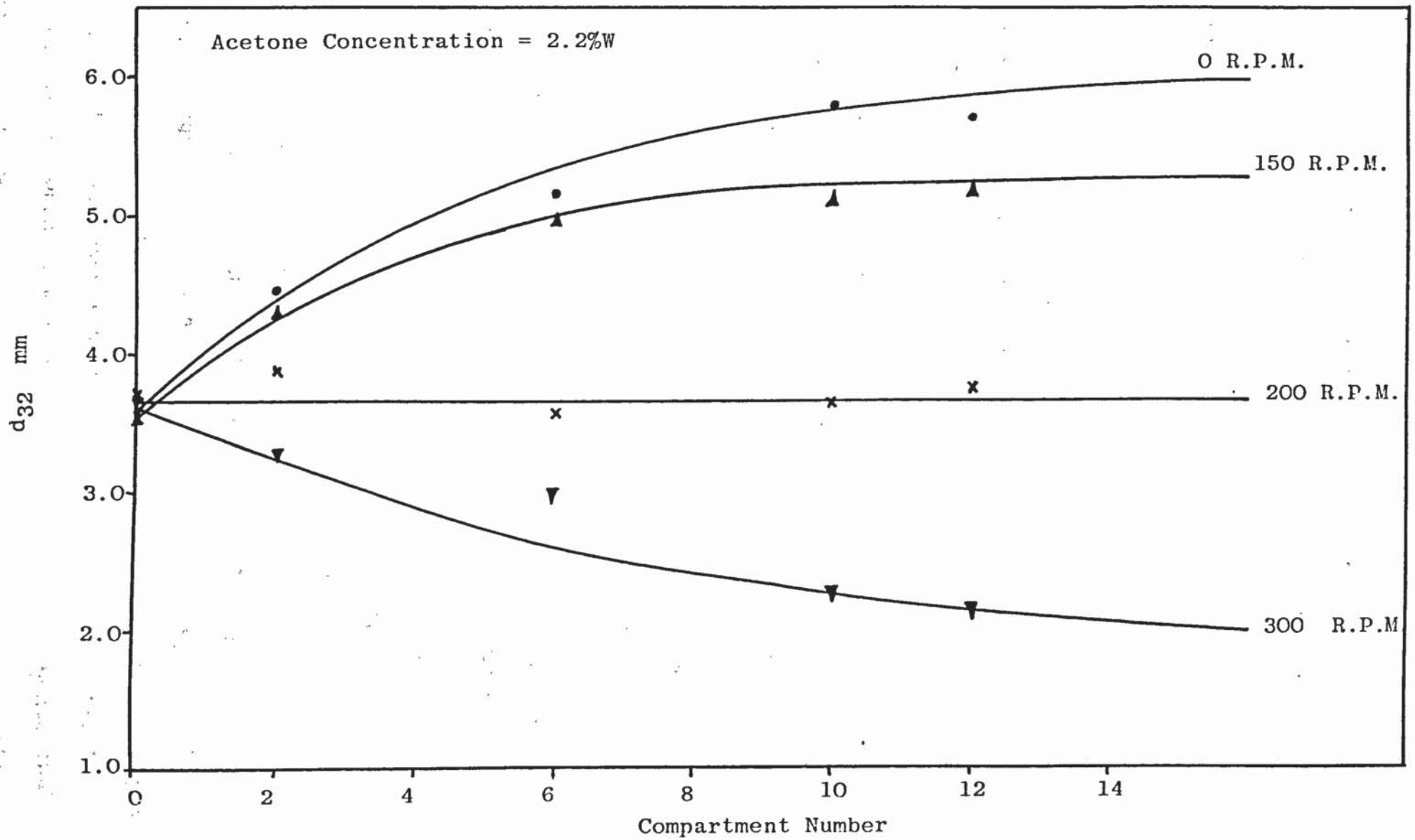

Fig. 7.8 Drop size profile along column, under mass transfer

After choosing the representative compartment, two or three photographs were taken for this compartment for all the rest of the mass transfer experiment in either direction of mass transfer.

7.2.3 Mass Transfer Experiments

Experiments involving the transfer of acetone from either phase were performed at acetone concentrations in the feed stream of less than 6% in order to avoid the formation of emulsions that might happen at higher acetone concentration. Phases flowrates were kept below 70% of the flooding flowrates under non-mass transfer conditions as recommended (1). In all cases of solute transfer from dispersed to continuous phase the initial acetone concentration in the continuous phase was always zero. However, when the organic phase was the extract, the initial concentration was between 0 - 0.5% in most cases. To reduce the concentration of the organic phase to the above level, back extraction were carried out with fresh filtrated water, which was then discarded.

The procedure followed during these runs was: before starting experiments the two phases were mutually saturated by circulating each phase in a closed loop for approximately 5 hours. Afterwards they were left overnight to settle and separate. The raffinate solution was made up to the required solution was made up to the required concentration of acetone, normally between 1.5 to 5% by weight and the initial concentration of acetone in the extract phase was 0% when it was the aqueous continuous phase and about 0.5% acetone when it was the organic dispersed phase.

The column was then filled with the continuous phase and the agitator adjusted to the required speed. The dispersed phase was introduced into the column and its flowrate adjusted to the set for the experiment. When an interface level was attained the continuous phase flowrate was adjusted to the required value. Initial runs were carried out to determine the time taken for the column to reach steady state conditions and this was done by taking 20 ml. samples from the outlet streams at 3 minute intervals until identical acetone concentrations were obtained for consecutive time intervals. This was found to be about 15 minutes. After steady state conditions had been reached, 20 mls samples were taken from the sample ports along the column and at the respective outlets. Drop size and hold-up were measured as described earlier in Section 6.2.1 and 7.2.2.

Results of the mass transfer runs in each direction of transfer were evaluated and the mass transfer coefficient calculated as discussed in Section 8.2.

CHAPTER EIGHT

Treatment of Results.

Application of published work (28, 29, 31, 32, 33, 78, 93, 114) to large scale an R.D.C. is very limited. Most of this work has been based on small scale R.D.C. data and sometimes for one specific system. So the treatment of the results of this work have been directed to provide a better understanding of large scale R.D.C. hydrodynamics as well as the mass transfer performance.

8.1 Non-Mass Transfer Studies

8.1.1 Flooding

The flooding data used to plot Figure 7.1 is presented in Table 8.1 below. These data have been used to test Logsdail, Thornton and Pratt (28) flooding relation as

$$V_{d.f} = 2\ \overline{V}_N\ X_f^2(1-x_f) \qquad (8.1)$$

where x_f is the dispersed phase hold-up at a flooding point and can be estimated by Equation 3.13

$$x_f = \frac{(L-8L)^{0.5}-3L}{4(1-L)} \qquad (3.13)$$

where $L = \frac{V_{d.f}}{V_{c.f}}$ (8.2)

The characteristic velocity $\overline{V}_N$ was evaluated from experimental data under conditions of flooding by substituting $V_{d.f}$ and $V_{c.f}$ into Equation 3.13 to give x_f for each determination; then plotting $v_{d.f}$ against $x_f^2(1-x_f)$ in accordance with Equation 8.1. Values of $\overline{V}_N$ were obtained from the slopes of the lines shown in Figure 8.1, equal to $2\overline{V}_N$.

Table 8.1 Flooding Data

$V_{c.f}$ cm/sec	$V_{d.f}$ cm/sec		
	200 r.p.m.	250 r.p.m.	300 r.p.m.
0.587	0.849	0.760	0.692
0.660	0.760	0.681	0.605
0.756	0.671	0.597	0.524
0.901	0.576	0.503	0.445

8.1.2 Drop Size

The observed Sauter mean drop size d_{32} values were compared with the predicted values by most of the published correlations (31, 32, 33, 57, 93). Large differences have been observed in most cases. Therefore

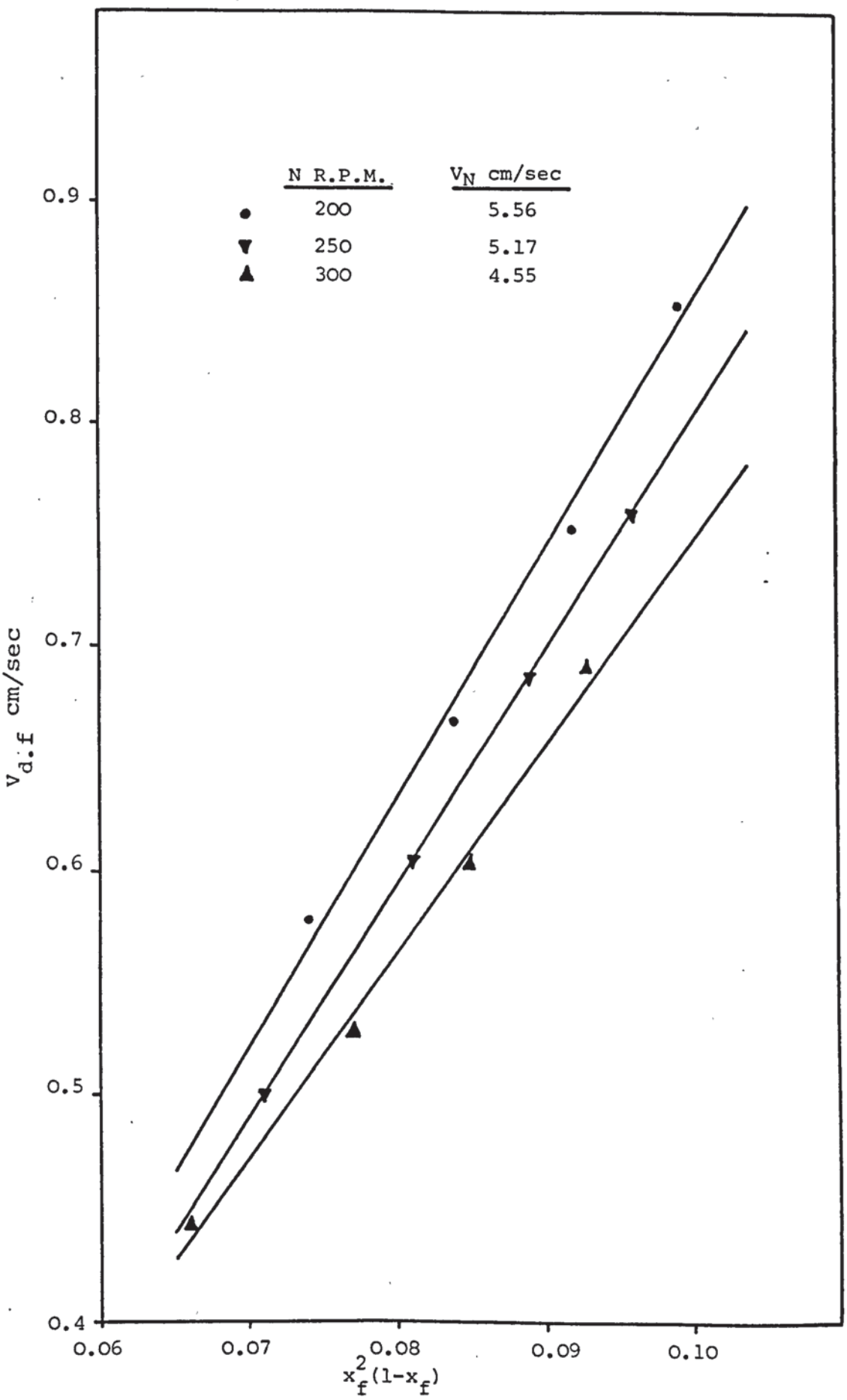

Fig. 8.1 Correlation of Flooding Data

to produce a more realistic model the drop size results obtained from this study have been correlated as a function of the following dimensionless groups

$$\frac{d_{32}}{D_r} \propto \left[\frac{V_d H \rho_c}{\mu_c X}\right]^a \left[\frac{N^2 D_r^3 \rho_c}{\sigma}\right]^b \left[\frac{V_d^2}{g_c D_c X^2}\right]^c \left[\frac{n}{N_c}\right]^d \qquad (8.3)$$

A multilinear least square computer program was written (Appendix 5) and applied to estimate the values of the exponents and the resulting correlation is represented by equation (8.4)

$$\frac{d_{32}}{D_r} = 5.52 \times 10^{-8} \left[\frac{V_d H \rho_c}{\mu_c X}\right]^{1.14} \left[\frac{N^2 D_r^3 \rho_c}{\sigma}\right]^{-0.14} \left[\frac{V_d^2}{g_c D_c X^2}\right]^{-0.38} \left[\frac{n}{N_c}\right]^{-0.06} \qquad (8.4)$$

By extending the dimensional analysis in Equation 8.3 to include the column dimensions group $\left[\frac{H}{D_c - D_s}\right]^e$ as well as the density difference group $\left[\frac{\Delta\rho}{\rho_c}\right]^f$ and by analysing published results (78, 114) together with the results of this study the following correlation was obtained

$$\frac{d_{32}}{D_r} = 1.48 \left[\frac{V_d H \rho_c}{\mu_c X}\right]^{-0.23} \left[\frac{N^2 D_r^3 \rho_c}{\sigma}\right]^{-0.004} \left[\frac{V_d^2}{g_c D_c X^2}\right]^{0.44} \left[\frac{\Delta\rho}{\rho_c}\right]^{-0.57} \left[\frac{H}{D_c - D_s}\right]^{-0.24} \left[\frac{n}{N_c}\right]^{-0.07} \qquad (8.5)$$

8.1.3 Drop Size Distribution

Figure 7.4 shows the drop size distribution as drop cumulative volume against drop diameter for compartment No. 14 for two rotor speeds, viz 200 and 300 r.p.m. The cumulative volume of the drop size sample is calculated as

$$v = \Sigma n_i \left(\frac{\pi}{6} d_i^{\,3}\right) \qquad (8.6)$$

Appendix 3 shows a sample of calculation of the drop size distribution. Log-probability graph paper was used to plot the drop size cumulative volume against the drop diameter. From this graph d_{10}, d_{50} and d_{90} were determined and the upper limit distribution parameters d_m, a' and δ were calculated by applying equations proposed by Mugele and Evans (108) as

$$\frac{d_m}{d_{50}} = \frac{d_{50}(d_{90}+d_{10}) - 2d_{90}d_{10}}{d_{50}^{\,2} - d_{90}d_{10}} \qquad (8.7)$$

$$a' = \frac{d_m - d_{50}}{d_{50}} \qquad (8.8)$$

$$\delta = \frac{0.907}{\ln\left[\frac{d_{90}}{d_m - d_{90}} - \frac{d_m - d_{50}}{d_{50}}\right]} \qquad (8.9)$$

The drop size distribution function of Mugele and Evans (Equation 4.8) was compared with the experimental drop size distribution. These comparisons are shown in Figure 8.2A and 8.2B. A further check to the agreement of the upper limit distribution law of Mugele and Evans with the experimental distribution were carried out by comparing d_{32} for the data calculated from Equation 7.1 and d'_{32} from the upper limit distribution as in Equation 4.13

$$d'_{32} = \frac{d_m}{1+a' e^{0.25\delta^{-2}}} \qquad (4.13)$$

The deviation of d'_{32} from that of d_{32} is 5.2% at 200 r.p.m. and 3.6% at 300 r.p.m.

8.1.4 Dispersed Phase Hold-up

All the correlations proposed to calculate the dispersed phase hold-up in an R.D.C. have been compared with the experimental values of this study and great divergencies have been found as shown in Figure 8.5.

The dispersed phase hold-up has in the past been analysed in one of two ways. In the first the hold-up is considered to be a function of the characteristic velocity $\overline{V}_N$. Secondly, the hold-up has been correlated by dimensional analysis. In the first method it was assumed that Equation 3.9 is applicable to an R.D.C., and studies were directed to the production of a more

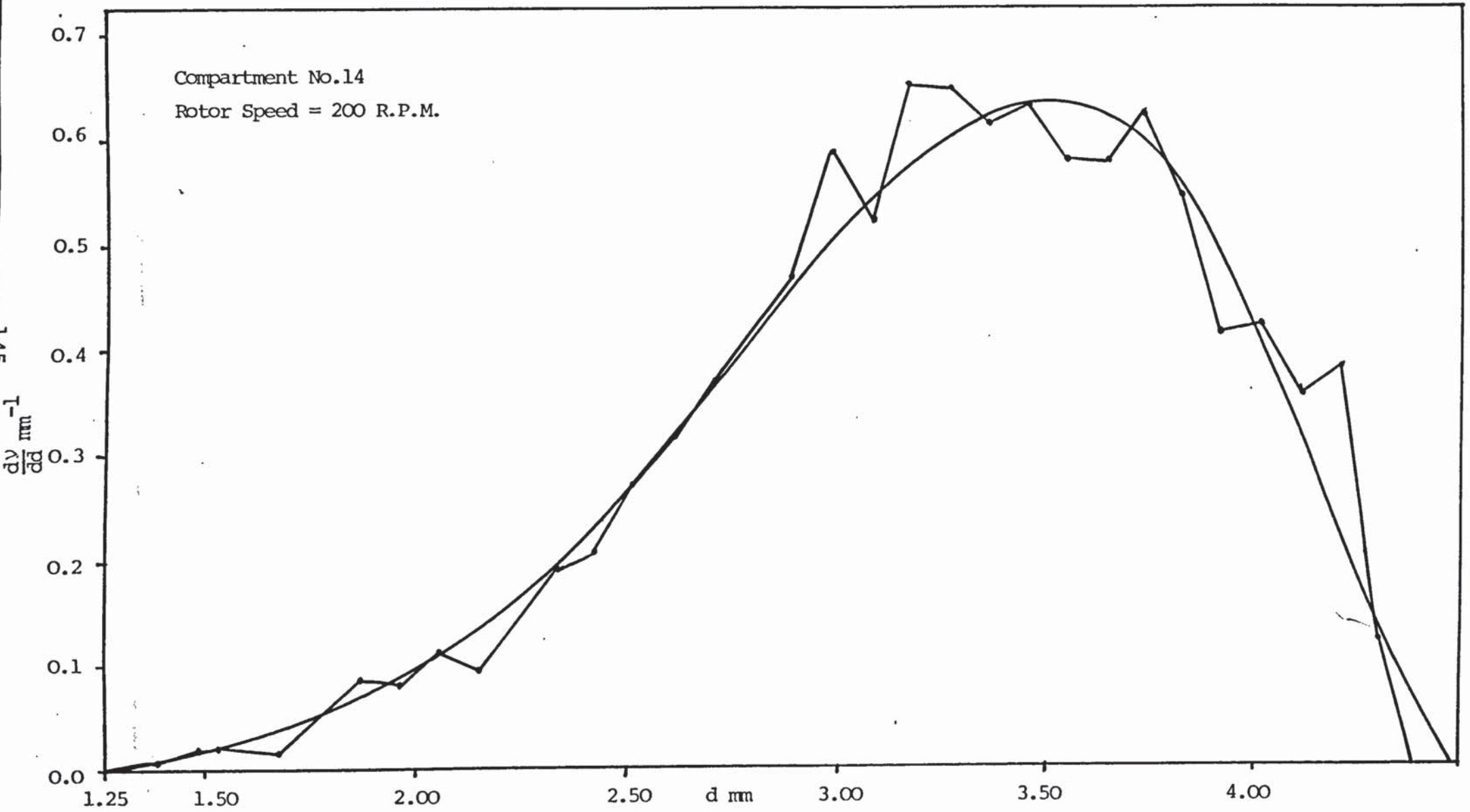

Figure 8.2A - Comparison of Experimental Drop Size Distribution with Upper Limit Distribution Function

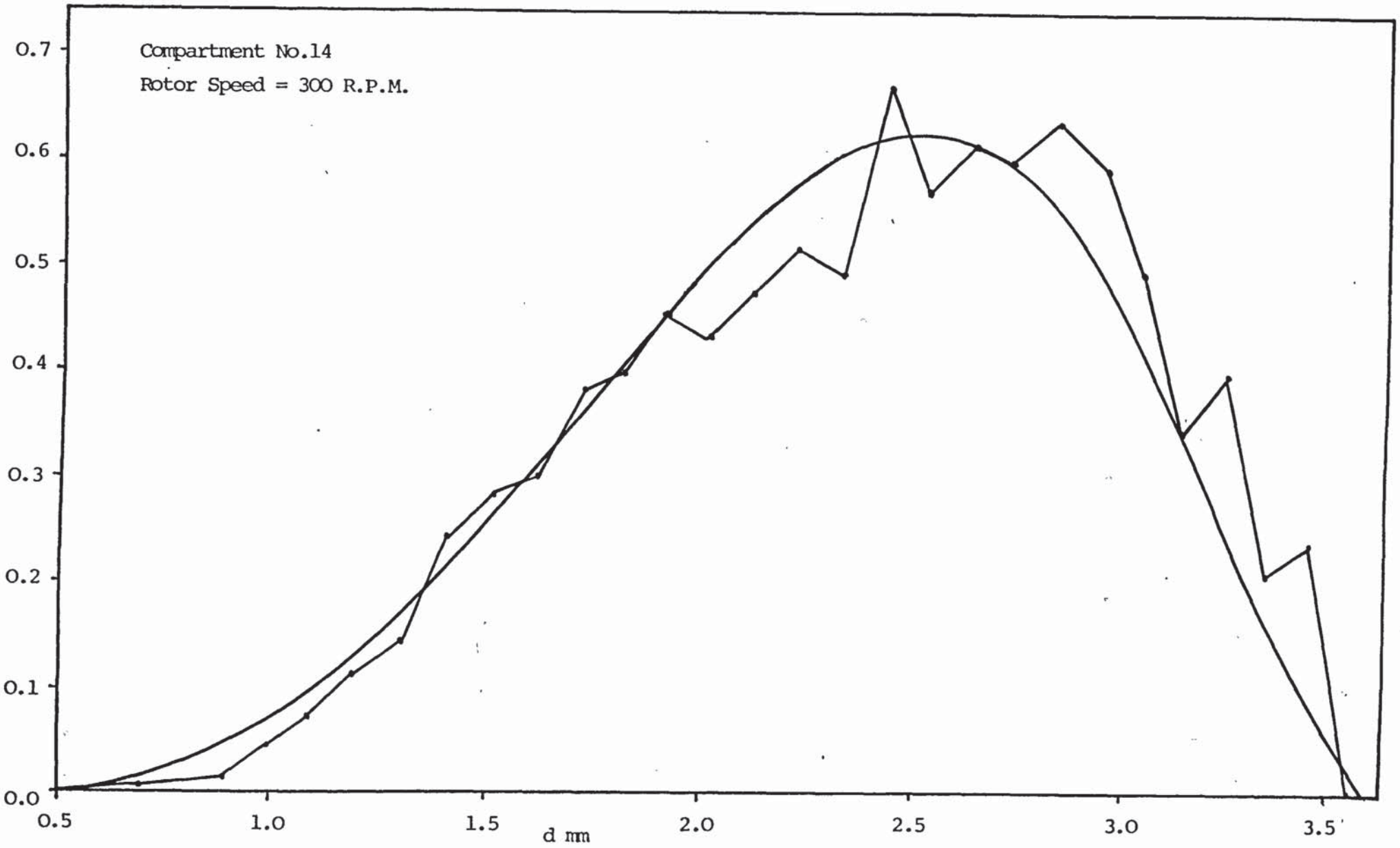

Figure 8.2B - Comparison of Experimental Drop Size Distribution with Upper Limit Distribution Function

accurate correlation for V_N as a function of the physical properties of the system and the column geometry. Since all the correlations previously published were based on results obtained from columns of small diameter and due to the large divergences showed in Figure 8.3 by these correlations from that of the experimental values, an attempt was made to produce a new correlation from which the characteristic velocity V_N can be determined as a function of the physical properties of the system and the column geometry. This was done by determining the experimental values of V_N from Equation 3.9 after rearrangement as follows

$$V_N = \frac{V_d}{X(1-X)} + \frac{V_c}{(1-X)^2} \qquad (8.10)$$

where V_d, V_c and X are the experimental measured values. Then V_N was correlated with the typical dimensionless groups as those used in the previously published correlations. By using the multilinear least square computer regression program (Appendix 5), the new characteristic velocity correlation with the new exponents is

$$\frac{V_N \mu_c}{\sigma} = 6.24 \times 10^{-3} \left[\frac{\Delta\rho}{\rho_c}\right]^{0.783} \left[\frac{g_c}{D_r N^2}\right]^{0.234} \left[\frac{D_s}{D_r}\right]^{1.778} \left[\frac{H}{D_r}\right]^{1.362} \left[\frac{D_r}{D_c}\right]^{1.922} \qquad (8.11)$$

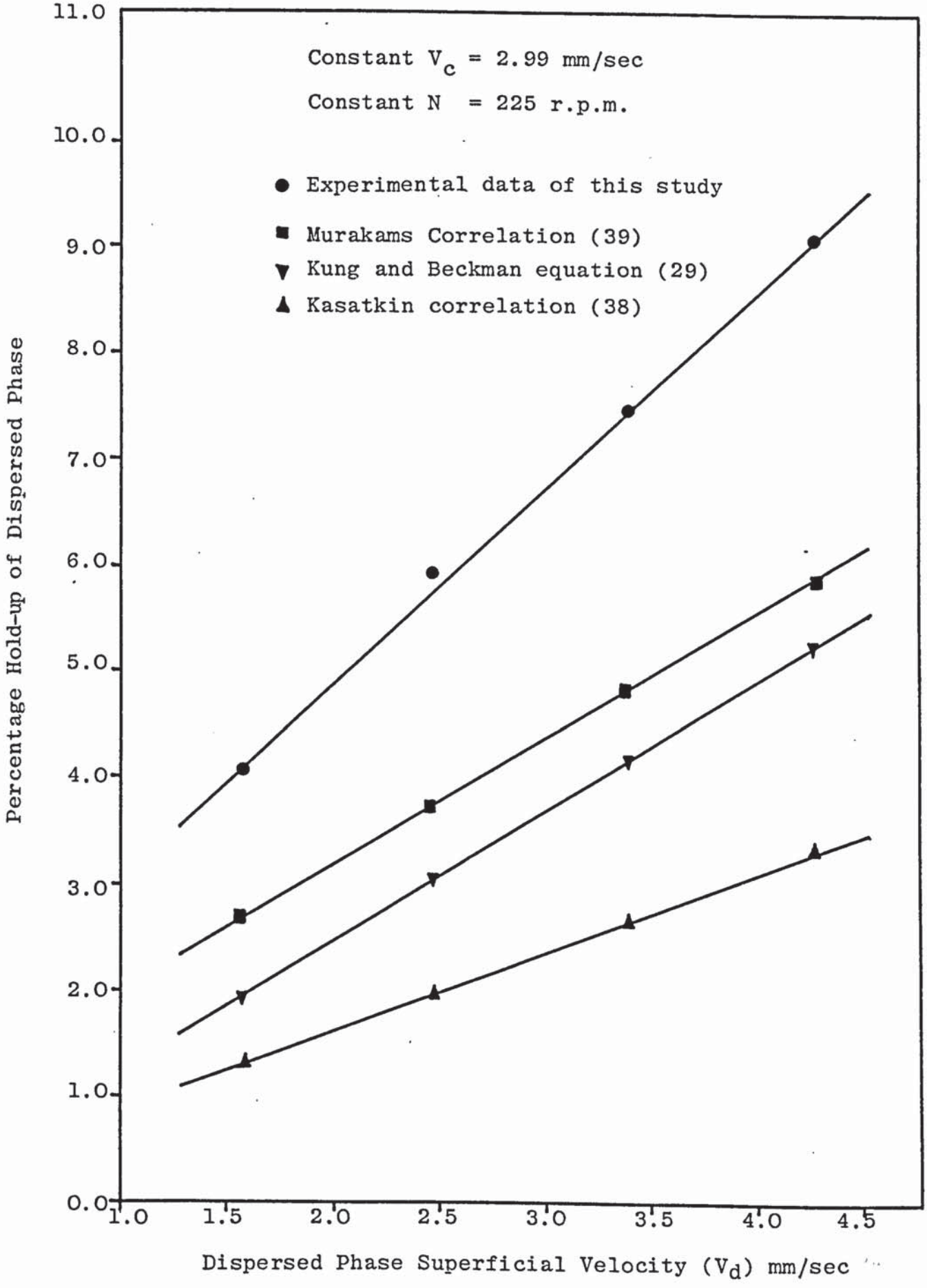

Figure 8.3 - Comparison of experimental hold-up data with that predicted from previously published correlations.

Some of the published data (28, 29, 182) for small R.D.C.'s have again been analysed together with the results of this work and the correlation produced is

$$\frac{V_N \mu_c}{\sigma} = 4.45 \times 10^{-4} \left[\frac{\Delta\rho}{\rho c}\right]^{-0.941} \left[\frac{g_c}{D_r N^2}\right]^{0.205} \left[\frac{D_s}{D_r}\right]^{1.601} \left[\frac{H}{D_r}\right]^{0.689} \left[\frac{D_r}{D_c}\right]^{1.786} \qquad (8.12)$$

In the second approach the dispersed phase hold-up was correlated as a function of the physical properties of the system, the column geometry and the power input in the rotor. The hold-up was found to be dependent on the same dimensionless group as follows (38, 39)

$$X\alpha \left[\frac{NDr}{Vc}\right]^a \left[\frac{V_d}{V_c}\right]^b \left[\frac{D_s^2 - D_r^2}{D_c^2}\right]^c \left[\frac{H}{D_c}\right]^d \left[\frac{D_r}{D_c}\right]^e \left[\frac{\Delta\rho}{\rho_c}\right]^f \left[\frac{\rho_c V_c D_c^2}{\sigma}\right]^g \left[\frac{V_c^2}{g_c D_c}\right]^h \left[\frac{\rho_c V_c D_c}{\mu_c}\right]^i \qquad (8.13)$$

The values of the exponents were estimated by applying the regression computer program and by using the data of this work as well as previous reported data (28, 29, 182). The resulting correlation is

$$X = 1.05\times10^{14}\left[\frac{ND_r}{V_c}\right]^{0.521}\left[\frac{V_d}{V_c}\right]^{0.775}\left[\frac{D_s^2-D_r^2}{D_c^2}\right]^{-0.187}$$

$$\left[\frac{H}{D_c}\right]^{-0.873}\left[\frac{D_r}{D_c}\right]^{0.201}\left[\frac{\Delta\rho}{\rho c}\right]^{4.843}\left[\frac{\rho_c D_c V_c^2}{\sigma}\right]^{1.082}$$

$$\left[\frac{V_c^2}{g_c D_c}\right]^{0.892}\left[\frac{\rho_c V_c D_v}{\mu_c}\right]^{-2.367} \qquad (8.14)$$

8.2 Mass Transfer Coefficient

8.2.1 Experimental Mass Transfer Coefficient

The overall experimental dispersed phase mass transfer coefficient under each set of operating conditions was calculated using Equation 1.1

$$N = K\ A(\Delta\ C_m) \qquad (1.1)$$

where N is the rate of mass transfer which is calculated from the mass balance across the column. A is the interfacial area which is estimated by using Equation 1.3 which is

$$a = \frac{6_x}{d_{32}} \qquad (8.15)$$

where a is the specific interfacial area as cm^2 per cm^3 of the column volume. Hence

$$A = a \cdot V \tag{8.16}$$

where V is the total column volume.

Simpson's Rule was applied to determine the actual mean driving force (ΔC_m) by using the acetone concentration profile along the column. Acetone concentration was measured in samples of the continuous phase taken from compartment number 1, 3, 6, 9 and 12. The driving force in these compartments can be determined as Δy_1, Δy_3, Δy_6, Δy_9 and Δy_{12} respectively, where

$$\Delta y = y^* - y \tag{8.17}$$

and y is the acetone concentration the aqueous phase. So Simpson's Rule is

$$\Delta y_m = \frac{1}{18}\left[\Delta y_{in} + 4\Delta y_1 + 2\Delta y_3 + 4\Delta y_6 + 2\Delta y_9 + 4\Delta y_{12} + \Delta y_{out}\right] \tag{8.18}$$

Δy_m was then converted to ΔC_m by dividing it by the extract phase density.

So the overall experimental mass transfer coefficient can be calculated as

$$K_{Exp} = \frac{N}{A \Delta C_m} \tag{8.19}$$

Tables 8.2 and 8.3 shows the results of the mass transfer coefficient and Appendix 4 shows a sample of the mass transfer coefficient calculation.

8.2.2 Theoretical Mass Transfer Coefficient

A novel method of calculation has been carried out to evaluate the overall theoretical dispersed phase mass transfer coefficient K_{cal}. These calculations involve the use of the drop distribution diagram to determine the volume percentage of the stagnant, circulating and oscillating drops in the drop sample population, and compartment No.6 has been taken as the representative compartment for the whole column. Droplet Reynolds number has been used as a measure of the state of the drops as follows (125, 132, 146)

Stagnant drops	$Re < 10$
Circulating drops	$10 < Re < 200$
Oscillating drops	$Re > 200$

where droplet Reynolds number is

$$Re = \frac{d\rho_c V_o}{\mu_c} \qquad (8.20)$$

where d is the drop diameter and V_o is the vertical relative velocity of drops in the RDC determined by applying Misek's equation (46)

$$V_o = \left[\frac{V_d}{X} + \frac{V_c}{1-X}\right] \qquad (8.21)$$

Table 8.2 Mass Transfer Results

Run No.	Direction of Transfer	N RPM	V_c cm/sec	V_d cm/sec	X_{in}	X_{out}	y_{in}	y_{out}
1	D→C	150	0.66	0.28	1.45	0.34	0.00	0.37
2	"	200	0.66	0.28	1.45	0.22	0.00	0.41
3	"	250	0.66	0.28	1.45	0.19	0.00	0.42
4	"	300	0.66	0.28	1.45	0.19	0.00	0.42
5	"	0.0	0.66	0.28	2.20	0.82	0.00	0.46
6	"	150	0.66	0.28	2.20	0.41	0.00	0.60
7	"	200	0.66	0.28	2.20	0.33	0.00	0.62
8	"	300	0.66	0.28	2.20	0.27	0.00	0.64
9	"	150	0.31	0.24	3.03	1.24	0.00	1.09
10	"	200	0.31	0.24	3.03	1.14	0.00	1.15
11	"	250	0.31	0.24	3.03	1.06	0.00	1.20
12	"	300	0.31	0.24	3.03	0.98	0.00	1.25
13	"	100	0.31	0.28	3.96	1.58	0.00	1.70
14	"	200	0.31	0.28	3.96	1.34	0.00	1.87
15	"	300	0.31	0.28	3.96	1.18	0.00	1.98
16	"	350	0.31	0.28	3.96	1.09	0.00	2.05
17	"	100	0.31	0.28	4.91	2.28	0.00	1.88
18	"	150	0.31	0.28	4.91	2.12	0.00	1.99
19	"	200	0.31	0.28	4.91	1.81	0.00	2.21
20	"	300	0.31	0.28	4.91	1.48	0.00	2.45

(Cont..)

Table 8.2 (Cont..)

Run No.	Direction of Transfer	N RPM	V_c cm/sec	V_d cm/sec	X_{in}	X_{out}	y_{in}	y_{out}
21	D←C	100	0.31	0.24	0.45	1.10	5.52	5.12
22	"	150	0.31	0.24	0.45	1.22	5.52	5.05
23	"	200	0.31	0.24	0.45	1.28	5.52	5.01
24	"	300	0.31	0.24	0.45	1.32	5.52	4.98

Table 8.3 Mass Transfer Results.

Run No.	N gm/sec	Hold-up %	Eff. column height cm	d_{32} cm	Inter-facial area A cm^2	Δ Cm gm/cm^3	K_{Exp} cm/sec
1	3.84	3.98	367	0.46	303010.1	0.064	1.96×10^{-4}
2	4.25	4.52	371	0.35	457204.1	0.054	1.72×10^{-4}
3	4.35	5.02	367	0.31	567118.6	0.053	1.45×10^{-4}
4	4.35	5.76	369	0.24	845090.9	0.053	9.71×10^{-5}
5	4.76	0.90	373	0.54	59323.0	0.113	7.10×10^{-4}
6	6.21	3.95	363	0.49	279237.3	0.102	2.18×10^{-4}
7	6.46	4.68	361	0.36	447833.3	0.079	1.83×10^{-4}
8	6.67	6.03	363	0.26	803371.5	0.071	1.17×10^{-4}
9	5.31	3.16	356	0.51	21049.6	0.166	1.52×10^{-4}
10	5.61	3.78	358	0.37	349010.8	0.157	1.02×10^{-4}
11	5.85	4.29	360	0.32	460548.8	0.152	8.36×10^{-5}
12	6.08	5.51	378	0.24	828128.9	0.148	4.96×10^{-5}
13	8.27	2.82	359	0.51	182277.7	0.221	2.05×10^{-4}
14	9.10	3.70	357	0.39	323199.8	0.184	1.53×10^{-4}
15	9.65	4.74	371	0.26	645423.4	0.177	8.45×10^{-5}
16	9.97	6.62	373	0.21	1122052.9	0.167	5.32×10^{-5}
17	9.13	2.61	356	0.54	164196.0	0.283	1.96×10^{-4}
18	9.69	2.82	358	0.52	185265.5	0.258	2.03×10^{-4}
19	10.77	3,34	355	0.44	257150.8	0.241	1.74×10^{-4}
20	11.91	4..10	360	0.32	434038.3	0.226	1.21×10^{-4}

Table 8.3 (Cont..)

Run No.	N gm/sec	Hold-up %	Eff. column height cm	d_{32} cm	Inter-facial area A cm^2	Δ Cm gm/cm^3	K_{Exp} cm/sec
21	1.94	3.08	385	0.310	365012.2	0.0124	4.29×10^{-4}
22	2.28	4.39	377	0.304	519505.2	0.0185	2.37×10^{-4}
23	2.48	5.53	362	0.288	663282.9	0.0207	1.81×10^{-4}
24	2.60	6.24	355	0.252	838822.4	0.0211	1.47×10^{-4}

to find the maximum diameter of the stagnant drops in the whole drop population, set Re=10

$$\frac{d_s \rho_c V_o}{\mu_c} = 10 \qquad (8.22)$$

where d_s is the maximum diameter of the stagnant drops regime To find the minimum diameter of oscillating drops regime. Set

$$Re = 200$$

$$\frac{d_o \rho_c V_o}{\mu_c} = 200 \qquad (8.23)$$

where d_o is the minimum diameter of the oscillating drops regime. The circulating drops regime is determined in what between d_s and d_o. As it shows in Table 8.4, d_s is too small to be analysed by the technique used in this study (Section 7.1.2). So the drop population was considered to contain circulating and oscillating drops only with d_o the boundary between the two regimes.

(i) Circulating Drops Regime

Volume percentages of the circulating drops was determined from the drop distribution diagrams. The individual mass transfer coefficients of the dispersed and continuous phase for the circulating drop were calculated as follows:

a) Dispersed phase mass transfer coefficient was estimated by the Kronig and Brink (138) equation

Table 8.4 Results of Calculation of Vo, ds and do

Run No.	Direction of Transfer	N RPM	V_c cm/ sec	V_d cm/ sec	X %	V_o cm/ sec	d_s cm	d_o cm
1	D→C	150	0.66	0.28	3.98	7.72	0.014	0.266
2	"	200	0.66	0.28	4.52	6.89	0.015	0.298
3	"	250	0.66	0.28	5.02	6.27	0.016	0.328
4	"	300	0.66	0.28	5.76	5.56	0.018	0.370
5	"	0.0	0.66	0.28	0.90	31.78	0.003	0.065
6	"	150	0.66	0.28	3.95	7.78	0.013	0.264
7	"	200	0.66	0.28	4.68	6.68	0.015	0.308
8	"	300	0.66	0.28	6.03	5.35	0.019	0.384
9	"	150	0.31	0.24	3.16	7.92	0.013	0.260
10	"	200	0.31	0.24	3.78	6.67	0.015	0.308
11	"	250	0.31	0.24	4.29	5.92	0.017	0.347
12	"	300	0.31	0.24	5.51	4.68	0.022	0.439
13	"	100	0.31	0.28	2.82	10.25	0.010	0.201
14	"	200	0.31	0.28	3.70	7.89	o.013	0.261
15	"	300	0.31	0.28	4.74	6.23	0.017	0.330
16	"	350	0.31	0.28	6.62	4.56	0.023	0.451
17	"	100	0.31	0.28	2.61	11.05	0.009	0.186
18	"	150	0.31	0.28	2.82	10.25	0.010	0.201
19	"	200	0.31	0.28	3.34	8.70	0.012	0.236
20	"	300	0.31	0.28	4.10	7.15	0.014	0.288

Table 8.4 (Cont..)

Run No.	Direction of Transfer	N RPM	V_c cm/ sec	V_d cm/ sec	X %	V_o cm/ sec	d_s cm	d_o cm
21	D←C	100	0.31	0.24	3.08	8.11	0.013	0.255
22	"	150	0.31	0.24	4.39	5.79	0.018	0.358
23	"	200	0.31	0.24	5.53	4.67	0.022	0.444
24	"	300	0.31	0.24	6.24	4.18	0.025	0.496

$$k_{d.c} \simeq \frac{17.9 D_d}{\bar{d}_c} \qquad (8.24)$$

where $\bar{d}_c$ is the circulating drop mid-sector diameter and D_d is the molecular diffusion of acetone in the dispersed phase, estimated by Wilke and Pin Chang (181) correlation.

b) Continuous phase mass transfer coefficient was estimated by Garner et al (154) correlation
Equation 5.40

$$\frac{k_{c.c}\bar{d}_c}{D_c} = -126 + 1.8\ Re^{0.5}\ Sc^{0.42} \qquad (5.40)$$

where D_c is the molecular diffusion of acetone in the continuous phase estimated by as in D_d.

The overall mass transfer coefficient of the circulating drops $K_{o.c}$ is calculated as

$$\frac{1}{K_{o.c}} = \frac{1}{k_{d.c}} + \frac{m}{k_{c.c}} \qquad (8.25)$$

Results of the circulating drop coefficients shown in Table 8.5.

(ii) Oscillating Drops Regime

The rest of the drop population was considered as the oscillating drop regime. The individual mass transfer coefficients of the dispersed and continuous phases for this regime were calculated as follows:

Table 8.5 Circulating Drop Coefficient

Run No.	Direction of Transfer	$k_{d.c}$ cm/sec	$k_{c.c}$ cm/sec	$K_{o.c}$ cm/sec	ν
1	D→C	8.46×10^{-6}	1.75×10^{-3}	8.19×10^{-6}	0.005
2	"	8.94×10^{-6}	1.19×10^{-3}	8.47×10^{-6}	0.300
3	"	1.03×10^{-5}	1.42×10^{-3}	9.80×10^{-6}	0.400
4	"	1.01×10^{-5}	1.26×10^{-3}	9.54×10^{-6}	0.750
5	"	4.01×10^{-5}	5.41×10^{-3}	3.80×10^{-5}	0.001
6	"	8.70×10^{-6}	1.80×10^{-3}	8.40×10^{-6}	0.004
7	"	1.16×10^{-5}	1.50×10^{-3}	1.10×10^{-5}	0.300
8	"	9.37×10^{-6}	1.23×10^{-3}	8.72×10^{-6}	0.800
9	"	8.80×10^{-6}	1.82×10^{-3}	8.50×10^{-6}	0.003
10	"	9.29×10^{-6}	1.49×10^{-3}	8.89×10^{-6}	0.200
11	"	9.68×10^{-6}	1.35×10^{-3}	9.20×10^{-6}	0.600
12	"	9.29×10^{-6}	1.13×10^{-3}	8.76×10^{-6}	0.900
13	"	1.16×10^{-6}	2.31×10^{-3}	1.12×10^{-5}	0.002
14	"	1.08×10^{-5}	1.81×10^{-3}	1.04×10^{-5}	0.028
15	"	9.64×10^{-5}	1.46×10^{-3}	9.19×10^{-6}	0.750
16	"	1.04×10^{-6}	1.11×10^{-3}	9.75×10^{-6}	0.930
17	"	1.27×10^{-5}	2.62×10^{-3}	1.23×10^{-5}	0.001
18	"	1.13×10^{-5}	2.34×10^{-3}	1.09×10^{-5}	0.002
19	"	1.01×10^{-5}	2.00×10^{-3}	9.74×10^{-6}	0.023
20	"	9.29×10^{-5}	1.65×10^{-3}	8.92×10^{-6}	0.500

(Cont..)

Table 8.5 (Cont..)

Run No.	Direction of Transfer	$k_{d.c}$ cm/sec	$k_{c.c}$ cm/sec	$K_{o.c}$ cm/sec	ν
21	D←C	1.29×10^{-5}	1.54×10^{-3}	1.22×10^{-5}	0.110
22	"	8.45×10^{-6}	1.06×10^{-3}	7.98×10^{-6}	0.550
23	"	8.07×10^{-6}	9.22×10^{-4}	7.58×10^{-6}	1.000
24	"	9.22×10^{-6}	9.26×10^{-4}	9.59×10^{-6}	1.000

a) Dispersed phase mass transfer coefficient was first estimated by Rose and Kintner (125) Equation 5.28.

$$k_{d.o} = 0.45\ (D_d\ \omega)^{0.5} \qquad (5.28)$$

and then by Angelo et al (118) equation

$$k_{d.o} = \frac{\sqrt{4D_d\omega(1+\varepsilon+\frac{3}{8}\varepsilon^2)}}{\pi} \qquad (8.26)$$

where ε is the eccentricity which is estimated by Al-Hassan's (135) correlation as

$$\varepsilon = 0.434\ \left(\frac{\omega\bar{d}_o}{V_o}\right)^{-0.46} \left(\frac{\bar{d}_o V_o^2\ \rho_c}{\sigma}\right)^{-0.53} \left(\frac{\mu V_o}{\sigma}\right)^{-0.11} \qquad (8.27)$$

where $\bar{d}_o$ is the oscillating drop mid-sector diameter.

b) Continuous phase mass transfer coefficient was estimated by Garner et al (126) correlation equation 5.42.

$$\frac{k_{c.o}\bar{d}_c}{D_c} = 50 + 0.0085\ Re\ Sc^{0.7} \qquad (5.42)$$

The overall mass transfer coefficient of the oscillating drop $K_{o.o}$ was first estimated as follows:

$$\frac{1}{K_{o.o}} = \frac{1}{k_{d.o}} + \frac{m}{k_{c.o}} \qquad (8.28)$$

where $k_{d.o}$ is the dispersed phase coefficient calculated

by Rose and Kintner (125) equation. Secondly by Angelo et al (118) equation as

$$K_{o.o} = k_{d.o}\left[\frac{1}{1+m\sqrt{\frac{D_d}{D_c}}}\right] \qquad (8.29)$$

where $K_{d.o}$ is the dispersed phase coefficient calculated by Angelo et al (118). Results of the oscillating drop coefficients presented in Table 8.6. The theoretical mass transfer coefficient for the whole drop population was then calculated as

$$K_{cal} = K_{o.c}\,\nu + K_{o.o}\,(1-\nu) \qquad (8.30)$$

Two values of K_{cal} were obtained for each run, this is correspond two values of $K_{o.o}$, first from Rose et al (125) and Garner et al (126) correlations and the second $K_{o.o}$ from Angelo et al (118) correlations. Table 8.7 presenting K_{cal} values together with the experimental K_{Exp}.

Table 8.6 Oscillating Drop Coefficients

Run No.	Direction of Transfer	1-ν	Rose et al (125) - Garner et al (126)			Angelo et al (118)	
			$k_{d.o}$	$k_{c.o}$	$K_{o.o}(1)$	$k_{d.o}$	$K_{o.o}(2)$
1	D→C	0.995	1.64×10^{-3}	2.14×10^{-3}	2.48×10^{-4}	5.06×10^{-3}	5.68×10^{-4}
2	"	0.700	1.92×10^{-3}	1.91×10^{-3}	2.29×10^{-4}	5.26×10^{-3}	5.91×10^{-4}
3	"	0.600	1.98×10^{-3}	1.75×10^{-3}	2.12×10^{-4}	6.59×10^{-3}	7.40×10^{-4}
4	"	0.250	1.87×10^{-3}	1.55×10^{-3}	1.90×10^{-4}	5.93×10^{-3}	6.65×10^{-4}
5	"	0.999	1.47×10^{-3}	8.78×10^{-3}	6.59×10^{-4}	3.97×10^{-3}	4.46×10^{-4}
6	"	0.996	1.57×10^{-3}	2.16×10^{-3}	2.48×10^{-4}	4.84×10^{-3}	5.41×10^{-4}
7	"	0.700	1.91×10^{-3}	1.86×10^{-3}	2.24×10^{-4}	6.11×10^{-3}	6.86×10^{-4}
8	"	0.200	1.81×10^{-3}	1.49×10^{-3}	1.83×10^{-4}	6.03×10^{-3}	4.77×10^{-4}
9	"	0.997	1.53×10^{-3}	2.20×10^{-3}	2.50×10^{-4}	4.66×10^{-3}	5.23×10^{-4}
10	"	0.800	1.87×10^{-3}	1.86×10^{-3}	2.23×10^{-4}	5.63×10^{-3}	6.32×10^{-4}
11	"	0.400	1.94×10^{-3}	1.65×10^{-3}	2.01×10^{-4}	6.24×10^{-3}	7.01×10^{-4}
12	"	0.100	1.66×10^{-3}	1.30×10^{-3}	1.61×10^{-4}	5.83×10^{-3}	6.55×10^{-4}
13	"	0.998	1.53×10^{-3}	2.84×10^{-3}	3.09×10^{-4}	4.45×10^{-3}	4.99×10^{-4}
14	"	0.972	1.84×10^{-3}	2.19×10^{-3}	2.57×10^{-4}	5.85×10^{-3}	6.57×10^{-4}
15	"	0.250	1.98×10^{-3}	1.74×10^{-3}	2.11×10^{-4}	5.59×10^{-3}	6.28×10^{-4}
16	"	0.070	1.64×10^{-3}	1.27×10^{-3}	1.57×10^{-4}	5.84×10^{-3}	6.56×10^{-4}
17	"	0.999	1.47×10^{-3}	3.07×10^{-3}	3.25×10^{-4}	4.37×10^{-3}	4.91×10^{-4}
18	"	0.998	1.51×10^{-3}	2.84×10^{-3}	3.08×10^{-4}	4.47×10^{-3}	5.02×10^{-4}
19	"	0.977	1.69×10^{-3}	2.41×10^{-3}	2.75×10^{-4}	5.55×10^{-3}	6.23×10^{-4}

(Cont..)

Table 8.6 (Cont..)

Run No.	Direction of Transfer	1-ν	Rose et al (125) - Garner et al (126)			Angelo et al (118)	
			$k_{d.o}$	$k_{c.o}$	$K_{o.o}(1)$	$k_{d.o}$	$K_{o.o}(2)$
20	D→C	0.500	1.98×10^{-3}	1.99×10^{-3}	2.38×10^{-4}	6.78×10^{-3}	7.61×10^{-4}
21	D←C	0.890	1.94×10^{-3}	2.25×10^{-3}	2.64×10^{-4}	6.10×10^{-3}	6.84×10^{-4}
22	"	0.450	1.87×10^{-3}	1.96×10^{-3}	1.96×10^{-4}	6.13×10^{-3}	6.88×10^{-4}
23	"	0.000	-	-	-	-	-
24	"	0.000	-	-	-	-	-

Table 8.7 Experimental and Theoretical Overall Mass Transfer Coefficients

Run No.	K_{Exp}	$K_{cal}(1)$ Rose and Garner	$K_{cal}(2)$ Angelo et al
1	1.96×10^{-4}	2.47×10^{-4}	5.65×10^{-4}
2	1.72×10^{-4}	1.63×10^{-4}	416×10^{-4}
3	1.45×10^{-4}	1.31×10^{-4}	4.48×10^{-4}
4	9.71×10^{-5}	5.47×10^{-5}	1.73×10^{-4}
5	7.10×10^{-4}	6.58×10^{-4}	4.46×10^{-4}
6	2.18×10^{-4}	2.47×10^{-4}	5.39×10^{-4}
7	1.83×10^{-4}	1.60×10^{-4}	4.84×10^{-4}
8	1.17×10^{-4}	4.36×10^{-5}	1.42×10^{-4}
9	1.52×10^{-4}	2.49×10^{-4}	5.21×10^{-4}
10	1.02×10^{-4}	1.80×10^{-4}	5.07×10^{-4}
11	8.36×10^{-5}	8.59×10^{-5}	2.86×10^{-4}
12	4.96×10^{-5}	2.40×10^{-5}	7.34×10^{-4}
13	2.05×10^{-4}	3.09×10^{-4}	4.98×10^{-4}
14	1.53×10^{-4}	2.50×10^{-4}	6.39×10^{-4}
15	8.45×10^{-5}	5.96×10^{-4}	1.64×10^{-4}
16	5.32×10^{-5}	2.01×10^{-5}	5.50×10^{-4}
17	1.96×10^{-4}	3.25×10^{-4}	4.91×10^{-4}
18	2.03×10^{-4}	3.08×10^{-4}	5.01×10^{-4}
19	1.74×10^{-4}	2.69×10^{-4}	6.09×10^{-4}
20	1.21×10^{-4}	1.23×10^{-4}	3.85×10^{-4}
21	4.29×10^{-4}	2.36×10^{-4}	6.10×10^{-4}
22	2.37×10^{-4}	9.26×10^{-5}	3.14×10^{-4}
23	1.81×10^{-4}	7.58×10^{-6}	7.58×10^{-6}
24	1.47×10^{-4}	8.59×10^{-6}	8.59×10^{-6}

CHAPTER NINE

Discussion of Results.

9.1 Non-Mass Transfer Studies

9.1.1 Flooding

Conventional flooding was observed as described in the literature (25, 26, 33). This was characterised by the complete rejection of the dispersed phase, a dense layer of droplets forming at the heavy phase outlet at the bottom of the column. This phenomena can be explained on the basis of the gravitational and buoyancy force existing in the column at the flooding point. As the flooding point is approached by increasing the dispersed flowrate, at constant continuous phase flowrate and rotor speed, dispersed phase hold-up builds up causing a substantial increase in the continuous phase velocity in the direction opposite to the flow of the dispersed phase. As described in Section 7.1.1 intensive mixing was observed immediately prior to flooding; this is due to drops residing for a longer period in the highly turbulent region, causing severe drops break-up. Flooding therefore

occurs for two reasons, firstly smaller buoyancy forces are associated with smaller droplets and secondly the continuous phase velocity in the opposite direction becomes greater. This causes a dense layer of drops to move downwards until it reaches the heavy phase outlet at the bottom of the column. As previously reported (2, 25, 26) flooding was not an instant phenomenon. The time needed for the column to reach flooding usually depended on the flowrates and rotor speeds; it decreased with increase in rotor speed. This may have arisen due to the rapid increase in the number of smaller drops, accumulating in the column during normal operation near flooding, eventually causing the column to flood prematurely.

As illustrated in Figure 8.1 flooding data ought to be correlated approximately by the characteristic velocity approach of Logsdail et al (28). Good straight lines were in fact obtained for V_d against $X_f^2(1-X_f)$. These lines assist interpolation and, to some extent, extrapolation of the flooding capacity data of this column. However, deviations would be expected at higher flowrates and energy input levels, that is under conditions when the extent of drop-interaction becomes appreciable.

9.1.2 Drop Size

The variation of drop size along the column at different rotor speeds are presented in Figure 7.3. These demonstrate that the drop size changed rapidly in the first four compartments and a stable drop size was not attained

after fourteen compartments when agitator speeds were 300 r.p.m. Very little change was observed in the drop size when the rotor speed was 100 r.p.m.: this may suggest that this speed is below the critical rotor speed which has been defined by Laddha (15): "The energy spent at the rotor may not be sufficient to overcome the interfacial tension force". Generally, droplet break-up occurred as described in Section 4.2, viz by the dynamic pressure acting upon a drop, surpasses the magnitude of the cohesive surface force and the droplet stays in the high-shear zone for sufficient period of time. The above droplet break-up mechanisms can be clearly explained in large R.D.C. due to the high tip speed can be generated even at low rotor speed (2) and the longer paths that droplets follow near the rotating disc which is the high shear zone in the column. Probably these are some of the omitted parameters in the scale-up or the application of a correlation based on a small scale R.D.C. data. This also explains why most of the d_{32} values obtained from previously published correlations (31, 32, 33, 57, 93) were higher than experimental data.

As previously reported (2, 25, 26, 30, 40, 180) continuous phase flowrate has no noticeable affect on the drop size. Generally, as illustrated in Figure 9.1, drop sizes increased with increasing hold-up and dispersed phase flowrate and decreased with increasing rotor speed. The data used in plotting Figure 9.1 were applied to develop the drop size correlation of Equation 8.4. The evaluation of this correlation is shown below.

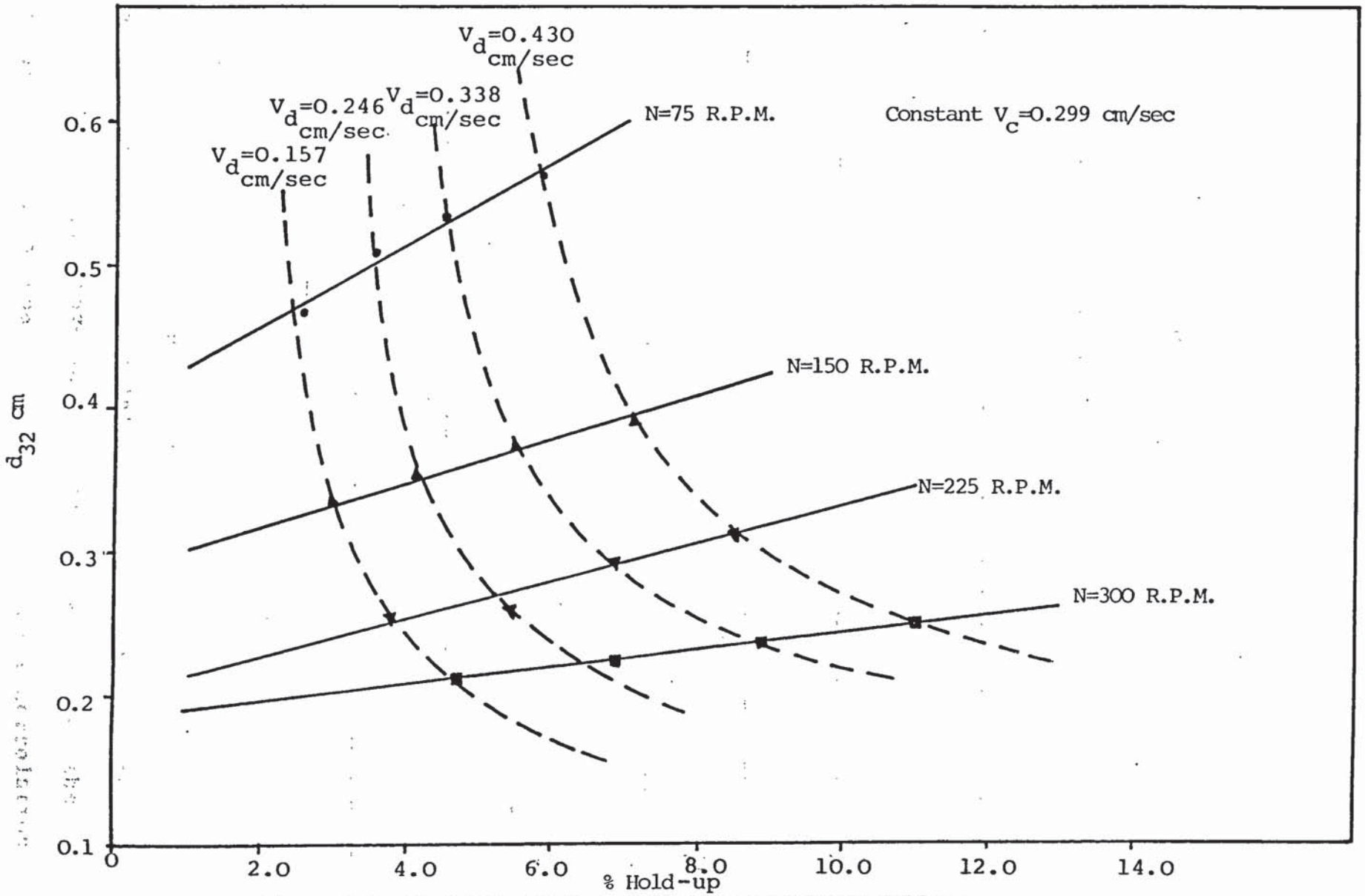

Figure 9.1 Variation of Mean Drop Size Vs Percent Hold-up

$$\frac{d_{32}}{D_r} = 5.52\times10^{-8}\left[\frac{V_d H \rho_c}{\mu_c X}\right]^{1.14}\left[\frac{N^2 D_r^3 \rho_c}{\sigma}\right]^{-0.14}$$

$$\left[\frac{V_d^2}{g_c D_c X^2}\right]^{-0.38}\left[\frac{n}{N_c}\right]^{-0.06} \qquad (8.4)$$

Table 9.1 Evaluation of Correlation 8.4

Group	Group's Range	Term's Range (X^y)	Effect on Predicted Value of d_{32}
$\frac{d_{32}}{D_r}$	0.01 - 0.025	-	-
$\frac{V_d H \rho_c}{\mu_c X}$	7500-17000	2.6×10^4-6.65×10^4	Significant
$\frac{N^2 D_r^3 \rho_c}{\sigma}$	400-7500	0.28-0.43	Significant
$\frac{V_d^2}{g_c D_c X^2}$	0.3×10^{-3}-1.3×10^{-3}	12.5-21.8	Significant
$\frac{n}{N_c}$	0.14-1.00	1.00-1.13	Small

The above table shows the range of the dimensionless groups covered by the above correlation; term's represent the ranges of the dimensionless groups raised to the exponents shown in the correlation. It is clear that the first three groups have very significant effects on the predicted value of d_{32}. The last group in the correlation

$(\frac{n}{N_c})$ accounts for the relative height of the column through the ratio (No. of compartment/total no. of compartment). The small value of 0.06 confirms the very small effect of this group on the prediction of d_{32}. However, the advantage of this group is to assist the prediction of the drop size profile along the column. Comparison between the experimental values and the regression values of d_{32} for the above correlation is shown in Figure 9.2 where it was found that the average percentage error was 8%. The average percentage error was calculated as

$$\% \text{ Average Error} = \frac{\Sigma\sqrt{(\text{Exp. Value} - \text{Reg. Value})^2}}{\text{Number of data points}} \qquad (9.1)$$

Figure 9.2 also shows that 70% of the experimental results were correlated within $\mp$ 10% and 87% within $\mp$ 15%. The second drop size correlation, Equation 8.5 was developed by analysing published results (78, 114) together with the results of this study.

Parameter's Ranges:

Column diameter (D_c)	15.0 - 45.00 cm
Disc diameter (Dr)	7.5 - 22.50 cm
Stator diameter (D_s)	10.0 - 33.75 cm
Compartment height (H)	5.3 - 22.50 cm
Density (ρ_c)	1.00 - 1.14 gm/cm^3
Viscosity (μ_c)	0.0102 - 0.091 gm/cm.sec
Interfacial tension (σ)	26.0 - 50.0 dyne/cm

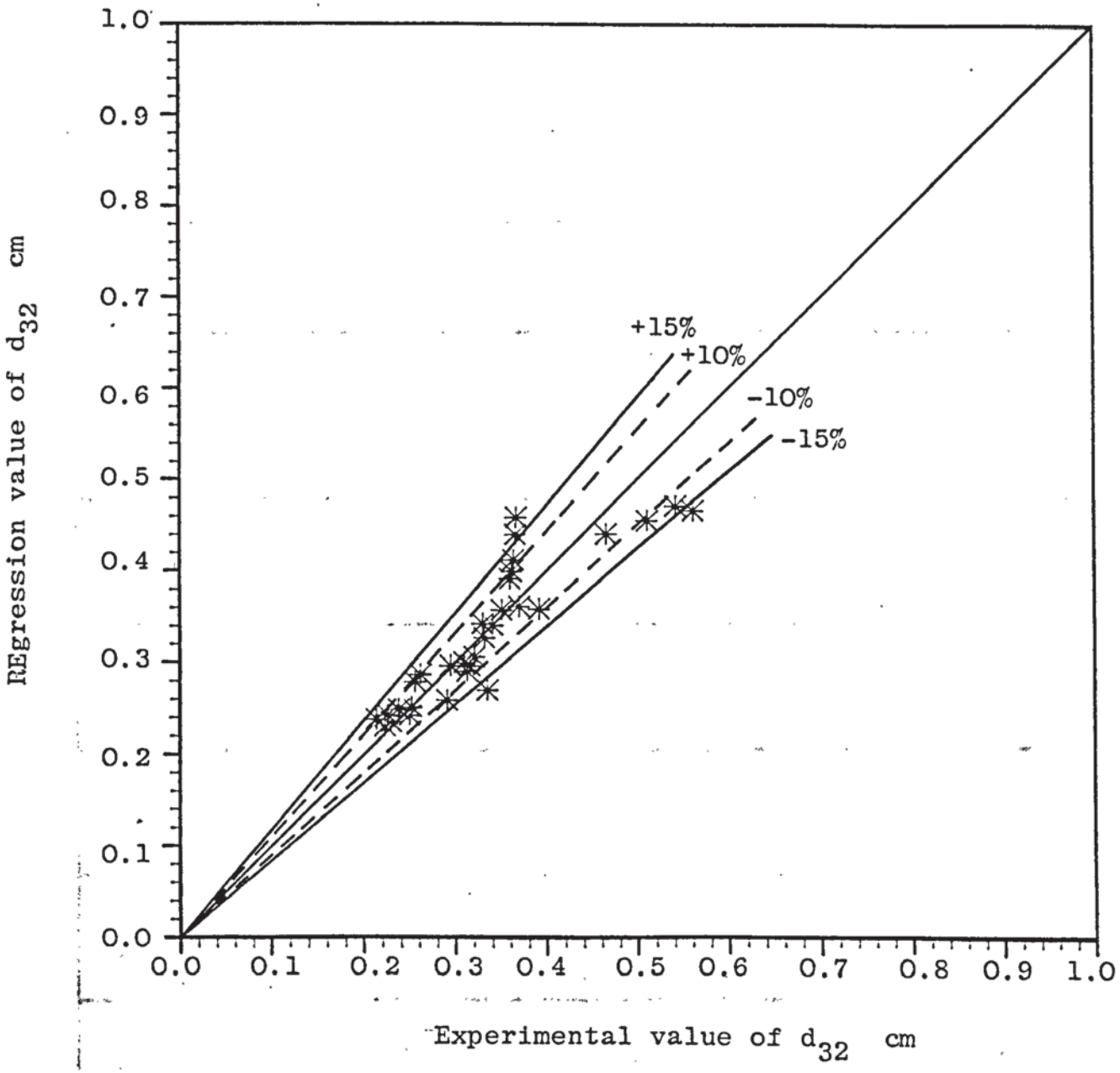

Figure 9.2 - Comparison of experimental data with regression values predicted from correlation 8.4.

$$\frac{d_{32}}{D_r} = 1.48\left[\frac{V_d H \rho_c}{\mu_c^X}\right]^{-0.23}\left[\frac{N^2 D_r^3 \rho_c}{\sigma}\right]^{-0.004}\left[\frac{V_d^2}{g_c D_c X^2}\right]^{0.44}$$

$$\left[\frac{\Delta\rho}{\rho_c}\right]^{-0.57}\left[\frac{H}{D_c - D_s}\right]^{-0.24}\left[\frac{n}{N_c}\right]^{-0.07}$$

Table 9.2 Evaluation of Correlation 8.5

Group	Group's Range	Term's Range (X^Y)	Effect on Predicted Value of d_{32}
$\frac{d_{32}}{D_r}$	0.01-0.05	-	-
$\frac{V_d H \rho_c}{\mu_c^X}$	28.0-14500	0.11-0.46	Significant
$\frac{N^2 D_r^3 \rho_c}{\sigma}$	400-7500	0.96-0.98	Very small
$\frac{V_d^2}{g_c D_c X^2}$	1.2×10^{-5}-1.4×10^{-3}	0.007-0.06	Significant
$\frac{\Delta\rho}{\rho_c}$	0.05-0.30	5.50-2.00	Significant
$\frac{H}{D_c - D_s}$	0.5-2.00	0.85-1.20	Significant
$\frac{n}{N_c}$	0.07-1.00	1.00-1.20	Small

Table 9.2 clearly shows the advantage of a wider range of groups covered by Equation 8.5 over Eqaution 8.4. Surprisingly the exponent of the Weber number $(\frac{N^2 D_r^3 \rho_c}{\sigma})$ is very small in this correlation so that this group has a very small effect on the predicted value of d_{32}. This is contrary to what is commonly reported i.e. that Weber number represents the power input to the agitated system and therefore controls the drop size. The low value of the exponent on this term, arises from the multilinear least square computer program in Appendix 5. However, the effect of rotor speed is partly accounted for in the groups $(\frac{V_d H \rho_c}{\mu_c^X})$ and $(\frac{V_d^2}{g_c D_c X^2})$.

Clearly hold-up is not independent of rotor speed (for example Figure 7.6); thus the residence time of drops in the turbulent regions where break-up occurs is also a function of rotor speed. Hence a doubling of rotor speed for any given system will, notwithstanding the low exponent on the Weber number from Equation 8.5, result in a reduction in the drop size of the order of 0.75, hence confirming that the correlation does comply with the experimental observation. The effect of the last group $(\frac{n}{N_c})$ is small too, but its significance is in the estimation of the drop size profiles along the column. Figure 9.3 shows the comparison between the experimental values and the regression values of d_{32} predicted by Equation 8.5. It was found that the average percentage error for this correlation was 17%, further 64% of the data were within ∓15% and 78% with ∓25%. The average percent error between the predicted values from Equation 8.5 and the experimental values of this study was less than 17.0%.

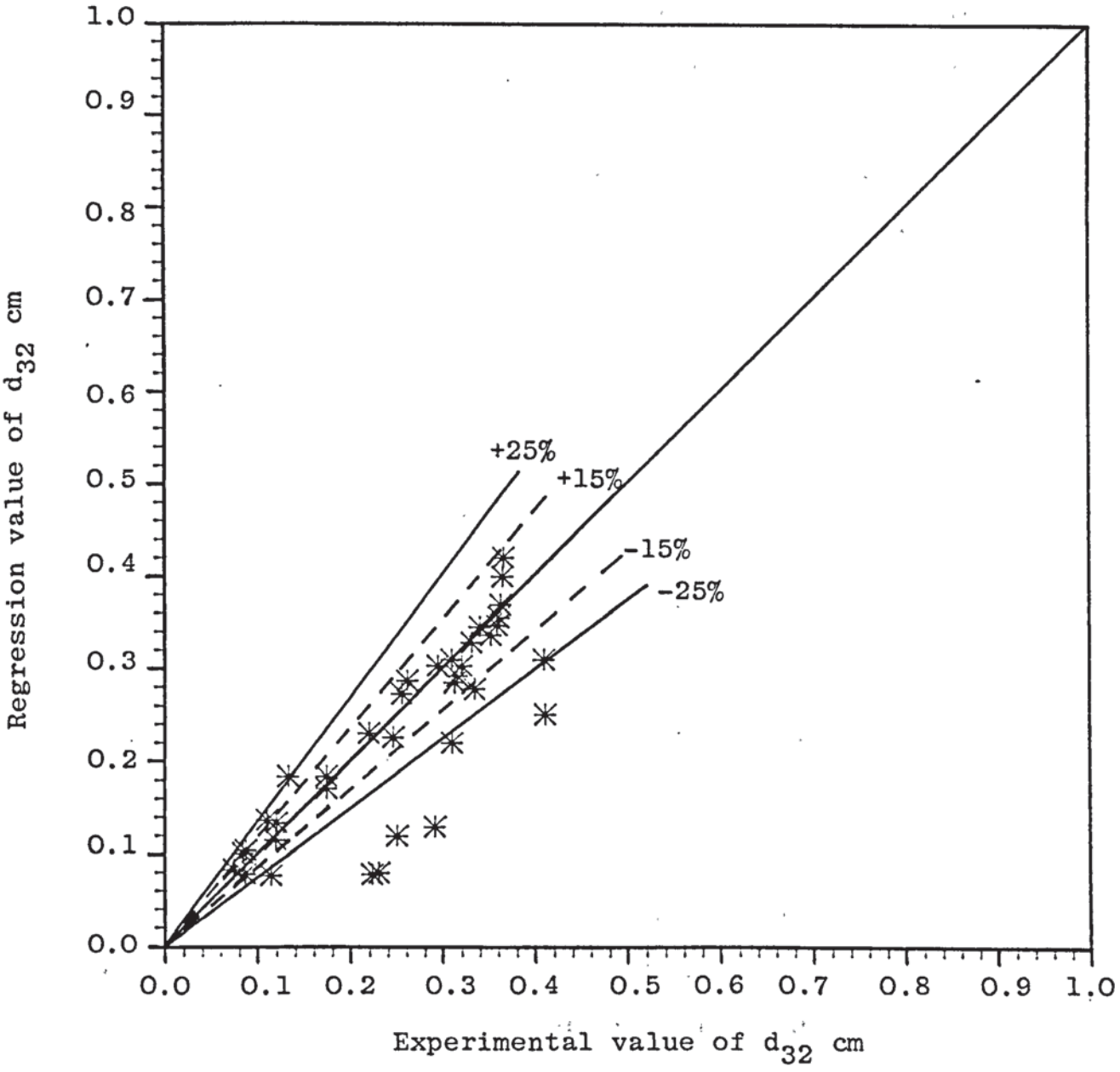

Figure 9.3 - Comparison of experimental d_{32} data with regression values predicted from correlation 8.5.

9.1.3 Drop Size Distribution

As shown in Figure 7.4, the range of drop sizes observed were between 0.9 mm and 5.0 mm for 200 r.p.m. and 0.5 mm and 3.5 mm for 300 r.p.m. These ranges are slightly wider in the small drop sizes side, than previously reported (2, 25, 26). The shape of the drop size distribution curves of Figure 7.4 are similar to that of Olney's (78) and different to that of Arnold's (47). Arnold found that the experimental drop size distribution on a log-probability graph paper are straight lines for Oldshue-Rushton column. Figures 8.2A and 8.2B show excellent agreement between the experimental volume-drop size and the upper limit distributions of Mugele and Evans (108) and this agreement is confined by comparing d_{32} for the experimental data calculated by equation 7.1 and d'_{32} calculated from the upper limit distribution equation 4.13. The deviation of d'_{32} from that of d_{32} was very small as mentioned in Section 8.1.2. The upper limit distribution curves of Figures 8.2A and 8.2B were replotted together on Figure 9.4 for comparison. The drop size spectrum tries to become wider as well as shifting towards the smaller drop sizes as the rotor speed increases. Wider spectrum means more drop sizes over the whole spectrum. This may be explained on the basis of increased hold-up and energy input. As the hold-up increased higher drop interaction rates were possible due to smaller interdrop distances, while higher energy input generates intensive mixing, hence there are more chances for the larger drops breaking down repeatedly producing many smaller droplets.

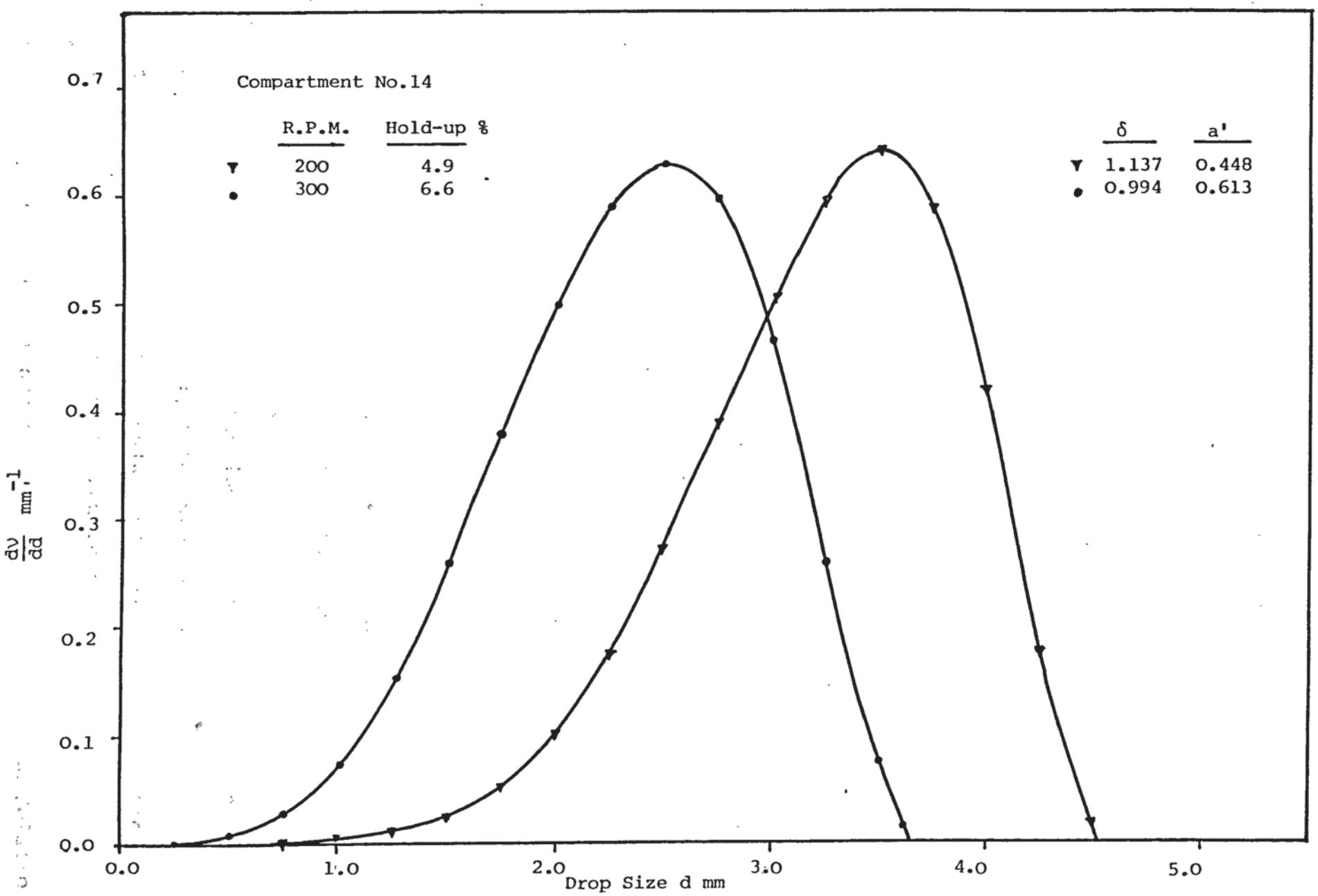

Fig. 9.4 Drop Size Distribution of the Upper Limit Distribution

The skewness parameter a of the upper limit distribution function was less than unity for the two curves which indicated a wider range of drops of sizes less than d_{50}. While the uniformity parameter δ of the 300 r.p.m. curve is less than that of the 200 r.p.m. curve and that indicating a wider drop size spectrum of the 300 r.p.m. curve (78).

9.1.4 Dispersed Phase Hold-up

The variation of average hold-up with the operating conditions, *ie* , dispersed phase flow velocity, rotor speed and continuous phase flow velocity are illustrated in Figures 7.5, 7.6 and 7.7. Generally, at fixed rotor speed and continuous phase velocity, the average hold-up increased with increasing dispersed phase velocity. The rate of increase was greater at higher rotor speed and at dispersed phase flowrate beyond a point corresponding to 40-50% of the flooding point. Figure 7.7 illustrated the significant effect of the continuous phase velocity. This is in agreement with earlier findings of Khandelwal (2) and Al-Hemiri (25) and unlike other studies (26, 47) in which no significant effect of the continuous phase flow was recorded. Clearly the effect of continuous flow velocity was due to the increase in the drop mean residence times. At high rotor speeds the drop sizes decreased, and the drops would therefore tend to be more easily entrained by the countercurrent flow.

The poor performance of previously published correlations

to predict the hold-up in large R.D.C.'s is not surprising since they are not only based on R.D.C.'s of small diameter but the majority (15, 28, 29) of studies have been conducted on the basis of Pratt's (42) characteristic velocity. Correlations with the characteristic velocity have been achieved in the cases of spray columns and packed columns, but not, however, in the case of a R.D.C. so, to provide more accurate prediction of the characteristic velocity V_N, Equations 8.11 and 8.12 were developed in the way mentioned in Section 8.13. Below is the evaluation of these correlations

(i) Correlation of V_N for data of this work only:

$$\frac{V_N \mu_c}{\sigma} = 6.24 \times 10^{-3} \left[\frac{\Delta\rho}{\rho_c}\right]^{0.783} \left[\frac{g_c}{D_r N^2}\right]^{0.234} \left[\frac{D_s}{D_r}\right]^{1.778} \left[\frac{H}{D_r}\right]^{1.362} \left[\frac{D_r}{D_c}\right]^{1.922} \qquad (8.11)$$

Table 9.3 Evaluation of Correlation 8.11

Group	Group's Range	Term's Range (X^y)	Effect on Predicted Value of V_N
$\frac{V_N \mu}{\sigma}$	7.8×10^{-4}-2.9×10^{-3}	-	-
$\frac{\Delta\rho}{\rho_c}$	0.2146	0.30	Constant
$\frac{g_c}{D_r N^2}$	0.88-27.90	0.97-2.2	Significant

(Cont..)

Table 9.3 (Cont..)

Group	Group's Range	Term's Range (X^Y)	Effect on Predicted Value of V_N
$\frac{D_S}{D_r}$	1.2-1.90	1.4-3.1	Significant
$\frac{H}{D_r}$	0.8-1.25	0.74-1.36	Significant
$\frac{D_r}{D_c}$	0.44-0.62	0.21-0.40	Significant

The density difference group is a very important group to be included in such a correlation as a standard form correlation of the characteristic velocity. However, only one liquid system was studied in this project and the effect of this group will be constant for all the data. Nevertheless the liquid system used is considered to be a model for liquid-liquid extraction and all the physical properties do not vary very greatly.

All the other dimensionless groups have a significant effect on the predicted value of V_N; however the groups range for the column dimensions are relatively small. This is because the column internal dimensions, *ie*, D_r, D_S and H, were kept constant through the whole study, and the effect of the small changes in D_r, D_S and H on the hold-up was predicted by using the general hold-up correlation, Equation 8.14 which gave a very accurate prediction,

as will be seen in the discussion later in this section, of the dispersed phase hold-up at conditions below 50% of the flooding point. These predicted values of hold-up were then treated as experimental values in the way mentioned in Section 8.13. Comparison between the experimental and regression values of V_N is shown in Figure 9.5, with an average percent error for all the data only 8.8% and 65% of the data were within ∓10% and 91% within ∓15%.

(ii) Correlation of V_N for data of this work and published work (28, 29, 182):

$$\frac{V_N \mu_c}{\sigma} = 4.45 \times 10^{-4} \left[\frac{\Delta\rho}{\rho_c}\right]^{-0.941} \left[\frac{g_c}{D_r N^2}\right]^{0.205} \left[\frac{D_s}{D_r}\right]^{1.601} \left[\frac{H}{D_r}\right]^{-0.689} \left[\frac{D_r}{D_c}\right]^{1.786} \qquad (8.12)$$

The advantage of wider ranges of the groups covered by this correlation over previous characteristic velocity correlations resulted in a slight increase in the average percentage error of 4.6% to 13.4%. Figure 9.6 gives a comparison between the experimental and regression values of V_N, 51% of the data were correlated within ∓10% and 82% within ∓20%. The average percent error of the data of this work and the predicted values by this correlation was less than 10%.

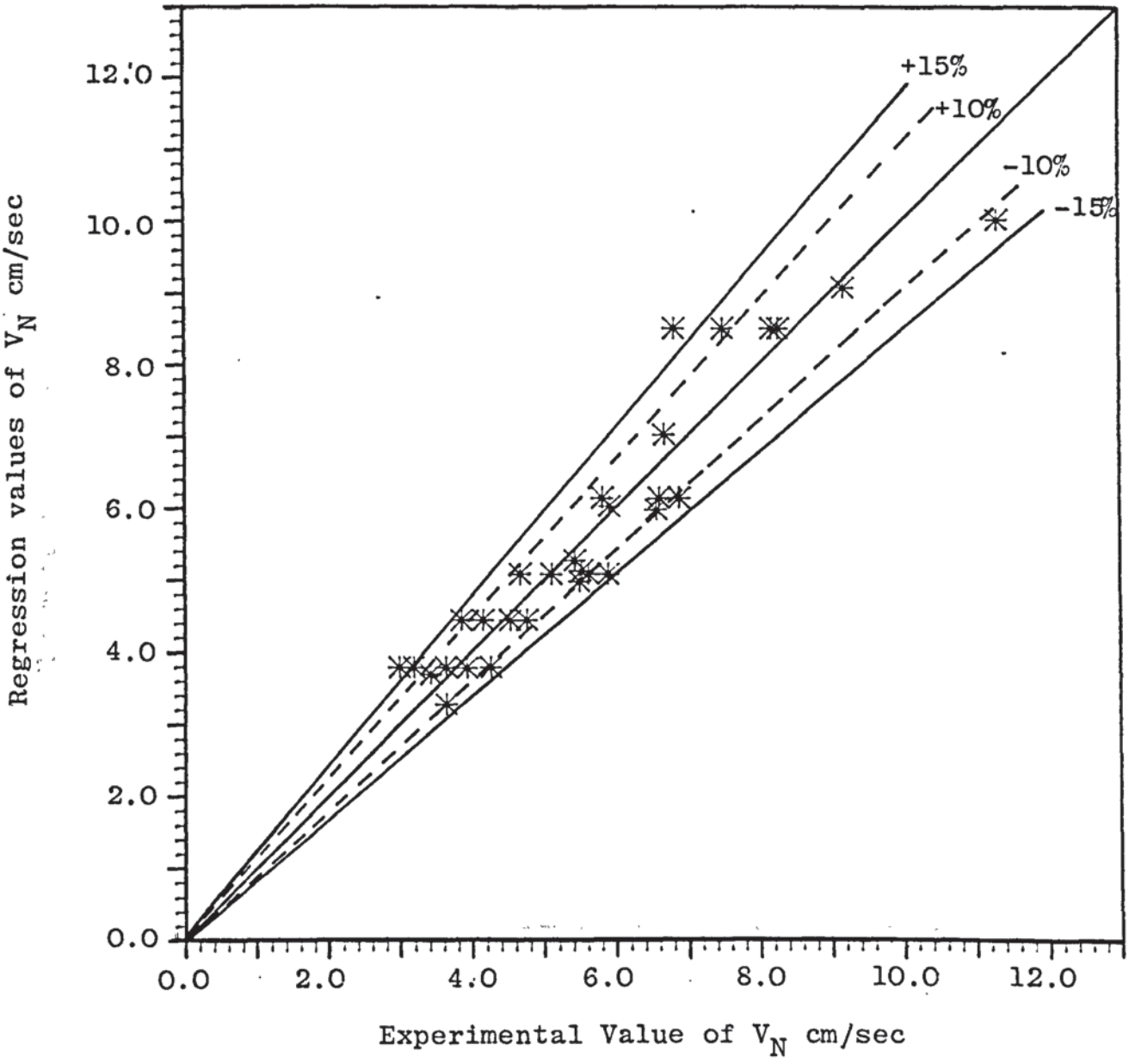

Figure 9.5 - Comparison of experimental V_N data with regression values predicted from correlation 8.11.

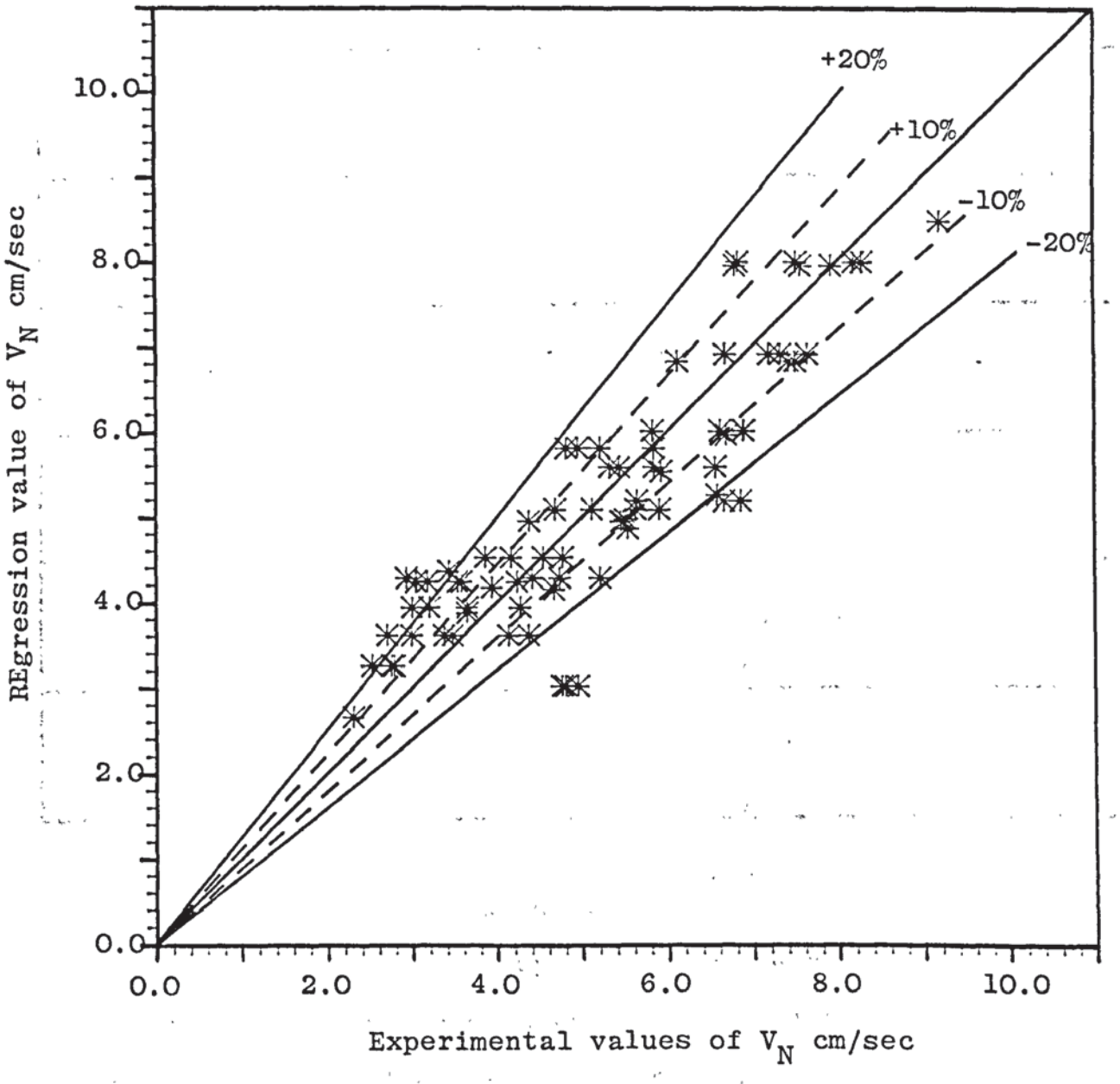

Figure 9.6 - Comparison of experimental V_N data with regression values predicted from correlation 8.12.

Table 9.4 Evaluation of Correlation 8.12

Group	Group's Range	Term's Range (X^y)	Effect on Predicted Value of V_N
$\frac{V_N \mu_c}{\sigma}$	7.8×10^{-4}-2.5×10^{-3}	-	-
$\frac{\Delta\rho}{\rho c}$	0.13-0.22	4.20-6.80	Significant
$\frac{g_c}{D_r N^2}$	0.88-27.90	0.97-1.98	Significant
$\frac{D_s}{D_r}$	1.06-2.67	1.1-4.8	Significant
$\frac{H}{D_r}$	0.53-1.25	0.65-1.20	Significant
$\frac{D_r}{D_c}$	0.25-0.63	0.085-0.440	Significant

Besides the doubt about the validity of the characteristic velocity approach to correlate hold-up in R.D.C., another problem arises by solving the characteristic velocity-hold-up equation

$$\frac{V_d}{X} + \frac{V_c}{1-X} = V_N(1-X) \qquad (3.9)$$

which becomes after rearrangement.

$$V_N X^3 - 2V_N X^2 + (V_d - V_c + V_N)X - V_d = 0 \qquad (9.2)$$

as this equation is of the third degree, and gives three roots from which only one, is a reasonable hold-up. The problem arises when two of the roots are close positive numbers and less then 1.0 which reoccurs quite often, specially in conditions near the flooding point.

Hence correlating the dispersed phase hold-up directly as described in Section 8.1.3 in terms of the column geometry, physical properties of the system and the operating conditions by Equation 8.14 is more accurate than the above approach. Correlation 8.14 was developed by including some of published results of Logsdail et al (28) and Kung (182) and the outcome correlation can be evaluated as follows:

$$X = 1.05 \times 10^{14} \left[\frac{ND_r}{V_c}\right]^{0.521} \left[\frac{V_d}{V_c}\right]^{0.775} \left[\frac{D_s^2 - D_r^2}{D_c^2}\right]^{-1.867}$$

$$\left[\frac{H}{D_c}\right]^{-0.873} \left[\frac{D_r}{D_c}\right]^{0.201} \left[\frac{\Delta\rho}{\rho_c}\right]^{4.843} \left[\frac{\rho_c D_c V_c}{\sigma}\right]^{1.082}$$

$$\left[\frac{V_c^2}{g_c D_c}\right]^{0.892} \left[\frac{\rho_c V_c D_c}{\mu_c}\right]^{-2.367} \qquad (8.14)$$

Parameter's ranges:

Column diameter (D_c)	7.6 - 45.0 cm
Disc diameter (D_r)	3.2 - 22.5 cm
Stator diameter (D_s)	5.1 - 33.8 cm
Compartment height (H)	1.9 - 22.5 cm
Interfacial tension (σ)	14.2 - 39.2 cm
Density difference ($\Delta\rho$)	0.11 - 0.21 gm/c.c

Table 9.5 Evaluation of Correlation 8.14

Group	Group's Range	Term's Range (X^y)	Effect on Predicted Value of X
$\frac{ND_r}{V_c}$	28.4-745.0	5.7-31.4	Significant
$\frac{V_d}{V_c}$	0.12-3.10	0.19-2.40	Significant
$\frac{D_s^2-D_r^2}{D_c^2}$	0.05-0.44	4.6-268.5	Very significant
$\frac{H}{D_c}$	0.25-0.83	1.18-3.35	Significant
$\frac{D_r}{D_c}$	0.25-0.63	0.76-0.91	Small
$\frac{\Delta\rho}{\rho_c}$	0.116-0.214	2.9×10^{-5}-6.0×10^{-4}	Significant
$\frac{\rho_c D_c V_c}{\sigma}$	0.002-0.500	0.001-0.470	Significant
$\frac{V_c^2}{\rho_c D_c}$	7.1×10^{-7}-7.0×10^{-5}	3.3×10^{-6}-1.9×10^{-4}	Significant
$\frac{\rho_c V_c D_c}{\mu_c}$	50.0-1315	4.1×10^{-8}-9.5×10^{-5}	Very significant

Table No. 9.5 shows that the effect of the ratio $(\frac{D_r}{D_c})$ is smaller than expected for the effect of rotating disc, but looks as though it has been compensated by the large effect of the group $(\frac{D_s^2-D_r^2}{D_c^2})$.

The large positive exponent of the density difference group was surprising and is contrary to what was expected as larger density differences for the same column geometry and operating conditions means less hold-up as drops settling velocity will increase. Comparison between the experimental and the regression values of the dispersed phase hold-up are illustrated in Figure 9.7 where it can be seen that there is good agreement at the lower values of hold-up corresponding to conditions below 60% of the flooding point. Deviations increase as conditions approach the flooding point, since some of the data included in the regression of this correlation belong to the flooding rates data of Logsdail et al (28). Deviations were expected for these data due to fluctuations in the column at the flooding point. Generally the performance of the hold-up correlation is good as the average percent error was found to be 14.0% and 72% of the data were correlated with $\mp$15% and 82% within $\mp$20%. The average percentage error of the data of this work and the predicted values by this correlation was less than 9.0%.

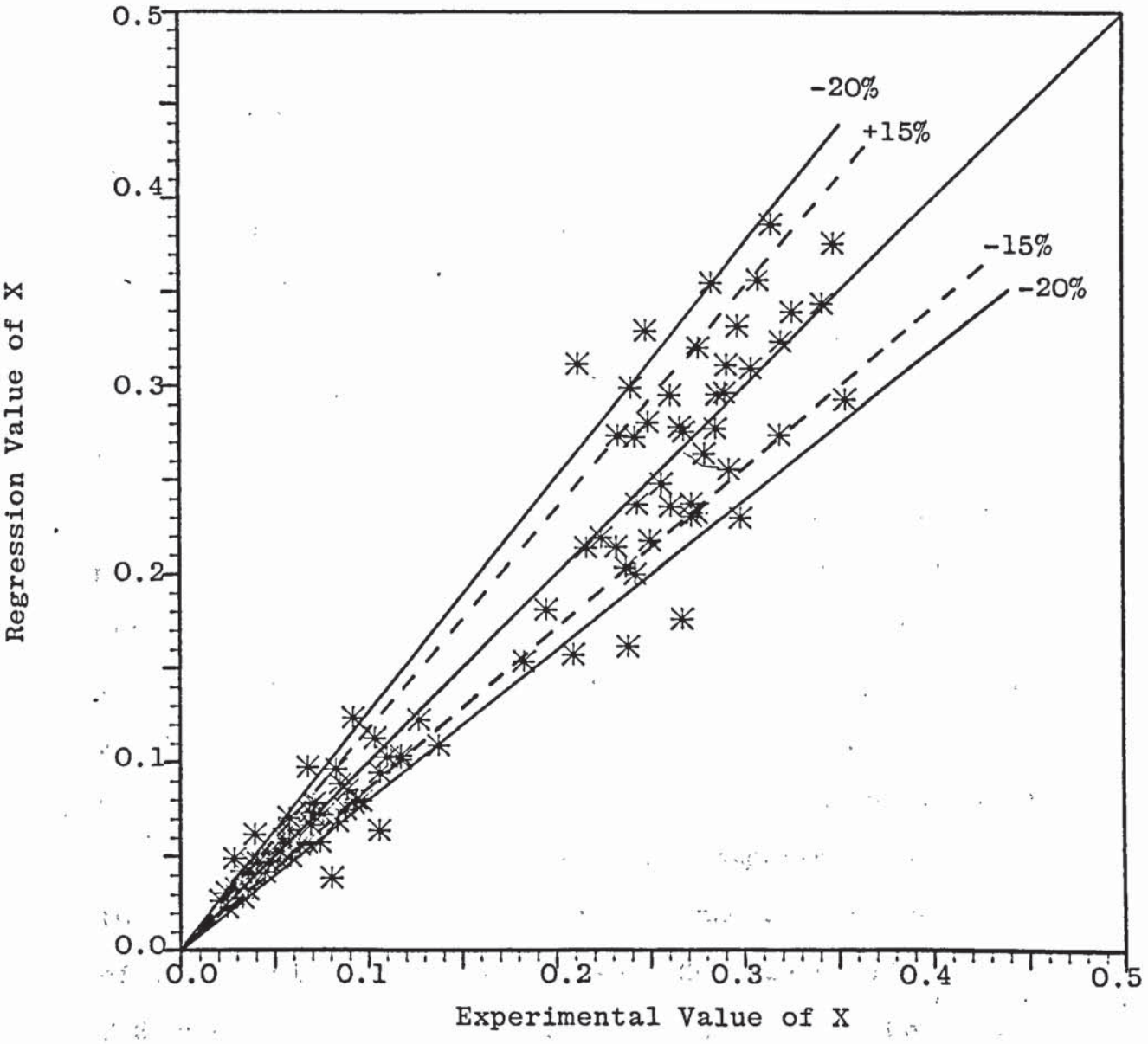

Figure 9.7 - Comparison of experimental hold-up data with regression values predicted from correlation 8.14.

9.2 Mass Transfer Studies

9.2.1 Drop Size

From visual and photographic observations it was found that the drop size under mass transfer conditions is strongly dependant upon the direction of mass transfer. Generally, the Sauter mean drop sizes (d_{32}), for the non-mass transfer runs, were larger than those obtained when mass transfer ocurred was from the continuous to the dispersed phase but lower than those obtained for solute transfer in the opposite direction under the same operating conditions; *ie.*, phases flowrates and rotor speed. The larger d_{32} for acetone transferring from dispersed phase to continuous may be attributed to enhanced interdroplet coalescence which increases the mean drop sizes, For rotor speeds below the critical speed mentioned in Section 9.1.2 the rate of coalescence overcomes the rate of drop break-up resulting in larger mean drop sizes as the swarm of drops *rise* through the column. The photograph in Figure 9.8 shows a comparison of drop sizes in compartment No.2 at the bottom and compartment No.12 at the top at a rotor speed of 150 r.p.m. and acetone concentrations of 2.20% in the dispersed phase. More generally Figure 7.8 shows the mean drop size variation along the column at different rotor speeds and constant acetone concentration of 2.20%. The four curves in Figure 7.8 represent the drop size measurement during mass transfer runs 5, 6, 7 and 8, listed in Table 8.2. The inlet drop sizes, via the distributor in the bottom of the column

were noticeably smaller when the mass transfer direction was from continuous to dispersed phase. This is illustrated in the photograph of compartment No.2 in Figure 9.9 and by comparing it with that in the bottom photograph in Figure 9.8. That is the variation of the mean drop sizes along the column was very small at rotor speed of 300 r.p.m. and nearly constant for those rotor speeds near and below the critical rotor speed of 200 r.p.m. This may again be attributed to the reduction or absence of interdrop coalescences.

9.2.2 Dispersed Phase Hold-up

The average hold-up was measured for each mass transfer run and, as expected, was found to increase with increasing flow rates and rotor speed. Under similar operating conditions with those for non-mass transfer conditions different values of the hold-up were obtained. They were higher when acetone was transfered from the continuous to the dispersed phase, and lower when acetone was transfered from dispersed to continuous. This can be related as mentioned in the previous section, (9.2.1), to different rates of coalescence for the different transfer directions, i.e. for D→C, increased coalescence caused the mean drop diameter to increase and the residence time to be shorter resulting in lower hold-up. For C→D the reduction, or absence of coalescence resulted in smaller drops with longer residence times and hence higher values of hold-up.

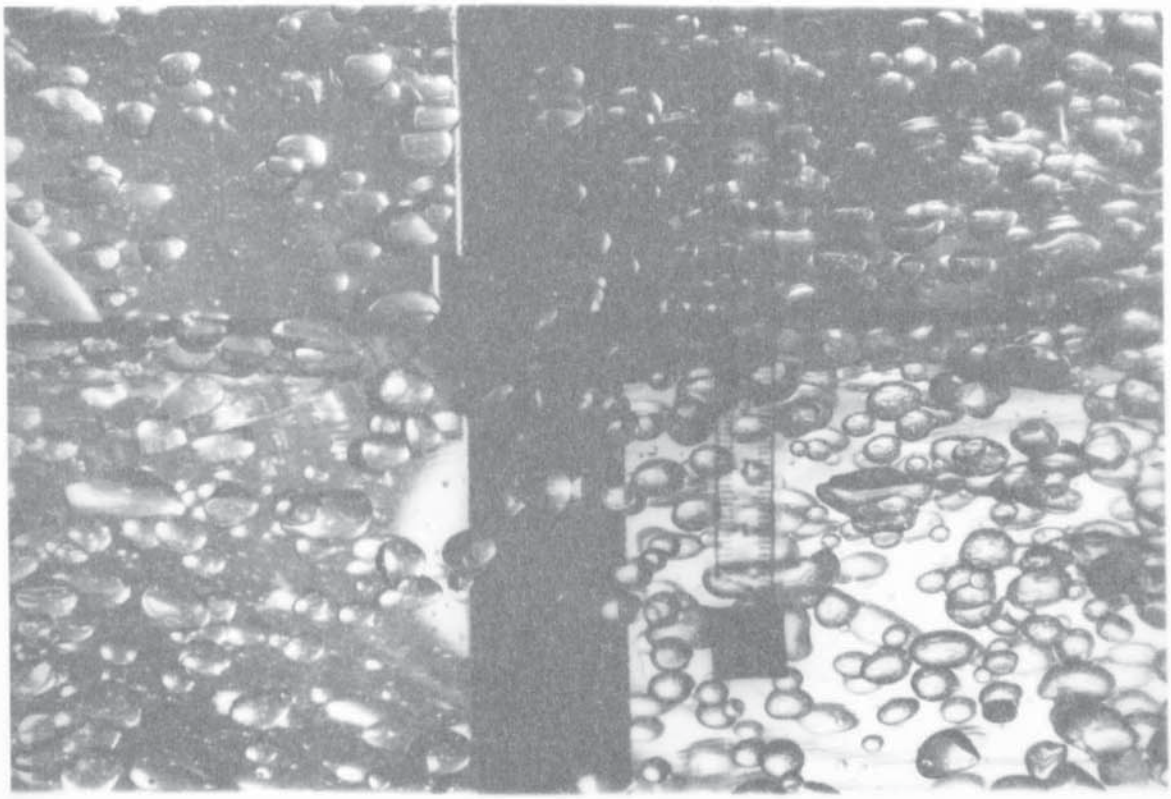

Compartment No. 12 d_{32} = 0.52 cm Acetone conc. = 2.20%

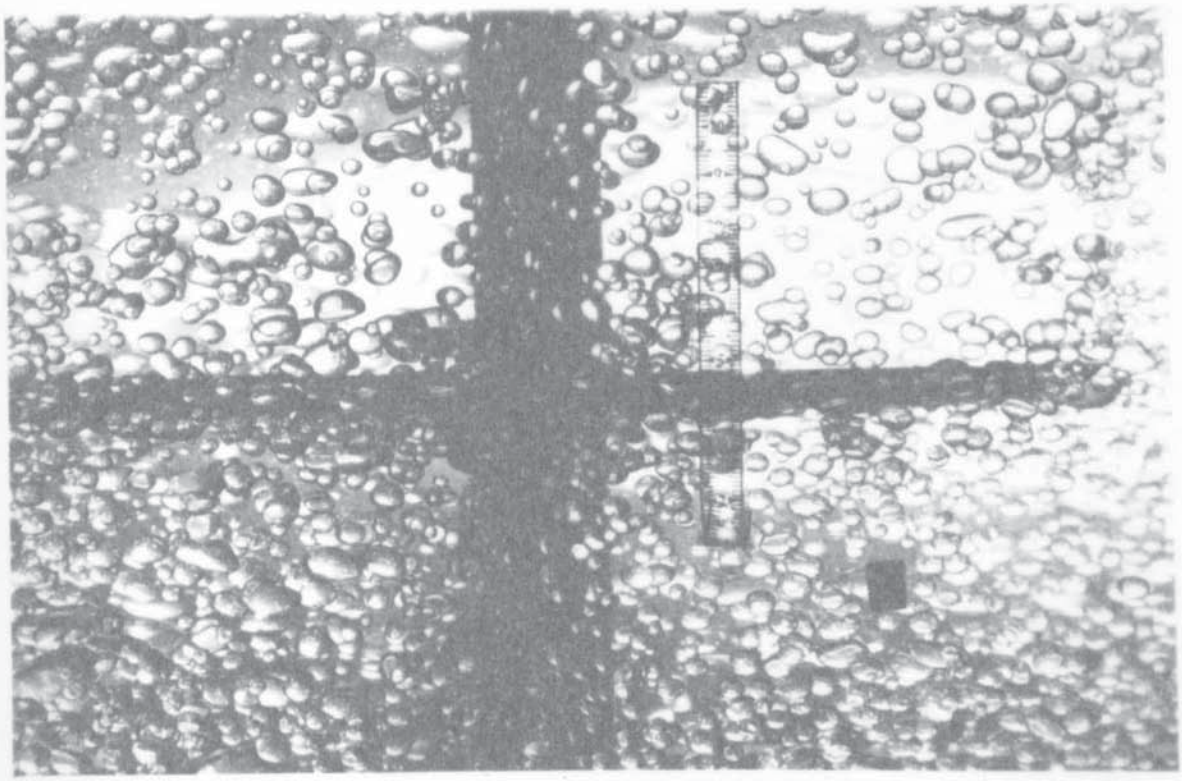

Compartment No. 2 d_{32} = 0.43 cm Acetone conc. = 2.20%

Figure 9.8 Variation in drop size between compartments No. 2 and 12 under mass transfer at rotor speed of 150 rpm.

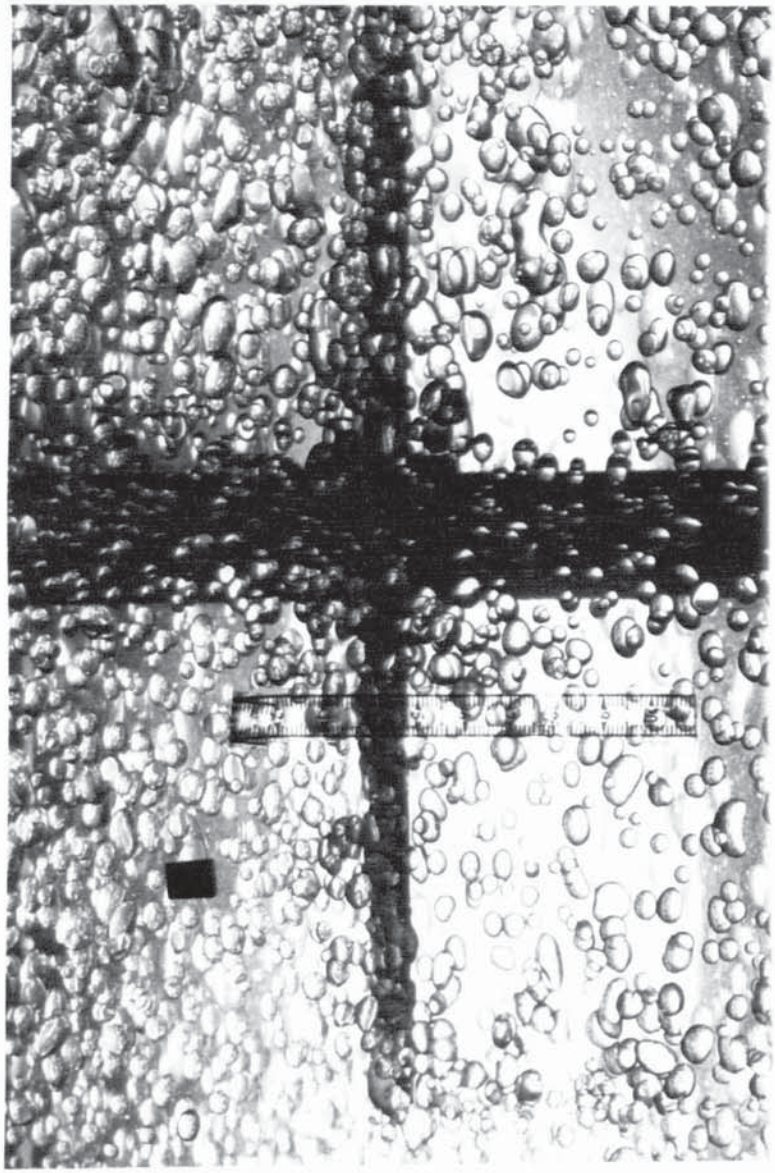

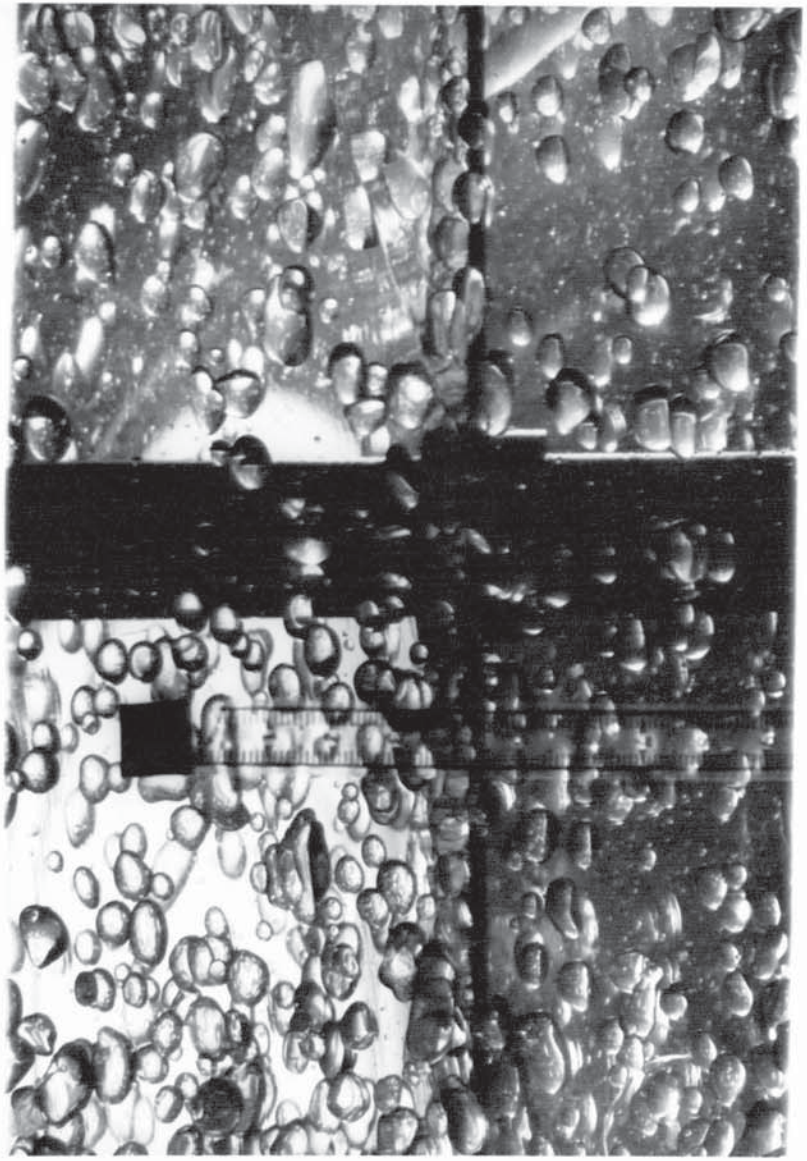

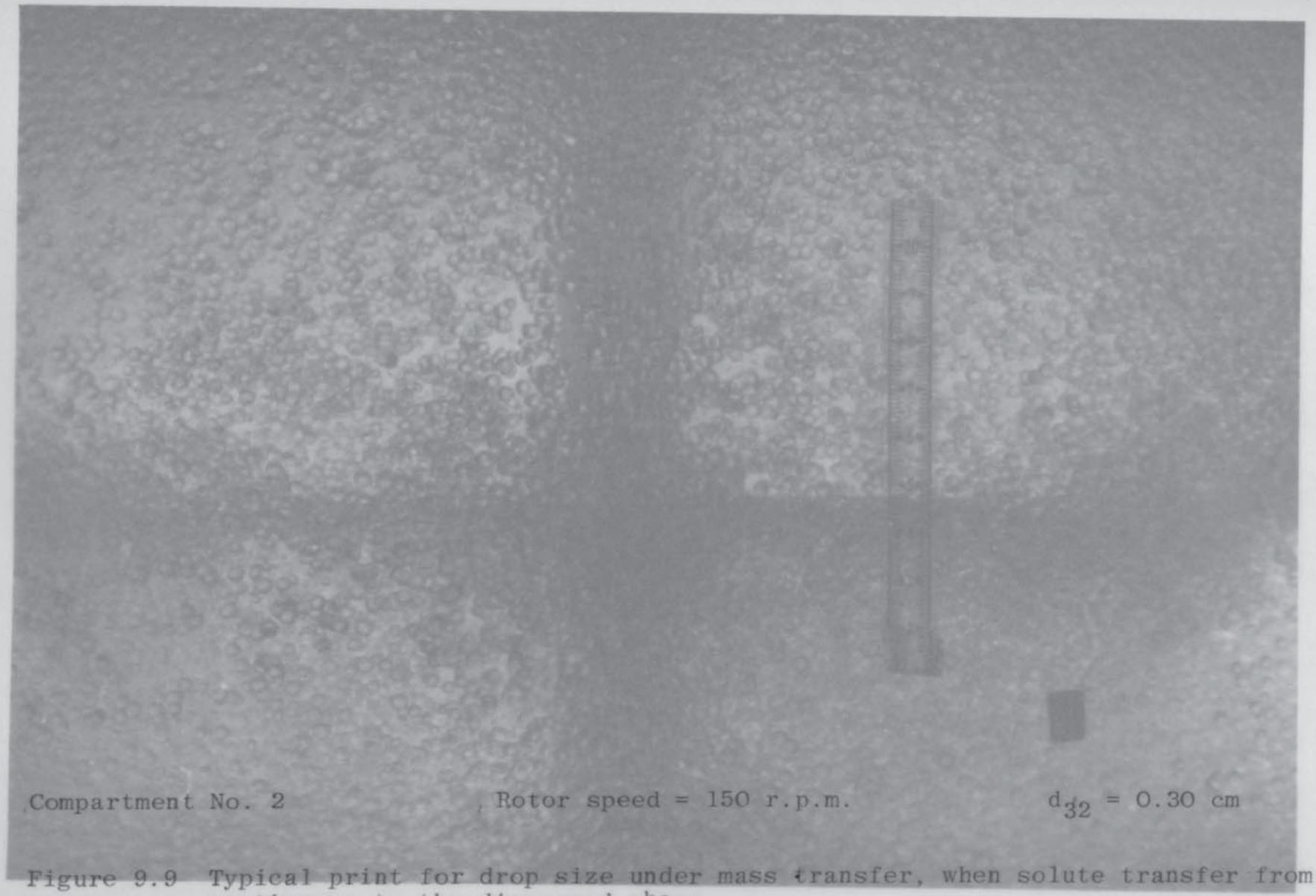

Figure 9.9 Typical print for drop size under mass transfer, when solute transfer from the continuous to the dispersed phase.

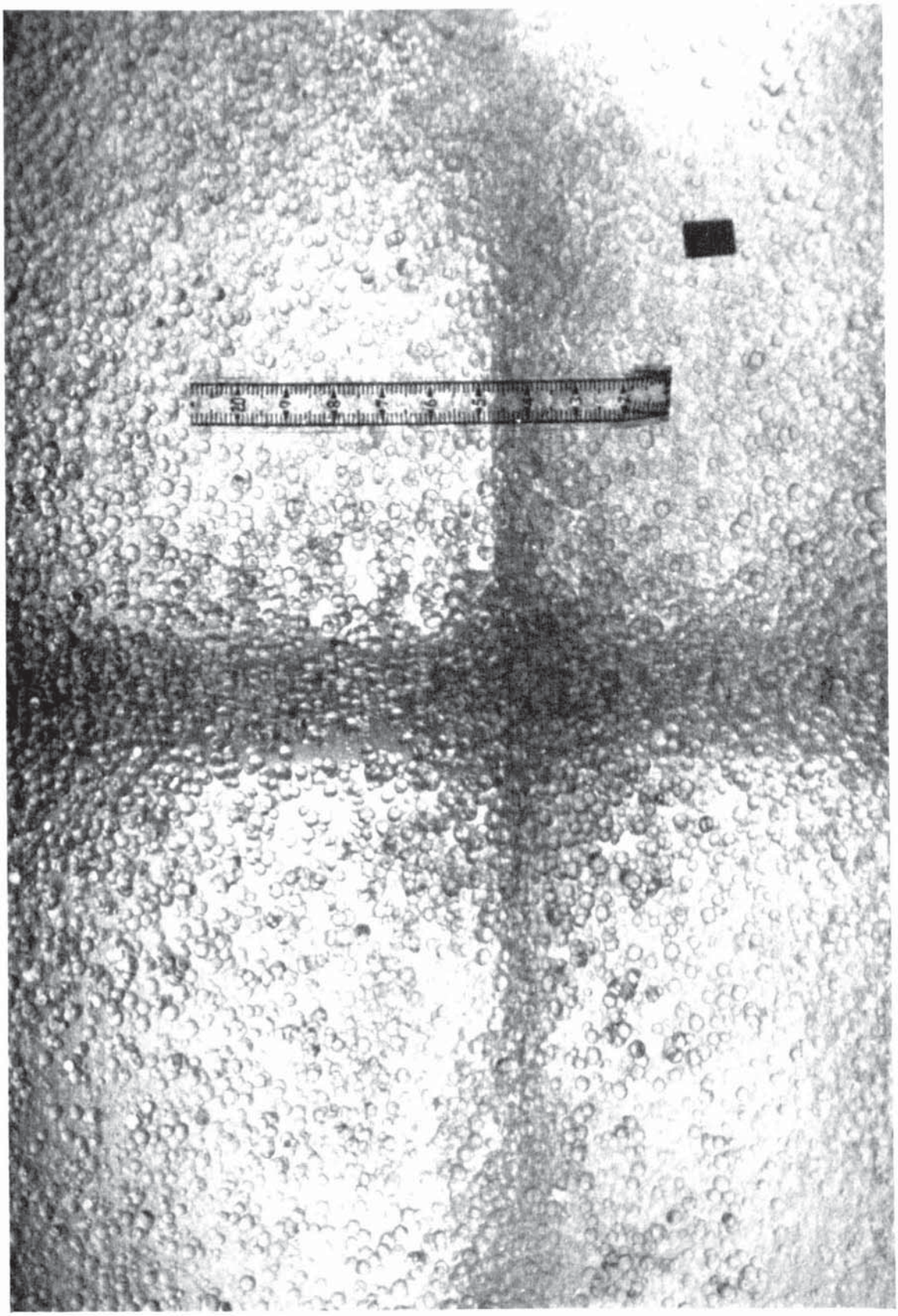

9.2.3 Mass Transfer Coefficient

9.2.3.1 Experimental Mass Transfer Coefficient

The overall experimental dispersed phase mass transfer coefficient recorded in this study was considerably greater than those recorded in some of the previous studies (2, 25). This was mainly due to a smaller driving force evaluated by Simpson's Rule as described in Section 8.2.1. Simpson's Rule has a great advantage over the log-mean driving force in the agitated column for a very obvious reason, that is the shape of the operating line and distribution curve resulting from the flow pattern of the phases within the column not being plug flow (33, 48).

From Table 8.2 it can be seen that the rate of mass transfer increased with increasing rotor speed, while on the other hand, the experimental mass transfer coefficient decreased. This is expected since an increase in rotor speed causes more drops to break-up and the proportion of the small droplets will be greater for which the mass transfer coefficient becomes smaller, with the result that stagnant or circulating droplets replace some of the oscillating drops. The real gain in the higher energy input is in the interfacial area which increases more rapidly than the decrease in the mass transfer coefficient because of the higher hold-up of smaller drops, as expected in Equation 8.15, i.e.

$$a = \frac{6x}{d_{32}} \qquad (8.15)$$

Hence the overall volumetric mass transfer coefficient $(Ka)_{Exp}$ will illustrate more clearly the effect of the rotor speed. Table 9.6 shows that $(Ka)_{Exp}$ increases with increase in the rotor speed, but the rate of increases become smaller as the rotor speed becomes higher which suggests that there is an optimum point in which the column can be run more efficiently by gaining maximum mass transfer at a specified rotor speed. This rotor speed can be easily detected by plotting $(Ka)_{Exp}$ against the rotor speed for each set of phases flowrates as shown in Figure 9.10 . There it can be seen that $(Ka)_{Exp}$ increases with the increase in either phase flowrate. Table 9.6 and Figure 9.10 also demonstrate the insignificant effect of the rotor speed on $(Ka)_{Exp}$ for C→D runs, this due to the fact that there is very little charge in drop size with rotor speed.

9.2.3.2 Theoretical Mass Transfer Coefficient

Since a fairly wide range of drop size exists in the dispersion in the agitated extractor, it is likely that more than one transfer mechanism would take place over the wide spectrum of drop sizes. Therefore assumption of uniform drop size could lead to serious errors when interpreting mass transfer and related processes in discrete-drop apparatus. The use of the drop size distribution in calculating the mass transfer rate was recommended by Olney (78), Chartres and Korchinsky (114, 115, 116), but it has not been applied in the same way as it has been used in this study and as described in Section 8.2.2.

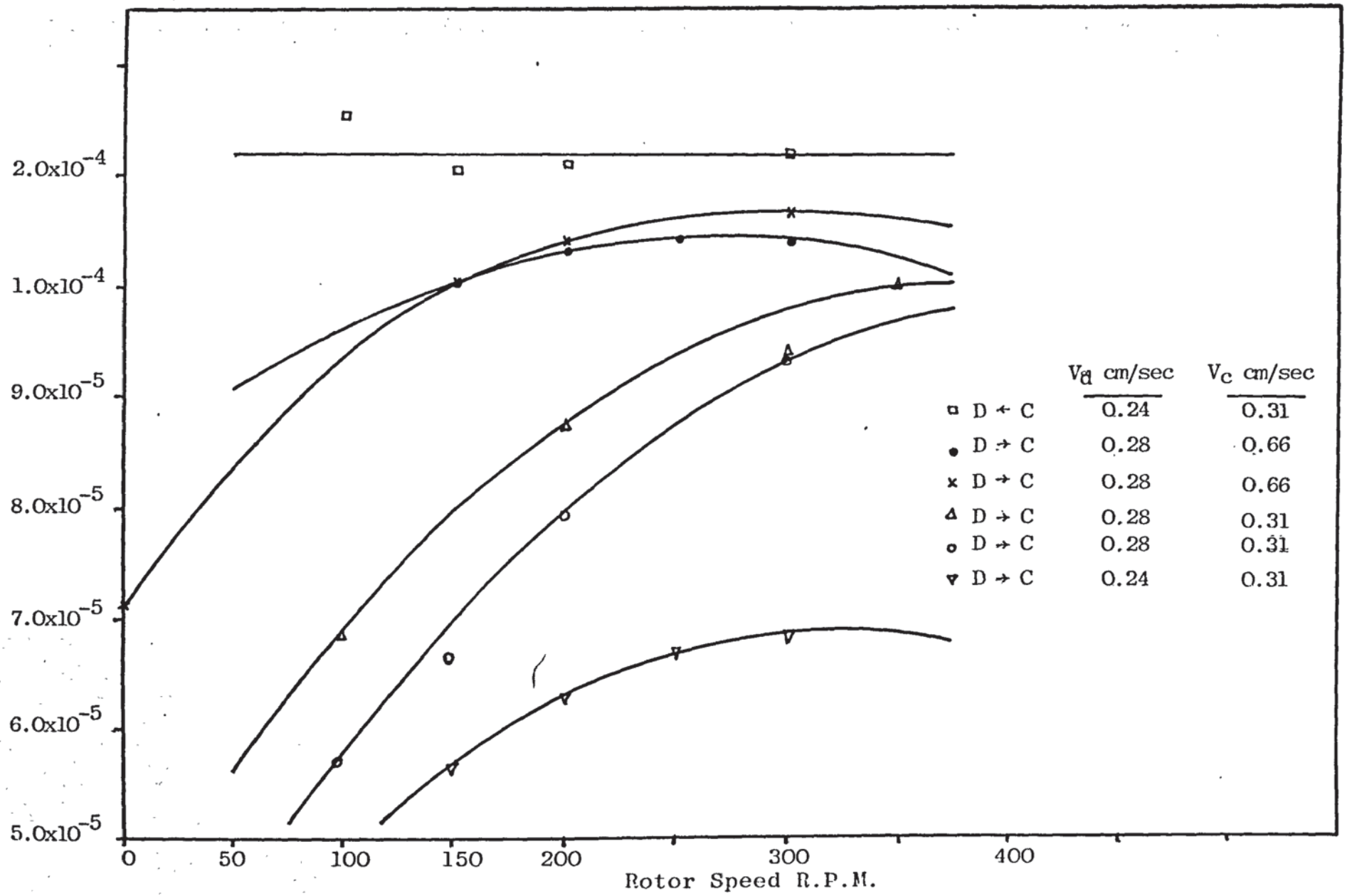

Fig. 9.10 Variation of $(Ka)_{Exp}$ with rotor speed

Table 9.6 Effect of Rotor Speed on $(Ka)_{Exp}$

Run No.	Direction of Transfer	Rotor Speed R.P.M.	Hold-up %	d_{32} cm	K_{Exp} cm/sec	$(Ka)_{Exp}$ l/sec
1	D→C	150	3.98	0.46	1.96×10^{-4}	1.02×10^{-4}
2	"	200	4.52	0.35	1.72×10^{-4}	1.32×10^{-4}
3	"	250	5.02	0.31	1.45×10^{-4}	1.41×10^{-4}
4	"	300	5.76	0.24	9.71×10^{-5}	1.40×10^{-4}
5	"	0.00	0.90	0.54	7.10×10^{-4}	7.10×10^{-5}
6	"	150	3.95	0.49	2.18×10^{-4}	1.05×10^{-4}
7	"	200	4.68	0.36	1.83×10^{-4}	1.43×10^{-4}
8	"	300	6.03	0.26	1.17×10^{-4}	1.63×10^{-4}
9	"	150	3.16	0.51	1.52×10^{-4}	5.65×10^{-5}
10	"	200	3.78	0.37	1.02×10^{-4}	6.25×10^{-5}
11	"	250	4.29	0.32	8.36×10^{-5}	6.72×10^{-5}
12	"	300	5.51	0.24	4.96×10^{-5}	6.83×10^{-5}
13	"	100	2.82	0.51	2.05×10^{-4}	6.80×10^{-5}
14	"	200	3.70	0.39	1.53×10^{-4}	8.71×10^{-5}
15	"	300	4.74	0.26	8.45×10^{-5}	9.24×10^{-5}
16	"	350	6.62	0.21	5.32×10^{-5}	1.01×10^{-4}
17	"	100	2.61	0.54	1.96×10^{-4}	5.68×10^{-5}
18	"	150	2.82	0.52	2.03×10^{-4}	6.61×10^{-5}
19	"	200	3.34	0.44	1.74×10^{-4}	7.92×10^{-5}
20	"	300	4.10	0.32	1.21×10^{-4}	9.30×10^{-5}
21	D←C	100	3.08	0.310	4.29×10^{-4}	2.56×10^{-4}
22	"	150	4.39	0.304	2.37×10^{-4}	2.05×10^{-4}
23	"	200	5.53	0.288	1.81×10^{-4}	2.09×10^{-4}
24	"	300	6.24	0.252	1.47×10^{-4}	2.17×10^{-4}

The experimental overall mass transfer coefficients were found to be greater than those calculated by the methods described in Section 8.2.2. This is believed to be due to the fact that oscillations are superimposed on the circulating droplets due to the existence of a swarm of drops in close proximity inducing adjacent drops to oscillate in the highly turbulent regions near the discs. On the other hand, the use of filtered tap water, industrial grade solvent and the scale of operation may have an opposite effect on the circulating drops making them behave as stagnant drops with very low mass transfer coefficients. Table 9.2 gives a comparison between the experimental overall mass transfer coefficients and the theoretical mass transfer coefficients. This comparison is discussed as follows.

a) The mass transfer calculated by the Rose and Kintner and Garner equations (given in Table 8.7 as $K_{cal}^{(1)}$ and compared in Table 9.7, as $K_{Exp}/K_{cal}^{(1)}$). The ratio can be seen to varyfrom 0.57 to 2.68 for the runs in which mass transfer occured from D→C, and from 1.82 to 23. 88 for those in which mass transfer occured from C→D. This wide range for C→D experiments may be due to the large proportion of the circulating drops predicted by the drop distribution diagram actually oscillating and persisting for longer time in the high turbulent regions underneath the discs. The same reason may be used to explain the high ratio obtained for the D→C runs as in runs 4, 8, 12 and 16. the circulating drops are predominant as shown in Table 8.5.

Table 9.7 Comparison between Experimental and Theoretical Mass Transfer Coefficients

Run No.	Direction of Transfer	$\frac{K_{Exp}}{K_{cal}^{(1)}}$	$\frac{K_{Exp}}{K_{cal}^{(2)}}$	$\frac{K_{Exp}}{K_{o.c}}$	$\frac{K_{Exp}}{K_{o.o}^{(1)}}$	$\frac{K_{Exp}}{K_{o.o}^{(2)}}$
1	D→C	0.79	0.35	23.93	0.79	0.35
2	"	1.05	0.35	15.64	0.75	0.25
3	"	1.11	0.32	14.80	0.68	0.20
4	"	1.78	0.56	10.18	0.51	0.15
5	"	1.08	1.59	18.68	1.08	1.60
6	"	0.88	0.40	25.95	0.88	0.40
7	"	1.14	0.38	16.64	0.82	0.27
8	"	2.68	0.82	13.42	0.64	0.17
9	"	0.61	0.29	17.88	0.61	0.29
10	"	0.57	0.20	11.47	0.46	0.16
11	"	0.97	0.29	9.09	0.42	0.12
12	"	2.07	0.68	5.66	0.31	0.08
13	"	0.67	0.41	18.30	0.67	0.41
14	"	0.61	0.24	14.71	0.60	0.23
15	"	1.42	0.52	9.19	0.40	0.13
16	"	2.65	0.97	5.46	0.34	0.08
17	"	0.60	15.93	15.93	0.60	0.40
18	"	0.66	18.62	18.62	0.66	0.40
19	"	0.65	17.86	17.86	0.63	0.28
20	"	0.98	13.57	13.57	0.51	0.16
21	D←C	1.82	35.16	35.16	1.63	0.63
22	"	2.56	29.70	29.70	1.21	0.34
23	"	23.88	23.88	23.88	-	-
24	"	17.11	17.11	17.11	-	-

All these runs were at high rotor speeds of 300 and 350 r.p.m. as shown in Table 8.2. The experimental mass transfer coefficients were generally lower for lower phase flowrates than those for high phases flowrates at identical rotor speeds; for example in runs 9 and 10 which can be compared with runs 1 and 2. While almost no charge was found in the calculated mass transfer coefficient for these runs because the phase flow rates are not allowed for any of the equations used in the calculations. The only implicit inclusion of flow rates are in equations 5.40 and 5.42 through the droplet Reynold's number i.e. $\frac{d\rho_c V_o}{\mu_c}$. The vertical relative velocity of drops V_o is calculated by Misek's equation 8.21 which relates the phases velocities with hold-up and the resulting figure gives no indication whatsoever to phase flowrates used, as shown in Table 8.4. The above reasons explain why some of the comparisons of $K_{Exp}/K_{cal}^{(1)}$ are too low i.e. between 0.57 and 0.79.

b) The Mass Transfer coefficient calculated by Angelo et al (118) equations are shown in Table 8.6 $K_{cal}^{(2)}$ and are compared in Table 9.7, as the ratio $K_{Exp}/K_{cal}^{(2)}$. Comparative results are generally low for the D→C runs, which means that the calculated mass transfer coefficient is higher than that estimated experimentally. This is generally because the values produced by Angelo et al (118) equations are usually higher than those produced by the Rose and Kintner model (125) as previously reported (135). Again the comparison ratios deteriorate at lower phases flowrates and this might be attributed to the inadequate allowance for phased flowrates in the equation used in the

calculation. However, comparison of the results of runs 8 and 16 are much better than those for Rose and Kintner ($K_{Exp}/K_{cal}^{(1)}$); this is due to the fact that the contribution of the oscillating drops regime is very small as shown in Table 8.6. Run no. 5 was exceptional as $K_{cal}^{(1)}$ was higher than $K_{cal}^{(2)}$ as in Table 8.6, this is believed to be due to the fact that the continuous mass transfer coefficient calculated by the Garner et al (154) correlation is exceptionally high because of the very high Vo as shown in Table 8. 4 and 8.6. The absence of oscillating drops from the calculation of $K_{cal}^{(2)}$ for runs 23 and 24 as shown in Table 8.6, increases the ratio considerably to 23.88 and 17.11 respectively, and this can be explained as before in the $K_{Exp}/K_{cal}^{(1)}$ for the C→D runs.

c) The circulating and oscillating drop overall mass transfer coefficients, $K_{o.c}$, $K_{o.o}^{(1)}$ and $K_{o.o}^{(2)}$ (shown in Table 8.5 and 8.6). The comparison ratios shown in Table 9.7 confirms the need for the drop size distribution to be involved in the calculations of the theoretical overall mass transfer coefficient. The circulating drop overall mass transfer coefficient $K_{o.c}$ varied between 5.46 and 29.70 times K_{Exp}. Again this may be attributed to the tendency of circulating drops to oscillate due to the presence in swarms of drops adjacent to oscillating drops in a high turbulent region. The comparison ratio decreases as the proportion of circulating drops ν increases, as shown in Table 8.5. Comparison ratio of $K_{Exp}/K_{o.o}^{(1)}$ are generally below 1.0 for D→C runs and this ratio becomes nearer to 1.0 as the proportion of the oscillating drops $1-\nu$ increases.

Only Run no. 5 has a ratio just over 1.0 for D→C runs. This run was carried out at zero rotor speed, at which inter-droplet coalescence was enhanced and large drops were observed along the column, and it is not surprising that the experimental mass transfer coefficient was high. Only in two runs, no. 21 and 22, of the four runs of C→D were oscillating drops present in high proportions in their drop size distribution diagram and surprisingly the comparison ratio with K_{Exp} are higher than 1.0; that is 1.63 and 1.21 respectively. The experimental mass transfer coefficients were noticeably high for these two runs, due to very small driving force, as shown in Table 8.3, and the ratio with the calculated $K_{o.o}^{(1)}$ became higher than 1.0. Finally in Table 9.7 is the comparison ratio of $K_{Exp}/K_{cal}^{(2)}$ which is less than 1.0 for all the runs with the exception of run no. 5 due to the same reason as mentioned earlier for $K_{cal}^{(1)}$. Again all the ratios are less than those involving $K_{cal}^{(1)}$. This is believed to be due to the fact that all the results produced by Angelo et al (118) equations were higher than those produced by Rose and Kintner model (125), and with exception of run 5 the continuous mass transfer coefficient calculated by Garner et al (154) was very high as seen in Table 8.6.

The theoretical overall mass transfer coefficients $K_{cal}^{(1)}$ shows generally very good comparable results with the experimental coefficients, and the range of the ratios between the coefficients ($K_{Exp}/K_{cal}^{(1)}$) is very narrow compared with that previously reported by Al-Hemiri (25), who used the traditional calculation method. No stagnant

drops were included in the calculation because of the limitation of the photographic technique used in measuring the drop size and drop size distribution. However, they exist in the dispersion but their contribution to the overall mass transfer coefficient will be insignificant because the proportion will be very small compared to the whole drop population.

The use of droplet Reynold's number, as a measure of the state of the drops in classifying them as, stagnant, Circulating and oscillating drops, is inadequate for accurate classification in agitated systems. This may be a cause for a small error in the drops proportions fraction i.e. ν and $(1-\nu)$, which may have very little effect on the final values of the theoretical overall mass transfer coefficient.

CHAPTER TEN

Conclusions

The main conclusions arising from this work are as follows.

1. Non-mass Transfer Studies

i) Drop size:

a) None of the previous published correlations based on small-scale R.D.C., give a satisfying prediction of the drop size in a large scale R.D.C.

b) The drop size correlation developed in this study. Equations 8.4 and 8.5 give a more accurate prediction of the drop size in a large R.D.C.

c) The effect of rotor speed, dispersed phase flow rate. Column geometry, interfacial tension and density difference, upon drop size was confirmed.

ii) Drop Size Distribution:

The Mugele-Evans upper-limit distribution function accurately represents experimental drop size distributions of dispersion in a R.D.C.

iii) Dispersed Phase Hold-up:

a) Most of the previously published correlations failed to produce a satisfactory prediction of the dispersed phase hold-up in a large scale R.D.C.

b) The characteristic velocity approach to estimate the dispersed phase hold-up using Equation 3.9 is not a very reliable means for the R.D.C. However, the two correlations developed in this study. Equation 8.11 and 8.12 give more accurate estimations for the characteristic velocity than those previously published over the range shown in the corresponding table mentioned in Section 9.1.4.

c) Correlation 8.14 gives very reliable prediction of the dispersed phase hold-up for a wide range of column geometries and operating conditions.

2. Mass Transfer Study

i) Both drop size and dispersed phase hold-up are different when mass transfer is occuring compared to non-mass transfer conditions. Therefore data obtained under non-mass transfer conditions must be applied with caution in column design.

ii) Direction of Mass Transfer:

with the system studied, solute transfer from dispersed to continuous phase enhanced coalescence, and transfer

in the opposite direction reduced it.
The consequences of enhanced coalescence were larger drop sizes and less hold-up, and vice-versa.

iii) Experimental Overall Mass Transfer Coefficient:

a) The use of driving force profile along the column to calculate the mean driving force viz Simpson's Rule results in more precise experimental overall mass transfer coefficient.

b) There is an optimum rotor speed at which maximum mass transfer occurs due to maximum overall volumetric mass transfer coefficient $(Ka)_{Exp}$ at that point.

iv) Theoretical Overall Mass Transfer Coefficient:

a) With drop size distribution.
The use of the dorp size distribution in the calculation of the theoretical overall mass transfer coefficient gives results that are very comparable with experimental coefficients and the method of calculation mentioned in Section 8.2.2 represents a first step in making such a calculation more rigorous.

b) Without drop size distribution:
The wide deviation in the calculated mass transfer coefficient based on a uniform-drop size assumption, from that of the experimental

coefficient K_{Exp}, confirms that different mass transfer mechanisms occur simultaneously as the drop size distribution must be included in the calculation process.

c) Mass transfer coefficient models:
The oscillating drop mass transfer coefficient models of Rose et al (125) and Garner et al (154), generally give closer results to the experimental coefficient than that of Angelo et al (118).

In conclusion the correlations and methods of calculation presented in this work should, when used as part of an established design procedure (183) result in a more precise design of columns for commercial duties.

CHAPTER ELEVEN

Recommendation for Further Work

1. The prediction of drop size and dispersed phase hold-up under mass transfer conditions are less reliable by the correlations developed in this work for non-mass transfer conditions. More work is needed to determine a correction factor with respect to solute concentrations and mass transfer direction.

2. To improve the calculation of the theoretical overall mass transfer coefficient with the involvement of drop size distribution, more work is needed to find a new basis for classifying the state of drops viz stagnant, circulating or oscillating in the agitated contactor. In addition to droplet Reynold's number the correlations should include the Weber number ($N^2\rho_c D_r^3/\sigma$) as well.

3. The effect of the phase flowrate on the theoretical mass transfer coefficient is negligible but it was found to be very significant on the experimental coefficient. This suggests improvements in the correlations and models for the mass transfer coefficient with respect to phases flowrates will be very appreciable.

4. The effect of the axial mixing in either phase or both on the column performance has long been one of the major problems encountered in agitated extractor operation. Therefore quantitative assessment of this phenomenon would be very useful.

APPENDICES

APPENDICES

APPENDIX I

Physical Properties of Liquid-Liquid System.

APPENDIX 1

Physical Properties of Liquid-Liquid System.

1.1 Physical Properties of Clairsol-350

Clairsol-350: purchased as an industrial grade solvent from Carless Solvents Ltd. with the following properties.

Density = 0.7830 gm/cc at 20°C

Kinematic viscosity = 2.112 cs at 20°C

Flash Point = 71.1 °C

Boiling Range = 205 - 230 °C.

Average molecular weight ≈ 160 - 170 gm/gmmole

Interfacial Tension with Filtered Tap Water = 32.9 dyne/cm at 20°C.

1.2 Physical Properties of Filtered Tap Water.

Density = 0.9970 gm/cc at 20°C.

Kinematic viscosity = 0.0102 cs at 20°C.

APPENDIX II

Calibration Charts, Equilibrium Distribution and Interfacial Tension Graph.

Contents of Appendix II

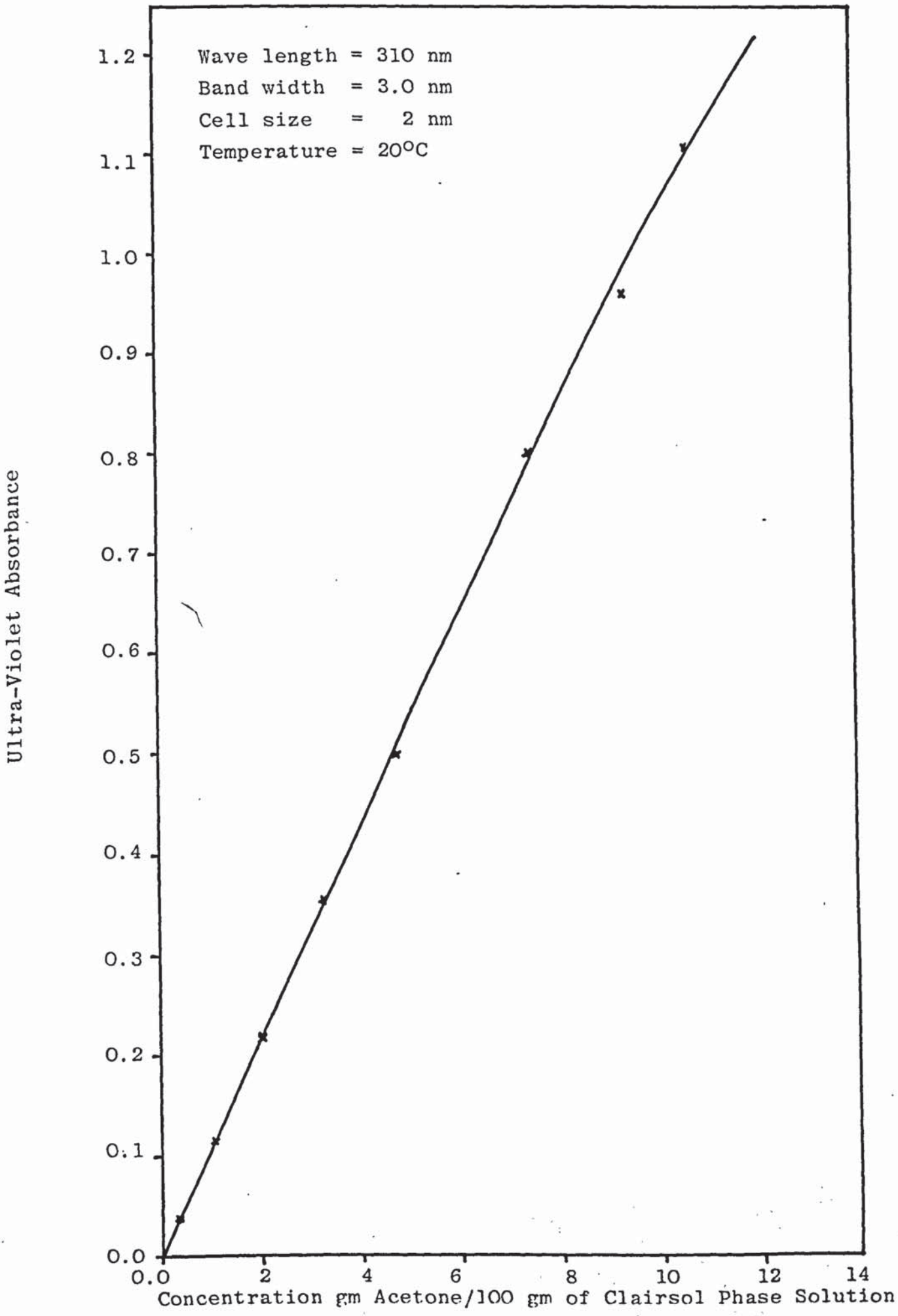

Fig. I Concentration of Acetone in Clairsol Phase vs Ultra-Violet Absorbance

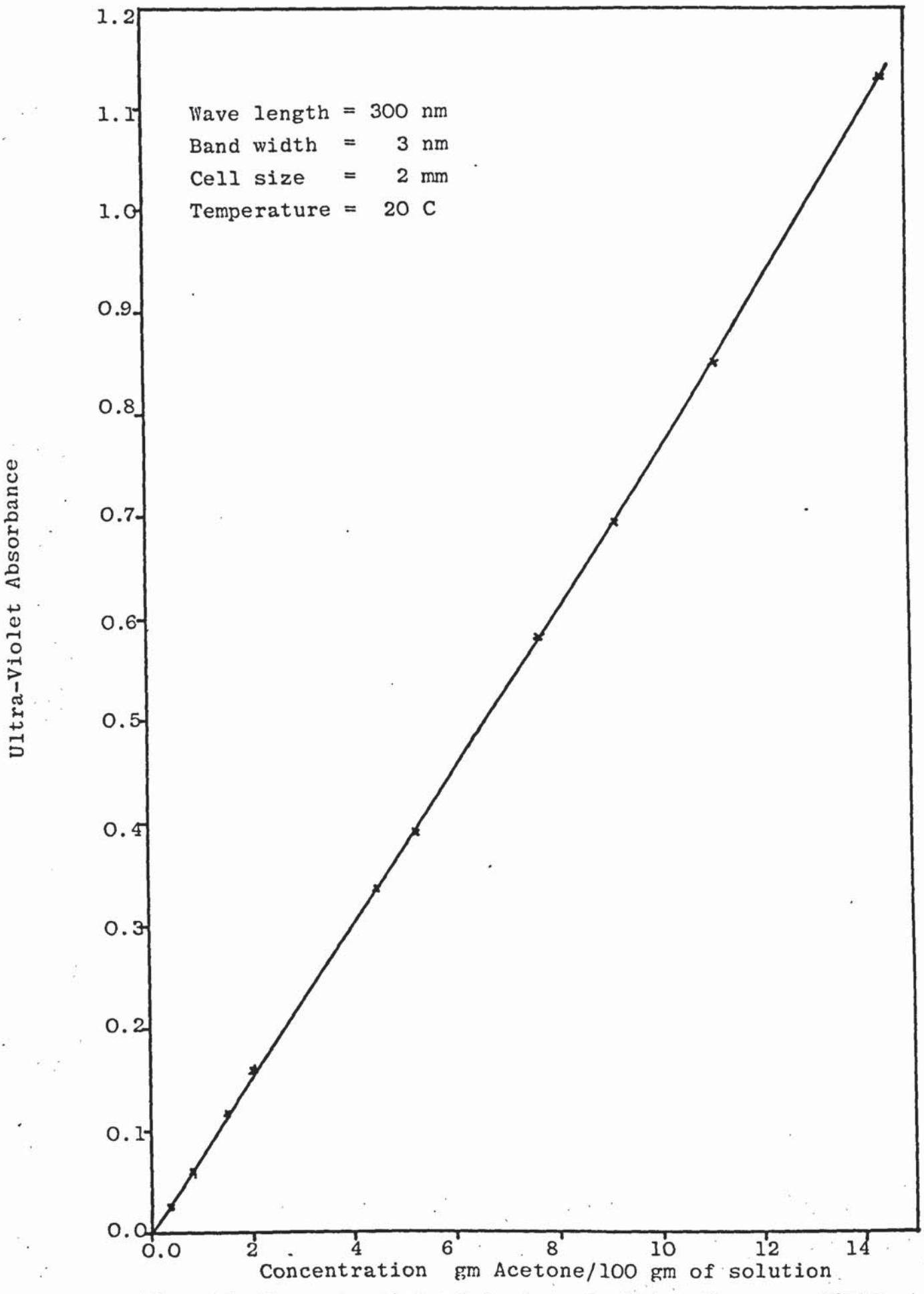

Fig. II Concentration of Acetone in Water Phase vs Ultra-Violet Absorbance

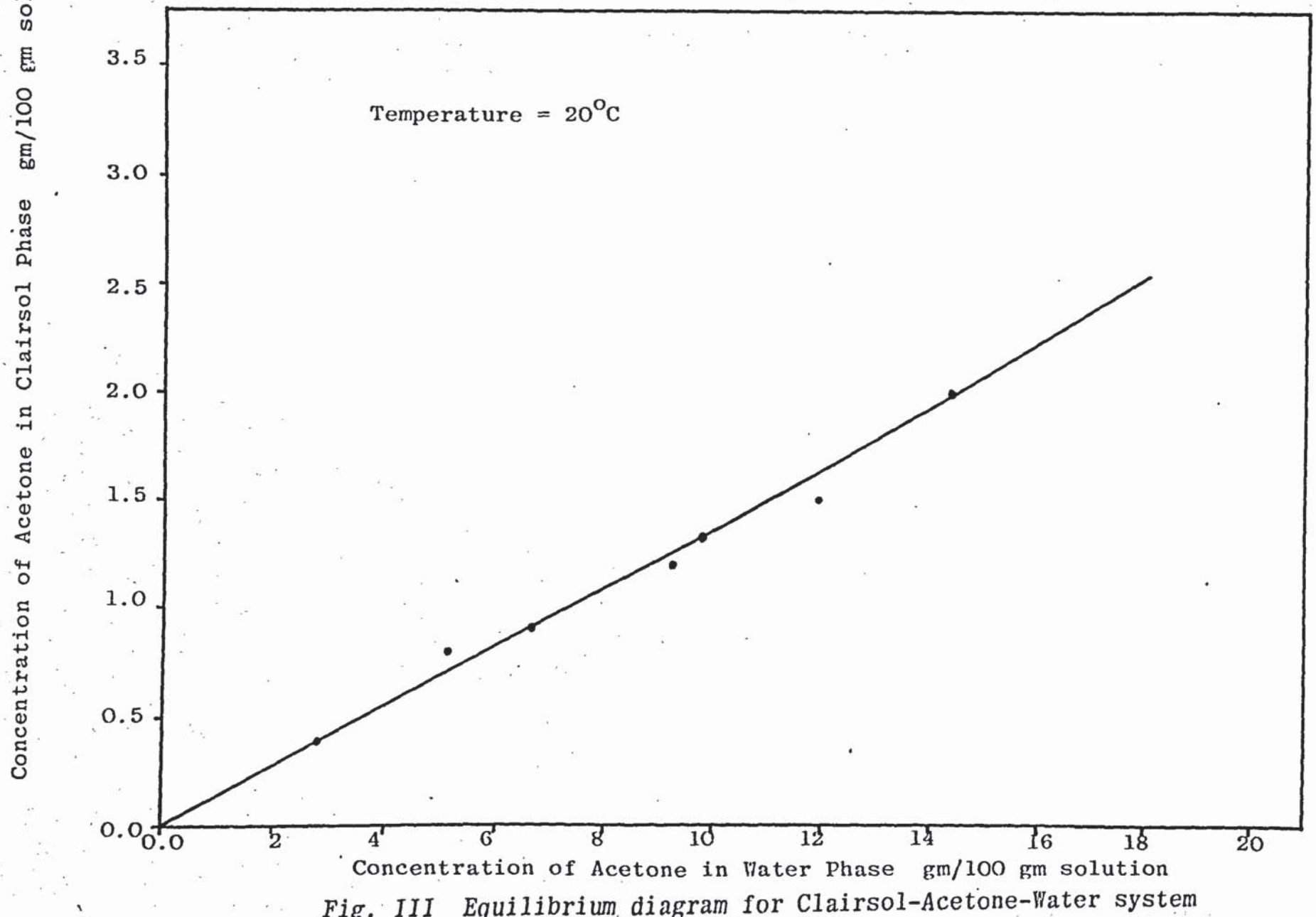

Fig. III Equilibrium diagram for Clairsol-Acetone-Water system

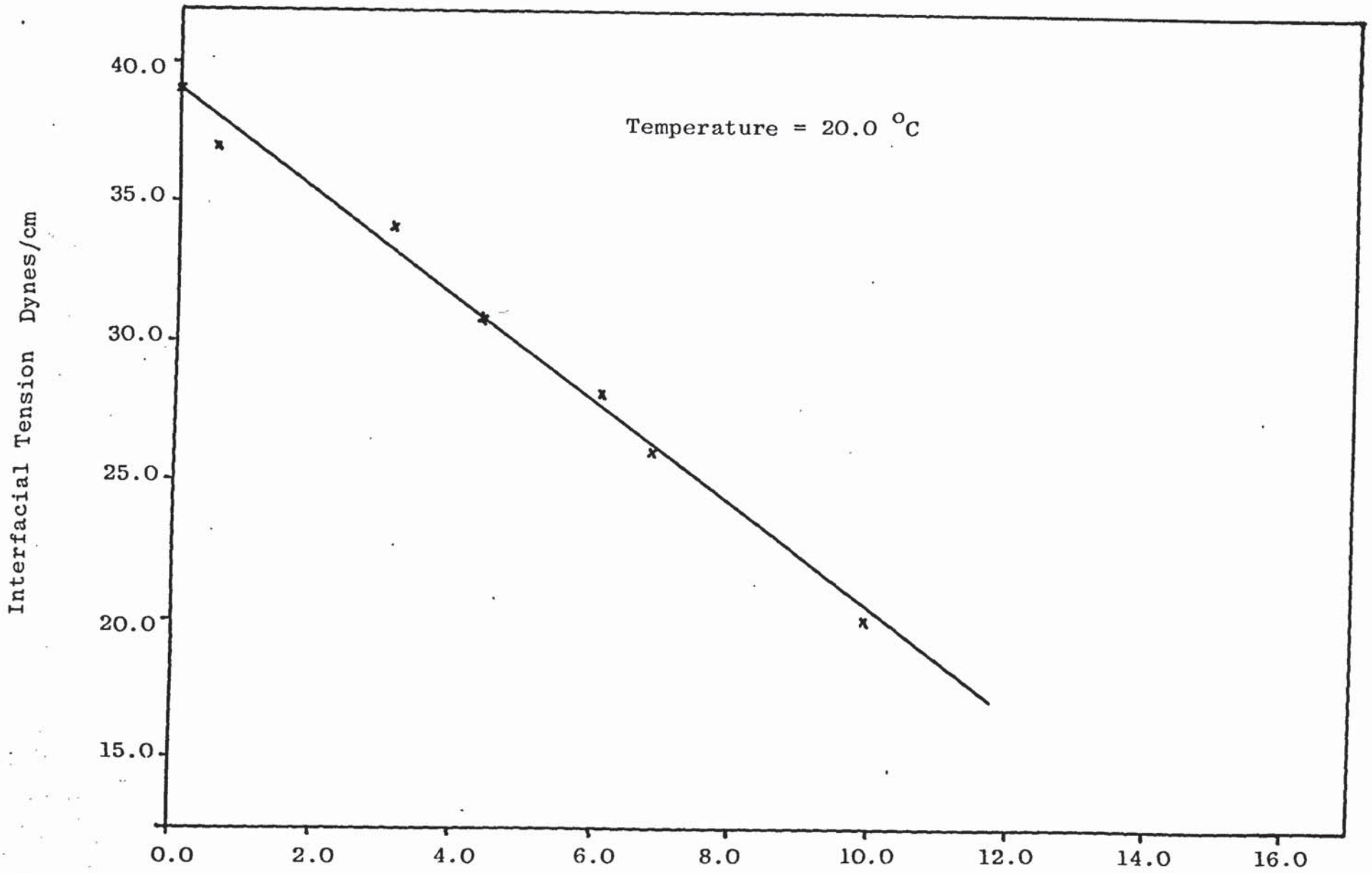

Fig. IV Variation of interfacial tension (with water) with concentration of acetone in clairsol phase

APPENDIX III

Simple Calculation of Drop Size (d_{32}) and Drop Size Distribution

Compartment No. = 14

Rotor Speed = 300 R.P.M.

Magnification = 1.80

Hold-up % = 6.6

1) Drop Size Count

$$d_{actual} = \frac{d_{observed}}{Magnification}$$

$$d_{32} = \frac{\Sigma nidi^3}{\Sigma nidi^2} \qquad (7.1)$$

2) Drop Size Distribution

Cumulative drops volume = $\nu_i = \Sigma_{ni}(\frac{\pi}{6}d_i^3)$ (8.6)

$$\% \text{ Cumulative drops volume} = \frac{\nu_i}{\nu_{Total}} \times 100$$

$$\frac{d\nu}{dd} = \frac{\nu_{f.i} - \nu_{f.i-1}}{d_i - d_{i-1}}$$

where ν_f is the fractional cumulative drop volume

$$\nu_{f.i} = \frac{\nu_i}{\nu_{Total}}$$

Table III.I shows the drop size distribution results.

d_{32} = 2.23 mm.

Drop size distribution curve shown in Figure 7.4,from the distribution curve.

Table III.I Drop Size Distribution Results

l	$d_{observed}$ mm	d_{actual} mm	n	ν_{mm^3}	$\nu\%$	$\frac{d\nu}{dd}$ mm^{-1}
1	0.86	0.478	1	0.057	0.006	0.0001
2	1.05	0.583	2	0.265	0.030	0.002
3	1.23	0.683	4	0.932	0.106	0.008
4	1.60	0.889	6	3.139	0.355	0.012
5	1.78	0.989	8	7.191	0.814	0.046
6	1.97	1.094	10	14.050	1.590	0.074
7	2.15	1.194	11	23.850	2.700	0.111
8	2.34	1.300	12	37.660	4.270	0.148
9	2.52	1.400	15	59.210	6.710	0.244
10	2.70	1.500	14	83.950	9.510	0.280
11	2.89	1.606	13	112.140	12.700	0.302
12	3.07	1.706	13	145.940	16.520	0.382
13	3.26	1.811	12	183.260	20.750	0.400
14	3.44	1.911	11	223.450	25.800	0.455
15	3.62	2.011	9	261.780	29.640	0.434
16	3.81	2.117	9	306.490	34.700	0.479
17	3.99	2.217	8	352.130	39.860	0.517
18	4.18	2.322	7	398.020	45.060	0.492
19	4.36	2.422	8	457.530	51.700	0.674
20	4.54	2.522	6	507.930	57.510	0.571
21	4.73	2.628	6	564.950	63.960	0.611
22	4.91	2.728	5	618.100	69.980	0.602
23	5.10	2.833	5	677.620	76.720	0.639
24	5.28	2.933	4	730.470	82.700	0.598
25	5.46	3.033	3	774.290	87.670	0.496
26	5.65	3.139	2	806.680	91.330	0.347
27	5.83	2.239	2	842.270	95.360	0.403
28	6.02	3.344	1	861.850	97.580	0.210
29	6.20	3.444	1	883.230	100.000	0.242
Σ	-	-	-	208	883.230	-	-

at $\nu\% = 10$ $\quad d_{10} = 1.52$ mm

$\nu\% = 50$ $\quad d_{50} = 2.38$ mm

$\nu\% = 90$ $\quad d_{90} = 3.08$ mm

$$\frac{d_m}{d_{50}} = \frac{d_{50}(d_{90}+d_{10})-2d_{90}d_{10}}{d_{50}^2 - d_{90}d_{10}} \qquad (8.7)$$

$$\frac{d_m}{2.38} = \frac{2.38(3.08+1.52)-2x3.08x1.52}{(2.38)^2-3.08x1.52}$$

$$d_m = 3.838 \text{ mm}$$

$$a' = \frac{d_m-d_{50}}{d_{50}} \qquad (8.8)$$

$$a' = \frac{3.838 - 2.38}{2.38}$$

$$a' = 0.613$$

$$\delta = \frac{0.907}{\text{In}\left(\frac{d_{90}}{d_m-d_{90}} \cdot \frac{d_m-d_{50}}{d_{50}}\right)} \qquad (8.9)$$

$$\delta = \frac{0.907}{\text{In}\left(\frac{3.08}{3.838-3.08} \cdot \frac{3.838-2.38}{2.38}\right)}$$

$$\delta = 0.994$$

Figure 8.2B shows the experimental drop size distribution in comparison with upper limit distribution function.

APPENDIX IV

Sample Calculation of Overall Mass Transfer Coefficient

Calculation of Run 2. (Results shown in Tables 8.2, 8.3, 8.4, 8.5 and 8.6).

(1) The Overall Experimental Mass Transfer Coefficient.

Hold-up = 4.52% d_{32} = 0.35 cm

V_c = 0.66 cm/sec V_d = 0.28 cm/sec

Effective column height = 371 cm Rotor Speed = 200 r.p.m.

Column Cross Sectional area = 1590.43 cm^2

$y^* = 7.34x$ Equilibrium line equation as shown in Appendix 11, Diagram III.

i.e. m = 7.34

	y	X	y*	$\Delta y = y^* - y$
Bottom	0.410	1.45	10.643	10.233
Comp. 1	0.357	1.292	9.483	9.126
Comp. 3	0.303	1.130	8.294	7.991
Comp. 6	0.192	0.798	5.857	5.665
Comp. 9	0.134	0.625	4.588	4.454
Comp. 12	0.070	0.433	3.178	3.108
Top	0.000	0.224	1.643	1.643

The specific interfacial area $a = \frac{6X}{d_{32}}$ (8.15)

$$a = \frac{6 \times 0.0452}{0.35} = 0.775 \ cm^2/cm^3$$

Total interfacial area = A = a.V (8.16)

where V is the effective column volume.

$$A = 0.775 \times 371 \times 1590.43$$

$$A = 457204.1 \text{ cm}^2$$

The mean driving force Δy_m was estimated by applying Simpson's Rule as

$$\Delta y_m = \frac{1}{18}\left[\Delta y_{Top} + \Delta y_{Bot} + 4(\Delta y_1 + \Delta y_6 + \Delta y_{12}) + 2(\Delta y_3 + \Delta y_9)\right]$$

$$\Delta y_m = \frac{1}{18}\left[10.233 + 1.643 + 4(9.126 + 5.665 + 3.108) + 2(7.991 + 4.454)\right]$$

$$\Delta y_m = 5.31 \frac{\text{gm Acetone}}{\text{100 gm aqueous solution}}$$

Density of aqueous phase solution = 0.985 gm/cc

$$\Delta C_m = \frac{5.31}{100 \times 0.985} = 0.054 \frac{\text{gm Acetone}}{\text{cm}^3 \text{ solution}}$$

Rate of Mass Transfer $N = Q_c \rho_c (y_{out} - y_{in}) = Q_d \rho_d (x_{in} - x_{out})$

$$N = 0.66 \times 1590.43 \times 0.985 \ (0.00411 - 0.0000)$$

$$N = 4.25 \text{ gm/sec}$$

$$\therefore \quad K_{Exp} = \frac{N}{A \Delta C_m} \qquad (8.19)$$

$$K_{Exp} = \frac{4.25}{457204.1 \times 0.054}$$

$$\therefore \quad K_{Exp} = 1.72 \times 10^{-4} \text{ cm/sec}$$

(II) Theoretical Overall Mass Transfer Coefficient

The vertical relative velocity of drops of V_o in the R.D.C. was determined by applying Misek's equation (46),

$$V_o = \left[\frac{V_d}{X} + \frac{V_c}{1-X}\right] \qquad (8.21)$$

$$V_o = \left[\frac{0.28}{0.0452} + \frac{0.66}{1-0.0452}\right]$$

$$V_o = 6.886 \quad \text{cm/sec}$$

The maximum diameter of the stagnant drops in the whole drop population when droplet Reynolds number Re=10 was found from

$$\frac{d_s \rho_c V_o}{\mu_c} = 10$$

$$\therefore \quad d_s = \frac{10 \times 0.0102}{0.985 \times 6.886}$$

$$d_s = 0.015 \text{ cm}$$

The minimum diameter of the oscillating drops regime when Re=200 was,

$$d_o = \frac{200 \times 0.0102}{0.985 \times 6.886}$$

$$d_o = 0.298 \text{ cm}$$

The drop size distribution diagram of Figure V shows that d_s is too small to be included in the calculation. Hence the drop population is considered to contain only circulating and oscillating drops, with d_o the boundary between the two regimes. Therefore from the drop size distribution diagram, the fractional proportion of circulating drops $\nu = 0.30$, and the oscillating drops fractional proportion = $1 - \nu = 0.7$

1. Circulating Drop Regime:

a) Dispersed phase mass transfer coefficient was estimated by the Kronig and Brink (138) equation,

$$k_{d.c} \simeq \frac{17.9 D_d}{\bar{d}_c} \qquad (8.24)$$

$D_d = 1.298 \times 10^{-7}$ cm^2/sec for diffusion of acetone in clairsol

$\bar{d}_c = 0.26$ cm from drop size distribution diagram Figure

$$\therefore \quad k_{d.c} = \frac{17.9 \times 1298 \times 10^{-7}}{0.26}$$

$$k_{d.c} = 8.94 \times 10^{-6} \text{ cm/sec}$$

b) Continuous phase mass transfer coefficient was estimated by Garner et al (154) correlation,

$$\frac{k_{c.c}\bar{d}_c}{D_c} = -126 + 1.8\, Re^{0.5} S_c^{0.42} \qquad (5.42)$$

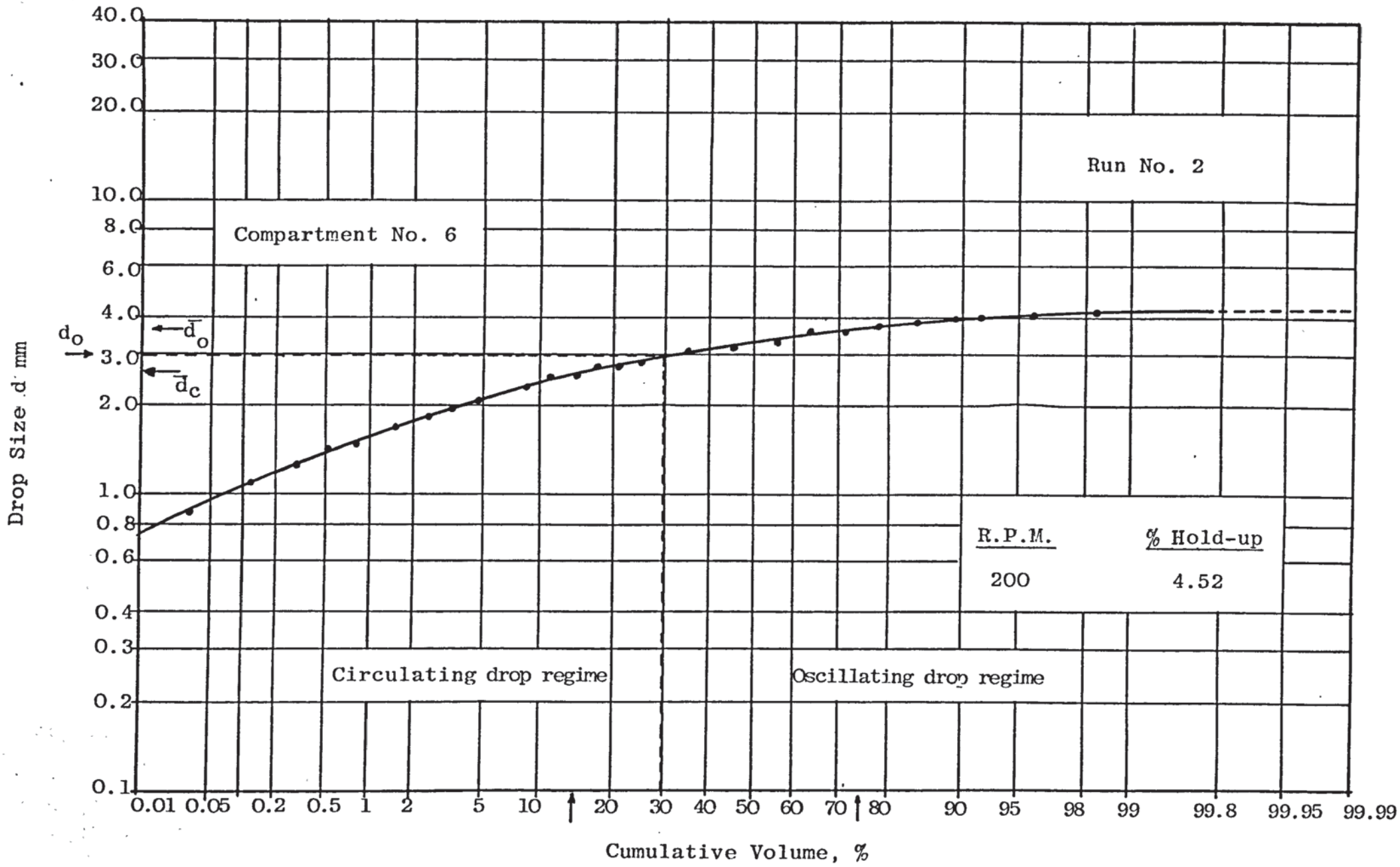

Figure V -- Drop size distribution of compartment No. 6 for Run 2

$D_c = 1.119 \times 10^{-7}$ cm^2/sec for diffusion of acetone in water.

$$\frac{k_{c.c} \times 0.26}{1.119 \times 10^{-7}} = -126 + 1.8 \left(\frac{0.25 \times 0.985 \times 6.886}{0.0102}\right)^{0.5} \left(\frac{0.0102}{0.985 \times 1.119 \times 10^{-7}}\right)^{0.42}$$

$$\therefore \quad k_{c.c} = 1.19 \times 10^{-3} \text{ cm/sec}$$

c) Overall Mass Transfer Coefficient of the Circulating Drops

$$\frac{1}{K_{o.c}} = \frac{1}{k_{d.c}} + \frac{m}{k_{c.c}} \qquad (8.25)$$

$$\frac{1}{K_{o.c}} = \frac{1}{8.94 \times 10^{-6}} + \frac{7.34}{1.19 \times 10^{-3}}$$

$$K_{o.c} = 8.47 \times 10^{-6} \text{ cm/sec}$$

2. Oscillating Drop Regime:

a) Dispersed phase mass transfer was firstly estimated by Rose and Kintner (125) equation,

$$k_{d.o} = 0.45 \, (D_d \omega)^{0.5} \qquad (5.28)$$

where

$$\omega^2 = \frac{\sigma b}{r^3} \left[\frac{n(n-1)(n+1)(n+2)}{(n+1)\rho_d + n\rho_c}\right] \qquad (5.26)$$

$$n = 2$$

$$b = \frac{\bar{d}_o^{0.225}}{1.242}$$

$\bar{d}_o$ = 0.37 cm from drop size distribution diagram Figure IV.1.

$$b = \frac{(0.37)^{0.225}}{1.242} = 0.644$$

$$r = \frac{0.37}{2} = 0.185 \text{ cm}$$

$$\sigma = 35.0 \text{ dyne/cm}$$

$$\omega^2 = \frac{35.0 \times 0.644}{(0.185)^3}\left[\frac{2(2-1)(2+1)(2+2)}{(2+1)0.783+2\times0.985}\right]$$

$$\omega = 140.65 \text{ 1/sec}$$

$$k_{d.o} = 0.45(1.298\times10^{-7}\times140.65)^{0.5}$$

$$k_{d.o} = 1.92\times10^{-3} \text{ cm/sec}$$

Secondly by Angelo et al (118) Equation,

$$k_{d.o} = \sqrt{\frac{4Dd\omega(1+\varepsilon+\frac{3}{8}\varepsilon^2)}{\pi}} \qquad (8.26)$$

where

$$\varepsilon = 0.434\left(\frac{\omega\bar{d}_o}{V_o}\right)^{-0.46}\left(\frac{\bar{d}_o V_o^3 \rho_c}{\sigma}\right)^{-0.53}\left(\frac{\mu V_o}{\sigma}\right)^{-0.11} \qquad (8.27)$$

$$\varepsilon = 0.434\left(\frac{140.65\times0.37}{6.886}\right)^{-0.46}\left(\frac{0.37(6.886)^3\times0.985}{35}\right)^{-0.53}$$

$$\left(\frac{0.0102\times6.886}{35}\right)^{-0.11}$$

$$\varepsilon = 0.177$$

$$k_{d.o} = \sqrt{\frac{4x1.298x10^{-7}x140.65(1+0.177+\frac{3}{8}x(0.177)^2}{\pi}}$$

$$k_{d.o} = 5.26 \times 10^{-3} \text{ cm/sec}$$

b) Continuous phase mass transfer coefficient was estimated by Garner et al (126) correlation,

$$\frac{k_{c.o}\bar{d}_o}{D_c} = 50 + 0.0085 \text{ Re } Sc^{0.7} \qquad (5.42)$$

$$\frac{k_{c.o}x0.37}{1.119x10^{-7}} = 50 + 0.0085(\frac{0.37x6.886x0.985}{0.0102}$$

$$(\frac{0.0102}{0.985x1.119x10^{-7}})^{0.7}$$

$$k_{c.o} = 1.91 \times 10^{-3} \text{ cm/sec}$$

c) The overall mass transfer coefficient of oscillating drops.

Firstly for Rose and Kintner (125) and Garner et al (126)

$$\frac{1}{K_{o.o}} = \frac{1}{k_{d.o}} + \frac{m}{k_{c.o}} \qquad (8.28)$$

$$\frac{1}{K_{o.o}} = \frac{1}{1.92x10^{-3}} + \frac{7.34}{1.91x10^{-3}}$$

$$K_{o.o}^{(1)} = 2.29 \times 10^{-4} \text{ cm/sec}$$

Secondly by Angelo et al (118) equation,

$$K_{o.o} = k_{d.o}\left[\frac{1}{1+m\sqrt{\frac{Dd}{Dc}}}\right] \qquad (8.29)$$

$$K_{o.o} = 5.26 \times 10^{-3}\left[\frac{1}{1+7.34\sqrt{\frac{1.298\times10^{-7}}{1.119\times10^{-7}}}}\right]$$

$$K^{(2)}_{o.o} = 5.91 \times 10^{-4} \text{ cm/sec}$$

So the theoretical overall mass transfer coefficient for the whole drop population

$$K_{cal} = K_{o.c}\nu + K_{o.o}(1-\nu) \qquad (8.30)$$

$$K^{(1)}_{cal} = 8.47 \times 10^{-6} \times 0.30 + 2.29 \times 10^{-4}(1-0.30)$$

$K^{(1)}_{cal} = 1.63 \times 10^{-4}$ cm/sec for Rose and Kintner and Garner et al,

or

$$K^{(2)}_{cal} = 8.47 \times 10^{-6} \times 0.30 + 5.91 \times 10^{-4}(1-0.30)$$

$K^{(2)}_{cal} = 4.16 \times 10^{-4}$ cm/sec for Angelo et al.

APPENDIX V

*Multi-Linear Least Square Computer Program (used for regression analysis of the dispersed phase hold-up data).

```
     *****    ****   ****    *****   *****     **      *
**   *        *      *   *       *       *     *      *
**   *        *      *   *       *       *     *      *
     ****     *      ****    *****   *****     *      * *
**   *        *      *       *       *         *      * *
**   *        *      *       *       *         *      *****
     *****    ****   *       *****   *****   *****      *

#LISTING OF :ECP2214.HOLD(188/) PRODUCED ON 25MAR82 AT 16.07.01

#G8.65E AT ASTON     IN ':ECP2214.KIFAH' ON  5APR82 AT 08.03.59

DOCUMENT     HOLD

      0        TRACE 0
      1        MASTER HOLD UP
      2        DIMENSION X(104,9),Y(104),AA(104),B(104,9),XBAR(104),
      3       *          NS(55),VN(104),VC(104),VD(104),XH(104),
      4       *          VIS(7),DEN(7),DENDF(7),RN(104),CH(104),
      5       *          SIG(7),DT(7),CALXH(104),ERROR(104),DR(104),
      6       *          YHAT(104),DS(104),A(104)
      7        READ (1,1) NSET1,NSET2,NSET3,NSET4,NSET5
      8     1  FORMAT (5I0)
      9        WRITE (2,2) NSET1,NSET2,NSET3,NSET4,NSET5
     10     2  FORMAT (//,2X,6HNSET1=,I4,8X,6HNSET2=,I4,8X,
     11       *          6HNSET3=,I4,8X,6HNSET4=,I4,8X,
     12       *          6HNSET5=,I4)
     13        DO 200 I=1,5
     14        READ (1,3) DEN(I),DENDF(I),VIS(I),SIG(I),DT(I),GRAV
     15     3  FORMAT (6F0.0)
     16        WRITE (2,41)
     17    41  FORMAT (//,2X,1HI,8X,7HDENSITY,8X,12HDENSITY DEF.,
     18       *          7X,9HVISCOSITY,7X,12HINT. TENSION,7X,
     19       *          13HCOL. DIAMETER,8X,12HGRAVITY ACC.)
     20        WRITE (2,4)  I,DEN(I),DENDF(I),VIS(I),SIG(I),
     21       *             DT(I),GRAV
     22     4  FORMAT (/,2X,I1,6X,F8.4,9X,F8.4,10X,F8.4,10X,F8.4,
     23       *          12X,F8.4,12X,F8.4)
     24        WRITE (2,31)
     25    31  FORMAT (///,2X,2H J,8X,2HRN,12X,2HVC,12X,2HVD,12X,
     26       *          2HVN,12X,2HXH,12X,2HDS,12X,2HDR,11X,2HCH)
     27        IF(I.EQ.1) GO TO 101
     28        IF(I.EQ.2) GO TO 102
     29        IF(I.EQ.3) GO TO 103
     30        IF(I.EQ.4) GO TO 104
     31        IF(I.EQ.5) GO TO 105
     32   101  NS(I)=NSET1
     33        GO TO 100
     34   102  NS(I)= NSET2
     35        GO TO 100
     36   103  NS(I)=NSET3
     37        GO TO 100
     38   104  NS(I)=NSET4
     39        GO TO 100
     40   105  NS(I)=NSET5
     41   100  DO 201 K=1,NS(I)
     42        IF(I.EQ.1)  GO TO 56
```

```
      IF(I.EQ.2)  GO TO 57
      IF(I.EQ.3)  GO TO 58
      IF(I.EQ.4)  GO TO 59
      IF(I.EQ.5)  GO TO 60
56    J=K
      GO TO 55
57    J=K+NS(I-1)
      GO TO 55
58    J=K+NS(I-2)+NS(I-1)
      GO TO 55
59    J=K+NS(I-3)+NS(I-2)+NS(I-1)
      GO TO 55
60    J=K+NS(I-4)+NS(I-3)+NS(I-2)+NS(I-1)
55    READ (1,5) RN(J),VC(J),VD(J),VN(J),XH(J),DS(J),DR(J)
     *          ,CH(J)
 5    FORMAT(8F0.0)
      WRITE (2,8) J,RN(J),VC(J),VD(J),VN(J),XH(J),DS(J),
     *            DR(J),CH(J)
 8    FORMAT (/,2X,I2,4X,F8.4,6X,F8.4,6X,F8.4,6X,F8.4,6X
     *         ,F8.4,6X,F8.4,6X,F8.4,6X,F8.4)
      B(J,1) =RN(J)*DR(J)/VC(J)
      B(J,2) =VD(J)/VC(J)
      B(J,3) =((DS(J)**2)-(DR(J)**2))/(DT(I)**2)
      B(J,4) =CH(J)/DT(I)
      B(J,5) =DR(J)/DT(I)
      B(J,6) =DENDF(I)/DEN(I)
      B(J,7) =DEN(I)*DT(I)*(VC(J)**2)/SIG(I)
      B(J,8) =VC(J)**2/(GRAV*DT(I))
      B(J,9) =DEN(I)*VC(J)*DT(I)/VIS(I)
      Y(J)   =ALOG(XH(J))
      X(J,1) =ALOG(B(J,1))
      X(J,2) =ALOG(B(J,2))
      X(J,3) =ALOG(B(J,3))
      X(J,4) =ALOG(B(J,4))
      X(J,5) =ALOG(B(J,5))
      X(J,6) =ALOG(B(J,6))
      X(J,7) =ALOG(B(J,7))
      X(J,8) =ALOG(B(J,8))
      X(J,9) =ALOG(B(J,9))
201   CONTINUE
200   CONTINUE
      WRITE (2,9)
 9    FORMAT (///,10X,8HY MATRIX)
      DO 203 IK= 1,J
      WRITE (2,10) IK,Y(IK)
10    FORMAT (/,4X,I3,10X,F10.4)
203   CONTINUE
      WRITE (2,11)
11    FORMAT (//,10X,8HB MATRIX)
      DO 280 II=1,J
      WRITE (2,12) II,(B(II,JJ), JJ=1,9)
12    FORMAT (/,3X,I3,9(3X,F9.5))
280   CONTINUE
      WRITE (2,13)
13    FORMAT (//,10X,8HX MATRIX)
      DO 204  KK=1,J
      WRITE (2,14) KK,(X(KK,JJ), JJ=1,9)
14    FORMAT (/,3X,I3,9(3X,F9.5))
204   CONTINUE
      NB=9
```

```
      NX=9
      NN=NB*NB
      M=J
      CALL LESQ(X,Y,NB,M,A,B,XBAR,YHAT,AA,NN)
      WRITE (2,888)
888   FORMAT (/,5X,3H L ,5X,24HEXPERIMANTAL VALUE OF XH,
     *          10X,22HREGRESSION VALUE OF XH,10X,
     *          15HPERCENTAG ERROR)
      SUMER =0.0
      DO 777 L=1,M
      IF(L.LE.31)  GO TO 111
      IF(L.LE.83)  GO TO 222
      IF(L.LE.101) GO TO 333
      IF(L.LE.119) GO TO 444
      IF(L.LE.135) GO TO 556
111   I=1
      GO TO 666
222   I=2
      GO TO 666
333   I=3
      GO TO 666
444   I=4
      GO TO 666
556   I=5
666   CALXH(L) =EXP(YHAT(L))
      ERROR(L) =ABS(CALXH(L)-XH(L))*100/XH(L)
      SUMER    =SUMER+ERROR(L)
      WRITE (2,999) L,XH(L),CALXH(L),ERROR(L)
999   FORMAT (/,5X,I3,16X,F8.5,26X,F8.5,20X,F8.4)
777   CONTINUE
      AVERR =SUMER/FLOAT(M)
      WRITE (2,707) AVERR
707   FORMAT (///,20X,23HAVERAGE PERCENT ERROR =,F10.4)
      CALL MINIMAX(M,XH,XMIN,XMAX)
      CALL MINIMAX (M,CALXH,YMIN,YMAX)
      IF (XMIN.LT.YMIN) YMIN =XMIN
      IF (YMIN.LT.XMIN) XMIN =YMIN
      IF (XMAX.GT.YMAX) YMAX =XMAX
      IF (YMAX.GT.XMAX) XMAX =YMAX
      CALL OPENGINOGP
      CALL SHIFT2(70.0,70.0)
      CALL AXIPOS(1,0.0,0.0,150.0,1)
      CALL AXIPOS(1,0.0,0.0,150.0,2)
      CALL AXISCA(1,10,0.0,0.50,1)
      CALL AXISCA(1,10,0.0,0.50,2)
      CALL AXIDRA(2,1,1)
      CALL AXIDRA(-2,-1,2)
      CALL MOVTO2 (0.0,0.0)
      CALL LINTO2 (150.0,150.0)
      CALL LINTO2(0.0,150.0)
      CALL MOVTO2(150.0,150.0)
      CALL LINTO2(150.0,0.0)
      CALL GRASYM (XH,CALXH,M,8,0)
      CALL DEVEND
555   STOP
      END
      SUBROUTINE LESQ(X,Y,N,M,A,B,XBAR,YHAT,AA,N2)
      DIMENSION X(M,N),Y(M),A(N2),B(N),XBAR(N),YHAT(M),
     *          AA(N,N)
      WRITE(2,16)
```

```
163    16  FORMAT(10X,38HMULITIPLE LINEAR REGRESSION ALGORITHM:)
164
165 C            CALCULATE AVERAGE  X  AND  Y VALUES
166
167         DO 205 I=1,N
168         SUMX=0.0
169         DO 206 J=1,M
170    206  SUMX=SUMX+X(J,I)
171    205  XBAR(I)=SUMX/FLOAT(M)
172         SUMY=0.0
173         DO 207 K=1,M
174    207  SUMY=SUMY+Y(K)
175         YBAR=SUMY/FLOAT(M)
176         WRITE(2,17)
177    17   FORMAT(//,2X,23HVARIABLE AVERAGE VALUES :)
178         WRITE(2,18) (II,XBAR(II), II=1,N)
179    18   FORMAT(/,3(2X,5HXBAR(,I2,4H) = ,1PE14.7))
180         WRITE(2,19) YBAR
181    19   FORMAT(/,2X,7HYBAR=  ,1PE14.7)
182
183 C          CALCULATE REGRESSION MATRICES
184
185         KK=1
186         DO 208 I=1,N
187         DO 209 J=1,N
188         SUMA=0.0
189         SUMB=0.0
190         DO 210 K=1,M
191         SUMA=SUMA+(X(K,I)-XBAR(I))*(X(K,J)-XBAR(J))
192    210  SUMB=SUMB+(Y(K)-YBAR)*(X(K,I)-XBAR(I))
193         AA(I,J)=SUMA
194         A(KK)=SUMA
195         KK=KK+1
196    209  B(I)=SUMB
197    208  CONTINUE
198         WRITE(2,191)
199    191  FORMAT(//,10X,9HAA MATRIX :)
200         DO 211 II=1,N
201    211  WRITE(2,20) (AA(II,JJ), JJ=1,N)
202     20  FORMAT(/,8(2X,E10.4))
203         WRITE(2,21)
204     21  FORMAT(//,10X,8HB MATRIX :)
205         WRITE(2,22) (B(KK), KK=1,N)
206     22  FORMAT(/,8(2X,E10.4))
207
208 C          SOLVE REGRESSION MATRICES FOR COEFFICIENTS
209
210         CALL STMG(A,B,N,KS,N2)
211         SUMX=0.0
212         DO 212 I=1,N
213    212  SUMX=SUMX+B(I)*XBAR(I)
214         AZERO=YBAR-SUMX
215         WRITE(2,23)
216    23   FORMAT(10X,37HVALUES OF THE REGRESSION COEFFICIENTS:)
217         WRITE(2,24) (JJ,B(JJ), JJ=1,N)
218    24   FORMAT(/,2(2X,5HAHAT(,I2,4H) = ,1PE16.8,8X))
219         WRITE(2,25) AZERO
220    25   FORMAT(/,2X,8HAZERO=  ,1PE16.8 :)
221         AHATO=EXP(AZERO)
222         WRITE(2,26) AHATO
```

```
223    26  FORMAT(/,2X,10HAHAT(0) = ,1PE16.8)
224
225 C         CALCULATE S AND R TEST
226
227         STEST=0.0
228         DO 213 J=1,M
229         SUMS1=0.0
230         DO 214 K=1,N
231    214  SUMS1=SUMS1+B(K)*X(J,K)
232         YHAT(J)=AZERO+SUMS1
233         DIFF=(Y(J)-YHAT(J))**2
234    213  STEST=STEST+DIFF
235         SUMST=0.0
236         DO 215 I=1,M
237    215  SUMST=SUMST+(Y(I)-YBAR)**2
238         SUMSR=SUMST-STEST
239         RTEST=SUMSR/SUMST
240         WRITE(2,27)
241    27   FORMAT(////,5X,19HEXPERIMENTAL VALUES,18X
242        *                ,17HREGRESSION VALUES  )
243         DO 516 KK=1,M
244   516   WRITE(2,28) KK,Y(KK),KK,YHAT(KK)
245    28   FORMAT(/,2X,2HY(,I3,4H) = ,1PE16.8,10X
246        *            ,5HYHAT(,I3,4H) = ,1PE16.8)
247         WRITE(2,29) SUMST,STEST,RTEST
248    29   FORMAT(///,2X,8HSUMST = ,1PE16.8,/,2X,4HS = ,
249        *            1PE16.8,10X,10X,7HR**2 = ,1PE16.8  )
250         RETURN
251         END
252         SUBROUTINE STMG(A,B,N,KS,NS)
253         DIMENSION A(NS),B(N)
254         TOL=0.0
255         KS=0
256         JJ=-N
257         DO 217 J=1,N
258         JY=J+1
259         JJ=JJ+N+1
260         BIGA=0.0
261         II=JJ-J
262         DO 218 I=J,N
263
264 C           SEARCH FOR MAXIMUM COEFFICIENT IN COLUMN
265
266         IJ=II+I
267         IF(ABS(BIGA)-ABS(A(IJ))) 20,218,218
268    20   BIGA=A(IJ)
269         IMAX=I
270   218   CONTINUE
271
272 C       TEST FOR PIVOT LESS THAN TOLERANCE (SING. MATRIX)
273
274         IF(ABS(BIGA)-TOL) 35,35,40
275    35   KS=1
276         RETURN
277
278 C           INTERCHANGE ROWS IF NECESSARY
279
280    40   I1=J+N*(J-2)
281         II=IMAX-J
282         DO 50 K=J,N
```

```
      I1=I1+N
      I2=I1+II
      SAVE=A(I1)
      A(I1)=A(I2)
      A(I2)=SAVE

C          DIVIDE EQUATION BY LEADING COEFFICIENT

   50 A(I1)=A(I1)/BIGA
      SAVE=B(IMAX)
      B(IMAX)=B(J)
      B(J)=SAVE/BIGA

C          ELIMINATE NEXT VARIABLE

      IF(J-N) 57,70,57
   57 IQS=N*(J-1)
      DO 217 IX=JY,N
      IXJ=IQS+IX
      II=J-IX
      DO 60 JX=JY,N
      IXJX=N*(JX-1)+IX
      JJX=IXJX+II
   60 A(IXJX)=A(IXJX)-(A(IXJ)*A(JJX))
  217 B(IX)=B(IX)-(B(J)*A(IXJ))

C             BACK   SOLUTION

   70 NY=N-1
      II=N*N
      DO 219 J=1,NY
      IA=II-J
      IB=N-J
      IC=N
      DO 219 K=1,J
      B(IB)=B(IB)-A(IA)*B(IC)
      IA=IA-N
  219 IC=IC-1
      RETURN
      END
      SUBROUTINE MINIMAX (M,X,XMIN,XMAX)
      DIMENSION X(M)

      XMIN =X(1)
      XMAX = X(1)

      DO 1 I = 1,M
         IF(XMIN.GT.X(1))  XMIN=X(1)
         IF(XMAX.LT.X(1))  XMAX=X(1)
    1 CONTINUE


      XMIN =FLOAT(IFIX(XMIN-(0.15*XMIN)))
      XMAX =FLOAT(IFIX(XMAX+(0.15*XMAX)))
      RETURN
      END
      FINISH
****
```

APPENDIX VI

Paper presented at the Second Symposium on Separation Science and Technology for Energy Application.

Gatlinburg, Tennessee, U.S.A.

5-8 May, 1981.

and Published in Separation Science and Technology, Volume 16, Number 9, Page 1217-1245, (1981).

Aston University

Pageă removed for copyright restrictions.

NOMENCLATURE

The symbols have the following meaning unless otherwise stated in the text:

A	Total interfacial area, cm^2
A	Surface area of an oscillating drop, cm^2
A_n	Eigenvalue in Equation (5.15).
A_o	Initial surface are of an oscillating drop, cm^2.
a	Interfacial area per unit column volume, cm^2/cm^3.
a	Horizontal radius of spheriod in Equation (5.24).
a'	Distribution parameter (Skewness parameter).
a_d	Surface area of drop in equation (5.5) and (5.6).
a_o	Initial horizontal radius in Equations (5.22) and (5.24).
a_p	Amplitude in x-axis in Equations (5.22) and (5.24).
b	Vertical radius of spheriod in Equation (5.25).
b_o	Initial vertical radius in Equation 5.23.
ΔC	Concentration driving force, gm/cm^3.
ΔC_m	Actual mean concentration driving force, gm/cm^3.
C	Solute concentration, gm/cm^3.
C^*	Equilibrium solute concentration, gm/cm^3.
D	Molecular diffusivity, cm^2/sec.
D_c	Column diameter, cm
D_E	Effective diffusivity in Equation (5.20), cm^2/sec.
D_N	Nozzle inside diameter in Equation (4.1), cm.
D_r	Diameter of rotor disc, cm
D_s	Diameter of stator opening, cm.
ΔD	Distance between agitator and colum wall $(D_c-D_r)/2$, cm.

d	Diameter of drop, cm.
d_F	Diameter of detatched drop in Equation (4.1), cm.
d_{max}, d_m	Maximum stable drop size, cm.
d_o	Mean drop size, cm.
d_{32}	Sauter mean drop diameter, cm.
d_{10}	Drop diameter at 10% cumulative drops volume. cm.
d_{50}	Drop diameter at 50% cumulative drops volume, cm.
d_{90}	Drop diameter at 90% cumulative drops volume, cm.
E	Axial mixing coefficient, cm^2/sec
E_m	Extraction efficiency.
e	Eddy diffusivity, cm^2/sec.
F	Constant in Equation (4.1), Harkins and Brown correlation factor.
F_B	Superficial flow rate of interstage mixing per unit cross sectional area of column, cm/sec.
g, g_c	Acceleration due to gravity, cm/sec^2.
H	Compartment height, cm.
H_c	Overall column height, cm.
H_E	Effective column height, cm.
H.T.U.	Height of transfer unit, cm.
h	Column height at certain point, cm.
K	Overall mass transfer coefficient, cm/sec.
K_{cal}	Overall theoretical mass transfer coefficient, cm/sec
K_{df}	Mass transfer coefficient during drop formation, cm/sec.
K_{Exp}	Overall experimental mass transfer coefficient, cm/sec.
$K_{o.c}$	Overall mass transfer coefficient of circulating drop, cm/sec.
$K_{o.o}$	Overall mass transfer coefficient of oscillating drop, cm/sec.
Ka	Overall volumetric mass transfer coefficient, 1/sec.

r_o	Initial radius of drop in Equations (5.5) and (5.6).
S	Distance between the centres of the drops in Equation (4.5), cm.
t	Time, sec.
t_f	Time of drop formation, sec.
U_N	Dispersed phase average velocity through the nozzle in Equation (4.1), cm/sec.
V	Phase superficial velocity, cm/sec.
$\overline{V}$	Mean Langrangin turbulent velocity fluctuation in Equation (4.5), cm/sec.
V*	The critical approach velocity in Equation (4.5), cm/sec.
V_F	Drop volume after break off from the nozzle in Equation (4.1), cm^3.
$V_N, \overline{V}_N$	Characteristic drop velocity, cm/sec.
V_o	Vertical relative velocity of drops, cm/sec.
V_o	Characteristic velocity of turbulence pulsations in Equations (4.6) and (4.7), cm/sec.
V_s	Slip velocity, cm/sec.
V_t	Drop terminal velocity, cm/sec.
W	Function of oscillating drop characteristics defined by Equation (5.22).
X	Solute concentration in the raffinate phase, gm/100 gm.
X	Dispersed phase hold-up.
X	Length of droplet X-axis in Equation (5.23), cm.
X_f	Dispersed phase hold-up at flooding point
X_i	Dispersed phase hold-up at phase inversion point.
X_o	Ficticious film thickness in Equation (5.23), cm.
x	Distance, cm.
Y,y	Solute concentration in the extract phase, gm/100 gm.
Δy_m	Actual mean concentration driving force, gm/100 gm

Z	Coefficient of coalescence.

Dimensionless Groups

F_r	Froude number $\frac{V_c^2}{g_c D_c}$
F_r	Modified Froude number $\frac{V_d^2}{g_c D_c X^2}$
G_a	Galileo number $\frac{d^3 \rho^2 g}{\mu^2}$
N_p	Power number $\frac{P}{N^3 D^5 \rho}$
$(Pe)_c$	Peclet number $\frac{V_c H}{E_c}$ for continuous phase.
$(Pe)_d$	Peclet number $\frac{V_d H}{E_d}$ for dispersed phase.
Re	Disc Reynolds number $\frac{D_r^2 N \rho}{\mu}$
Re	Droplet Reynolds number $\frac{dV_o \rho}{\mu}$
Re	Column Reynolds number $\frac{V_d H \rho_c}{\mu x}$
Sc	Schmidt number $\frac{\mu}{\rho D}$
Sh	Sherwood number $\frac{kd}{D}$
We	Disc Weber number $\frac{N^2 D_r^3 \rho_c}{\sigma}$
We	Droplet Weber number $\frac{dV_o^2 \rho_c}{\sigma}$

Greek Letters

α	Back flow coefficient.
α	Back mixing correlation factor.
α	Constant in Equation (3.19).
γ	Surface tension, dyne/cm.
δ	Uniformity distribution parameter.
ε $\bar{\varepsilon}$	Energy input per unit mass and time, erg/(gm.sec).

K_1, K_2	Constant in Equations (3.21) and (4.6).
K_3, K_4	Constant in Equation (4.7).
k_c	Continuous phase mass transfer coefficient, cm/sec.
$k_{c.c}$	Continuous mass transfer coefficient of circulating drop, cm/sec.
$k_{c.o}$	Continuous phase mass transfer coefficient of oscillating drop, cm/sec.
k_d	Dispersed phase mass transfer coefficient, cm/sec.
$k_{d.c}$	Dispersed phase mass transfer coefficient of circulating drop, cm/sec.
$k_{d.o}$	Dispersed phase mass transfer coefficient of oscillating drop, cm/sec.
k_{HB}	Mass transfer coefficient calculated by means of Handlos and Baron, cm/sec.
L	Characteristic dimension of turbulence, cm.
m	Equilibrium distribution coefficient.
N	Rate of mass transfer, gm/sec.
N	Rotor speed, R.P.S.
N'	Rotor speed, R.P.M.
N_c	Total number of compartments.
N.T.U.	Number of transfer unit.
n	Compartment number.
n_o	Number of uncombined drop per unit volume in equationa (4.6) and (4.7), $1/cm^3$.
P	Power input, erg/sec.
Q	Volumetric flow rate, cm^3/sec.
Q	Volumetric flow rate of dispersed phase through nozzle in Equation (4.1), cm^3/sec.
Rr	Phase flow ratio at inversion.
r	Radius of sphere of volume equal to that of a drop, cm.
$r_{s.d}$	Stable drop radius, cm.

ε	Amplitude of oscillation.
ε_o	Function of amplitude of oscillation defined by Equation (5.29).
λ_n	Eigenvalue in Equation (5.15).
μ	Viscosity, gm/cm.sec.
ν	Kinematic viscosity, cm^2/sec.
ν	Cumulative volume of drops, cm^3.
ρ	Density, gm/cm^3.
ρ_m	Mean density = $\rho_d x+\rho_c(1-x)$, gm/cm^3.
$\Delta\rho$	Density difference, gm/cm^3.
σ	Interfacial tension, dyne/cm.
τ	Dimensionless time.
ψ	Coalescence frequency in Equation (4.5).
ψ_1	Function of Schmidt group defined by Equation (3.29).
ψ_2	Function of the physical properties defined by Equation (3.31).
ω	Frequency of oscillation, 1/sec.
π	Constant = 3.1416.

Subscripts.

A	Refers to phase A.
av	Average
B	Bottom of the column.
C	Continuous phase.
C	Column.
C	Circulating drop.
Crit	Critical
Cul	Calculated or Theoretical.
d	Drop.
d	Dispersed phase.

E	Effective.
E	Extract phase.
Exp	Experimental.
F	Feed.
f	Flooding condition.
f	Drop formation.
i	Initial.
i	Ith Stage.
m	Mean.
m, max	Maximum.
N	Nozzle.
n	Nth stage,
o	Initial.
o	Oscillating drop.
o	Overall.
R	Raffinate phase.
R	Drop release.
r	Rotating disc.
s	Stagnant drop.
s	Stator opening.
s	Slip.
s.d	Stable drop.
T	Top of the column.
Vg	Geometric mean.
VS	Sauter-mean. Volume to surface ratio of droplets.
1	Refers to the end of the column where solutions are concentrated.
2	Refers to the end of the column where solutions are dilute.

Superscripts.

*	Refers to equilibrium condition.
–	Mid-sector or average.

REFERENCES

1. Treybal, R.E., Liquid Extraction, McGraw-Hill, New York, 2nd Edition (1963).

2. Khandelwal, A.N., Ph.D. Thesis, University of AStON in Birmingham, U.K. (1978).

3. Reman, G.H., Proceeds. 3rd World Pet. Cong. den Haag (1951) Section 3, 121.

4. Misek, T., Chem. Eng., 68, 58 (1961).

5. Marek, J, Misek, T., and Windmer, F., Soc. Chem. Eng., Symp., University of Bradford, U.K. 31st October, (1967).

6. Marek, J., Misek, T. Soc. Chem. Eng. Conf. on Solvent Extraction, London, March, (1969).

7. Old Shue, J.Y. and Rushton, J.H., Chem. Eng. Prog. 48, 297 (1952).

8. Simonis, H., Process Eng., 110, Nov. (1972).

9. Scheibel, E.G., U.S. Pat., 2, 493,265, (1950).

10. Kuhni, A.G., Verfarheus Technik and Apparateban, CH-4123, Aleschwuil-Basel, Schweitz.

11. Thornton, J.D., Trans. Instn. Chem. Engrs., 35, 316, (1957).

12. Coggan, G.C., Instn. Chem. Engrs., 35, 316, (1957).

13. Todd, D.B., Chem. Engng., 69, 156, (1962).

14. Logsdail, D.H. et al, Chap. 5, "Recent Advances in Liquid Extraction", Pergamon, London, (1971).

15. Laddha, G.S., Degalassan, T.E. and Kannapan, R., The Can. J. Chem. Engng., 56, 137, (1978).

16. Kagan, S.Z., Trukhanov, U.G., Kostin, P.A. and Kudryanstev, E.W., Int. Chem. Eng., 4, 473 (1964).

17. Reman, G.H., Olney, R.B., Chem.Eng.Prog., 51, 141 (1955).

18. Theyze, U.G., Wall, R.J., Train, K.E. and Olney, R.B., Oil.Gas Jnl., 59, 70, (1961).

19. Anon. Pet. Processes, 10, 230, (1955).

20. Misek, T. and Rozkos, B., Int. Chem. Eng., 6, 130, (1966).

21. Reman, G.H. and Van der Vusse, J.G., Pet. Refiner, 34, 9, 129, (1955).

22. Reman, G.H., Pet. Refiner, 36, 269, (1957).

23. Reman, G.H. and Van der Vusse, J.G., Genie Chemie, 74, 106, (1956).

24. Cronan, C.S., Chem. Eng., 65, 54 (1958).

25. Al-Hemiri, A.A.A., Ph.D. Thesis, University of Aston in Birmingham, U.K., (1973).

26. Sarkar, S., Ph.D. Thesis, University of Aston in Birmingham, U.K., (1976).

27. Rod, V., Bri. Chem. Eng., 16, 617, (1971).

28. Logsdail, D.H., Thornton, J.D. and Pratt, H.R.C., Trans. Inst. Chem. Eng., 35, 301, (1957).

29. Kung, K.Y. and Beckmann, R.B., A.I.Ch.E., Jnl., 7, 319, (1961).

30. Mumford, C.J., Ph.D. Thesis, University of Aston in Birmingham, U.K., (1970).

31. Misek, T., Coll. Czech. Comm. 29, 1767, (1964).

32. Misek, T., Rotating Disc Extractor, Statni Nakadatelstvi Technicke Literatury, Prague, (1964).

33. Strand, C.P., Olney, R.B. and Ackerman, G.H., A.I.Ch.E. Jnl., 8, 252, (1962).

34. Vermijis, H.J.A. and Kramers, H., Chem. Eng. Sci., 3, 55, (1954).

35. Gayler, R., Roberts, M.W. and Pratt, H.R.C., Trans. Instn. Chem. Engrs., 31, 57, (1953).

36. Thornton, J.D., Chem. Eng. Sci., 5, 201, (1956).

37. Thornton, J.D. and Pratt, H.R.C., Trans. Instn. Chem. Engrs., 31, 289, (1953).

38. Kasatkin, A.G.,Kagan, S.Z. and Trukhanov, G.V., Appl. Chem. (USSR), 35, 1903, (1962).

39. Murakami, A., Misonou, A. and Inoue, K., Int. Chem. Eng., 18, 16, (1978).

40. Misek, T., Coll. Czech. Comm., 28, 426, (1963).

41. Jeffreys, G.V., Al-Aswad, K.K.M. and Mumford, C.J., Paper presented in the 2nd Symp. on Sep. Sci. and Tech. for Energy App., Gatlinburg, Tenn. U.S.A., May, (1981).

42. Pratt, H.R.C., Ind. Chemist, 31, 505, (1955).

43. Rowe, P.N. et al, Trans. Instn, Chem. Engrs., 43, 14, (1965).

44. Rozkos, B., Research Rep. 918/69, VUCHZ Praha.

45. Reman, G.H., Chem. Eng. Prog., 62, 56, (1966).

46. Misek, T., Coll. Czech. Chem. Comm., 28, 570, 1631 (1963).

47. Arnold, D.R., Ph.D. Thesis, University of Aston in Birmingham, U.K. (1974).

48. Sleicher, C.A., A.I.Ch.E. Jnl., 5, 145, (1959).

49. Westerterp, K.R. and Landsman, P. , Chem. Eng. Sci., 17, 363, (1962).

50. Stainthorp, F.P. and Sudall , N., Trans. Inst. Chem. Engr., 42, 198, (1964).

51. Stemerding, S., Lumb, E.C. and Lips, J., Chem. Eng. Tech., 35, 844, (1963).

52. Misek, T. and Rod, V., "Calculation of Contactors with Longitudinal Mixing", "Recent Advances in Liquid-Liquid Extraction", Pergamon Press, Oxford, (1971).

53. Misek, T., Paper presented in CHISA II Congress, Marienbad, Czech, (1965).

54. Bruin, T., Trans. Inst. Chem. Eng., 51, 355, (1973).

55. Elenkov, D. and Temniskov, I., Comptes Rendus Acad. Bulg. Sci., 6, 679, (1974).

56. Venkataramana, J., Degaleesan, T.E. and Laddha, G.S., The Can. J. Chem. Engng., 58, 206, (1980).

57. Blazej, L., Vajda, M., Bafrncova, S. and Havalda, J., Chem. Zvesti, 32, 328, (1978).

58. Blazej, L., Vajda, M., Bafrncova, S. and Havalda, J., Chem. Zvesti, 32, 341, (1978).

59. Miyauchi, T., Mitsutake, H. and Harase, I., A.I.Ch.E.Jnl., 12, 508, (1966).

60. Murakami, A. and Misonou, A., Int. Chem. Eng., 18, 22, (1978).

61. Misek, T., Coll. Czech. Chem. Comm., 40, 1686, (1975).

62. Rod, V., Coll. Czech. Chem. Comm., 33, 2855, (1968).

63. Adamson, A.W., "Physical Chemistry of Surfaces", Interscience Publishers Inc., (1960).

64. Osipau, L.I., Surface Chemistry, Rheinhold Publishing Corp., (1962).

65. Garner, F.H., Ellis, S.R.M. and Hill, J.W., A.I.Ch.E.Jnl., 1, 185, (1955) and Trans. Instn. Chem. Engrs., 34, 223, (1956).

66. Sobolic, R.H. and Himmelblan, D.M., A.I.Ch.E.Jnl., 6, 619, (1960).

67. Treybal, R.E., Ind. Eng. Chem., 51, 262, (1960).

68. Coggan, G.C., Instn. of Chem. Engrs. Symp. on Liquid-Liquid Extraction, April, (1967).

69. Sege, G. and Woodfield, F.M., Chem. Eng. Progr., 50, 396 (1954).

70. Davies, J.T., Ritchie, J.M. and Southward, D.C., Trans. Instn. Chem. Engrs., 38, 331, (1960).

71. Haynes, L.G., Himmelblau, D.M. and Shechter, R.S., I. and E.C. Process Design and Development, 7, 508 (1968).

72. Groothuis, H. and Kramers, H., Chem. Eng. Sci., 4, 17 (1955).

73. Young, E.F., Chem. Eng., 64, 241, (1957).

74. Miyauchi, T. and Vermeulen, T., Ind. Engng. Chem. Funds., 2, 113, (1963).

75. Hartland, S. and Mechlenburgh, J.C., Chem. Eng. Sci., 21, 1209, (1966).

76. Rod, V., Bri. Che. Eng., 9, 300, (1964).

77. Danckwerts, P.V., Chem. Eng. Sci., 2,1, (1953).

78. Olney, R.B., A.I.Ch.E.Jnl., 10, 827, (1964).

79. Misek, T. and Rod, V., Paper presented on CHISA II Congress, Marienbad, Czech, (1965).

80. Mumford, C.J. and Jeffreys, G.V., Paper presented to 3rd CHISA Congress, Marianske Lazne, Spet., (1969).

81. Jeffreys, G.V. and Ellis, E.M.R., CHISA, (1962).

82. Heertjes, P.M. and De Nie, L.H., Mass Transfer to Drops, Recent Advances in Liquid-Liquid Extraction. Edited by Hanson, C., Pergamon Press, (1971).

83. Harkins, W.D. and Brown, F.E., Jnl. Am. Chem. Soc., 41, 499, (1919).

84. Treybal, R.E. and Howarth, C.B., Ind. Eng. Chem., 42, 1174, (1950).

85. Null, H.R. and Johnson, H.F., A.I.Ch.E.Jnl., 4, 273, (1958).

86. Meister, J.B., Ph.D. Thesis, Cornall Univ. New York, (1966).

87. Scheels, G.E. and Meister, B.J., A.I.Ch.E.Jnl., 14, 9, (1968).

88. Kolmogoroff, A.N., Doklady Acad. Nank, U.S.S.R., 30, 301, (1941); 31, 538, (1941); 66, 825, (1949).

89. Hinze, J.O., I.A.Ch.E.Jnl., 1, 289, (1955).

90. Clay, P.H., Proc. Roy. Acad. Sci., (Amsterdam), 43, 852, 979, (1940).

91. Levich, V.G., "Physicochemical Hydrodynamics". Prentice-Hall, New Jersey, (1962).

92. Jeffreys, G.V. and Mumford, C.J., Proc. Int. Solvent, Ext. Conf., The Hague, (ISEC), Vol. 1, 667, (1971).

93. Mumford, C.J. and Al-Hemiri, A.A.A., Proc. Int. Solvent Ext. Conf., Lyon, (ISEC), Vol.2, 1591, (1974).

94. Blazej, L., Vajda, M., Bafrncova, S. and Havalda, J., Chem. Zvesti, 32, 314, (1978).

95. Lawson, G.B., Ph.D. Thesis, University of Manchester, (1967).

96. Jeffreys, G.V. and Davies, G.A., "Recent Advances in Liquid-Liquid Extraction, C. Hanson (ed.), Pergamon Press, N.Y., (1971).

97. Gillespie, T. and Rideal, E.K., Trans. Faraday Soc., 52, 1736, (1956).

98. Jeffreys, G.V. and Hawksley, J.L., Jnl.Appl.Chem., 12, 329, (1962).

99. Cockbain, E.G. and McRoberts, T.S.,Jnl. Coll. Sci., 8, 440, (1953).

100. Elton, G.A. and Picknett, R.G., Proc. 2nd Int. Cong. on Sufacr Activity, Vol.1, 288-307, Butterworths, London, (1957).

101. Jeffreys, G.V. and Lawson, G.B., Trans. Instn. Chem. Engrs., 43, 294 (1965).

102. Smith, D.V. and Davies, G.A., Can. Ins. Chem. Eng., 48, 628, (1970).

103. Howarth, W.J., Chem. Eng. Sci., 19, 33, (1966).

104. Madden, A.J. and Damarell, G.L., A.I.Ch.E.Jnl., 8, 233, (1962).

105. Misek, T., Coll. Czech. Comm., 29, 2086, (1964).

106. Miller, R.S. et al, A.I.Ch.E.Jnl., 9, 196, (1963).

107. Sleicher, C.A., A.I.Ch.E.Jnl., 8, 471, (1962).

108. Mugele, R.A. and Evans, H.D., Ind. Eng. Chem., 43, 1317, (1951).

109. Bouyatiotis, B.A. and Thornton, J.D., Instn. Chem. Engrs. Symp. Series, No.26, (1967).

110. Chen. H.T. and Middleman, S.A., A.I.Ch.E.Jnl., 13, 989, (1967).

111. Sprow, F.B., Chem. Eng. Sci., 22 435, (1967).

112. Brown, D.E. and Pitt, K., Proc. Chemeca 70, Butterworth, Australia, (1970).

113. Giles, J.G., Hanson, C. and Marsland, J.Proc.Int. Solvent, Ext. Conf., The Hague (ISEC) 74, (1971).

114. Chartes, R.H. and Korchinsky, W.J., Trans. Inst. Chem.Engrs., 53, 247, (1975).

115. Korchinsky, W.J. and Azimzadeh-Khataylo, S., Chem. Engng. Sci., 31, 871, (1976).

116. Chartres, R.H. and Korchinsky, W.J., Trans. Inst. Chem. Eng., 56, 91, (1978).

117. Sherwood, T.K. et al, Ind. Eng. Chem., 31, 1144, (1939).

118. Angelo, J.B., Lightfoot, E.N. and Howard, O.W., A.I.Ch.E.Jnl., 12, 751, (1966).

119. Heertjes, P.A., Holve, W.A. and Talsma, H., Chem. Eng. Sci., 3, 122, (1954).

120. Sawistowski, H. and Goltz, G.E., Trans. Instn. Chem. Engrs., 41, 174, (1963).

121. Skelland, A.H.P. and Minhas, S.S., A.I.Ch.E.Jnl., 17, 1316, (1971).

122. Heertjes, P.A. and de Nie, L.H., Chem. Eng. Sci., 21, 755, (1966).

123. Coulson, J.H. and Skinner, S.J., Chem. Eng. Sci., 1, 197, (1951).

124. Popovich, A.T., Jervis, R.E. and Trass, O., Chem. Eng. Sci., 19, 357, (1969).

125. Rose, P.M. and Kintner, R.C., A.I.Ch.E.Jnl., 12, 530, (1966).

126. Garner, F.H. and Tayeban, H., An. R. Soc.Esp. Quim., 56B, 479, (1960).

127. Forsyth, J.S. et al, Proc. Int. Solvent Conf., Lyon, (ISEC), Vol.1, 417, (1974).

128. Hughmark, G.A., Ind. Eng. Chem. Funds., 6, 408, (1967).

129. Kinard, G.E., Manning, F.S. and Manning, W.P., Brit. Chem. Eng., 8, 326, (1963).

130. Licht, W. and Pensing, W.F., Ind. Eng. Chem., 45, 1885, (1953).

131. Ilkovic, D., Coll. Czech. Chem. Comm., 6, 498, (1934).

132. Hadamard, C.R. and Rybezynski, A., Acad. Sci., Paris, 152, 1735, (1911).

133. Levich, V., Shur. Obstrch. Khim., 19, 18, (1949).

134. Garner, F.H. and Skelland, A.H.P., Chem. Eng. Sci., 4, 149, (1955).

135. Al-Hassan, T.S., Ph.D. Thesis, University of Aston in Birmingham, U.K., (1979).

136. Newman, A.B., Trans. Am. Inst. Chem. Engrs., 27, 203, (1931).

137. Vermulen, T., Ind. Eng. Chem., 45, 1664, (1953).

138. Kronig, R. and Brink, J.C., Appl. Sci. Res., A-2, 142, (1960).

139. Calderbank, P.H. and Korchinski, I.J.O., Chem Eng.Sci. 6.65, (1956).

140. Handlas, A.E. and Baron, T., A.I.Ch.E.Jnl., 3, 127, (1957).

141. Skelland, A.H.P. and Wellek , R.H., A.I.Ch.E.Jnl., 10, 491, (1964).

142. Johnson, A.I. and Hamielec, A.E., A.I.Ch.E.Jnl., 6, 145, (1960).

143. Olander, D.R., A.I.Ch.E.Jnl., 12, 1018, (1966).

144. Gunn, R. Jnl. Geophys. Res., 54, 383 (1949).

145. Garner, F.H. and Haycock, P.J., Pro. Roy. Soc., A. 252, 457, (1959).

146. Schroeder, R.R. and Kintner, R.C., A.I.Ch.E.Jnl., 11, 5 (1965).

147. Ellis, W.B., Ph.D. Thesis, University of Maryland, U.S.A., (1966).

148. Linton, M. and Sutherland, Chem. Eng. Sci., 12, 214, (1960).

149. Sideman, S. and Shafrai, H., Cand. Chem. Eng. J., 42, 107, (1964).

150. Griffith, R.M., Chem.Eng.Sci., 12, 198, (1960).

151. Garner, F.H. and Suckling, R.D., A.I.Ch.E.Jnl., 4, 114, (1958).

152. Garner, F.H., Jenson, V.C. and Keey, R., T.I.C.E., 37, 197, (1957).

153. Boussinesq, J., C.R.Acad. Sci. Paris, 156, 983, 1035, 1124, (1913).

154. Garner, F.H., Foord, A. and Tayeban, M., Jnl. Appl., Chem. 9, 315, (1959).

155. Mekasut, L., Molinier, J. and Angelino, H., Chem. Eng., Sci., 33, 821, (1978).

156. Thorsen, G. et al, Chem. Eng. Sci., 23, 413, (1968).

157. Yamaguchi, M., Watanabe, S. and Katayama, T., Jnl.Chem. Eng., Japan, 8, 415, (1975).

158. Yamaguchi, M., Fujimato, and Katayama, T., Jnl. Chem.Eng. Japan, 8, 361, (1975).

159. Hendrix, C.D. et al, A.I.Ch.E.Jnl., 13, 1072, (1967).

160. Groothuis, H. and Zuiderweg, F.J., Chem. Eng. Sci., 12, 288, (1960).

161. Sawistowski, H., Recent Advances in Liquid-Liquid Extraction, Edited by Hanson, C., Pergamon, Press, N.Y., (1971).

162. McFerrin, A.R. and Davidson, R.R., A.I.Ch.E.Jnl., 17, 1021, (1971).

163. Licht, W. and Conway, J.B., Ind. Engng. Chem., 47, 1151 (1950).

164. Heertjes, P.M. and de Nie, L.H., Chem. Eng. Sci., 26, 697, (1971).

165. Sternling, C.V., and Schriven, L.E., A.I.Ch.E.Jnl., 5, 574, (1959).

166. Orell, A. and Westwater, J.W., A.I.Ch.E.Jnl., 8, 350, (1962).

167. Maroudas, N.G. and Sawistowski, H., Chem.Eng. Sci., 19, 919, (1965).

168. Sehrt, B. and Linde, H., Proc. 3rd Int.Conf. on Surface Active Materials, Akademie Verlag, Berlin, (1967).

169. Haydon, D.A., Proc. Roy. Soc., A243, 483, (1958).

170. Davies, J.T., "Turbulence Phenomena", Academic Press, New York, (1972).

171. West, F.B., Herman, A.J., Chong, A.T. and Thomas, L.E.A., Ind. Eng. Chem., 44, 625, (1952).

172. Garner, F.H. and Hale, A.R., Chem. Eng. Sci., 20, 737, (1965).

173. Holm, A. and Terjesen, S.G., Chem. Eng. Sci., A.265, (1955).

174. Lindland, K.P. and Terjesen, S.G., Chem. Eng. Sci., 5,1, (1956).

175. Frumkin, A. and Levich, V.G., Zh. Fiz. Khim., 21, 1183, (1947).

176. Huang, W.S. ans Kintner, R.C., A.I.Ch.E.Jnl., 15, 735, (1969).

177. Kintner, R.C., Advan. Chem. Eng., 4, 51, (1963).

178. Goltz, G.E. and Glew, D.N., Analy. Chem., 29, 816, (1957).

179. Siedel, A., Solubilities of Inorganic and Metal Organic Compounds, Vol.II, 4th Edition, (1965).

180. Honekamp, J.R. and Burkhart, L.E., Ind. Eng. Chem. Proc. Design and Dev., 1, 3, 177, (1962).

181. Wilke, C.R. and Pin Chang, A.I.Ch.E.Jnl., 1, 264, (1955).

182. Kung, E.Y., Ph.D. Thesis, Carnegie Institute of Tedhnology, College of Eng. and Sci., U.S.A., (1959).

183. Austin, D.G. and Jeffreys, G.V., The Manufacture of Methyl Ethyl Ketone, from 2-Butanol, Instn. of Chem. Eng., 193, (1979).